The Wide Field X-ray Telescope

A Vast Legacy for Astrophysics and Cosmology

Proceedings of the Bologna WFXT Workshop, November 25-26, 2009

Edited by: P. Rosati, S. Borgani, R. Gilli, M. Paolillo and P. Tozzi

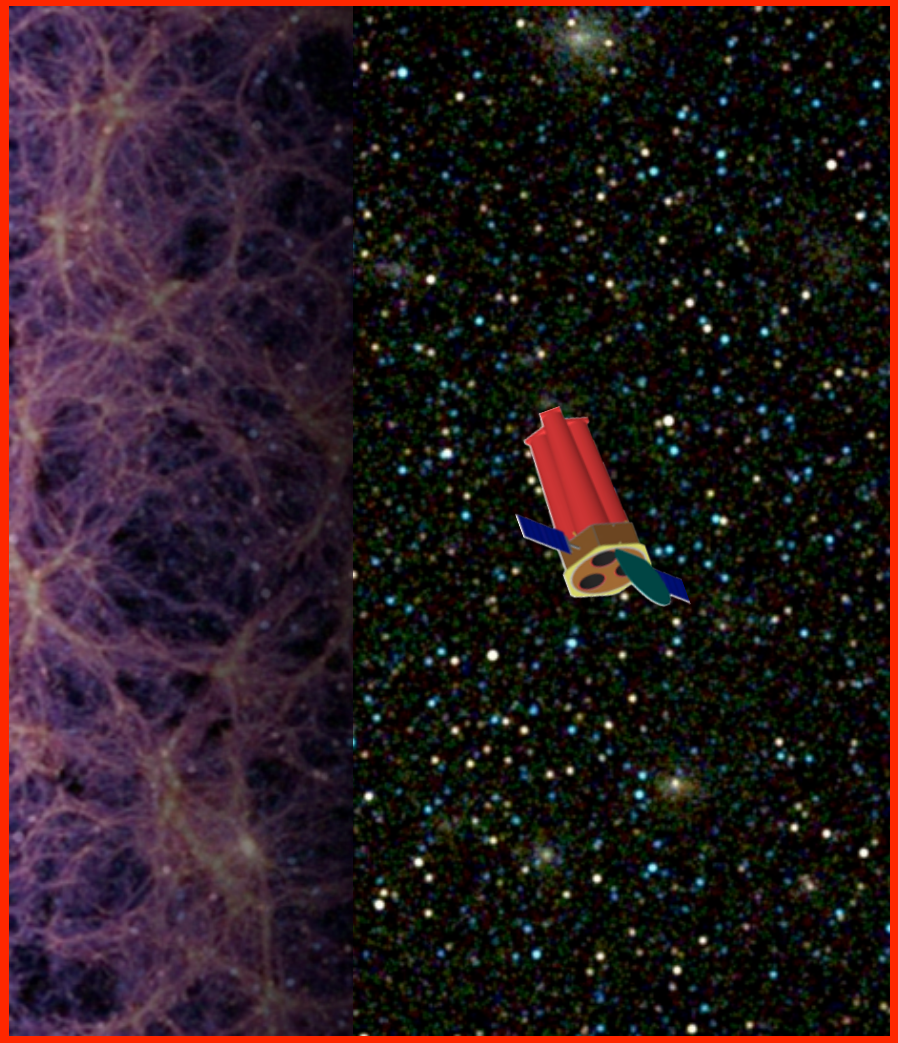

MEMORIE DELLA SOCIETÀ ASTRONOMICA ITALIANA
SUPPLEMENTI Vol.17

MEMORIE

DELLA

SOCIETÀ ASTRONOMICA ITALIANA SUPPLEMENTI

Vol. 17 - 2011

Direttore responsabile: Piercarlo Bonifacio

MEMORIE DELLA SOCIETÀ ASTRONOMICA ITALIANA

Supplements Vol. n.17 2011

The Wide Field X-ray Telescope

Bologna, November 25-26, 2009

editors: P.Rosati, S.Borgani, R.Gilli, M.Paolillo, P.Tozzi

TABLE OF CONTENTS

ACTIVE GALACTIC NUCLEI

GALAXIES

STARS AND COMPACT OBJECTS

SYNERGIES WITH FUTURE FACILITIES

The Wide Field X-ray Telescope

Bologna, November 25-26, 2009

Scientific Organizing Committee

Stefano Borgani (Dip. di Fisica, Sezione di Astronomia, Università di Trieste, Italy),
Sergio Campana (INAF - Osservatorio Astronomico di Brera, Italy),
Roberto Gilli (INAF - Osservatorio Astronomico di Bologna),
Maurizio Paolillo (Università Federico II, Dip. di Scienze Fisiche, Napoli, Italy),
Giovanni Pareschi (INAF - Osservatorio Astronomico di Brera, Italy),
Piero Rosati (ESO, European Southern Observatory, Garching bei München, Germany),
Salvo Sciortino (INAF - Osservatorio Astronomico di Palermo, Italy),
Paolo Tozzi (INAF - Osservatorio Astronomico di Trieste, Italy)

Sponsorship

INAF - Osservatorio Astronomico di Bologna
INAF - IASF Bologna
INAF - Osservatorio Astronomico di Brera
ASI (Agenzia Spaziale Italiana)

FOREWORD

Riccardo Giacconi, September 2010

Important discoveries in all branches of Astronomy and in particular in X-Ray Astronomy have often come about by a combination of physical intuition, technological improvements, and a boundless faith in the richness of Nature. It is clear that theories about the Universe only go so far as can be achieved given our current knowledge and our mathematical skills.

Nature has no such limitations and has already solved the questions we are asking; very simply Nature is. This perhaps is why so many discoveries in Astronomy are real discoveries rather than verifications. The existence of binary X-ray sources, of efficient energy production by in fall of matter on collapsed objects, the existence of an extragalactic X-ray background, and the existence of intergalactic plasmas were revealed in most cases by unexpected discoveries from broad surveys in the X-ray domain.

While faith in the bounty of Nature is justified, it is also important to realize that understanding Nature requires skill in providing discovery space and care in listening to its replies.

I am convinced that the Wide Field X-Ray Telescope (WFXT) will provide the required technological advance to open a significant new discovery space. The expectations discussed at this meeting are a testimony of the broad range of scientific questions that will become accessible through the proposed surveys. My own interest in wide field X-ray optics stems from my encounters with X-ray emission from clusters of galaxies with the UHURU, EINSTEIN and ROSAT observatories and the number of questions that those surveys left unresolved. It was clear that to obtain unbiased samples we needed to be able to recognize clusters at large Zs through their X-ray properties alone, and that we needed to obtain significant deep and large statistical samples to enable the study of the formation and evolution of these structures.

In the late 80s Richard Burg, Christopher Burrows and I came to the realization that what was needed was new X-ray optics, which combined reasonably high resolution ($\sim$5 arc seconds) and a wide field of view ($\sim$ 1 degree), in other words an X-ray Schmidt telescope. We submitted a paper on this subject to the Astrophysical Journal in April 1990 (it was published in June 1992 on Ap.J., 392, 760-765). We succeeded in showing that such optical design was entirely feasible and no more difficult to achieve practically than the EINSTEIN or the ROSAT optics (see figures below).

In 1995 we submitted a NASA Explorer proposal with the specific goal of a cluster survey out to $z > 1$. The proposal was rejected on the basis of the prejudice which dominated the theoretical and observational community in the early-mid 90s that clusters did not exist at $z > 0.5$. The pioneering efforts of Piero Rosati and later the results from *Chandra* and *XMM-Newton* demonstrated that this was nonsense. Still other proposals to ESA, ASI and NASA up to 2002 were not successful.

Development of the new X-ray optics fabrication techniques in the US has proceeded very slowly and the scarce available funds were mainly used for in house work at NASA centers with little success. In Italy ASI funded the efforts of the Brera Observatory that succeeded, with industrial support, in demonstrating the feasibility of wide field optics (1 degree) with angular resolution of 5-7 arc seconds.

We were encouraged to submit the description of a medium sized survey mission (which would become the ultimate survey for many decades) to the Decadal Survey of the National Academy of Sciences. This included a description of the mission, its cost and a projected launch date of six years after go ahead. Four supporting articles outlined the expected scientific returns ranging from stars and galaxies, clusters of galaxies, quasars and cosmology.

It is unfortunate that this mission that has broad community support was received at a time of great financial difficulties for NASA due to the ballooning costs (mainly due to NASA mismanagement) both in the the manned exploration and scientific programs. The concerns with the state of development and the future of IXO , which appears headed in the same direction, dominated the consideration of X-ray astronomy. If understandable, it was disappointing to find no mention of WFXT in the NASA report.

Still I remain convinced that WFXT is a necessary mission in X-ray Astronomy to fill the gap of 100,000 in sensitivity between the deep and all sky surveys. WFXT will generate a legacy set of 500,000 clusters to $z \sim 2$, 10,000,000 AGNs to $z \sim 6$, and 100,000 normal and starburst galaxies. For a fraction of this sample ($\sim 10\%$) will provide direct physical characterization, with no need of follow up observations.

WFXT will have a strong impact on a wide range of disciplines and provide unique synergy to present and planned observatories such as IXO, JWST, ELTs and ALMA. I have complete confidence that X-Ray Astronomy will continue in the future to contribute greatly to our understanding of the Universe, and that WFXT will play an important role in its progress.

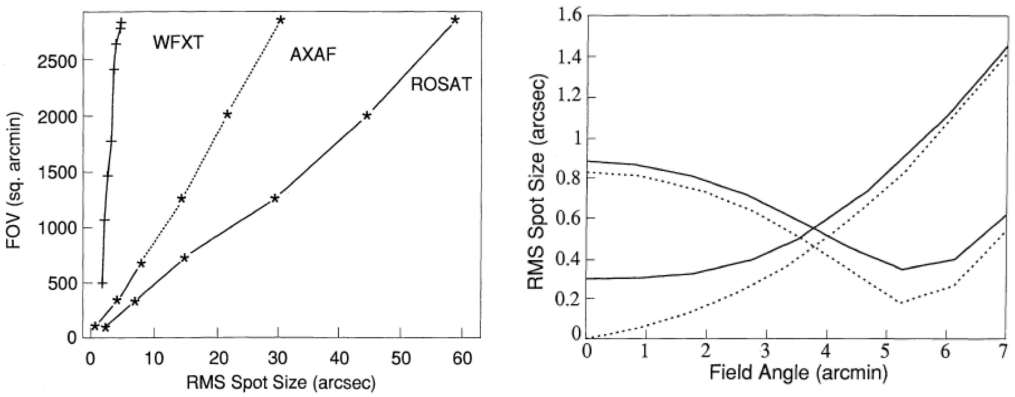

Fig. 1. [From Burrows, Burg & Giacconi, 1992, ApJ, 392, 760] *Left*: The cumulative field of view for ROSAT, AXAF (a.k.a. *Chandra*), and the *Wide Field X-ray Telescope*. The total available field area is plotted as a function of the average image quality. *Right*: the rms spot size for the outer shell of AXAF, in the existing and optimized designs (raising curves). The solid curves have an assumed image blur of $0.5''$caused by surface roughness added in quadrature to the dotted curves which represent the raytrace results. The optimized design (WFXT) has best image quality near $5''$. It remains sub-arcsecond over the full field. The existing paraboloid-hyberboid design is best on-axis, but when averaged over the field is about a factor of 2 worse than optimized design.

Mem. S.A.It. Suppl. Vol. 17, 8

Memorie della
Supplementi

Wide Field X-ray Telescope: Mission Overview

P. Rosati[1], S. Borgani[2,3], R. Gilli[4], M. Paolillo[5], P. Tozzi[6], S. Murray[7], R. Giacconi[7], A. Ptak[7], M. Weisskopf[8], W. Forman[9], C. Jones[9], and the WFXT Team

[1] ESO-European Southern Observatory, D-85748 Garching bei München, Germany
[2] Dipartimento di Fisica, Sezione di Astronomia, Università di Trieste, Via Tiepolo 11, I-34143 Trieste, Italy
[3] INFN, Sezione di Trieste, Via Valerio 2, I-34127 Trieste, Italy
[4] INAF-Osservatorio Astronomico di Bologna, Via Ranzani 1, I-40127 Bologna, Italy
[5] Università Federico II, Dip. di Scienze Fisiche, Via Cintia, I-80126, Napoli, Italy
[6] INAF-Osservatorio Astronomico di Trieste, Via Tiepolo 11, I-34143, Trieste, Italy
[7] Department of Physics and Astronomy, The Johns Hopkins University, Baltimore MD, USA
[8] NASA Marshall Space Flight Center, Space Science Office, VP62, Huntsville, AL 35812, USA
[9] Harvard-Smithsonian Center for Astrophysics, Cambridge, MA, USA

Abstract. The Wide Field X-Ray Telescope (WFXT) is a medium-class mission designed to be 2-orders-of-magnitude more sensitive than any previous or planned X-ray mission for large area surveys and to match in sensitivity the next generation of wide-area optical, IR and radio surveys. Using an innovative wide-field X-ray optics design, WFXT provides a field of view of 1 square degree (10 times Chandra) with an angular resolution of 5″(Half Energy Width, HEW) nearly constant over the entire field of view, and a large collecting area (up to 1 m^2 at 1 keV, > 10x Chandra) over the 0.1-7 keV band. WFXTs low-Earth orbit also minimizes the particle background. In five years of operation, WFXT will carry out three extragalactic surveys at unprecedented depth and address outstanding questions in astrophysics, cosmology and fundamental physics. In this article, we illustrate the mission concept and the connection between science requirements and mission parameters.

1. Introduction

Exploring the high-redshift Universe, to the epochs of cluster formation all the way back to the primordial populations of galaxies and super massive black holes (SMBHs) requires sensitive, high angular resolution, wide X-ray surveys to complement deep, wide-field surveys in other wavebands. The Wide Field X-Ray Telescope (WFXT) was designed to be 2-orders-of-magnitude more sensitive than any previous or planned X-ray mission for large area surveys and to match in sensitivity the next generation of wide-area optical, IR and radio surveys. In its current concept (Murray et al. 2008) [1], WFXT is a medium-class PI mission with a broad science grasp which will build a unique astrophysical data set, consisting of $\gtrsim 5 \times 10^5$ clusters of galaxies to $z \sim 2$, $> 10^7$ AGN to $z > 6$, and $\sim 10^5$ normal and starburst galaxies at $z \lesssim 1$. These large sam-

[1] http://www.wfxt.eu, http://wfxt.pha.jhu.edu

ples will provide a description of the cosmic evolution of baryons, map the large scale structure of the Universe, constrain and test cosmological models and fundamental physics (such as the nature of Dark Matter, Dark Energy and gravity), determine the black hole accretion history to early epochs and its intimate link with galaxy formation, and provide an unprecedented view of nearby galaxies including our own. The science breadth of WFXT is only outlined below and fully described by the specific contributions in this volume, which span a range of prominent science cases.

The high survey efficiency of WFXT, compared with other past or planned X–ray missions, is obtained by using for the first time a wide-field optical design, first proposed by Burrows, Burg, & Giacconi (1992). By adopting a polynomial shape of the X–ray mirros, WFXT's angular resolution is optimized over the entire 1 deg^2 field of view, as opposed to the classical Wolter-I optics whose angular resolution is optimized mainly on-axis and degrades with the square of the off-axis angle (see Conconi et al. (2010), Elsner et al. (2010) and Pareschi et al. in this volume). The resulting *Grasp*$= A \cdot \Omega_{\rm eff}$ of the survey mission, i.e. the product of the telescope collecting area and the effective field of view (FoV) at the desired angular resolution, is significantly larger when compared to all other past or proposed X-ray missions, making it an unprecedented survey instrument, able to carry out both wide and deep surveys (see Fig.1/*left*). With such an enahanced discovery potential, WFXT will provide optimum samples for both giant ground-based telescopes for more sensitive, but narrow-field space facilities in the optical-IR and X-ray. WFXT, however, is not only a path finder for future missions, its large collecting area allows direct physical characterization of a large fraction of sources (AGN and Clusters) via X-ray spectroscopy with no need of follow-up observations. Synergy with other missions further enhances its scientic potential and breadth. WFXT is conceived for the entire astronomical community. Like the Sloan Digital Sky Survey (SDSS[2]), all WFXT data will become public through a series of annual Data Releases that will constitute a vast scientific legacy for decades.

[2] http://www.sdss.org/

2. Science goals and performance requirements

To define the top level mission requirements, four major science cases were identified and submitted as white papers to the Astro2010 Decadal Survey of the National Academy of Sciences: 1) Physics and Evolution of Cluster of Galaxies (Giacconi et al. 2009, Borgani et al. this volume); 2) Growth and Evolution of Supermassive Black Holes (Murray et al. 2009, Gilli et al. this volume); 3) Cosmology with Galaxy Clusters, (Borgani et al. this volume, Vikhlinin et al. 2009); 4) The very Local Universe (Ptak et al. 2009). Three extragalactic surveys, performed during five years of operation, are required to fully meet the science goals described in these papers: a *WIDE* survey covering most of the extragalactic sky ($\sim 20,000$ deg^2) at $\sim$ 500 times the sensitivity, and twenty times better angular resolution than the ROSAT All Sky Survey; a *MEDIUM* survey mapping $\sim$3000 deg^2 to deep Chandra and XMM sensitivity; and a *DEEP* survey probing $\sim$ 100 deg^2, ($\sim$ 1000 times the area of the Chandra Deep Fields), to the deepest Chandra sensitivity, with typical sampling timescales of days to months. Survey parameters are given in Table 1. Flux limits and areas for the three surveys are shown in Fig.1/left, along with those of existing and planned X-ray surveys.

The capability of an X-ray observatory to carry out a survey, at a given resolution, is given by the product of the *Grasp* defined above and the time available for observation T. WFXT maximizes $A \times \Omega_{\rm eff} \times T$ through its wide-field optics design and a dedicated survey strategy which has an obvious advantage compared to general facilities, such as *Chandra* and *XMM-Newton*, which have devoted $< 10\%$ of their time to surveys. The mirror design is no more complex than a Wolter-I telescope, but yields a resolution of 5–10$''$ over the entire 1 deg^2 field (Pareschi et al., this volume). To demonstrate the advantage of such a mission, Fig. 1/right shows the cumu-

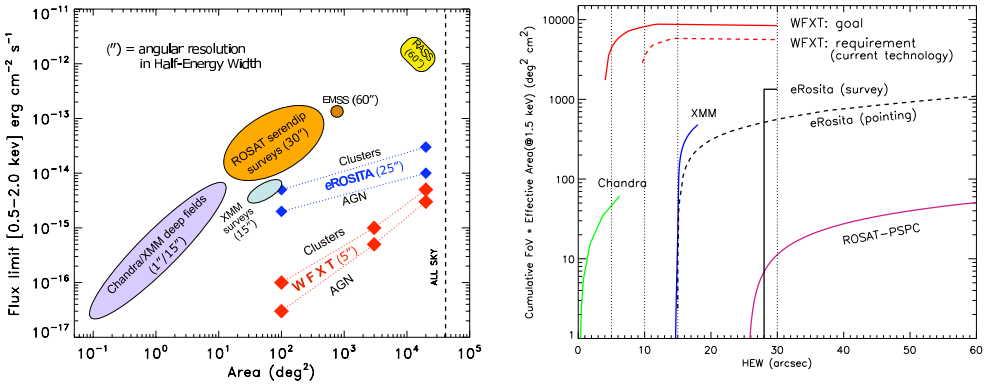

Fig. 1. *Left*: Flux limits and sky coverage for past and planned X-ray surveys. The three WFXT surveys provide an unsurpassed combination of sensitivity and sky area. *Right*: WFXT cumulative Grasp = $\Omega \times$ A, as function of angular resolution (HEW). WFXT's grasp is orders of magnitude greater than any other X-ray mission. Parameters for the planned mission *eROSITA* are taken from Cappelluti et al. in this volume.

Table 1. Description of the WFXT surveys $^{(\star)}$

Quantity	Survey		
	Deep	Medium	Wide
Ω (deg^2)	100	3000	20,000
Exposure	400 ksec	13 ksec	2 ksec
Total Time $^{(\star\star)}$	1.67 yr	1.66 yr	1.67 yr
$S_{\rm min}(0.5-2\,{\rm keV})$ point-like erg s^{-1} cm^{-2} at 5σ $^{(\star\star\star)}$	3×10^{-17} (1×10^{-16})	5×10^{-16} (1×10^{-15})	3×10^{-15} (5×10^{-15})
Total AGN detected	5×10^5	4×10^6	1×10^7
$S_{\rm min}(0.5-2\,{\rm keV})$ extended erg s^{-1} cm^{-2} at 5σ	1×10^{-16} (3×10^{-16})	1×10^{-15} (2×10^{-15})	5×10^{-15} (7×10^{-15})
Total Clusters/Groups	3×10^4	2×10^5	3×10^5

$^{(\star)}$ Values refer to goal performance parameters, those in parenthesis to minimal requirements of A_{eff} = 0.6 m^2, HEW = 10″

$^{(\star\star)}$ Total observing time assumes 76% observing efficiency

$^{(\star\star\star)}$ Flux limits in the hard 2–7 keV band are about 10 times higher

lative field of view as a function of angular resolution for five missions, derived from their half-energy widths at different off-axis angles. Even at 10″ resolution, allowed by the wide-field design with current technology, WFXT can survey a given area to a comparable flux limit in $\sim \frac{1}{100}$ of the time that Chandra requires. For example, the simulation in Fig.3 of a single 13 Ksec observation (a *MEDIUM* survey tile) shows that WFXT would cover 1 deg^2 at the sensitivity obtained by Chandra in a total observation of 1.8 Ms of the COSMOS field (Elvis et al. 2009). The wide-field X-ray optics and mirror construction technology are also key to understand the clear advantage with respect to the upcoming *eROSITA* survey mission (Cappelluti et al., this volume) which provides a significant step forward compared to the ROSAT All-Sky Survey.

The angular resolution is a key parameter for the scientific success of such a mission. A minimum requirement of 10″ for the half-energy width is dictated by the need to improve source sensitivity, to discriminate point from extended emission, to minimize source confusion and to allow an efficient identification of optical counterparts. The latter is an essential process for the work-flow of any science case.

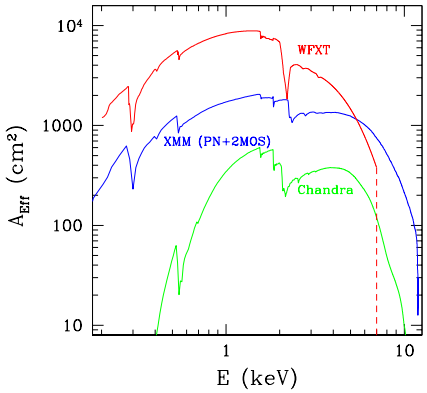

Table 2: WFXT Mission Performance Requirements

Parameter	*Requirement*	*Goal*
Area (1 keV)	$6,000\,cm^2$	$10,000\,cm^2$
Area (4 keV)	$2,000\,cm^2$	$3,000\,cm^2$
Field of View	1^o diameter	1.25^o diameter
Angular Resolution	$< 10''$ HEW	$\leq 5''$ HEW
Energy Band	0.2 - 5 keV	0.1 - 7 keV
Energy Resolution	$\frac{E}{\Delta E} > 10$	$\frac{E}{\Delta E} > 20$
Time Resolution	< 3 seconds	< 1 second
Orbit	550 km cir., $< 6°$ incl.	
Mission Lifetime	5 years	

Fig. 2. WFXT collecting effective area (goal) compared with *Chandra* and *XMM-Newton* .

While a commonly used figure of merit for the discovery potential of a survey mission is the *Grasp*, a more appropriate figure of merit in X-ray surveys for the discovery speed, i.e. the ability to discover and identify sources should scale as $A\Omega T \times \mathrm{HEW}^{-2}$, since the number of possible counterparts scale with the area of the error circle. For deep observations, no longer signal limited, the dependence on the angular resolution will be even faster (up to HEW^{-3} in the background limited regime). Specifically, a $10''$ HEW yields a 1.5–$2''$positional accuracy thus easing the identification of millions of sources, a daunting task with resolutions exceeding $10''$. While $10''$ is feasible with present technology (Pareschi et al. this volume), a goal of HEW $\approx 5''$approximately constant across the FoV has been chosen. This will *i)* further increase the sensitivity for point and extended sources (e.g. groups), *ii)* enable AGN/cluster discernment at any redshift, *iii)* enable confusion-free deep imaging, *iv)* provide *Chandra*-like positional accuracy ($\lesssim 1''$) with a source identification success rate of $>$ 90% (Brusa et al. this volume), *v)* resolve cool cores of $z \gtrsim 1$ clusters (Santos et al. 2010) (essential for cosmological applications, see Borgani et al. this volume), and *vi)* allow the detection of sharp features (shocks, cold fronts, cavities) in the intra-cluster medium (ICM).

The required effective area of the telescope at 1 kev is 0.6 m^2, with a goal of up to 1 m^2, to still fit within the mass budget and costs of a medium class mission with current or forseeen technology. This large collecting area ultimately enables wide surveys at unprecedented depth (Fig.1) within the 5 year life time of the mission, and thus allows very large volumes of the Universe to be explored to large redshifts. In turn, this *i)* allows one to trace the X-ray luminosity function of clusters and AGN (and underlying mass functions of clusters and SMBHs) over a wide range of masses and redshifts, and *ii)* enables physical characterization of large samples of sources via their spectral analysis (see Borgani et al. and Gilli et al. in this volume for predictions of expected number of clusters and AGN and a detailed discussion of related science cases). As shown in Fig.2, it is also important to note that the current (goal) design delivers an effective area as large as the one of *XMM* at 5 keV, this provides a significant benefit when measuring temperatures and redshifts (using the Fe K line) from the spectral fits of clusters as well as the detection of large populations of obscured AGN (see Tozzi et al. in this volume).

The $A\Omega$ and angular resolution combination also translates in very interesting WFXT capabilities in the time domain, enabling short temporal sampling observations and simultaneous monitoring of large sky areas, which will allow one to detect and study variable and transient X-ray populations of galactic and extra-

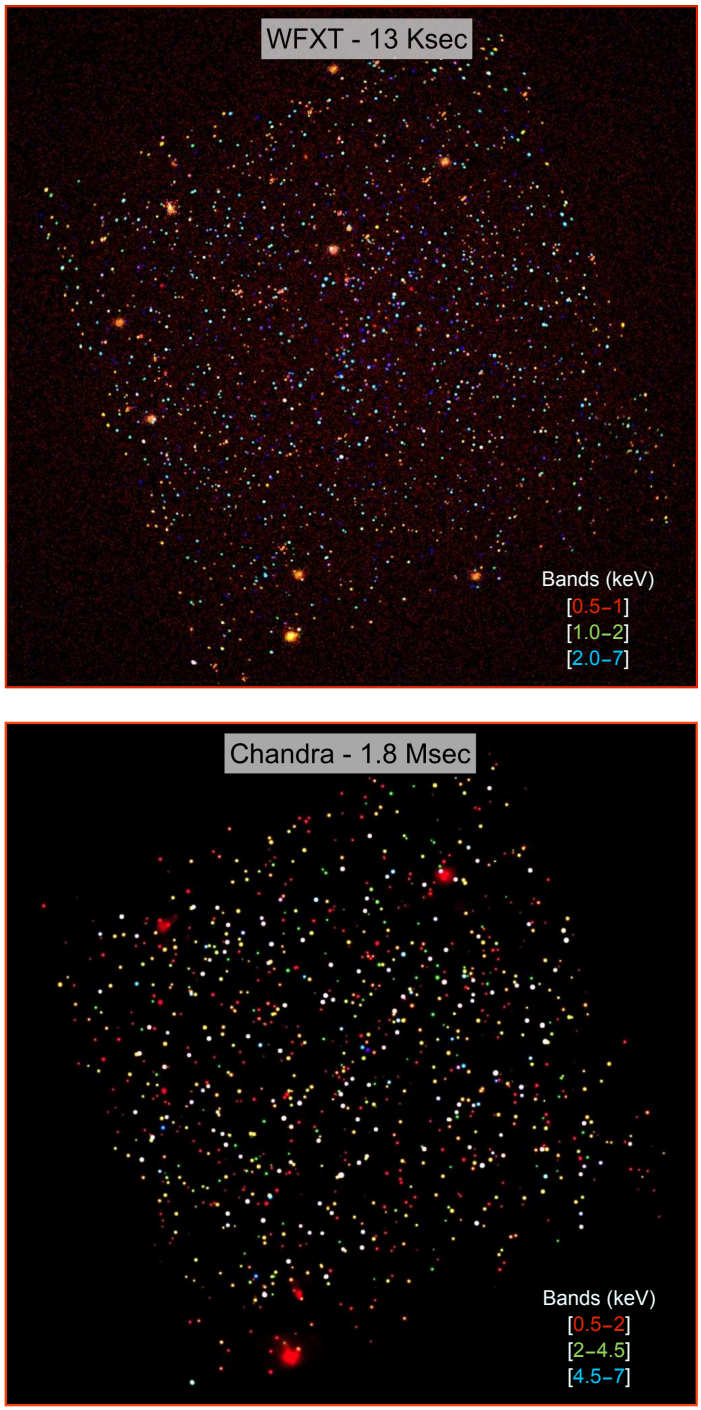

Fig. 3. Simulated WFXT image of the COSMOS field (top) observed with Chandra over 1 deg^2 (bottom) (Elvis et al. 2009). The flux limit of the two images is similar ($\sim 5 \times 10^{-16}$ erg s^{-1}cm^{-2} in 0.5-2 keV). However the WFXT image (1 deg^2) is obtained with a single 13 ksec exposure (as part of the Medium survey), with an angular resolution (5″ HEW) close to Chandra's average ($\sim 3''$). The WFXT simulation was constructed from the Chandra COSMOS catalog Elvis et al. (2009) with methods described in Tozzi et al. (this volume). Bluer sources emit harder X-rays in the 0.5–7 keV band.

Table 3. WFXT Science and Performance Requirements

Performance Requirement	*Observational/Science Requirements*
PSF HEW <10″(goal of 5″) across FoV	*(i)* Sensitivity for point and extended sources *(ii)* Minimize source confusion *(iii)* Discriminate extended sources from AGN at $z > 1$ *(iv)* Resolve cluster cool cores (50–100 kpc) at any redshift (10″ corresponds to 80 kpc at $z = 1$) *(v)* efficient identification of optical counterparts
Large grasp = FoV×A_{Eff} FoV ≥ 1 deg^2 0.6(0.2) < A_{Eff} <1(0.3) m^2 at 1(4) keV	High survey efficiency and vast discovery space: *(a)* to detect large numbers of sources thus measuring luminosity functions over a wide range of masses/luminosities and redshifts; *(b)* to guarantee high S/N spectra for significant subsets thus enabling physical characterization of clusters and AGN, including redshift measurements (with X-ray spectroscopy, without the need of follow-up observations); *(c)* to detect and characterize large number of variable and transient sources (AGN, GRB, SNe etc.)
Low particle background achieved by low Earth orbit	*(i)* Improved limiting flux for point/extended sources; clusters out to large redshifts (proto-clusters at $z \sim 2$); *(ii)* Detect low surface brightness diffuse emission for nearby galaxies and clusters (out to and beyond the virial radius)
Spectral resolution ($10 < E/\Delta E < 20$)	*(i)* Detect the Fe-K emission in clusters and AGN; *(ii)* Spectral characterization of clusters, AGN and galaxies

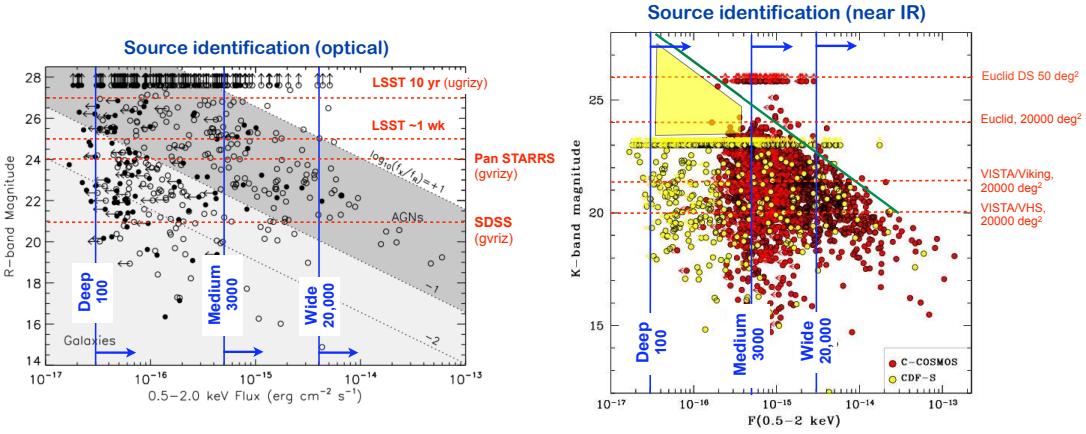

Fig. 4. Source identification strategy for WFXT X-ray sources in the Optical and near-IR based on the distributions of flux ratios from *Chandra* deep surveys in the R-band (Luo et al. 2008) and K_{AB}-band (courtesy of C.Vignali). Current and planned future wide-area surveys are indicated at different magnitude limits.

galactic sources (see Paolillo et al. this volume).

In addition, WFXT's low-Earth orbit reduces the particle background to take full advantage of the instrument sensitivity and high-quality PSF. This is important for the detection and spectral analysis of low-surface brightness features such as distant groups, the most distant clusters and the outskirts of nearby clusters (Ettori& Molendi, this volume).

We summarize in Table 2 the performance requirements and goals of the mission, and in

Table 3 how these parameters are connected to the observational and science requirements.

3. Synergies with other surveys

While we have emphasized how several science objectives can be achieved with the WFXT data only using the X-ray spectral analysis of significant sub-samples of sources with sufficient signal-to-noise, there is no doubt that the synergy of WFXT with the next generation of multi-wavelength deep wide-area surveys will greatly expand the scientific grasp of the mission and will consolidate its vast legacy value for decades.

The multi-wavelength properties of more than 10^7 sources will be available from the combination of current and future wide-area surveys, such as Pan-STARRS[3] and LSST[4] in the optical bands, and in the near-IR surveys (VISTA, WISE, and JDEM/Euclid possibly by the end of the decade), which will allow their identifcation and a measurement of their photometric redshifts. Obtaining deep imaging in the near-IR over the entire extra-galactic sky to identify the most obscured (and most distant) AGN and distant clusters will remain the main challenge, a task which only space-based surveys at $1-2\,\mu m$, such as those proposed for the Euclid[5] or JDEM[6] missions, can perform. We illustrate in Fig.4 the identification strategies of AGN for the three WFXT surveys, based on their optical/nearIR-to-X-ray flux ratios measured in deep *Chandra* surveys. The extension of the multi-wavelength coverage to longer wavelengths, in the submm (CCAT[7]) and radio with SKA[8] (see Padovani, this volume), will complete the information on the spectral energy distribution of different source populations with crucial implications on our understanding of their physics and evolution.

For example, WFXT observations of thousands of clusters will provide redshifts and detailed physical insights, such as temperature and entropy profiles, metallicity of the ICM, mass density profiles of gas and dark matter (DM). By combining this information with optical and near-IR photometry of the cluster galaxies and with future high sensitivity Sunyaev-Zeldovich surveys, one will be able to obtain a comprehensive picture of the evolution of the baryons in their hot and cold phases and how star formation and AGN activity affects the physics of the ICM. By combining these data with lensing studies carried out with ground (e.g. LSST) and space (e.g. Euclid) observations, one will obtain detailed DM mass density profiles on a range of redshifts and masses which can be compared with current structure formation models thus setting strong constraints on the foundations of the ΛCDM paradigm.

The spectroscopic follow-up study of large subsamples of WFXT sources will remain a serious challenge. Dedicated wide-field, high-multiplexing spectrographs on 8m class telescopes currently under study will be suitable for a wide range of science cases. The systematic spectroscopic identification work in large ($\sim 10^4$ deg^2) survey areas can partly be carried out with near-IR slitless surveys, which are part of the Euclid/JDEM mission concepts. A more effective approach to the study of a large variety of sources over a wide redshift range would require wide-area slit-spectroscopy from space, such as the one proposed for the SPACE(Cimatti et al. 2009) mission.

Moreover, in combination with more sensitive, narrow-field observatories, WFXT will be an outstanding source of interesting high redshift clusters and AGN for follow-up studies with JWST (or its successors), ALMA, the next generation of giant (30-40m) ground-based telescopes, and X-ray observatories (i.e., IXO and Gen-X).

4. Conclusions

In this article, we have illustrated the concept of the WFXT mission and how the mission requirements flow from the main science drivers and observational requiremens. We re-

[3] http://pan-starrs.ifa.hawaii.edu/public/home.html
[4] http://www.lsst.org
[5] http://sci.esa.int/euclid
[6] http://jdem.gsfc.nasa.gov/
[7] http://www.submm.org/
[8] http://www.skatelescope.org/

fer the reader to all the contributions in this volume for a detailed discussion of several science cases, which range from the formation and evolution of SMBHs and clusters to stellar populations and compact objects in the Galaxy; from Cosmology to the physics of clusters and AGN, including the study of early-type and star-forming galaxies. This collection of science cases is by no means complete, but can be considered the basis on which the scientific potential of WFXT can be further explored as the technological development continues. It is important to emphasize that the gain margin of WFXT compared to previous or planned X-ray missions in conducting surveys is so large that its scientific impact would remain very strong even if cost or technological challenges will drive a redefinition of its performance parameters. In the suite of requirements under study, as explained above, the angular resolution remains the one parameter on which is very difficult to compromise, as *Chandra* observations have unambigously and definitively taught us.

When examining the range of wide-area high-sensitivity surveys being planned for this decade, in the optical, IR, submm and radio regimes, WFXT stands out as the only one which will be able to match these surveys in coverage, sensitivity and angular resolution at soft X-ray wavelengths. Coordinated surveys from X-ray to radio wavelengths, which have been carried out in small areas of the sky ($\lesssim$ 1 deg^2) over the last decade, have definitively established the crucial value of the multi-wavelength approach in astrophysics which has fueled phenomenal progress in many areas. X-ray observations have been key to such a progress as they have the unique ability to probe phenomena and unveil sources powered by gravity. On the other hand, systematic wide-area surveys have demonstrated that they are able to produce major discoveries and address fundamental questions, as also underscored by their high level of high-impact publications (Madrid & Macchetto 2009). We therefore argue that the lack of a mission like WFXT in the suite of future multi-wavelength wide-area surveys will ultimately limit their scientific potential.

Acknowledgements. We are grateful to Colin Norman and the entire WFXT Team for intense discussions over the years which have led to the current mission concept and development.

References

Burrows, C. J., Burg, R., & Giacconi, R. 1992, ApJ, 392, 760

Cimatti, A., Robberto, M., Baugh, C., et al. 2009, Experimental Astronomy, 23, 39

Conconi, P., Campana, S., Tagliaferri, G., et al. 2010, MNRAS, 405, 877

Elsner, R. F., O'Dell, S. L., Ramsey, B. D., & Weisskopf, M. C. 2010, SPIE conference, Vol. 7732, astro-ph/1006.5065

Elvis, M., Civano, F., Vignali, C., et al. 2009, ApJS, 184, 158

Giacconi, R., Borgani, S., Rosati, P., et al. 2009, in astro-ph/0902.4857, Vol. 2010, astro2010: The Astronomy and Astrophysics Decadal Survey

Luo, B., Bauer, F. E., Brandt, W. N., et al. 2008, ApJS, 179, 19

Madrid, J. P. & Macchetto, D. 2009, astro-ph/0901.4552

Murray, S., Gilli, R., Tozzi, P., et al. 2009, in astro-ph/0903.5272, Vol. 2010, astro2010: The Astronomy and Astrophysics Decadal Survey

Murray, S. S., Norman, C., Ptak, A., et al. 2008, in SPIE Conference, Vol. 7011

Ptak, A., Feigelson, E., Chu, Y., et al. 2009, in astro-ph/0902.4239, Vol. 2010, astro2010: The Astronomy and Astrophysics Decadal Survey

Santos, J. S., Tozzi, P., Rosati, P., & Boehringer, H. 2010, A&A in press, astro-ph/1008.0754

Vikhlinin, A., Murray, S., Gilli, R., et al. 2009, in astro-ph/0903.5320, Vol. 2010, astro2010: The Astronomy and Astrophysics Decadal Survey

Mem. S.A.It. Suppl. Vol. 17, 16

Memorie della
Supplementi

WFXT Technology Overview

G. Pareschi[1] and S. Campana[1]

Istituto Nazionale di Astrofisica – Osservatorio Astronomico di Brera, Via Bianchi 46, Merate (LC), 23807, Italy e-mail: giovanni.pareschi@brera.inaf.it

Abstract. The Wide Field X-ray Telescope (WFXT) is a medium class mission for X–ray surveys of the sky with an unprecedented area and sensitivity. In order to meet the effective area requirement, the design of the optical system is based on very thin mirror shells, with thicknesses in the 1–2 mm range. In order to get the desired angular resolution (10 arcsec requirement, 5 arcsec goal) across the entire 1×1 degree FOV (Field Of View), the design of the optical system is based on nested modified grazing incidence Wolter-I mirrors realized with polynomial profiles, focal plane curvature and plate scale corrections. This design guarantees an increased angular resolution at large off-axis angle with respect to the normally used Wolter I configuration, making WFXT ideal for survey purposes. The WFXT X-ray Telescope Assembly is composed by three identical mirror modules of 78 nested shells each, with diameter up to 1.1 m. The epoxy replication process with SiC shells has already been proved to be a valuable technology to meet the angular resolution requirement of 10 arcsec. To further mature the telescope manufacturing technology and to achieve the goal of 5 arcsec, we are considering different materials for the mirror shells with particular care to quartz glass (fused silica), a well-known material with good thermo-mechanical and polishability characteristics that could meet our goal in terms of mass and stiffness, with significant cost and time saving with respect to SiC. To bring the mirror shells to the needed accuracy a deterministic direct polishing method for the mirror shells is under investigation. A direct polishing method has already been used for past missions (as Einstein, Rosat, Chandra): the technological challenge now is to apply it for almost ten times thinner shells. Our approach is based on two main steps: first quartz glass tubes available on the market are grinded to conical profiles, and second the obtained shells are polished to the required polynomial profiles by Computer Numerical Control (CNC) polishing machine.

Key words. Telescopes — X–rays: general — instrumentation: high angular resolution

1. Introduction

The Wide Field X-ray Telescope (WFXT) is a proposed medium-class mission dedicated to survey the sky in the soft X–ray band (0.2–7 keV) [Murray et al. (2008); Rosati et al. this volume]. In five years of operations, WFXT will carry out three extragalactic surveys, allowing direct physical characterization of a very large amount of sources (in particular AGN and clusters of galaxies) via X–ray spectroscopy with no need of follow-up observations. All the acquired data will constitute a scientific legacy to address key questions about cosmic origins and physics of the cosmos. To those ends, WFXT foresees an X–ray Telescope Assembly whose main requirement

Send offprint requests to: G. Pareschi

Table 1. WFXT Mission Performance Requirements and Goals.

Parameter	WAXS/WFXT* (ASI call, 1998)	Panoram-X+ (ESA call, 2000)	Requirement (Current design)	Goal
Effective Area at 1 keV (cm^2)	310	600	6,000	10,000
Effective Area at 4 keV (cm^2)	80	250	2,000	3,000
Field of View 50% vignetting (deg)	1	1	1	1.25
$< \text{HEW} >_{\text{FOV}}$ at 1 keV (arcsec)	< 15	< 15	< 10	< 5
Energy Band (keV)	0.2–7	0.2–7	0.2–7	0.1–7
Energy Res. ($\Delta E/E$)	> 10	> 10	> 10	> 20
Time Resolution (s)	< 4	< 3	< 3	< 1

* WAXS/WFXT was a mission concept developed in reply to an ASI call for small missions in 1998. It is described in Chincarini et al. (1998).
* Panoram-X was a mission concept developed in reply to an ESA call for Flexi-missions in 2000.

is to be orders of magnitude more effective than previous and planned X–ray missions in carrying out surveys. This is obtained through a telescope design that makes use of polynomial profiles for the mirror shells together with focal plane curvature and plate scale corrections [Burrows et al. (1992); Conconi & Campana (2001); Conconi et al. (2010)]. This design guarantees an increased angular resolution at large off-axis angles with respect to the usually adopted Wolter I configuration; in this way, it is possible to get the desired almost-constant angular resolution on the entire Field of View (FOV). WFXT main scientific requirements and goals are reported in Table 1. In the following we will describe the design of the mirror module for the WFXT and the first tests carried out to reach the mission goals.

2. Mirror design

Focusing telescopes for X–ray astronomy are usually built in the Wolter I configuration, constituted by two mirror segments (the first parabolic and the second hyperbolic) joining at the intersection plane. This design guarantees a perfect image along the telescope optical axis but the image quality rapidly degrades for large off-axis angles. Being WFXT a mission for survey purposes, it is necessary to act on the mirror design in order to increase the off-axis response and optimize the performances over the entire field of view. The present design is based on shells with polynomial profiles [Burrows et al. (1992)]. Polynomial mirror profiles are described usually by forth or third order polynomial and optimization techniques can be implemented to optimize the angular response over a desired field of view [Conconi et al. (2010); Conconi & Campana (2001)]. The first step is to optimize a single mirror shell over a 30 arcmin field of view. This can be done by optimizing a merit function based on the linear combination of HEW and 80% energy encircled fraction in order to have a small spot and not too extended wings in the source Point Spread Function (PSF). This has been done parametrizing the mirror shells (diameter, focal length, etc.) and reducing the optimization to a single parameter. The following step is to optimize a mirror assembly. In this case we have to modify the merit function in order to include also as a weighting factor the effective area (at 1 and 4 keV) and we have to provide a scaling law for the mirror thicknesses and mirror shell lengths. In the best design each nested mirror shell presents a different length dependent on the radius, decreasing from the outermost to the innermost shell in such a way to keep the same curvature of the focal plane. A displacement of few mm between the intersection planes of the mirror shells is introduced to compensate for the different focal plate scale of the shells that causes focusing of X–ray in slightly different positions at any off-axis angle. The proposed design consists of three telescopes with focal length of 5500 mm and diameter ranging from 330 mm for the innermost to 1100 mm for the outermost mirror shell. Shells thickness ranges from 1.2 to 2.2 mm. The total

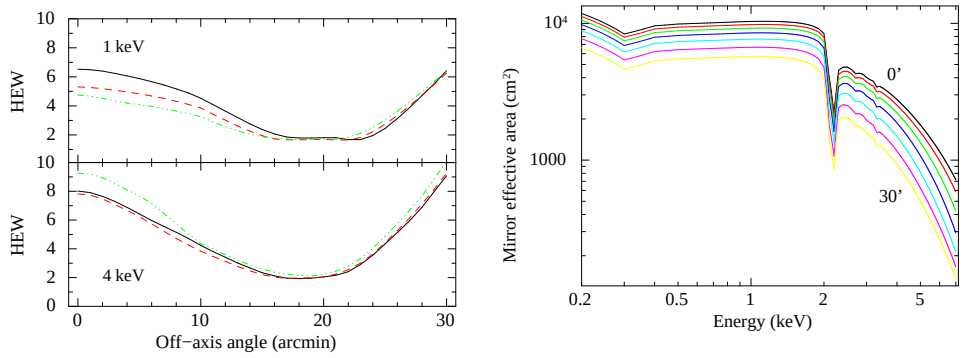

Fig. 1. Left: angular resolution for the WFXT telescope for three slightly different mirror design at 1 keV and 4 keV (the adopted one is marked with a dashed line). Right: Effective area of the three mirror modules (without the inclusion of the detector quantum efficiency and filter transmission).

length of each shell is different because of the butterfly-like adopted design. The main characteristics of the optical module are summarized in Table 2.

Table 2. Characteristics of the proposed WFXT surveying telescope.

Focal Length	5500 mm
Number of Optics Modules	3
Material	Quartz
Numbers of Shells	78
Radius [min max]	165 – 550 mm
Total length [min max]	200 – 440 mm
Thickness [min max]	1.2 – 2.2 mm
On-axis Effective Area* (1 keV)	9,236 cm^2
On-axis Effective Area* (4 keV)	2,565 cm^2
Total Weight (incl. mech. struct.)	930 kg

* this area refers to the total mirror area for the three modules and accounts for a 10% obstruction from the support structure.

3. Manufacturing the mirror shells

3.1. The SiC way

Starting from the late '90 we worked on the building of WFXT mirrors [Citterio et al. (1999); Ghigo et al. (1999)] (see Table 1). We explored different materials with respect to Nickel that were used to build the mirrors for missions such as BeppoSAX or XMM-Newton with the characteristic of being lighter but stiffer. These first attempts concentrated on SiC. The technique used to make a replica with SiC requires first to produce a SiC carrier which is the element that gives the mechanical structure to the mirror shell. The scheme for the manufacture of the SiC carrier is based on the Chemical Vapor Deposition (CVD) process. The SiC carrier is deposited on a mandrel manufactured with a material (for example graphite) capable to survive the high temperature of the process (1300 degrees). After removing the mandrel by burning it in the case of graphite, the carrier is grinded to achieve the precise shape required for the replication process. The carrier is then positioned on the gold coated superpolished mandrel leaving a gap of about 150 micron. The gap is filled with epoxy resin; after the curing of the resin, the mandrel is removed by cooling it. With this technique we were able to obtain a large single mirror shell (60 cm diameter) satisfying the mission requirement, i.e. with an HEW $<$ 10 arcsec over a 60 arcmin diameter FOV (see Fig. 2).

3.2. The glass way

The WFXT design as described above has been further refined. In order to reach the the stringent angular resolution requirement (5 arcsec

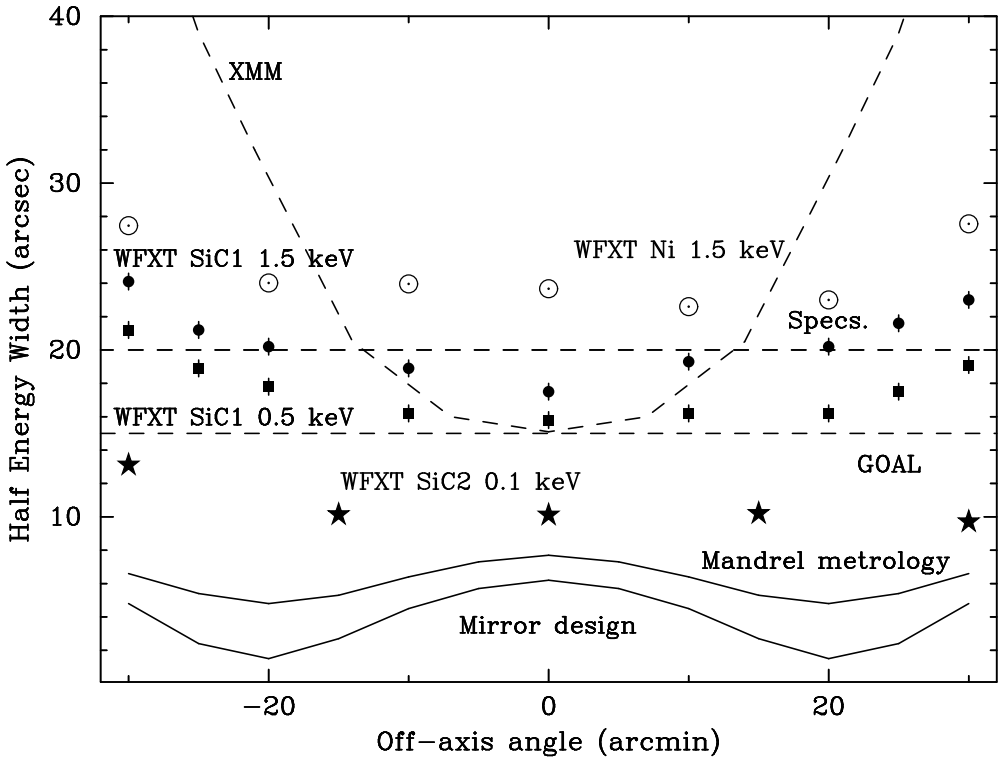

Fig. 2. Off-axis response of a WFXT mirror. Continuous lines indicate an early mirror design and mandrel metrology. Different mirror realizations were obtained with this mandrel either in Nickel (large dots) or in SiC: SiC1 (measured at 0.5 keV, filled squares, and at 1.5 keV, filled circles) and SiC2 (measured at 0.1 keV, filled stars). The SiC2 mirror shells satisfy the mission requirement of an HEW over a 60 arcmin diameter FOV.

HEW over a 60 arcmin diameter FOV) a different technology has to be explored. To meet the effective area and mass requirements, the shells need to be very thin, with wall thickness of few mm or less. SiC and quartz glass are two materials whose thermo-mechanical (T/M) properties (in particular low density and high rigidity) are very attractive and suitable to reach the necessary stiffness of the peculiar WFXT mirror shell configuration. The WFXT mirror shells are not only thin, but characterized by a very small Length-to-Diameter ratio (L/D 3 times smaller than for XMM-Newton mirrors) making more difficult their building. SiC and quartz can be adopted for the production of thin shells both by epoxy replication approach and by direct polishing approach. Quartz is adopted because of costs and production time reasons. Tubes of quartz glass to be used as raw material for shells production are available on the market. Learning from past experiences such as Chandra, and ROSAT, our approach is to follow a deterministic direct polishing method. In the last few years, new machines and polishing techniques have been developed with performances very promising in the perspective of directly optical machining thin mirror shells.

3.3. Thermo-mechanical aspects

The technological challenge is therefore to produce thin and short mirror shells. Several aspects have to be considered, in particular:

- Deformation during the machining and the metrology phase
- Propagation of deformations in thin and short shells
- Resistance to launch conditions

More details can be found in Proserpio et al. (2010).

The WFXT mirror shells are not only thin, but also characterized by a very small Length-to-Diameter ratio making their building more difficult because short mirror shells are more sensitive to perturbing effects related to edge loads since the they have a belt like rather than a tube like behavior. Under the same perturbing edge loads, short mirror shells show degradation 6–16 times larger with respect to long mirror shells and this ratio becomes even bigger in case of perturbing loads producing local deformed shapes. That happens because the angular resolution is strongly affected by the slope errors caused by azimuthal errors, which for a determined Out-Of-Roundness (OOR) error is inversely proportional to the mirror shell length. It is worth noting that the consideration of concentrated loads at the free edges of the shells is representative of the real conditions since normally the mirror shells are fixed to the mirror module structure by spot connections at the one or both end sections and, during metrology and integration, they rest on concentrated astatic supports at one-end section. Two astatic supports are available at INAF-OAB, one with 12 and the other with 16 sustaining points. It was verified by Finite Element Method (FEM) and ray-tracing analyses that with the available astatic supports, the deformations introduced on the shells are negligible, in the order of 0.5 arcsec HEW.

Preliminary FEM analyses have also been carried out in order to estimate a value for stress peaks in the quartz glass mirrors during launch, even if at this stage of the project, exact load levels, and operative and survival temperatures are not yet available and need to be evaluated in near future. A complete check of quartz components will require some more information, relevant to the characterization of the specific material, which are not known at the moment. Nevertheless, simple preliminary consideration can be performed based on engineering evaluations and past experiences. Considering a traditional X–ray telescope, the single mirror shells are connected to the telescope structure just at the end sections (one or both) through spokes wheel elements. Point connections between each mirror shell and the spokes wheel are realized by adhesive contacts. If such a configuration is adopted during FEM analyses, the maximum stresses in the glass might exceed the tensile stress limit in points of stress concentration. Local refinement of the analyses and the design are needed considering the use of a brittle material like quartz. Revised design criteria with respect to the traditional approach will allow obtaining surviving loads conditions. In addition to that, the use of chemical etching treatment of the shell surfaces in order to reduce the micro-cracks cause by the grinding is under investigation to improve the intrinsic stiffness of the quartz.

4. Building the first mirror shells

To fulfill the WFXT requirements a direct polishing approach on the thin mirror shells is under study. The proposed method foresees the direct figuring and polishing of mirror shells after grinding. The monolithic mirrors are made of materials with good mechanical properties (but easy to polish) like quartz. Quartz is indeed a well known material and its thermo-mechanical and polishability properties make it ideal for the realization of high precision optics, also for space application. It offers a number of advantages such as low density (2.203 g/cm^3), low thermal expansion coefficient (0.5×10^{-6} /K), high modulus of elasticity (70 GPa). The main drawback related to quartz is that the material is quite brittle. However, this does not represent an unsolvable problem since it can be overcome with suitable surface treatments (as chemical etching) in order to eliminate, or at least reduce, the surface damages coming from the machining

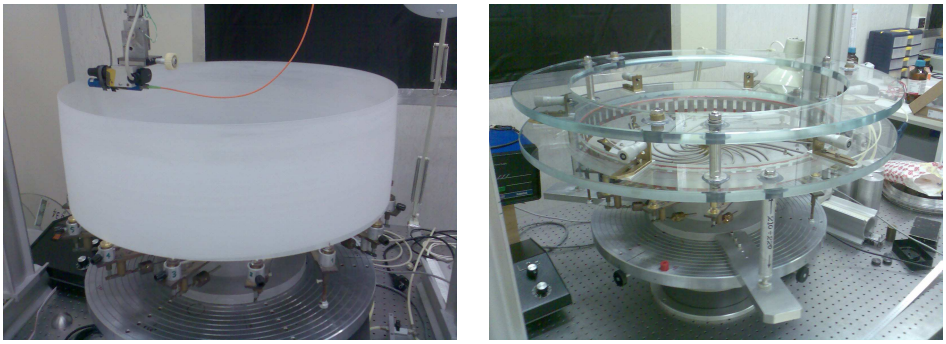

Fig. 3. Left: Raw quartz glass tube. Right: First shell integrated in its support structure.

steps, that tend to originate the cracks. On the other hand the direct polishing of X–ray telescope mirror shells made by quartz or glass material is a technology that has been proved since many years for the manufacturing of very high angular resolution X–ray telescopes (like Einstein, with 4 arcsec HEW, ROSAT, with 3 arcsec HEW, or Chandra with 0.5 arcsec HEW). The challenge now is to obtain a good angular resolution on the entire FOV but for considerably thinner (a factor 5–10 less) mirror shells.

In the last years, computer numerical control (CNC) polishing machines, able to perform a precise figuring also on thin substrates have been developed. The production flow here envisaged foresees to start from a quartz glass tube already available on the market. The tube is firstly ground with a double cone profile at the required thickness of a few millimeters. Then, it is figured and polished to the final polynomial profile making use of a "deterministic" figuring method and then superpolished. This implies that after the measurements of the actual profile of the mirror shell to be polished, a corrective matrix is determined and supplied to a CNC polishing machine which provides the corrective action according to the given error matrix. In a few iterations it is possible to reach the required specifications once we start from an acceptable profile after grinding with P-V roundness errors of a few tens of microns. Between the grinding and the polishing step it is necessary to integrate the shell in a suitable jig structure able to allow the metrology, machining and all the necessary steps before the assembling of the shell into the final structure (i.e. reflective coating deposition and X–ray characterization at an X–ray facility, at least until the telescope structure with spiders is not developed). This jig structure is also necessary for handling and will be used for the shell integration into the final mirror module structure. After that, it can be removed and used for another shell.

For the purpose of this study, 8 quartz glass shells have been realized to set the best parameters of the grinding phase and get useful hint on surface treatment to reduce surface imperfections that degrade the mechanical characteristics of the material. Two of these shells have been integrated in the suitable structure appositely designed to allow polishing, metrology, and all the necessary steps before the integration in the final structure. One of the integrated shells has been used for polishing tests. More details on the production of these demonstrative parts are presented in the following paragraphs, together with the present obtained results.

The polishing process is performed by the Zeeko firm by means of a IRP600 machine. The Zeeko Company not only makes use of an innovative figuring and polishing approach, but also it developed the capability of machining shells with diameter up to 1100 m and height up to 440 mm. The equipments of the Zeeko IRP-Series are CNC polishing systems, controlled on 7-axis, that use a patented tool to provide a distributed pressure and variable area

head for the polishing of aspheric and complex forms. By acting on the process parameters, such as tool pressure, precession angle, compression offset and head speed, it is possible to select the desired influence function, i.e. the 3D depression left by the spinning precessing tool as it is pressed onto a piece of the material to be polished. The influence function is generated to determine the best volumetric removal rate in dependence of the specific materials and requirements.

A number of tests have been performed during the study, in order to evaluate the applicability of this process for the manufacturing of the WFXT quartz glass shell. The effort was in particular focused on the problems caused by the deformations of the thin walls by effect of the tool pressure. The shell used for these preliminary tests was the first ground dummy shell used to test integration into Shell Supporting Structure that presents high out of roundness values (800 micron). The possibility of performing an intermediate coarser step "grolishing") before the polishing was investigated. Grolishing is needed to correct possible residual errors coming from the grinding step and to remove the external layer of surface damaged at a microscopic level. Different process parameters were investigated in order to define the best influence (or removal) function. Faster influence functions are used for bulk material removal. While slow removal functions provide better results in manipulating smaller scale errors. Those tests will be important to evaluate the possibility of obtain a proper polynomial profiles starting from the double-cone shape. More details can be found in Proserpio et al. (2010).

5. Conclusions

The ability of X–ray images to peer deep into the early Universe is a key in providing a way to study the evolution o f classes of objects over cosmological time-scales. For a broad perspective see the WFXT white papers submitted to the 2010 Decadal Survey [Murray et al. (2009); Giacconi et al. (2009); Vikhlinin et al. (2009); Ptak et al. (2009)]. In a large survey, these issues can all be addressed in a statistically significant way, in order to precisely constrain theories. At the same time, extremely powerful and rare phenomena within our own Galaxy, become evident only when large volumes are explored in the high-energy domain of X–rays. A deep (nearly) all-sky X–ray survey with high spatial resolution is therefore a natural, necessary step to complement and significantly extend the optical sky surveys as the classic Palomar or SDSS sky atlas as well as radio and near-infrared already available or available in the next decade.

Here we described the optimization of the optical design in relation to the scientific drivers of the WFXT mission. In particular, we describe step by step the design of a wide field X–ray telescope tailored for surveying the X–ray sky. A general indication of the manufacturing process of the mirrors have been presented. We presented the first results of the tests performed to evaluate the deterministic direct polishing technique for the realization of thin quartz glass mirror shells, to be implemented aboard the WFXT mission. The development aims at achieving the angular resolution goal level of the mission of 5 arcsec HEW across the FOV of 1 deg in diameter. Several quartz glass shells with double cone shape and diameters of 490 and 620 mm, lengths of 200 mm and thicknesses of 1.5–2 mm have been produced for the scope. Three grinding runs have been performed to improve the process and, at the end, the tolerances expected after grinding (OOR error $<$ 10 micron Peak-Valley) have been achieved. Two of the produced carriers have been integrated in a suitable jig, specifically designed for all the steps in the shell manufacturing up to the integration in the final telescope structure. It has been verified that the integration process in the jig is able to maintain or improve the original shape. One of the integrated shells has been used for the preliminary polishing tests performed by Zeeko using an innovative optical machining based on the Bonnet tool. Preliminary "grolishing" results suggest that the process can meet the angular resolution requirements if the mirror shells after grinding is characterized by an OOR error $<$ 60 micron. The evaluation of chemical etching to remove the sub-surface

damages on the surface of ground shells has started and analyses are in progress. Upcoming activities include polishing tests to evaluate the feasibility of obtaining mirror shells with a correct polynomial profiles. The mirror prototypes realized in this way will be X–ray tested in full illumination mode.

Acknowledgements. We are very grateful to the WFXT group at the Brera Observatory: S. Basso, R. Canestrari, O. Citterio, M. Civitani, P. Conconi, V. Cotroneo, M. Ghigo, E. Mattaini, G. Parodi L. Proserpio, D. Spiga and G. Tagliaferri. We are also indebted to the international WFXT collaboration and, in particular, to R. Giacconi, S. Murray and M. Weisskopf for supporting this work and for many useful discussions. This activity is funded by the Italian Space Agency (ASI) and by INAF.

References

Burrows, C. J., Burg, R., Giacconi, R. 1992, ApJ, 392, 760
Chincarini, G., et al. 1998, AN, 319, 125
Citterio, O., et al. 1999, Proc. SPIE, 3766, 198
Conconi, P., Campana, S. 2001, A&A, 372, 1088
Conconi, P., et al. 2010, MNRAS, 405, 877
Ghigo, M., et al. 1999, Proc. SPIE, 3766, 207
Giacconi, R., et al. 2009, arXiv:0902.4857
Murray, S., et al. 2008, Proc. of SPIE 7011
Murray, S., et al. 2009, arXiv:0903.5272
Proserpio, L., et al. 2010, Proc. SPIE, 7732, 77320D
Ptak, A., et al. 2009, arXiv:0902.4239
Vikhlinin, A., et al. 2009, arXiv:0903.5320

Mem. S.A.It. Suppl. Vol. 17, 24

Memorie della
Supplementi

Simulating the WFXT sky

P. Tozzi[1,2], J. Santos[1], H. Yu[1], A. Bignamini[3], P. Rosati[4], S. Borgani[2,3], S. Campana[5], P. Conconi[5], R. Gilli[6], M. Paolillo[7], A. Ptak[8], and the WFXT Team

[1] INAF – OATs, Via Tiepolo 11, I-34131 Trieste, Italy e-mail: tozzi@oats.inaf.it
[2] INFN Trieste, via Valerio 2, I-34127 Trieste, Italy
[3] Dipartimento di Fisica, Università di Trieste, via Tiepolo 11, I-34143 Trieste, Italy
[4] ESO - European Southern Observatory, D-85748 Garching bei Munchen, Germany
[5] INAF - OABrera, via Brera 28, 20121 Milano, Italy
[6] INAF - OABo, via Ranzani 1, I-40127 Bologna, Italy
[7] Università Federico II, Dip. di Scienze Fisiche, via Cintia, I-80126, Napoli
[8] NASA Goddard Space Flight Center, Maryland, USA

Abstract. We investigate the scientific impact of the Wide Field X-ray Telescope mission. We present simulated images and spectra of X–ray sources as observed from the three surveys planned for the nominal 5-year WFXT lifetime. The goal of these simulations is to provide WFXT images of the extragalactic sky in different energy bands based on accurate description of AGN populations, normal and star forming galaxies, groups and clusters of galaxies. The images are realized using a detailed PSF model, instrumental and physical backgrounds/foregrounds, accurate model of the effective area and the related vignetting effect. The simulated images can be used to evaluate the flux limits for detection of point and extended sources, the effect of source confusion at very faint fluxes, and in general the efficiency of detection algorithms. We also simulate the spectra of the detected sources, in order to address specific science topics which are unique to WFXT. Among them, we focus on the characterization of the Intra Cluster Medium (ICM) of high-z clusters, and in particular on the measurement of the redshift from the ICM spectrum in order to build a cosmological sample of galaxy clusters. The end-to-end simulation procedure presented here, is a valuable tool in optimizing the mission design, characterizing the WFXT discovery space and verifying the connection between mission requirements and scientific goals. Thanks to this effort, we can conclude on firm basis that an X-ray mission optimized for surveys like WFXT is necessary to bring X-ray astronomy at the level of the optical, IR, submm and radio wavebands as foreseen in the coming decade.

Key words. Cosmology: galaxy clusters; AGN: observations - X-rays: surveys

1. Introduction

The strong interest behind the Wide Field X–ray Telescope (WFXT) stems from the fact that no planned or foreseen X-ray mission is optimally designed for surveys. The tremendous scientific impact that we experienced in the last ten years thanks to the Chandra and XMM-Newton X-ray telescopes, largely relies on the previous all–sky surveys performed by satel-

Send offprint requests to: P. Tozzi

lites like Einstein or ROSAT, which were able to provide a large number of potentially interesting X-ray targets. A new, deeper, wide-angle X-ray survey is needed in order to perform a significant step forward in the field of X-ray astronomy. In addition, the innovative concept of WFXT (Murray et al. 2008)[1] will allow one not only to deliver catalogs of X-ray sources, but also to characterize most of them, and achieve several scientific goals well in advance of a multiwavelength follow-up. Eventually, the synergies with future surveys in other wavebands will greatly enhance its scientific impact (see Rosati et al. this volume). In our view, the WFXT mission will provide an immense legacy value for Galactic and extragalactic astronomy.

Simulations of data products from the planned WFXT surveys are crucial in order to quantify the scientific impact of the mission. In order to achieve this goal, we set up a procedure to build images of extragalactic fields and spectra of the sources according to the instrument design of WFXT. We put a strong effort in the modelization of the X-ray source populations, in order to investigate in detail several science cases which are unique to WFXT. Among these scientific cases we discuss the study of the ICM in groups and clusters of galaxies, the building of a cosmological sample of clusters whose redshift is obtained directly by the X-ray spectral analysis, and the characterization of the different classes of AGN up to redshift $z \sim 6$ (Giacconi et al. 2009; Murray et al. 2009; Vikhlinin et al. 2009). Many other science cases can be addressed with these simulations, including cases relevant for Galactic astronomy and the local Universe (Ptak et al. 2009), but are not discussed here.

This paper is organized as follows. In §2 we derive the main quantities which are relevant to the simulations like the background and foreground components and the typical conversion factors, and show how we build a mock WFXT image. In §3 we describe the modelization of the extragalactic source populations adopted in our simulations. In §4 we describe the results of a preliminary analysis using a simple detection algorithm to provide a conservative estimate of the capability of WFXT of detecting X-ray sources. In §5 we describe the spectral simulations and focus on the capability of measuring the redshift for a large sample of groups and clusters of galaxies. Finally our conclusions are summarized in §6.

[1] http://www.wfxt.eu; http://wfxt.pha.jhu.edu

2. Building WFXT simulated images

The details of the WFXT design are presented in the contribution by Pareschi & Campana in this volume. Here we recall the most relevant properties which affect our simulations. First we consider the sensitivity of the X-ray telescope. The total effective area of the three modules of the WFXT at the aimpoint is shown in Figure 1. In the soft band, the effective area of WFXT is about one order of magnitude larger than the total effective area of XMM (the sum of the PN and the two MOS), and about two orders of magnitudes larger than the Chandra one. The effective area in the hard band is comparable to the total value of XMM at 5 keV. Achieving a large effective area in the soft band while still keeping a significant area in the hard band (2-7 keV) is key to characterize the detected sources.

With its very large field of view (1 square degree), WFXT images suffer an important vignetting effect, which consists in a decrease of the effective area with the off–axis angle with respect to the aimpoint (assumed to be in the center of the image). This is an important aspect to be included in the simulations, since it allows us to compute correctly the number of detected photons for the sources randomly distributed in the field. The vignetting in both bands for a single pointing is shown in Figure 2.

The spectral resolution, defined as $E/\Delta E$, where ΔE is the Half Energy Width (HEW) of an emission line with zero intrinsic width, is shown in Figure 3. Spectral resolution is about a factor of 3 better than the Chandra (ACIS-I) resolution over the whole energy band, while it is comparable to the XMM resolution (PN) above 1 keV. Spectral resolution is crucial to perform line diagnostic. As we will see, the

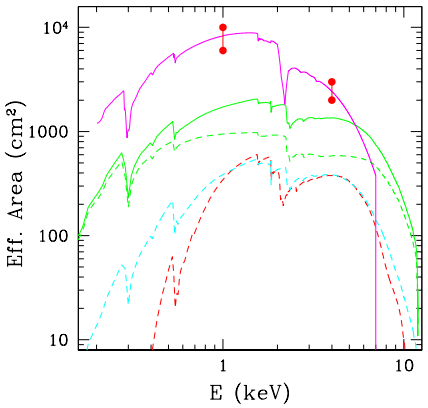

Fig. 1. Effective area for WFXT design (magenta) at the aimpoint for the sum of the three modules. Red dots show the requirement and the goal at 1 and 4 keV. The Chandra effective area is shown as a red dashed line, while the total XMM-Newton response is shown as a solid green line (green dashed for PN and cyan dashed for MOS).

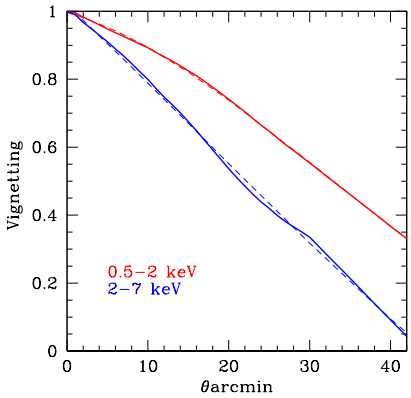

Fig. 2. Vignetting with respect to the aimpoint as a function of the off-axis angle at 1 keV (red solid line) and 4 keV (blue solid line). Dashed lines show the analytical fits used in the simulations.

Source	0.5 – 2 keV	2 – 7 keV
XRB, $\Gamma = 1.4$	2.25×10^{-13}	2.35×10^{-12}
AGN z=1, $N_H = 10^{21}$	2.19×10^{-13}	2.06×10^{-12}
AGN z=1, $N_H = 10^{23}$	3.45×10^{-13}	2.40×10^{-12}
SF Gal $\Gamma = 1.9$	2.16×10^{-13}	2.05×10^{-12}
ICM $z = 0.5, kT = 5$	2.22×10^{-13}	1.85×10^{-12}

Table 1. Typical Energy Conversion Factors (ECF) at the aimpoint. The units are erg s^{-1} cm^{-2}/(cts s^{-1}). We assume a typical Galactic absorption of $N_H = 3 \times 10^{20}$ cm^{-2}.

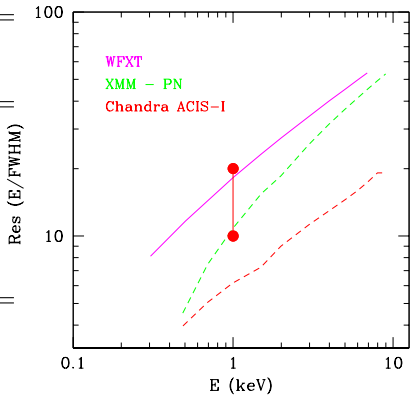

Fig. 3. Spectral resolution $E/\Delta E$ for WFXT (magenta solid line). Goal and requirement are shown as red dots. Spectral resolution for the XMM PN detector is shown in green, while the Chandra ACIS-I in red.

ability to measure the ubiquitous Fe K_α line in the ICM spectra is one of the key requirements in order to build a cosmological sample of groups and clusters of galaxies without recurring to time–expensive optical follow-up (see §5).

An important figure which is obtained directly from the WFXT spectral response, is the Energy Conversion Factor (ECF) appropriate to a given spectral shape (i.e., a given source class). The ECFs are defined as the ratio of the observed energy flux in a given band and the

observed photon rate in the same band, and are computed always at the aimpoint (so they must be weighted by the vignetting whenever the observed source is not at the aimpoint). In Table 2 we show the conversion factors for some typical extragalactic source in the soft and hard bands. These values are posted here as a reference: in the simulations the net photon rate of each source is computed exactly according to its spectral shape.

The next aspect we consider is the noise, which is due to the sum of several components. One is the particle (or instrumental) background, while the other contributions are from astrophysical sources. The galactic foreground is truly diffuse, with fluctuations of the order of a few percent. The extragalactic unresolved background is given by undetected point sources and it depends on the flux limit at which the extragalactic sources can be resolved, and therefore it is also a function of the exposure time. In our simulator we include the unresolved AGN contribution and the unresolved ICM contribution as a uniform distribution spread across the FOV. As a useful reference we show the expected average values in Table 2 in photons per second per field of view (one square degree). The particle background is very low thanks to the low Earth orbit proposed for WFXT. The Galactic background is by far the dominant component in the soft band (actually below 1 keV), while the extragalactic background, due to point sources (mostly AGN) and groups and clusters, strongly depends on the different exposure of the Wide, Medium and Deep surveys, given the different minimum flux at which it is possible to detect single sources.

The information given so far can be used to estimate the collected photons from several extragalactic sources in each of the three WFXT planned surveys. However, a proper estimate of the detectability, or the signal-to-noise ratio, of each source, depends also on the PSF. Thanks to the polynomial X-ray mirrors (Burrows et al. 1992) the PSF has an HEW of 5 arcsec almost constant across the entire field of view. This is the key property which makes WFXT the ultimate X-ray survey mission, since it allows one to detect and characterize pointlike and extended sources without hitting source–confusion down to very low fluxes. Together with the hard band sensitivity, the spatial resolution constitute the main difference of WFXT with respect to other planned X-ray missions like eRosita (Predehl et al. 2010).

Source	0.5 – 2 keV	2 – 7 keV
Particles	0.188	0.397
Galactic	21.4	0.0
AGN wide	9.5	3.13
AGN medium	3.9	1.65
AGN deep	0.8	0.17
Cluster wide	1.46	0.3
Cluster medium	0.79	0.14
Cluster deep	0.2	0.03

Table 2. Total background photon rates (cts/s) in the soft and hard bands for one FOV (1 deg^2)

A realistic image simulator needs a detailed modelling of the PSF. The HEW of the PSF is shown in Figure 4, at two different energies, 1 and 4 keV, representative of the soft and hard bands. Note that the images are realized taking into account all the features of the PSF, including its asymmetric shape (Conconi et al. 2010).

This short review of the WFXT instrumental properties is sufficient to comprehend the main ingredients of the WFXT mock images we realized. In order to achieve a realistic rendition of the X-ray sky, we now exploit what we have learned from deep X-ray extragalactic surveys to date on different source populations.

3. Source populations in extragalactic fields

In this work, we present only single–pointing images of extragalactic fields. The point source populations include four families of Active Galactic Nuclei (Unabsorbed, Compton–Thin, Mildly Compton–Thick and Heavily Compton–Thick), and normal and star forming galaxies, consistently with the observed luminosity function and extrapolated to high redshifts according to the Gilli et al.

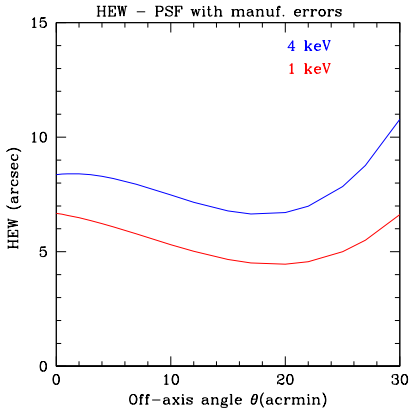

Fig. 4. Half Energy Width of the PSF (including estimated manufacturing errors) in the soft (1 keV, red line) and hard band (4 keV, blue line) as a function of the off–axis angle θ.

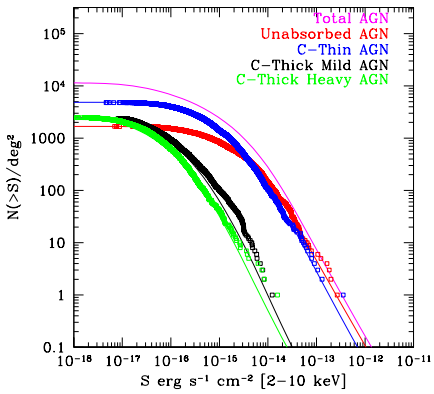

Fig. 5. The hard-band logNlogS from the mock input catalog of extragalactic point sources (empty squares) compared with the input model by Gilli et al. (2007) (solid lines). The contributions of unabsorbed, Compton-Thin and Compton-Thick AGN are plotted separately.

(2007) XRB synthesis model. The input logN-logS are shown in Figure 5. Two spectra of a Compton Thin and a Compton Thick AGN, as observed by WFXT, are shown in Figure 6. Each AGN type is simulated with a neutral Iron K_α line at 6.4 keV rest-frame with a typical equivalent width as commonly observed in each source class, as shown in Figure 7. The presence of the Iron line allows one to measure the redshift for a significant number of AGN, even though its equivalent width is expected to vary significantly from source to source. The feature at 2 keV in the spectra is due to a dip in the effective area (compare with Figure 1).

In addition to AGN, another important class of point sources is constituted by the star-forming galaxies. As we learned from the Chandra Deep Fields (Norman et al. 2004; Lehmer et al. 2008), star forming galaxies are expected to dominate the number counts below fluxes $\sim 10^{-17}$ cgs. WFXT will not reach fluxes lower than the limits achieved in the Chandra Deep Fields, however it will be able to detect thousands of star forming galaxies up to reshift one, providing an unbiased view of the cosmic star formation history with an unprecedented statistics (see contribution by P. Ranalli in this volume). We extract the galaxy catalog from the soft logN-logS relations (Ranalli et al. 2005). For all the galaxies we assumed an intrinsically unabsorbed power law spectrum with photon index $\Gamma = 2$.

Another important class of extragalactic sources are groups and clusters of galaxies. These sources are intrinsically extended since the X-ray emission is due to the thermal bremsstrahlung in the hot ICM. We extracted a population of groups and clusters from the Press & Schechter (1974) mass function, tuning the cosmological parameters in a ΛCDM universe in order to reproduce with reasonable accuracy the existing constraints on the observed number counts (see Figure 8) and the observed luminosity (Rosati et al. 1998) and temperature functions (Henry et al. 2009). Given their nature, X-ray extended sources have a variety of different morphologies and concentrations, which will be resolved in most cases thanks to the WFXT angular resolution. In order to render this aspect in our simulations, we used real Chandra images (i.e., at very high resolution) from a representative lo-

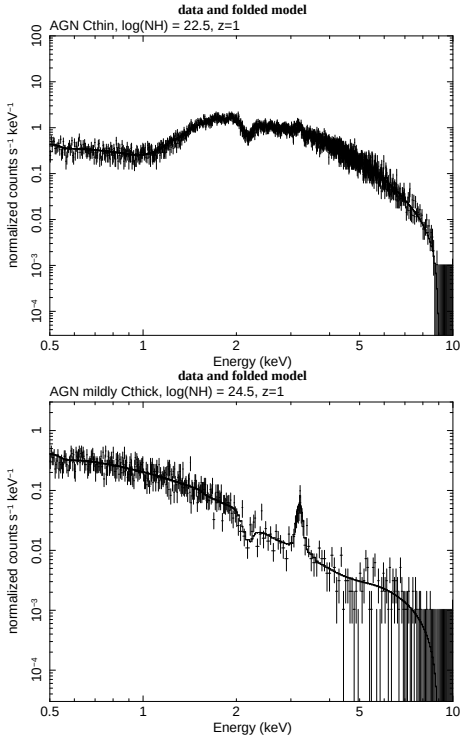

Fig. 6. Top panel: the spectrum of a typical compton-Thin AGN at z=1 with intrinsic absorption $log(N_H) \sim 22.5$ cm^{-2} and flux $F_S \sim 5 \times 10^{-14}$ erg s^{-1} cm^{-2} observed for 13.2 ks with WFXT. Bottom panel: the spectrum of a mildly Compton Thick AGN at z=1 with nominal intrinsic absorption $log(N_H) \sim 24.5$ cm^{-2}, soft flux $\sim 5.4 \times 10^{-14}$ erg s^{-1} cm^{-2}, observed for 13.2 ks with WFXT. In both cases a soft scattered component in addition to the primary absorbed one has been considered.

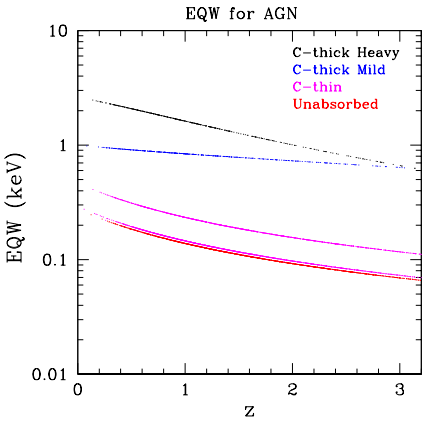

Fig. 7. Observed-frame equivalent width of the 6.4 keV neutral Fe K_α line adopted in our AGN population for different AGN types, as a function of redshift.

cal sample of groups and clusters in order to mimic the observed mix of flat and strongly peaked surface brightness profiles (see Figure 9). This procedure has been adapted from the cloning technique described in Santos et al. (2008). The presence of a cool–core may affect the detectability of the cluster emission particularly at high redshift, and therefore it will be an important aspect when quantifying the completeness of deep cluster samples. Clearly, some uncertainty is due to the evolution of cool-cores, which is currently measured to be mild (Santos et al. 2010). At present, we simply assume a fair mix of cool-core and non cool-core clusters as observed locally.

The WFXT images are created in three bands (0.5-1 keV, 1-2 keV, and 2-7 keV) and combined to produce color images (see Figure 10). We also produce the soft image (0.5-2 keV band) which will be used for source detection, together with the 2-7 keV hard band image. Each image is given by the sum of the three modules. The original pixel size is assumed to be 0.88 arcsec, while the final images are resized by a factor of three (corresponding to a pixel of 2.64 arcsec) thus adequately sampling the PSF across the FOV.

We showed the efficiency of WFXT by comparing one tile of the medium survey (corresponding to a single pointing of WFXT with a 13.2 ks exposure) with the Chandra image of the COSMOS field (Cappelluti et al. 2009) in the contribution by Rosati et al., this volume. The striking result is that WFXT is $\sim$ 150 times faster in obtaining an image of the same solid angle and same depth of Chandra COSMOS, and with a resolution only a factor of two below that of the Chandra mosaic. This direct comparison shows the tremendous survey efficiency of WFXT.

Fig. 10. A simulated WFXT extragalactic field with an exposure of 13.2 ks (corresponding to one tile of the Medium survey).

4. Source detection with WFXT

In principle, the large size of the WFXT images and the large number of sources which will be detected would require dedicated software. Indeed, we are planning to develope specific source detection algorithms and source extraction procedures in the next future. For the purpose of this Paper, we use the algorithm wavdetect which has been developed for Chandra and it is part of the `ciao` software. This procedure, despite not optimized for WFXT data, allows us to perform a rapid test on the quality of our simulated images.

We run `wavdetect` on the soft (0.5-2 keV) and hard (2-7 keV) images of a tile of the Medium survey (corresponding to an exposure time of 13.2 ks) with a standard set of parameters. The catalog of the detected sources is then matched with the input sources. In this way we have a catalog of the matched sources, a list of spurious and a list of undetected sources.

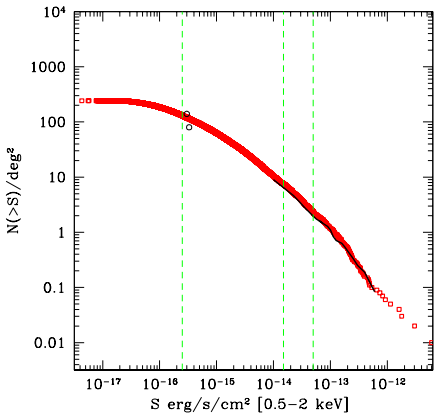

Fig. 8. Soft band logN-logS for groups and clusters of galaxies from the input catalog of 100 square degrees (corresponding to 100 WFXT fields), extracted from the PS-like mass function model (red squares). The black line refers to the ROSAT Deep Cluster Survey (RDCS) by Rosati et al. (1998). The two circles at low fluxes refer to the Chandra Deep Fields (Rosati et al. 2002). Vertical dashed lines show the approximate flux limits for detection corresponding to the three WFXT surveys.

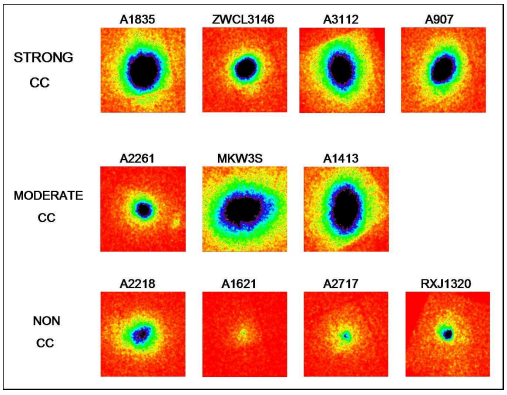

Fig. 9. Cluster templates (original Chandra images) used in the simulations, representing three classes with different cool-core strength (Santos et al. 2008).

Point sources are recovered with a position accuracy typically below 2 arcsec (see Figure 11). Note that part of this error is due to the asymmetry of the PSF, which is not corrected here, but it can be accounted for when the PSF model will be included in the detection algorithm. The number of detected photons for each source is in very good agreement with the input value within the poissonian error (see Figure 12). The sources are recovered efficiently down to 20 net photons, a value below which the number of undetected sources grows rapidly (see Figure 13). This value provide a very conservative estimate of the flux limit in WFXT images, and it can be considered constant with respect to the exposure time, since point sources are very mildly affected by the diffuse background. For an image of the Medium survey, 20 net photons correspond to a flux of 3.3×10^{-16} erg s^{-1} cm^{-2} in the soft band. At the same time, thanks to the low background, the number of spurious sources is negligible above 20 counts. We conclude that the constant PSF of WFXT allows one to detect sources with an almost flat sky coverage and negligible contamination down to very low flux levels. Eventually, it will be possible to decrease the detection limit by a factor of two with a more sophisticated detection algorithm.

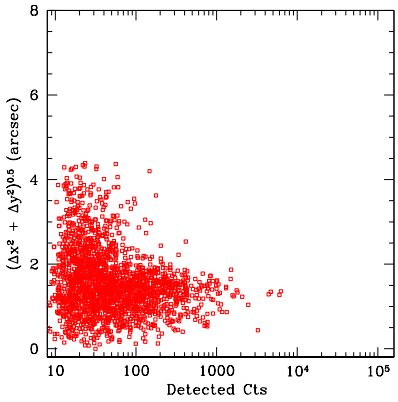

Fig. 11. Position error in arcsec as a function of the net detected counts for point sources, from a simulated soft band image of the Medium survey (13.2 ks).

The detected photons are in agreement with the input value also for extended sources

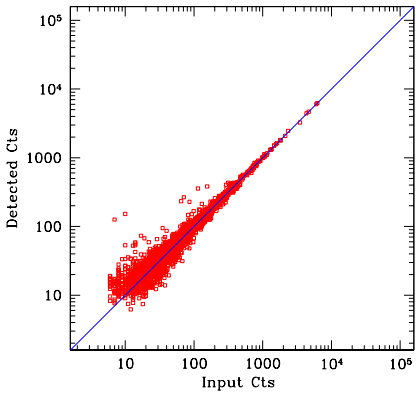

Fig. 12. Recovered vs input counts in the soft band for point sources (from a simulated soft band image of the Medium survey).

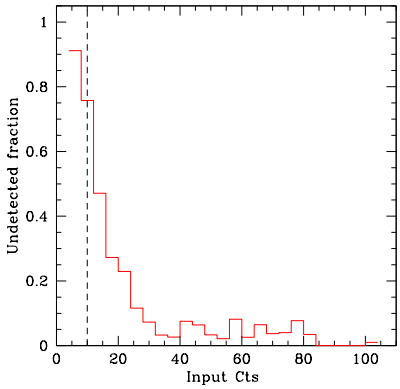

Fig. 13. Histogram distribution of the undetected point sources in the soft band as a function of the input photons (from a simulated image of the Medium survey).

(groups and clusters of galaxies) once a small offset due to the lost emission at low surface brightness is accounted for. However, at present, our schematic detection algorithm is not efficient in characterizing extended sources. Therefore, we set a conservative detection limit by requiring a typical S/N ratio of 5 from aperture photometry. To do this, we assume that for a typical group or cluster at medium and large redshifts, roughly 80% of the flux is included within 30 arcsec, corresponding to an extraction area of $A_{ext} = 2.18 \times 10^{-4}$ deg^2. We adopt an average conversion factor of 2.2×10^{-13} erg s^{-1} cm^{-2} for a typical ICM emission as in Table 2, and we use the background values shown in Table 2. We compute the S/N ratio as follows:

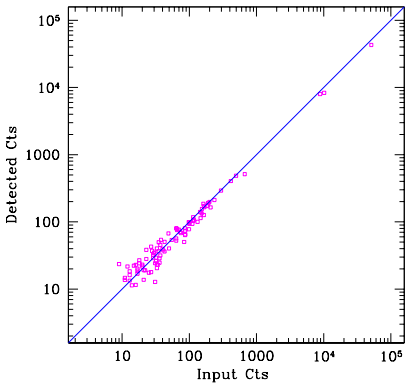

Fig. 14. Recovered vs input counts in the soft band for extended sources (from a simulated soft band image of the Medium survey).

$$BCK = BCK_{rate} \times T_{exp} \times A_{ext}\,, \quad (1)$$

$$S/N = CTS_{net}/\sqrt{CTS + 2\,BCK}\,. \quad (2)$$

Requiring $S/N > 5$, the condition on the minimum number of net detected photons within the extraction regions is:

$$CTS_{det} = 12.5 \times (1 + \sqrt{1 + 0.32 \times BCK})\,, \quad (3)$$

corresponding to a flux of $F_{det} = CTS_{det} \times ECF/T_{exp}/0.8$, where the factor of 0.8 accounts for the lost flux (see Table 3).

5. Redshift measure via X-ray spectroscopy of distant clusters

Now we focus on the properties of the WFXT sample of X-ray clusters. As we showed in this

Survey	CTS_{ext}	CTS_{tot}	$F_{lim}/10^{-15}$
Wide	39.4	49.3	5.42
Medium	69	86.1	1.44
Deep	294	367	0.2

Table 3. Detection limits for extended sources: CTS_{ext} is the minimum number of detected photons in the extraction regions, CTS_{tot} is the detection limit in terms of total emitted photons, and F_{lim} is the total flux limit.

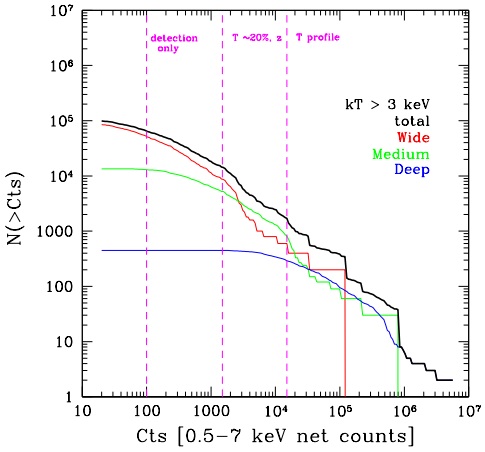

Fig. 15. Number of clusters with $kT > 3$ keV for the three WFXT surveys as a function of the detected photons (0.5-7 keV band). Vertical dashed lines correspond roughly to the average detection limit (100 photons), to the limit for spectral analysis (1500 net photons) and the the limit for spatially resolved spectral analysis (15000 net photons).

work, all the properties of the WFXT concur to deliver a very high quality set of data: the large effective area provides a high number of detected photons for sources down to low fluxes; the angular resolution allows us to avoid source confusion and remove the contribution of point sources from the diffuse emission of clusters and groups; finally the large field of view allows one to collect a large number of sources in a reasonable amount of time. To quantify the expected sample of clusters with $kT > 3$ keV from the three WFXT surveys, we show in Figure 15 the number of extended sources as a function of the detected photons.

Despite the bulk of the detected photons will be in the soft band, the relatively high effective area in the hard band (2-7 keV) will allow us to measure the ICM temperature and detect the K_α Fe line at any redshift whenever the equivalent width is $few \times 100$ eV. For the first time, this opens the possibility of building a sample of clusters with measured redshifts without recurring to time-consuming optical follow-up work.

To explore this relevant science case, we performed spectral simulations of a sample of groups and clusters extracted from the Press & Schechter (1974) mass function, whose temperatures and luminosities are assigned according to the observed *M-T* and *L-T* relations. The X-ray spectra are analyzed with `Xspec` with a `mekal` model where the redshift is left free to vary. Even though the Fe K_α line complex is ubiquitous in the ICM emission, the blind search of the Fe line is a difficult task. The background and the poisson noise in the rapidly decreasing signal in the hard band, may originate spurious lines which lead to catastrophic errors on the measured X-ray redshift. Another source of uncertainty is the intrinsic Fe abundance, which is significantly varying particularly in groups. Our automatic procedure to find the X-ray redshift (Yu et al. 2010, in preparation) shows that we will be able to detect the Fe K_α line complex in any extended source detected with more than 800 total photons. The number of catastrophic failures ($\Delta z \geq 0.1$) is kept low, and the typical error on the redshift is $\langle \Delta z \rangle \sim 0.022$. This can be seen in Figure 16.

The occurrence of catastrofic errors depends strongly on the total detected photons, and mildly on the intrinsic Fe abundance. As shown in Figure 17, where only clusters with more than 800 detected photons are considered, we can conservatively adopt a lower limit of 1500 net detected photons above which we can rely on the X-ray measured redshift. We can straightforwardly compute that the three

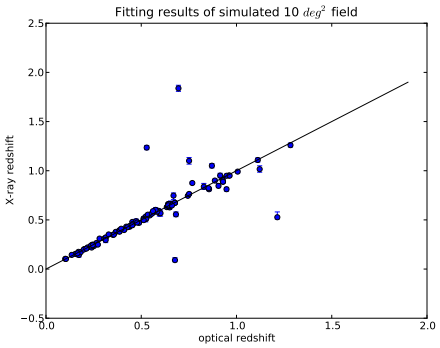

Fig. 16. X-ray measured redshift vs optical (input) redshift from the spectral analysis of a mock simulation of 10 square degrees of the Medium survey (exposure time of 13.2 ks). Vignetting effects are included (from Yu et al. 2010).

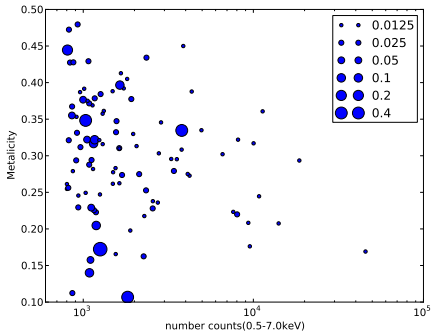

Fig. 17. Input Fe abundance vs detected number counts for the mock simulation of 10 square degrees of the Medium survey. The size of each dot is proportional to the error Δz with respect to the input value (from Yu et al. 2010).

WFXT planned surveys will provide a total of 15000-20000 clusters with $kT > 3$ keV (as shown in Figure 15) with measured X-ray redshift, a golden sample that can be directly used for precision cosmological tests with an unprecedented statistics (see Borgani et al. this volume).

6. Conclusions

The Wide Field X-ray Telescope has been designed in order to be optimized for surveys. Its goal is not only to detect the largest number of X-ray sources, but also to characterize them in order to address several science cases. The superiority of WFXT as an X-ray survey machine, is due to the combination of angular resolution ($HEW \sim 5$ arcsec), high effective area, and good sensitivity in the hard band. These properties open the discovery space of many scientific cases that are not addressed by any other present of future X–ray mission.

Thanks to the detailed imaging and spectral simulations presented in this work, we have investigated, among the many scientific cases within reach of WFXT, the construction of a cluster sample as large as 15000-20000 with redshift measured from the X-ray spectra, suitable for high precision cosmological tests. WFXT is therefore in the position of achieving the maximum scientific impact thanks to the high–quality characterization of the detected sources, of providing an extremely large number of targets suitable for next-generation X-ray missions like the International X-ray Observatory (IXO), with a unique legacy value to be added to the next–generation wide field surveys at other wavelengths.

The simulation tool presented in this work will provide an important testbed to refine the design of the mission in keeping with the scientific requirements. In particular, the imaging and spectral simulations will be used to develop specific detection algorithms and to refine analysis procedures. On the basis of the end-to-end analysis presented here, we reinforce our idea that an X-ray mission optimized for surveys like WFXT is necessary to bring X-ray astronomy at the level of the optical, IR, submm and radio wavebands as foreseen in the coming decade.

Acknowledgements. We acknowldge support under the ASI grant I/088/06/0 and the INFN PD51 grant.

References

Burrows, C. J., Burg, R., & Giacconi, R. 1992, ApJ, 392, 760
Cappelluti, N., Brusa, M., Hasinger, G., et al. 2009, A&A, 497, 635
Conconi, P., Campana, S., Tagliaferri, G., et al. 2010, MNRAS, 405, 877

Giacconi, R., Borgani, S., Rosati, P., et al. 2009, in ArXiv Astrophysics e-prints, Vol. 2010, astro2010: The Astronomy and Astrophysics Decadal Survey, 90

Gilli, R., Comastri, A., & Hasinger, G. 2007, A&A, 463, 79

Henry, J. P., Evrard, A. E., Hoekstra, H., Babul, A., & Mahdavi, A. 2009, ApJ, 691, 1307

Lehmer, B. D., Brandt, W. N., Alexander, D. M., et al. 2008, ApJ, 681, 1163

Murray, S., Gilli, R., Tozzi, P., et al. 2009, in ArXiv Astrophysics e-prints, Vol. 2010, astro2010: The Astronomy and Astrophysics Decadal Survey, 217

Murray, S., Norman, C., Ptak, A., et al. 2008, in Society of Photo-Optical Instrumentation Engineers (SPIE) Conference Series, Vol. 7011, Society of Photo-Optical Instrumentation Engineers (SPIE) Conference Series

Norman, C., Ptak, A., Hornschemeier, A., et al. 2004, ApJ, 607, 721

Predehl, P., Böhringer, H., Brunner, H., et al. 2010, in American Institute of Physics Conference Series, Vol. 1248, American Institute of Physics Conference Series, ed. A. Comastri, L. Angelini, & M. Cappi, 543–548

Press, W. H. & Schechter, P. 1974, ApJ, 187, 425

Ptak, A., Feigelson, E., Chu, Y., et al. 2009, in ArXiv Astrophysics e-prints, Vol. 2010, astro2010: The Astronomy and Astrophysics Decadal Survey, 240

Ranalli, P., Comastri, A., & Setti, G. 2005, A&A, 440, 23

Rosati, P., Borgani, S., & Norman, C. 2002, ARA&A, 40, 539

Rosati, P., della Ceca, R., Norman, C., & Giacconi, R. 1998, ApJ, 492, L21+

Santos, J. S., Rosati, P., Tozzi, P., et al. 2008, A&A, 483, 35

Santos, J. S., Tozzi, P., Rosati, P., & Boehringer, H. 2010, ArXiv e-prints

Vikhlinin, A., Murray, S., Gilli, R., et al. 2009, in Astronomy, Vol. 2010, AGB Stars and Related Phenomenastro2010: The Astronomy and Astrophysics Decadal Survey, 305

Mem. S.A.It. Suppl. Vol. 17, 36

Memorie della
Supplementi

Astrophysics and cosmology with galaxy clusters: the WFXT perspective

S. Borgani[1,2,3], P. Rosati[4], B. Sartoris[1,2,3], P. Tozzi[2,3], R. Giacconi[5], & the WFXT Team

[1] Dipartimento di Fisica, Sezione di Astronomia, Università di Trieste, Via Tiepolo 11, I-34143 Trieste, Italy e-mail: borgani,sartoris@oats.inaf.it
[2] INAF-Osservatorio Astronomico di Trieste, Via Tiepolo 11, I-34143 Trieste, Italy e-mail: tozzi@oats.inaf.it
[3] INFN, Sezione di Trieste, Via Valerio 2, I-34127 Trieste, Italy
[4] ESO-European Southern Observatory, D-85748 Garching bei München, Germany e-mail: prosati@eso.org
[5] Department of Physics and Astronomy, The Johns Hopkins University, Baltimore MD, USA

Abstract. We discuss the central role played by the X-ray study of galaxy clusters to reconstruct the assembly of cosmic structures. We shortly review the progress in this field contributed by the current generation of X-ray telescopes. Then, we focus on the outstanding scientific questions that have been opened by observations carried out in the last years by Chandra and XMM: (a) When and how is entropy injected into the inter-galactic medium (IGM)? (b) What is the history of metal enrichment of the IGM? (c) What physical mechanisms determine the presence of cool cores in galaxy clusters? (d) How is the appearance of proto-clusters at z 2 related to the peak of star formation activity and BH accretion? (e) What do galaxy clusters tell us about the nature of primordial density perturbations and on the history of their growth? We argue that the most efficient observational strategy to address these questions is to carry out a large-area X-ray survey, reaching a sensitivity comparable to that of deep Chandra and XMM pointings, but extending over several thousands of square degrees. A similar survey can only be carried out with a Wide-Field X-ray Telescope (WFXT), which combines a high survey speed with a sharp PSF across the entire FoV.

Key words. Cosmology – galaxy clusters – X-rays

1. Introduction

Galaxy clusters represent the place where astrophysics and cosmology meet: while their overall internal dynamics is dominated by gravity, the astrophysical processes taking place on galactic scale leave observable imprints on the diffuse hot gas trapped within their potential wells (Rosati et al. 2002; Voit 2005; Borgani & Kravtsov 2009). Understanding in detail the relative role played by different astrophysical phenomena in determining this cosmic cycle of baryons, and its relationship with the process of galaxy formation, is one of the most important challenges of modern cosmology. Clusters of galaxies represent the end result of the collapse of density

fluctuations over comoving scales of about 10 Mpc. For this reason, they mark the transition between two distinct dynamical regimes. On scales roughly above 10 Mpc, the evolution of the structure of the universe is mainly driven by gravity and the evolution still feels the imprint of the cosmological initial conditions. At scales below 1 Mpc the physics of baryons plays an important role in addition to gravity, thus making physical modeling far more complex. In the current paradigm of structure formation, clusters form via a hierarchical sequence of gravitational mergers and accretion of smaller systems. Within these small halos gas efficiently cools, forms stars and accretes onto supermassive black holes (SMBHs), living in massive galaxies, already at high redshift. While the star formation peaks at redshift $z \sim 2$–3, the intergalactic gas is heated to high, X-ray emitting temperatures by adiabatic compression and shocks, and settles in hydrostatic equilibrium within the cluster potential well, only at relatively low redshift, $z \lesssim 2$. The process of cooling and formation of stars and SMBHs can then result in energetic feedback due to supernovae or AGN, which inject substantial amounts of heat into the intergalactic medium (IGM) and spread heavy elements throughout the forming clusters.

Galaxy clusters are also very powerful cosmological tools. They probe the high end of the mass function of dark matter (DM) halos, whose evolution is highly sensitive to the underlying cosmological scenario and to the growth rate of cosmological perturbations (e.g., Borgani et al. 2001; Voit 2005). This information, combined with the shape and amplitude of the power spectrum of their large-scale distribution, offers a means of constraining the growth of cosmic structures over a wide range of scales. For these reasons, galaxy clusters are nowdays considered sensitive probes of the dark sector of the Universe and of the nature of gravity, complementary to CMB and SN-Ia tests, which are sensitive to the backgorund geometry and expansion rate. Based on relatively small samples of few tens of distant X–ray clusters extracted from ROSAT deep pointings, followed up by Chandra observations, independent analyses have recently shown that the evolution of the population of galaxy clusters does indeed provide significant constraints on cosmological parameters (e.g. Vikhlinin et al. 2009a; Mantz et al. 2009). This remarkable progress in cluster cosmology has been made possible by the introduction of robust X–ray mass proxies, such as the gas mass M_{gas} and the total thermal content of the ICM defined by the product of gas mass and temperature, $Y_X = M_{gas}T$ (e.g. Kravtsov et al. 2006). Quite interestingly, the scatter in the relation between such mass proxies and the total cluster mass is suppressed after excising core cluster regions, $\lesssim 0.15R_{500}$.

Such results demonstrate that, to fully exploit the potential of clusters for cosmological applications, detailed measurements of X–ray mass requires collecting an adequate number of photons and good spatial resolution to remove the contribution of core regions in distant objects. From one hand, the revitalization of cluster cosmology has indeed required the high data quality offered by the present generation of X-ray satellites. On the other hand, it highlights the constraining power that future X–ray surveys, like the one to be provided WFXT, could provide. The WFXT surveys would increase by several orders of magnitude the statistics of distant clusters for which data of comparable quality as that provided by Chandra observation.

As we will discuss in this contribution, the large grasp of WFXT combined with its sharp and stable PSF makes it the ideal instrument for astrophysical and cosmological studies of galaxy clusters (see also Giacconi et al. 2009, Vikhlinin et al. 2009b, and Rosati et al., in this volume).

2. WFXT to study clusters as astrophysical laboratories

Thanks to the high density and temperature reached by the gas within their potential wells, galaxy clusters mark the only regions where thermo- and chemo-dynamical properties of the IGM can be studied in detail at $z < 1$ from X–ray emission, and directly connected to the optical/near-IR properties of the galaxy population. A remarkable leap forward in the

quality of X-ray observations of clusters took place with the advent of the Chandra and XMM-Newton satellites. Thanks to their unprecedented sensitivity (and angular resolution in case of Chandra), they led to a number of fundamental discoveries concerning nearby, $z \lesssim 0.3$, clusters. For instance:

(a) The lack of strong emission lines at soft X-ray energies in the core regions placed strong limits on the amount of gas that can cool to low temperatures (Peterson & Fabian 2006), thus challenging the classical cooling flow model (Fabian 1994);
(b) Temperature profiles have been unambiguously observed to decline outside the core regions and out to the largest radii sampled so far, $\sim R_{500}$[1], while they gently decline toward the cluster center in relaxed systems(e.g. Vikhlinin et al. 2005; Pratt et al. 2007; Leccardi & Molendi 2008b);
(c) The level of gas entropy at R_{500} is in excess of what explainable by the action of supersonic accretion shocks (e.g. Sun et al. 2009; Pratt et al. 2009), while it is unexpectedly low in the innermost regions of relaxed clusters (e.g. Donahue et al. 2006);
(d) The intra-cluster medium (ICM) is not uniformly enriched in metals, instead metallicity profiles are observed to have a spike in the central regions, associated to the presence of the brightest cluster galaxy (BCG), while declining at least out to $\simeq 0.3R_{500}$.

While these observations shed new light on our understanding of the physical properties of the low-redshift intergalactic medium, (IGM), they opened at the same time at least as many questions. As we will discuss here below, an efficient way of addressing open questions in the ICM study is by carrying out high–sensitivity X-ray surveys, which provide a large number of clusters for which detailed studies can be carried out at low and high redshift. In Figure 1, we show a comparison for the yields of clusters expected from five years of operation of WFXT, compared with the expectations for the planned German-led mission eROSITA[2]. Besides the huge number of clusters that WFXT will detect at large redshift, this demonstrates that measurements of the physical properties of the ICM will be available for a large number of them.

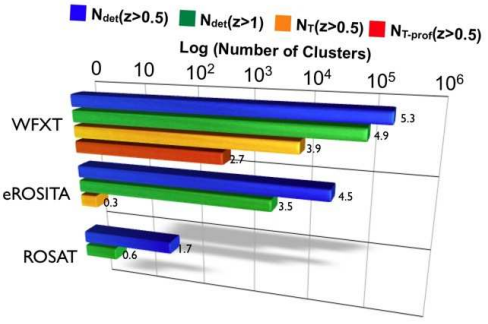

Fig. 1. The comparison between numbers of clusters expected for the surveys to be carried out by WFXT (as described in the contribution by Rosati et al. in this volume), by eROSITA, and as found in the ROSAT All Sky Survey (Voges et al. 1999). Blue and grees bars: number of clusters detected at $z > 0.5$ and $z > 1$, respectively; yellow and orange bars: number of clusters with at least 1.5×10^3 and 1.5×10^4 net photon counts in the [0.5-2] keV energy band, respectively.

When and how is entropy injected into the IGM? The standard explanation for the excess of entropy observed out to R_{500} is that some energetic phenomena should have heated the ICM over the cluster life-time (e.g. Voit 2005; Borgani & Kravtsov 2009). Models based on the so-called pre-heating (i.e. diffuse entropy injection before the bulk of the mass is accreted into the cluster halos) have been proposed as an explanation (e.g. Tozzi & Norman 2001; Borgani et al. 2002; Voit et al. 2003). However, these models predict quite large isentropic cores, which are not observed. Furthermore,

[1] We indicate with R_Δ the cluster-centric radius encompassing an average overdensity Δ times the critical cosmic density. For reference, $\Delta = 200$ is close to the virial overdensity while $\Delta = 500$ corresponds to about half the virial radius for a concordance ΛCDM model.

[2] Based on the specifications as provided in Mission Definition Document (`http://www.mpe.mpg.de/erosita/MDD-6.pdf`)

studies of the intergalactic medium (IGM), from observations of $z \gtrsim 2$ absorption systems in high-resolution optical spectra of distant QSOs, demonstrate that any pre-heating should take place only in highdensity regions (Shang et al. 2007; Borgani & Viel 2009). An alternative scenario is that ICM heating takes place at relatively low redshift, within an already assembled deep potential well. In this case, the natural expectation is that the same heating agent, presumably the central AGN, should be responsible for both establishing the cool core and increasing the entropy out to $\sim$ 1 Mpc scale, although it is not clear how AGN feedback can be distributed within such a large portion of the cluster volume.

Reconstructing the timing and pattern of entropy injection in the ICM has far reaching implications for tracing the past history of star formation and black hole (BH) accretion. While we expect that the two above scenarios leave distinct signatures on the evolution of the ICM entropy structure, available data from XMM and Chandra are too sparse to adequately understand this evolution.

The large number of clusters with $\sim 10^4$ counts available from the WFXT surveys would increase by orders of magnitude the statistics of a handful of clusters at $z > 0.5$ for which detailed entropy profiles have been measured so far. The measurement of ICM profiles for a large number of distant clusters will allow us to trace the interplay between IGM and galaxy population along 2/3 of the cosmological past light-cone. Furthermore, the low background and the possibility of resolving out the contribution of point sources will also allow us to measure such profiles out to R_{200} and beyond for bright galaxy clusters at $z < 0.2$ (see the contribution by Ettori & Molendi, in this volume).

What is the history of metal enrichment of the IGM? This question is inextricably linked to the previous one on the history of IGM heating. Measurements of the metal content of the ICM provide direct information on the past history of star formation and on processes (e.g., galactic ejecta powered by SN and AGN, ram-pressure stripping of merging galaxies, stochastic gas motions, etc.) that are expected to displace metal-enriched gas from star forming regions (e.g., Schindler & Diaferio 2008). So far, X–ray observations have provided valuable information on the pattern of enrichment only at low-redshift, $z \lesssim 0.3$ (Baumgartner et al. 2005; Mushotzky 2004; Werner et al. 2006). Profiles of the Fe abundance have been measured for nearby systems (e.g. Snowden et al. 2008; Leccardi & Molendi 2008a). However, these results are limited to rather small radii, $\lesssim 0.3R_{500}$, while the level of enrichment at larger radii should be quite sensitive to the timing of metal production and to the mechanism of metal transport. Furthermore, profiles of chemical abundances for other elements, such as O, Si, and Mg, are much more uncertain. Tracing the relative abundances of different chemical species, which are synthetized in different proportions by different stellar populations, is crucial to infer the relative role played by different SN types and to establish the time-scale over which the ICM enrichment took place. The situation is even more uncertain at $z > 0.3$. Although analyses based (mainly) on the Chandra archive show indications for an increase of the ICM enrichment since $z \sim 1$ (Balestra et al. 2007; Maughan et al. 2008), basically no information is available on the metallicity profiles and on abundance of elements other than Fe. To improve upon this situation, one needs (a) to push to larger radii the study of the distribution in the ICM of different chemical species in nearby clusters; (b) to measure profiles of the Fe abundance for hundreds of clusters at $z > 0.5$.

Iron metallicity profiles would be measured by WFXT for virtually all the clusters for which a temperature profile is obtained, although with ~ 2 times larger statistical errors. A very accurate measurement of the global Fe metallicity will be obtained for several thousands of clusters out to $z \sim 1.5$. For all the clusters of this sample, thermo-dynamical and chemical properties of the ICM will be characterized with unprecedented precision.

What physical mechanisms determine the presence of cool cores in galaxy clusters? XMM and Chandra unambiguously demonstrated that the rate of gas cooling in cluster cores is unexpectedly low. Such a low cooling

rate requires that some sort of energy feedback must heat the ICM so as to exactly balance radiative losses. AGN are generally considered as the natural solution to this problem (e.g. McNamara & Nulsen 2007). However, no consensus has been reached so far on the relative role played by AGN and by mergers in determining the occurrence of cool cores in galaxy clusters (e.g. Burns et al. 2008). Since merging activity and galactic nuclear activity are both expected to evolve with redshift, measurements of the occurrence of cool cores in distant clusters are necessary to address this issue. Although attempts have been pursued to characterize the evolution of the fraction of cool cores using Chandra data (e.g. Santos et al. 2008), no definite conclusion has been reached on the evolution of the fraction of cool core clusters.

The sharp and stable PSF of WFXT will allow one to resolve the core region of distant clusters (a cool-core of 50 kpc radius will subtend an angle of $\simeq 6$ arcsec at $z = 1$). The yield of hundreds of clusters at $z > 0.5$ for which more than 10^4 counts will be available, will allow us to accurately measure the evolution of the occurrence of cool cores and how this is related to the cluster dynamical state.

How is the appearance of proto-clusters related to the peak of star formation activity and BH accretion? Massive galaxies in todays clusters show only very modest ongoing star formation: they harbor a super-massive black hole usually living in a quiescent accretion mode and experience only "dry" mergers with much smaller galaxies. The situation should be radically different at $z \sim 2$. This is the epoch when proto-BCGs are expected to be assembling through violent mergers between actively star-bursting galaxies, moving within a rapidly evolving potential well. These proto-cluster regions accrete a large amount of gas that is suddenly heated to high temperature by mechanical shocks and, for the first time, starts radiating in X-rays. At the same time, BHs hosted within merging galaxies are expected to coalesce and their accretion disks to be destabilized by the intense dynamical activity, thereby triggering a powerful release of feedback energy. Evidence for such forming proto-clusters has been obtained by optical observations of a strong galaxy overdensity region, the so-called Spiderweb complex, surrounding a previously identified powerful radio galaxy at $z \simeq 2.1$ (Miley et al. 2006; Hatch et al. 2009). Cosmological simulations lend support to the expectation that similar structures trace the progenitors of massive cluster seen locally, and predict that this structure should already contain dense IGM, emitting in X-rays with $L_X \sim 10^{44}$ erg s^{-1} in the [0.5-2] keV band, with a temperature of several keV and enriched in metal at a level comparable to nearby clusters (Saro et al. 2009). As of today, no unambiguous detection of X-ray emitting gas permeating this region has been obtained (Carilli et al. 2002). While the detection of such a hot diffuse gas may be just at the limit of the capability of current X-ray telescopes, characterizing its physical properties (temperature and metallicity) is far beyond the reach of Chandra and XMM.

The study of proto-clusters at $z \gtrsim 2$ is still unexplored territory. For this reason, it is difficult to make predictions on how many of these structures could be observed by WFXT. By extrapolating our present knowledge of the relation between mass and X-ray luminosity, we expect to detect several hundreds of such objects over the whole sky. For the brightest of these clusters, it will even be possible to measure their redshift through X-ray spectroscopy with deeper follow-up exposures. At $z \sim 2$ the inverse Compton scattering of relativistic electrons, injected by AGN in core regions, off the CMB photons is much more effective than at low-z in producing a hard X-ray excess, thanks to the higher CMB temperature. Based on the expectation from hydrodynamic simulations, we estimated that 5 to 10 thousands of photons would be detectable by WFXT in a deep 400 ksec pointing on a $z \simeq 2$ proto-cluster, which is the progenotor of a today massive cluster, with $M_{200} \simeq 10^{15}\, h^{-1} M_\odot$. Such an observation would allow one: (a) to catch "in fieri" the pristine ICM enrichment; (b) to see in action the combined effect of strong mergers and intense nuclear activity within a forming cluster; (c) to discern the thermal and non-thermal emission from X-ray spectroscopy and infer the early

contribution of cosmic rays in pressurizing the ICM.

The goal of measuring physical properties of the ICM out to $z \sim 1$ and beyond can only be accomplished by a survey with the area and sensitivity achievable with WFXT. In fact, WFXT constitutes a two orders of magnitude improvement with respect to eROSITA (similar to the area-sensitivity enhancement that eROSITA will give with respect to the ROSAT All-Sky Survey), with in addition a 5 times better angular resolution (see the contribution by Cappelluti et al, in this volume).

3. Cluster cosmology with WFXT

WFXT will not be just a highly efficient cluster-counting machine. Its unique added value is that it will characterize the physical properties for a good fraction of these clusters and, therefore, calibrate them as robust tools for cosmological applications. Based on the specification of the WFXT surveys (see Rosati et al., this volume), we computed the constraints that can be placed on different classes of cosmological models. By following the approach described by Sartoris et al. (2010), we apply the Fisher-Matrix technique to forecast constraints on cosmology by combining information from number counts and power spectrum of clusters. The computation of these forecasts is based on the so-called self–calibration approach (e.g., Majumdar & Mohr 2003; Lima & Hu 2004). In this approach, we assume that X–ray observations provide an estimate of the actual cluster mass whose uncertain relation with the actual cluster mass is described by a suitable set of ''nuisance" parameters, to be fitted, with their own priors, along with cosmological parameters.

Sartoris et al. (2010) used this approach to place constraints on possible deviations from Gaussianity of the primordial density fluctuation field. The reference cosmological model assumed in this analysis, consistent with the WMAP-7 best–fitting model (Komatsu et al. 2010), assume: $\Omega_m = 0.28$ $\sigma_8 = 0.81$, $\Omega_k = 0$ for the curvature, $w(a) = w_0 + (1 - a)\, w_a$ with $w_0 = -0.99$ and $w_a = 0$ for the Dark Energy equation of state, $\Omega_{\rm b} = 0.046$ for the baryon contribution, $h = 0.70$ for the Hubble parameter, $n = 0.96$ for the primordial spectral index and $f_{\rm NL} = 0$ for the non–Gaussianity parameter. Furthermore, in the analysis we also include priors on cosmological parameters as expected from the Planck CMB experiment (Rassat et al. 2008).

We adopt the appropriate flux-dependent sky coverages for the three surveys (see Tozzi et al., this volume). To convert fluxes into masses, we use the relation between X–ray luminosity and M_{500} calibrated by Maughan (2007), where masses are recovered from Y_X, using Chandra data for 115 clusters in the redshift range $0.1 < z < 1.3$. The relation between measured and true mass is described by four nuisance parameters, which describe a possible intrinsic bias in the mass estimate, e.g. related to a residual violation of hydrostatic equilibrium (e.g. Rasia et al. 2006; Piffaretti & Valdarnini 2008; Lau et al. 2009), an intrinsic scatter in this relation and the evolution of these two parameters (see Sartoris et al. 2010, for a more detailed discussion).

In the left panel of Figure 2 we show the redshift distribution for all the clusters detected in the three WFXT surveys, having mass of at least $M_{500} > 5 \times 10^{13}\, h^{-1} M_\odot$. The right panel shows the same redshift distributions for the "Golden Samples", i.e. for all the clusters which are detected with at least 1500 net photon counts. The left panel demonstrates the huge potential of WFXT to detect a large number of clusters out to $z \sim 2$ and beyond. Furthermore, the right panel demonstrates that WFXT is not only a highly efficient survey machine to count clusters. In fact, its large grasp also provides a large enough number of photons and, therefore, to precise measurements of robust mass proxies, for about 20,000 clusters, with $\sim$ 1000 of them at $z > 1$. This represents a huge improvement with respect to the few tens of distant clusters available at present. This plot also shows the relevence of the Deep Survey to calibrate measurements of mass proxies beyond $z \sim 1$, thus complementing the larger statistics of lower-z clusters provided by the Medium and Wide surveys.

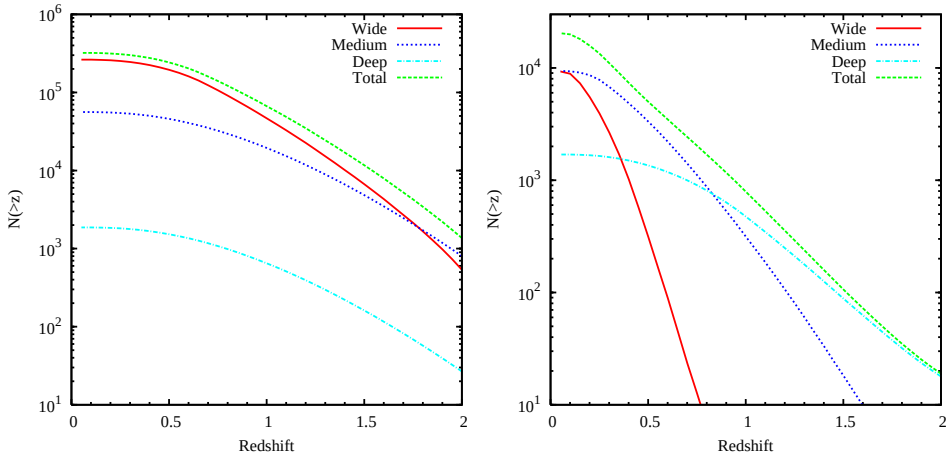

Fig. 2. The cumulative redshift distributions for the three WFXT surveys. The left panel is for all clusters detected, while the right panel is for the clusters in the "Golden Samples", corresponding to a 1500 photons detected. In both panels solid (red), dotted (blue) and dot-dashed (cyan) curves are for the Wide, Medium and Deep surveys, respectively, while the short-dashed (green) curve is for the sum of the three surveys.

We show in Figure 3 the joint constraints on the f_{NL} parameter, which define the deviation from Gaussianity (e.g. Verde 2010; Desjacques & Seljak 2010, for recent reviews) and the normalization of the power spectrum, σ_8, after marginalizing over all the other cosmological and nuisance parameters. As discussed by Sartoris et al. (2010) (see also Oguri 2009; Cunha et al. 2010), constraints on non-Gaussianity are weakly sensitive to the uncertain knowledge of the nuisance parameters. On the other hand, non-Gaussian constraints mainly comes from the shape of the power spectrum at the long wavelengths probing the possible scale dependence of the biasing parameter. For these reasons, we used in this analysis the large sets of detected clusters, without restricting to the "Golden Sample" for which nuisance parameters can be measured. This plot clearly shows that most of the constraints on non-Gaussianity comes form the Wide survey, which in fact has the potential to prove the long wavelength modes. Little information is carried instead by the Deep survey, which is instead very important for the calibration of mass proxies for distant clusters.

Figure 4 shows the constraints on the parameters defining the DE equation of state us-

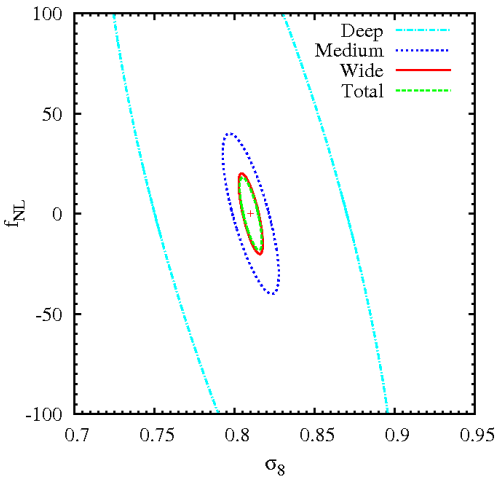

Fig. 3. Constraints at the 68 per cent confidence level on non–Gaussian parameter $f_{\rm NL}$ and power spectrum normalization σ_8 from the Deep, Medium and Wide surveys (solid red, long-dashed blue and short-dashed black curves, respectively), by combining number counts and power spectrum information. Also shown with the dotted magenta curve are the constraints obtained from the combination of the three surveys. No prior knowledge is assumed for the values of the nuisance parameters. The Fisher Matrix from Planck experiment is included in the calculation of all constraints.

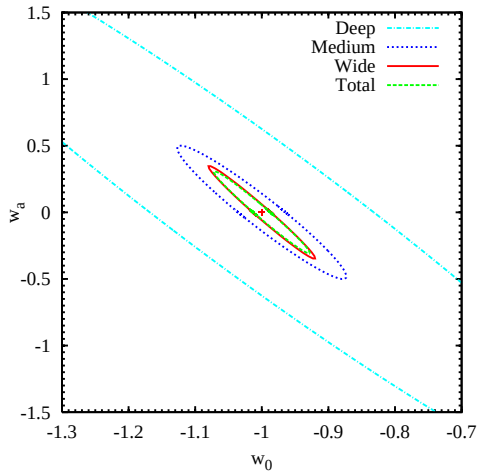

Fig. 4. The same as in Fig. 3, but for the constraints on the DE equation of state. The analysis is carried out for the same samples and same priors on nuisance parameters as in Fig.3.

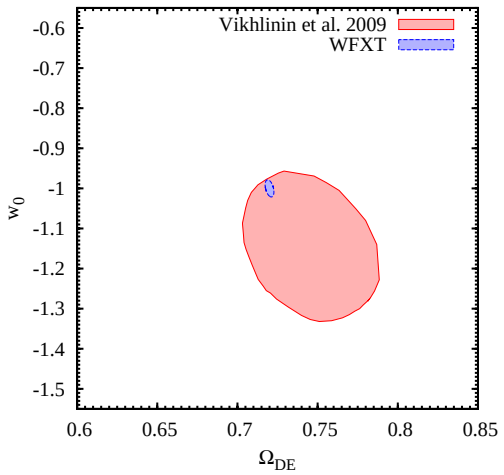

Fig. 5. A comparison between the constraints on the Ω_{DE}–w_0 plane obtained by Vikhlinin et al. (2009a) from a sample of clusters followed-up with Chandra (red shaded area), and as expected for the "Bright" WFXT surveys, by combining number counts and power spectrum information, under the assumption of strong strong priors on the nuisance parameters (light blue filled area). Both contours corresponds to $\Delta\chi^2 = 1$ (i.e. 68 per cent confidence level for one significant parameter) and are obtained under the assumption of flat Universe.

ing the samples and the same priors on nuisance parameters as for Fig.3. Also in this case, the large cluster statistics available in the Wide survey, makes it providing the dominant constraining power. The resulting value of the DETF Figure-of-Merit Albrecht et al. (2009), after combining the information from the three surveys, is $DETF = 512$.

Figure 5 emphasizes the improvement represented by WFXT with respect to present constraints from X–ray cluster surveys. In this plot, the red shaded area show the constraints on the Ω_{DE}–w_0 plane obtained by Vikhlinin et al. (2009a) from a sample combining nearby and distant cluster, originally identified from ROSAT data and followed-up with Chandra. Since Chandra follow-up provides at least $\sim 10^3$ photons per cluster, for consistency we compare it with the forecasts for the WFXT samples (light blue ellipse). The WFXT contour, which is obtained by combining number counts and power spectrum information, is off-centered with respect to the contours by Vikhlinin et al. (2009a) since their best–fitting model does not coincide with the reference cosmological model assumed for our Fisher–Matrix analysis of forecasts.

As well known, the evolution of the population of galaxy clusters is affected by cosmology both through the cosmic expansion history, which defines the volumes, and through the linear growth rate of perturbations (e.g. Haiman et al. 2001). In order to make a pure test of perturbation growth, we decided to carry out the Fisher-Matrix analysis by freezing the expansion history to the ΛCDM one, while using a suitable parametrization to describe the growth history. A commonly adopted approach to parametrize the growth of perturbations is based on the quantity

$$f(a) = \frac{d\log D_+(a)}{d\log a}\,, \qquad (1)$$

where a is cosmic expansion factor and $D_+(a)$ is the linear growth rate of density perturbations. The quantity $f(a)$ is well approximated

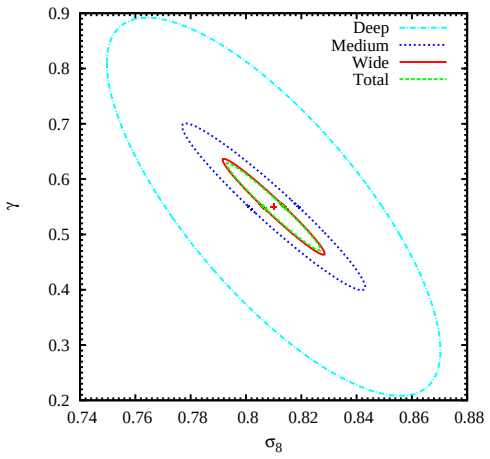

Fig. 6. Constraints on the power-spectrum normalization σ_8, and on the growth index γ from the three WFXT surveys and from their combination.

by the phenomenological relation (e.g. Wang & Steinhardt 1998)

$$f(a) \simeq \Omega_m(a)^\gamma \qquad (2)$$

with $\gamma = 0.55 + 0.05[1 + w(a = 0.5)]$ for large classes of DE models (e.g. Linder 2005). Therefore, testing the precision with which γ can be measured should be regarded as a test of the precision with which General Relativity (GR) can be verified on cosmological scales. For instance, $\gamma \simeq 0.68$ corresponds to the linear growth predicted by the popular DGP model of modified gravity (Dvali et al. 2000).

In order to test the constraints on the growth of perturbations obtainable from the WFXT surveys, we freeze cosmic expansion to ΛCDM, under the assumption that any modified gravity model should be almost indistinguishable from ΛCDM at the background level. Furthermore, we do not include any Dark Energy in our non-GR models, following the idea that a modification of GR should be alternative to DE to explain cosmic expansion. The results of our analysis based on the WFXT surveys are shown in Figure 6. Here we report the expected constraints on the γ–σ_8 plane, once we marginalize over the remaining parameters. This plot confirms that WFXT would indeed provide very useful constraints on possible deviations from the standard gravity, based on the growth of structure as traced by the evolution of the cluster population.

4. Synergies & legacy value

Addressing the outstanding questions outlined above will greatly benefit from a coordinated multi-wavelength activity between WFXT, future space missions and ground-based facilities (see also Rosati et al. in this volume, for a more detailed description of the synergies between WFXT and future instrumentation).

The identification and characterization of the galaxy populations hosted by the $\sim 2 \times 10^5$ clusters at $z > 0.5$, unveiled by WFXT, will be an essential process to obtain a comprehensive and self-consistent picture of the cosmic cycle of baryons in their hot and cold phase, by tracing the evolution of their underlying stellar populations and star formation histories. Deep optical coverage of large survey areas will be provided by the next generation of wide-field ground-based facilities, currently under development and scheduled for routine operations within the next few years, such as Pan-Starrs[3] and LSST[4].

The combination of WFXT with the ESA Euclid and the NASA JDEM missions, currently under development (Euclid and JDEM) will provide spectroscopic confirmation for a large fraction of $z > 0.5$ clusters identified by WFXT and a full characterization of member galaxies with high resolution optical imaging. Such Dark Energy missions are also designed to reconstruct the DM mass distribution via weak lensing tomographic techniques. This will allow direct lensing mass determination of thousands of massive clusters out to $z \sim 1$. Their comparison with X-ray derived masses will yield the much heralded cluster mass calibration and control of systematics for cosmological applications.

The Atacama Cosmology Telescope (ACT) and the South Pole Telescope (SPT) have recently opened a new era

[3] http://pan-starrs.ifa.hawaii.edu/
[4] http://www.lsst.org/

of Sunyaev-Zeldovich (SZ) cluster search (Staniszewski & et al. 2009). Next generation large single-dish mm telescopes, such as the Caltech-Cornell Atacama Telescope (CCAT `http://www.submm.org/`) will have enough sensitivity and angular resolution to carry out large-area SZ surveys, providing at the same time spatially resolved SZ imaging for moderately distant massive clusters. Taking advantage of the different dependence of the SZ and X-ray signals on gas density and temperature, their combination will provide a reconstruction of temperature and mass profiles, independent of X-ray spectroscopy (e.g. Ameglio et al. 2009; Golwala et al. 2009). This will offer further independent means of calibrating mass measurements of clusters.

With its unprecedented grasp and angular resolution, WFXT will be an outstanding source of interesting targets for follow-up studies of galaxy clusters with facilities such as JWST, ALMA, ELT and future X-ray observatories (i.e., IXO and Gen-X). For example, a combined study of X-ray luminous proto-cluster regions with ALMA, will test whether a phase of vigorous star formation (sub-mm bright galaxies) coexist with a BH accretion phase. Follow-up pointed observations with IXO of extreme clusters identified by WFXT at $z \sim 2$ will allow the study of metallicity and entropy structure of the pristine ICM. In general, the synergy with next generation multi-wavelength deep wide-area surveys and with high sensitivity instruments for pointed observations will unleash the full potential of WFXT in addressing a number of outstanding scientific questions related to cosmological and astrophysical applications of galaxy clusters.

Acknowledgements. This work has been supported by ASI–AAE Grant for Mission Feasibility Studies and by the INFN PD51 grant. The Authors would like to thank all the members of the WFXT team for a number of enlightening discussions.

References

Albrecht, A., Amendola, L., Bernstein, G., et al. 2009, ArXiv e-prints, 0901.0721

Ameglio, S., Borgani, S., Pierpaoli, E., et al. 2009, MNRAS, 394, 479

Balestra, I., Tozzi, P., Ettori, S., et al. 2007, A&A, 462, 429

Baumgartner, W. H., Loewenstein, M., Horner, D. J., & Mushotzky, R. F. 2005, ApJ, 620, 680

Borgani, S., Governato, F., Wadsley, J., et al. 2002, MNRAS, 336, 409

Borgani, S. & Kravtsov, A. 2009, ArXiv e-prints

Borgani, S., Rosati, P., Tozzi, P., et al. 2001, ApJ, 561, 13

Borgani, S. & Viel, M. 2009, MNRAS, 392, L26

Burns, J. O., Hallman, E. J., Gantner, B., Motl, P. M., & Norman, M. L. 2008, ApJ, 675, 1125

Carilli, C. L., Harris, D. E., Pentericci, L., et al. 2002, ApJ, 567, 781

Cunha, C., Huterer, D., & Dore, O. 2010, ArXiv e-prints

Desjacques, V. & Seljak, U. 2010, ArXiv e-prints

Donahue, M., Horner, D. J., Cavagnolo, K. W., & Voit, G. M. 2006, ApJ, 643, 730

Dvali, G., Gabadadze, G., & Porrati, M. 2000, Physics Letters B, 485, 208

Fabian, A. C. 1994, ARA&A, 32, 277

Giacconi, R., Borgani, S., Rosati, P., et al. 2009, in Astronomy, Vol. 2010, Astro2010: The Astronomy and Astrophysics Decadal Survey, 90

Golwala, S. R., Aguirre, J. E., Basu, K., et al. 2009, in Astronomy, Vol. 2010, astro2010: The Astronomy and Astrophysics Decadal Survey, 96–+

Haiman, Z., Mohr, J. J., & Holder, G. P. 2001, ApJ, 553, 545

Hatch, N. A., Overzier, R. A., Kurk, J. D., et al. 2009, MNRAS, 395, 114

Komatsu, E., Smith, K. M., Dunkley, J., et al. 2010, ArXiv e-prints, 1001.4538

Kravtsov, A. V., Vikhlinin, A., & Nagai, D. 2006, ApJ, 650, 128

Lau, E. T., Kravtsov, A. V., & Nagai, D. 2009, ApJ, 705, 1129

Leccardi, A. & Molendi, S. 2008a, A&A, 487, 461

Leccardi, A. & Molendi, S. 2008b, A&A, 486, 359

Lima, M. & Hu, W. 2004, Phys. Rev. D, 70, 043504
Linder, E. V. 2005, Phys. Rev. D, 72, 043529
Majumdar, S. & Mohr, J. J. 2003, ApJ, 585, 603
Mantz, A., Allen, S. W., Rapetti, D., & Ebeling, H. 2009, ArXiv e-prints, 0909.3098
Maughan, B. J. 2007, ApJ, 668, 772
Maughan, B. J., Jones, C., Forman, W., & Van Speybroeck, L. 2008, ApJS, 174, 117
McNamara, B. R. & Nulsen, P. E. J. 2007, ARA&A, 45, 117
Miley, G. K., Overzier, R. A., Zirm, A. W., et al. 2006, ApJ, 650, L29
Mushotzky, R. F. 2004, in Clusters of Galaxies: Probes of Cosmological Structure and Galaxy Evolution, ed. J. S. Mulchaey, A. Dressler, & A. Oemler, 123–+
Oguri, M. 2009, Physical Review Letters, 102, 211301
Peterson, J. R. & Fabian, A. C. 2006, Phys. Rep., 427, 1
Piffaretti, R. & Valdarnini, R. 2008, A&A, 491, 71
Pratt, G. W., Arnaud, M., Piffaretti, R., et al. 2009, ArXiv e-prints, 0909.3776
Pratt, G. W., Böhringer, H., Croston, J. H., et al. 2007, A&A, 461, 71
Rasia, E., Ettori, S., Moscardini, L., et al. 2006, MNRAS, 369, 2013
Rassat, A., Amara, A., Amendola, L., et al. 2008, ArXiv e-prints, 0810.0003
Rosati, P., Borgani, S., & Norman, C. 2002, ARA&A, 40, 539
Santos, J. S., Rosati, P., Tozzi, P., et al. 2008, A&A, 483, 35
Saro, A., Borgani, S., Tornatore, L., et al. 2009, MNRAS, 392, 795
Sartoris, B., Borgani, S., Fedeli, C., et al. 2010, ArXiv e-prints
Schindler, S. & Diaferio, A. 2008, Space Science Reviews, 134, 363
Shang, C., Crotts, A., & Haiman, Z. 2007, ApJ, 671, 136
Snowden, S. L., Mushotzky, R. F., Kuntz, K. D., & Davis, D. S. 2008, A&A, 478, 615
Staniszewski, Z. & et al. 2009, ApJ, 701, 32
Sun, M., Voit, G. M., Donahue, M., et al. 2009, ApJ, 693, 1142
Tozzi, P. & Norman, C. 2001, ApJ, 546, 63
Verde, L. 2010, ArXiv e-prints, 1001.5217
Vikhlinin, A., Kravtsov, A. V., Burenin, R. A., et al. 2009a, ApJ, 692, 1060
Vikhlinin, A., Markevitch, M., Murray, S. S., et al. 2005, ApJ, 628, 655
Vikhlinin, A., Murray, S., Gilli, R., et al. 2009b, in Astronomy, Vol. 2010, Astro2010: The Astronomy and Astrophysics Decadal Survey, 305
Voges, W., Aschenbach, B., Boller, T., et al. 1999, A&A, 349, 389
Voit, G. M. 2005, Reviews of Modern Physics, 77, 207
Voit, G. M., Balogh, M. L., Bower, R. G., Lacey, C. G., & Bryan, G. L. 2003, ApJ, 593, 272
Wang, L. & Steinhardt, P. J. 1998, ApJ, 508, 483
Werner, N., de Plaa, J., Kaastra, J. S., et al. 2006, A&A, 449, 475

Mem. S.A.It. Suppl. Vol. 17, 47

Memorie della
Supplementi

X-ray observations of cluster outskirts: current status and future prospects.

S. Ettori[1,2] and S. Molendi[3]

[1] Istituto Nazionale di Astrofisica – Osservatorio Astronomico di Bologna, Via Ranzani 1, I-40127 Bologna, Italy e-mail: stefano.ettori@oabo.inaf.it
[2] INFN, Sezione di Bologna, viale Berti Pichat 6/2, I-40127 Bologna, Italy
[3] INAF, IASF, via Bassini 15, I-20133 Milano, Italy e-mail: silvano@iasf-milano.inaf.it

Abstract.
Past and current X-ray mission allow us to observe only a fraction of the volume occupied by the ICM. After reviewing the state of the art of cluster outskirts observations we discuss some important constraints that should be met when designing an experiment to measure X-ray emission out to the virial radius. From what we can surmise *WFXT* is already designed to meet most of the requirements and should have no major difficulty in accommodating the remaining few.

Key words. galaxies: cluster: general – galaxies: fundamental parameters – intergalactic medium – X-ray: galaxies – cosmology: observations – dark matter

1. Introduction

Galaxy clusters form through the hierarchical accretion of cosmic matter. The end products of this process are virialized structures that feature, in the X-ray band, similar radial profiles of the surface brightness $S_{\rm b}$ (e.g. Vikhlinin et al. 1999, Neumann 2005, Ettori & Balestra 2009) and of the plasma temperature $T_{\rm gas}$ (e.g. Allen et al. 2001, Vikhlinin et al. 2005, Leccardi & Molendi 2008). Such measurements have definitely improved in recent years thanks to the arcsec resolution and large collecting area of the present X-ray satellites, like *Chandra* and *XMM-Newton*, but still remain difficult, in particular in the outskirts, because of the low surface brightness associated to these regions. Present observations provide routinely reasonable estimates of the gas density, $n_{\rm gas}$, and temperature, $T_{\rm gas}$, up to about R_{2500} ($\approx 0.3R_{200}$; R_Δ is defined as the radius of the sphere that encloses a mean mass density of Δ times the critical density at the cluster's redshift; R_{200} defines approximately the virialized region in galaxy clusters). Only few cases provide meaningful measurements at R_{500} ($\approx 0.7R_{200}$) and beyond (e.g. Vikhlinin et al. 2005, Leccardi & Molendi 2008, Neumann 2005, Ettori & Balestra 2009). Consequently, more than two-thirds of the typical cluster volume, just where primordial gas is accreting and dark matter halo is forming, is still unknown for what concerns both its mass distribution and its thermodynamical properties. This poses a significant limitation in our ability to charac-

Send offprint requests to: S. Ettori, S. Molendi

terize the physical processes presiding over the formation and evolution of clusters and to use clusters as cosmological tools, as also outlined in the Scientific Justification for the *WFXT* (Giacconi et al. 2009). Indeed the characterization of thermodynamic properties at large radii would allow us to provide constraints on the virialization process, while measures of the metal abundance would allow us to gain insight on the enrichment processes occurring in clusters Fabjan et al. (2010). Morever the X-ray emission at large radii could also be used to improve significantly measures of the gas and total gravitating masses thereby opening the way to a more accurate use of galaxy clusters as cosmological probes (e.g. Voit 2005).

In these proceedings, we take stock of the situation on cluster outskirts and suggest how to make progress. In Sect. 2, we provide an observational overview of currently available measures of cluster outer regions, while in Sect. 3 we discuss some important constraints that should be met when designing an experiment to measure X-ray emission out to the virial radius. In Sect. 4, we present an overview of future missions which have cluster outskirts observations as one of their goals, our main results are recapitulated in Sect. 5.

A Hubble constant of 70 h_{70} km s^{-1} Mpc^{-1} in a flat universe with $\Omega_{\rm m}$ equals to 0.3 is assumed throughout this manuscript.

2. What we know of cluster outskirts

2.1. Surface brightness and gas density profiles

The X-ray surface brightness is a quantity much easier to characterize than the temperature and it is still rich in physical information being proportional to the emission measure, i.e. to the gas density, of the emitting source. Recent work focused on a few local bright objects for which *ROSAT* PSPC observations with low cosmic background and large field of view have allowed to recover the X-ray surface brightness profile over a significant fraction of the virial radius (Vikhlinin et al. , 1999; Neumann , 2005).

In Ettori & Balestra (2009), we study the surface brightness profiles extracted from a sample of hot ($T_{\rm gas} > 3$ keV), high-redshift ($0.3 < z < 1.3$) galaxy clusters observed with *Chandra* and described in Balestra et al. (2007). A local background, B, was defined for each exposure by considering a region far from the X-ray center that covered a significant portion of the exposed CCD with negligible cluster emission. We define the "signal-to-noise" ratio, $S2N$, to be the ratio of the observed surface brightness value in each radial bin, $S_b(r)$, after subtraction of the estimated background, B, to the Poissonian error in the evaluated surface brightness, $\epsilon_b(r)$, summed in quadrature with the error in the background, ϵ_B: $S2N(r) = [S_b(r) - B] / \sqrt{\epsilon_b(r)^2 + \epsilon_B^2}$. The outer radius at which the signal-to-noise ratio remained above 2 was defined to be the limit of the extension of the detectable X-ray emission, R_{S2N}. We estimated R_{200} using both a $\beta-$model that reproduces the surface brightness profiles and the scaling relation quoted in eq. 1 and selected the 11 objects with $R_{S2N}/R_{200} > 0.7$ to investigate the X-ray surface-brightness profiles of massive clusters at $r > R_{500} \approx 0.7R_{200}$. Examples of the analyzed dataset are shown in Fig. 1. We performed a linear least-squares fit between the logarithmic values of the radial bins and the background-subtracted X-ray surface brightness. Overall, the error-weighted mean slope is -2.91 (with a standard deviation in the distribution of 0.46) at $r > 0.2R_{200}$ and $-3.59(0.75)$ at $r > 0.4R_{200}$. For the only 3 objects for which a fit between $0.5R_{200}$ and R_{S2N} was possible, we measured a further steepening of the profiles, with a mean slope of -4.43 and a standard deviation of 0.83. We also fitted linearly the derivative of the logarithm $S_b(r)$ over the radial range $0.1R_{200} - R_{S2N}$, excluding in this way the influence of the core emission. The average (and standard deviation σ) values of the extrapolated slopes are then $-3.15(0.46)$, $-3.86(0.70)$, and $-4.31(0.87)$ at $0.4R_{200}$, $0.7R_{200}$ and R_{200}, respectively.

These values are comparable to what has been obtained in recent analyses. Vikhlinin et al. (1999) find that a $\beta-$model with $\beta = 0.65 - 0.85$ describes the surface brightness profiles

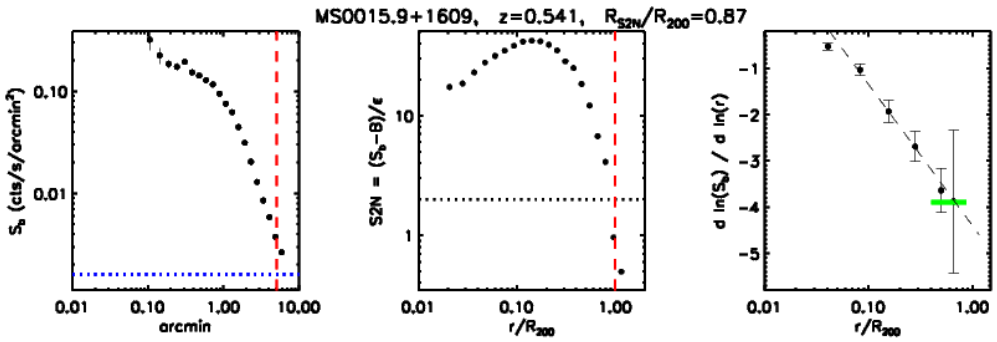

Fig. 1. From left to right: Example of a surface brightness profile with the fitted background (*horizontal dotted line*) and the radius R_{200} (*vertical dashed line*); the signal-to-noise profile evaluated as $S2N = (S_b - B)/\epsilon$, where the error ϵ is the sum in quadrature of the Poissonian error in the radial counts and the uncertainties in the fitted background, B; the best-fit values of the slope of the surface brightness profile as a function of r/R_{200}. These values are estimated over 6 radial bins (thick horizontal solid line: the slope evaluated between $0.4 \times R_{200}$ and R_{S2N} with a minimum of 3 radial bins; dashed line: best-fit of $d\ln(S_b)/d\ln(r/R_{200})$ with the functional form $s_0 + s_1 \ln(r/R_{200})$ over the radial range $0.1 \times R_{200} - R_{S2N}$, with the best-fit parameters quoted in Table 3 of Ettori & Balestra 2009).

in the range $0.3 - 1R_{180}$ of 39 massive local galaxy clusters observed with *ROSAT* PSPC. For a $\beta-$model with $x = r/r_c$, $\partial \ln S_b/\partial \ln x = (1 - 6\beta)\, x^2/(1 + x^2)$ and $\partial \ln n_{gas}/\partial \ln x = -3\beta\, x^2/(1 + x^2)$, impling that $\beta = 0.65 - 0.85$ corresponds to a logarithmic slope of the surface brightness of $-2.9/-4.1$, that is a range that includes our estimates. Neumann (2005) finds that the stacked profiles of few massive nearby systems located in regions at low ($< 6 \times 10^{20}$ cm^{-2}) Galactic absorption observed with *ROSAT* PSPC still provide values of β around 0.8 at R_{200}, with a power-law slope that increases from -3 when the fit is performed over the radial range $[0.1, 1]R_{200}$ to $-5.7^{+1.5}_{-1.2}$ over $[0.7, 1.2]R_{200}$.

These observational results are supported from the hydrodynamical simulations of X-ray emitting galaxy clusters performed with the Tree+SPH code GADGET-2 (Roncarelli et al. 2006). In the most massive systems, we measured a steepening of $S_b(r)$, independently from the physics adopted to treat the baryonic component, with a slope of $-4, -4.5, -5.2$ when estimated in the radial range $0.3 - 1.2R_{200}$, $0.7 - 1.2R_{200}$, $1.2 - 2.7R_{200}$, respectively. In particular, we note the good agreement between the slope of the simulated surface brightness profile of the representative massive cluster in the radial bin $0.7 - 1.2R_{200}$ (see values of b_A in Table 4 of Roncarelli et al. 2006 ranging between -4.29 and -4.54) and the mean extrapolated value at R_{200} of -4.43 measured in the *Chandra* dataset.

2.2. Temperature and metallicity profiles

Early attempts to produce temperature profiles were made with the *ROSAT* PSPC, these were mostly limited to low mass systems (e.g. David et al. 1996) where the temperatures were within reach of the PSPC soft response. Resolved spectroscopy of hot systems began with the coming into operation of *ASCA* (1994) and *BeppoSAX* (1996). Both missions enjoyed a relatively low instrumental background, which was a considerable asset when extending measures out to large radii, however they both suffered from limited spatially resolution. The situation was somewhat less severe with the *BeppoSAX* MECS than with the *ASCA* GIS since the former had a factor of 2 better angular resolution and a modest energy dependence in the PSF. These difficulties led to substantial differences in temperature measures, while on the one side Markevitch

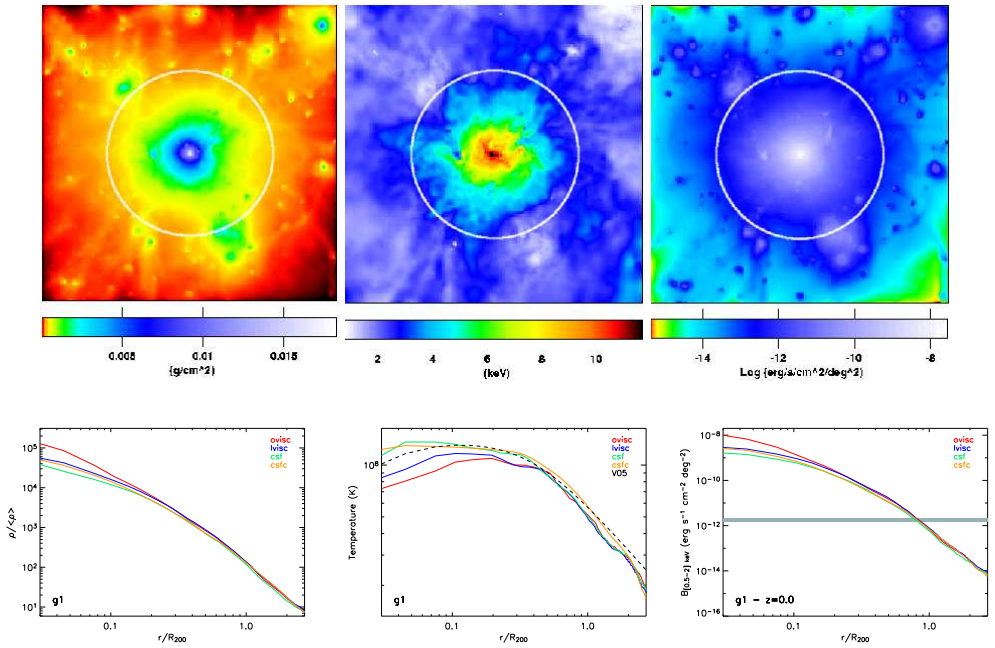

Fig. 2. From left to right; upper panels: Maps of the projected gas density, mass-weighted temperature and soft (0.5-2 keV) X-ray emission. The circles indicate the virial radius. The size of the side of each map is 12 Mpc, so they cover roughly up to $2.5R_{200}$. **Bottom panels**: Comparison between the gas density, mass-weighted temperature, soft X-ray surface brightness profiles for a cluster simulated by using 4 different physical models. A dashed line indicates the functional from Vikhlinin et al. (2006, eq. 9) that well reproduces the behavior of the temperature profile of nearby bright galaxy clusters observed with *Chandra*. The extragalactic unresolved background from Hickox & Markevitch (2006) in the soft X-ray band is indicated by the shaded region. From Roncarelli et al. (2006).

et al. (1998) using *ASCA* and De Grandi & Molendi (2002) using *BeppoSAX* MECS found evidence of declining temperature profiles, on the other, White (2000) using *ASCA* and Irwin et al. (1999) using *BeppoSAX* data found flat temperature profiles. The situation was somewhat clearer on abundance profiles were workers using *ASCA* (e.g. Finoguenov et al. 2000) and *BeppoSAX* data (De Grandi & Molendi 2001) consistently found evidence that cool core systems featured more centrally peaked profiles than NCC system. The coming into operation of the second generation of medium energy X-ray telescopes, namely *XMM-Newton* and *Chandra*, both characterized by substantially better spatial resolution, allowed more direct measures of the temperature profiles. The new *Chandra* (Vikhlinin et al. 2005) and *XMM-Newton* measurements (e.g. Pratt et al. 2007, Snowden et al. 2008) confirmed the presence of the temperature gradients measured with *ASCA* and *BeppoSAX*. In a detailed study of a sample of 44 objects observed with *XMM-Newton* (Leccardi & Molendi 2008) we found that temperature measurements could be extended out to about $0.7R_{180}$ (see Fig. 3). Since the major obstacle to the extension of measurements to large radii was the high background, most importantly the instrumental component, we adopted the source over background criterion originally introduced in De Grandi & Molendi (2002) to decide where to stop measuring profiles. The source to background ratio, defined as $\frac{I_{sou}}{I_{bkg}}$, where I_{sou} and I_{bkg} are the source and background intensities respectively,

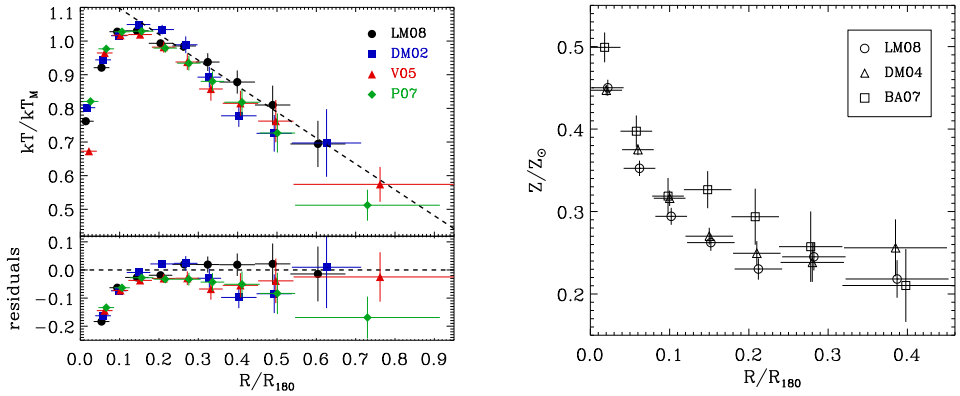

Fig. 3. Left panel: mean temperature profiles obtained from Leccardi & Molendi (2008; LM08, black circles), De Grandi & Molendi (2002; DM02, blue squares), Vikhlinin et al. (2005; V05, red upward triangles) and Pratt et al. (2007; P07, green diamonds). All profiles are rescaled by k$T_{\rm M}$ and R_{180}. The dashed line shows the best fit with a linear model beyond 0.2 R_{180} and is drawn to guide the eye. *lower panel:* residuals with respect to the linear model. The LM08 profile is the flattest one. **Right panel:** mean metallicity profiles obtained from Leccardi & Molendi (2008b; LM08, circles), De Grandi et al. (2004; DM04, triangle) and Baldi et al. (2007; BA07, squares). Abundances are expressed in Anders & Grevesse (1989) solar values and radii in units of R_{180}. The radii have been slightly offset in the plot for clarity.

should not be confused with the signal to noise ratio defined as $\frac{I_{sou}}{(I_{sou}+I_{bkg})^{1/2}} \cdot t$, where t is the exposure time. While the latter ratio is associated to the statistical error and therefore increases with exposure time, the former is associated to the systematic error and does not depend on the exposure time. Through a series of tests (see Sect. 5.2.1. and Fig. 11 of Leccardi & Molendi 2008) we determined that measurements could be trusted out to radii where the source to background ratio in the 0.7-10 keV band remained above a threshold of 0.6. In Leccardi & Molendi (2008) we made use for the first time of extensive simulations to estimate the impact of systematic errors on the measurements, part of the expertise we have acquired from that work has been used to perform the simulations discussed in Sect. 3.4. In the left panel of Fig. 3 we show a compilation of mean temperature profiles from different missions, all show evidence of a decline of the temperature beyond $0.2R_{180}$. Interestingly, as a result of the correction for systematic that we applied to our profile (see Sect. 5.3 and Fig. 14 of Leccardi & Molendi 2008) ours is the flattest amongst the profiles shown in the left panel of Fig. 3. The measurement of the metal abundance profile extends to radii that are somewhat smaller than those reached by the temperature profiles, this is because the most prominent emission line, the Fe Kα, is located in the high energy part of the spectrum where the instrumental background is particularly strong. In the right panel of Fig. 3 we show the mean abundance profile measured with different satellites. The flattening of the profiles beyond $0.2R_{180}$ is most likely indicative of an early enrichment of the ICM (Fabjan et al. 2010).

Unfortunately the high orbit of the *XMM-Newton* and *Chandra* satellites, as well as the fact that the design of the satellites was driven by scientific objectives other than the characterization of low surface brightness regions, led to a substantially higher and more variable background than with the previous satellite generation, thereby limiting the exploration of the temperature and abundance profiles to roughly the same regions already investigated with *ASCA* and *BeppoSAX* (see Fig. 3). Recently measures of temperature pro-

files have been made with the *Suzaku* X-ray imaging spectrometer (XIS). Although not ideal for cluster measurements, the XIS features a poor PSF and a small FOV, it does enjoy the considerable advantage of the modest background associated to the low earth orbit. The measures have been conducted on a handful of systems (A2204, Reiprich et al. 2009; A1795, Bautz et al. 2009; PKS0745-191, George et al. 2009; A1413, Hoshino et al. 2010) and extend beyond the regions explored with *Chandra* and *XMM-Newton*. However, the characterization is a limited one at best: only parts of the outermost annuli are explored and both radial bins and error bars are large. Moreover there are concerns as to the reliability of the measurements themselves. All measured temperature profiles are steeper than those predicted by simulations. This is particularly true of A1795 and PKS0745-191, where the temperature and the surface brightness are respectively steeper and flatter than those predicted by simulations. Consequently entropy profiles are flatter and, in the case of PKS0745-191, it features an inversion around $0.6R_{200}$, that could be associated to the presence of non virialized gas or, alternatively, to problems in the characterization of the source spectrum.

3. How we can map out to R_{200}

From the discussion in Sect. 2.2, it is rather obvious that past X-ray mission were not optimized for the spectral characterization of the low surface brightness emission typical of cluster outer regions. In this section we discuss how to design an experiment characterized by high sensitivity to low surface brightness emission. The sensitivity depends upon: 1) the surface brightness of the source, S_b, that scales with effective area of the experiment, A_E; 2) the solid angle covered by the field of view (FOV), Ω; 3) the surface brightness of the background, B. The quantity that needs to be maximized is then:

$$\frac{2\pi \int_0^{\theta_{max}} A_E(\theta)\theta d\theta}{B},$$

where θ is the off-axis angle and the integration is extended over the full FOV, i.e. $2\pi \int_0^{\theta_{max}} \theta d\theta = \Omega$. Therefore one needs to maximize the numerator, $2\pi \int_0^{\theta_{max}} A_E(\theta)\theta d\theta$, a quantity that is often referred to as "grasp", and minimize the background. To go well beyond what has been achieved with the instrumentation that has been designed thus far one needs to operate at three different levels: 1) the experiment design; 2) the observational strategy; 3) the data analysis strategy.

3.1. Experiment design

Let us start by considering the background and in particular the instrumental background, i.e. the part of the background that is not associated to genuine cosmic X-ray photons. A few things can be easily inferred by comparing background spectra from different mission. In Fig. 4 we report a recent compilation of such spectra from Hall et al. (2008). We note that: 1) front illuminated CCDs have lower background than background illuminated ones and that 2) the background on the low earth orbit is smaller than that in the high orbit. In this respect it is particularly instructive to compare the EPIC MOS with the *SWIFT* XRT background, since we are dealing with virtually the same detector in a high and low earth orbit. As shown in Hall et al. (2008), the *SWIFT* XRT background is about a factor 3 lower than the EPIC MOS background. Thus, from the inspection of Fig. 4 we learn that to keep the instrumental background low it is preferable to employ front illuminated CCDs on a low earth orbit. There are other issues that should be kept in mind: 1) a non-negligible fraction (say 15%) of the detector should be shielded from the sky, this will allow to constantly monitor the intensity of the instrumental background; 2) a tilted CCD configuration which allows to improve the imaging, will result in fluorescence Si line emission inhomogeneous distributed on the FOV, something similar is observed on MOS EPIC, this can be minimized by studying the most appropriate configuration; 3) while active shielding cannot be applied as long as the detector is a CCD, passive shielding can and should be considered. Most importantly the whole instrumental background issue should be addressed

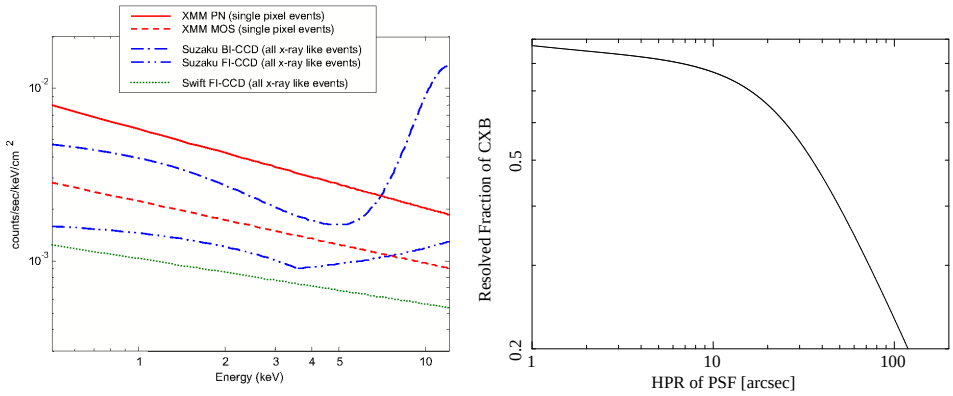

Fig. 4. Left panel: compilation of instrumental background spectra, only continuum components, for various X-ray missions equipped with CCD detectors from Hall et al. (2008). **Right panel:** Resolved fraction of extragalactic cosmic X-ray background as a function of angular resolution.The total background intensity is derived from measures by De Luca & Molendi (2004) and Mc Cammon et al. (2002). The LogN-logS is taken from Moretti et al. (2003). We also include an euclidian component to account for the unresolved 20% of the cosmic X-ray background (CXB). The normalization of this component is conservatively chosen in such a way that about 10% of the CXB is found at fluxes that are sufficiently small to efficiently mimic a diffuse component. The angular resolution necessary to reach a given flux limit is obtained by imposing that the source density at that flux limit is such that there is 1 source every 20 angular resolution elements, where the angular resolution element is a circle with a radius equal to the half-power-radius of the PSF.

from a global point of view. Detailed simulations of the physical interaction between particles and photons with the satellite, possibly complemented by exposures of the detector and associated structures to real particles and high energy photons, can be used to study solutions that will minimize the background.

If the experiment is properly designed then the instrumental background will be low and the cosmic background important. Above $\simeq$ 1 keV the dominant contributor to the cosmic X-ray background is the extragalactic background associated to unresolved sources, mostly AGN. Sufficiently high spatial resolution allows to resolve out a sizeable fraction of the sources producing the X-ray background (see Fig. 4b). With a resolution of 5 arcsec (Half-Power-Ratio, HPR) it is possible to resolve out about 80% of the background, provided of course sufficient counts are available to detect the sources. It should be noted that beyond an angular resolution of 15 arcsec the resolved fraction is not very sensitive to the resolution, see Fig. 4b. Another important point is that, to fully exploit the advantage of a large field of view, it is necessary that the high spatial resolution be available over the full FOV, polynomial optics Burrows et al. (1992) can provide this important feature. Another important contributor to the background is the so called straylight, this is associated to X-ray photons from outside the field of view which end up in the focal plane after reflecting only once on the mirrors. The effect of straylight can be significantly mitigated by introducing a precollimator in front of the telescope as was done in the case of the *XMM-Newton* optics.

3.2. Observing and data analysis strategies

An experiment design like the one described above contributes significantly in improving the sensitivity to low surface brightness emission, however further steps need to be taken to reach cluster outer regions. This is quite apparent when looking at the spectral simulation reported in Fig. 5 (for details see the fig-

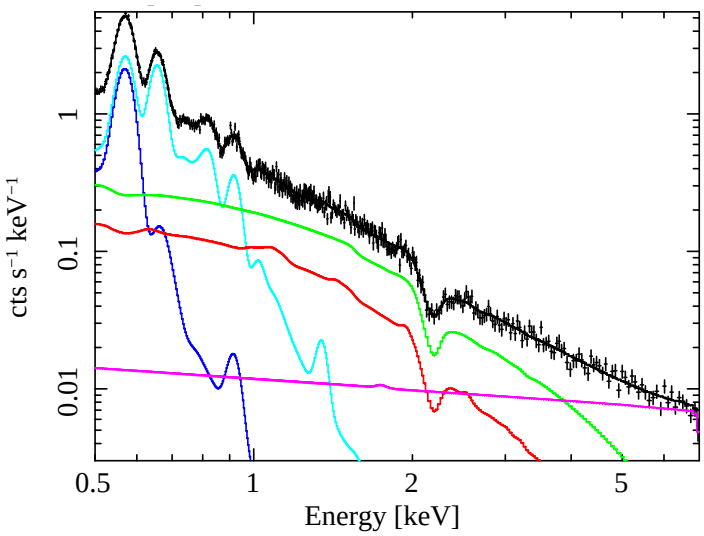

Fig. 5. Simulation of source and background spectra for a typical region at R200. Tne instrumental background estimates come from current missions. The cosmic X-ray background (CXB) is modeled with 3 components, for the soft X-ray background (SXRB) we adopt the modeling of the SXRB from McCammon et al. (2002), who have carried out the highest spatial resolution observation of the SXRB with a sounding rocket flight. The SXRB is modeled by 2 thermal components with temperatures of 0.1 keV and 0.225 keV both with solar abundances, normalizations come from Table 3 of McCammon et al. (2002). For the extragalactic background, comprising mostly unresolved AGNs, we assume a power-law of slope 1.4 and intensity 1/4 of that derived by De Luca & Molendi (2004), thereby assuming that 3/4 of the sources will be resolved out. The source surface brightness is assumed to be 3×10^{-16} erg cm^{-2}s^{-1}arcmin^{-2}, a typical value for cluster outskirts (see Sect. 2.1 for a detailed discussion), the extraction region is 100 arcmin^2, a value of 2×10^{20}cm^{-2} is assumed for the equivalent hydrogen column density, the cluster emission is modeled by a thermal plasma with kT=3 keV and metal abundance Z=0.15 $Z_\odot$, the exposure time was set to 100 ks. The model spectrum was convolved with response files (effective are and redistribution matrix) provided by the *WFXT* team.

ure caption). As can be seen background components of one kind or another dominate the spectrum at all energies. In the 1-3 keV range the source intensity is about 1/3 of the total, below 1 keV the galactic foreground dominates, while above 3 keV the residual extragalactic and the instrumental background do. These are of course estimates, for real clusters things may be a little different, however we will inevitably have a background that outshines the source. These are atypical conditions with respect to previous X-ray imaging missions. To make reliable measures will require devising specific observing and analysis strategies. Clearly the strongest requirement is that the background be characterized as well as possible, ideally one would like to measure the background associated to the source without the source, which is of course impossible. Considering that the instrumental component varies with time and that the galactic foreground varies with position on the sky, it is important to observe the background almost at the same time and almost at the same location of the source. A similar strategy has been adopted, albeit for reasons different from the ones considered here, by the *SWIFT* XRT experiment. During each 1.5 hour orbit, *SWIFT* observes a source field and 3 or 4 background fields. Thus background fields are observed almost simultaneously with the source field and with the same instrument set up. Moretti et al.

(2010) have shown that under these conditions the instrumental background can be characterized to the 3% level. Conversely, when background fields from different epochs are used, only a 10-15% level is achieved. The optimal solution that may be applied in a future mission, or on *SWIFT* for that matter, would be to use as part of the background fields, sky regions close to the source and dark earth observations. The former would allow to perform a spatial characterization of the galactic foreground, while the latter would permit a clean measurement of the instrumental background. Observations of both source and background fields need to be conducted to a high precision. Relative systematic errors on the spectra need to be kept at the few percent level. This is not a trivial requirement to meet, particularly since at this level of precision each detector element has to be considered as an independent detector. Assuming that each detector element will be calibrated to a relative precision of $\simeq 5\%$, systematics can be reduced to the desired level by viewing each sky element with a large number of detector elements. Observing strategies such as this have been used for decades in other bands of the electromagnetic spectrum when the source signal is smaller than the background. As examples, one may consider ground based infrared observations or cosmic microwave background measurements.

The comparison of the source plus background spectrum with the background spectrum is typically done via subtraction. In recent years, workers concentrating on cluster outer regions (e.g. Snowden et al. 2008, Leccardi & Molendi 2008) are finding that modeling is more effective. This is readily understood if one considers that the background is made of different components each capable of varying independently of the others. Unless there are good reasons to believe that the particular combination of background components associated to the source and background fields are next to identical, it is preferable to model the different components allowing for variations in relative intensity. Another issue that should be considered is that, under the atypical conditions of cluster outer regions, the standard maximum likelihood estimators commonly employed to derive physical parameters such as emission measure and temperature do not always work properly. In a recent paper (Leccardi & Molendi 2007), we have shown that the presence of a significant background component can lead to a substantially biased measure of the temperature. In the same paper, we describe a few quick fixes. Unfortunately, a general solution, based on a more powerful statistical estimator, has yet to be found.

3.3. A budget for systematics

Assuming that the above guidelines are followed, we expect to be able to maintain systematic errors to within a few percent. In the following, we provide a breakdown of the expected errors. A constant monitoring of the instrumental background by using the part of the detector not exposed to the sky plus dark earth and background field observations entwined with source observations should allow us to constrain this component to about 1% (as extrapolated from the results obtained on *SWIFT* XRT in Moretti et al. 2010). The extragalactic component of the cosmic background is a residual component, comprising unresolved sources and possibly a diffuse component. For a typical flux limit of 10^{-16} erg cm^{-2}s^{-1} in the 0.5-2.0 keV band, montecarlo simulations show that the cosmic variance for a 100 arcmin^2 field is less than 1% of the residual background component. The galactic foreground will be monitored by performing observations of fields contiguous to the source field. Moreover, observations over several 100 arcmin^2 should allow us to characterize this component to about 3-5%. Finally, assuming a typical relative calibration accuracy of 5% on individual detector elements and the application of substantial dithering, we expect to reach an overall relative spectral calibration of about 1%.

Table 1. Relative errors (in percentage) and deviations ϵ from the input values at 90% confidence level on the parameters of interest (normalization K, plasma temperature T and metal abundance Z of an apec component in XSPEC –Arnaud 1996) after joint-fit analysis of spectra simulated with an exposure time of 50 ksec. All the relative errors can be rescaled to different exposure times as $\sim \sqrt{t_{\rm exp}}$. β_{20} indicates a β value increased by 20 per cent. CC (nCC) indicates a (no) Cooling-Cores Cluster. The fluxes f are in units of 10^{-12} erg/s/cm^2 in the band (0.1 − 2.4) keV and are collected from http://bax.ast.obs-mip.fr/.

inputs	K	T	K	T	Z
	fixed Z				
Perseus (TURBOLENT/CC; $z = 0.0178, f = 1137.3, T = 6.3keV, n_{\rm H} = 1.5e21; R_{200} = 1.9$Mpc $= 88.2'$)					
$T = 3.16, Z = 0.15$	8 (+0.2ϵ)	15 (+0.5ϵ)	16 (+0.3ϵ)	17 (−1.3ϵ)	>100
$T = 2, Z = 0.15$	8 (−1.0ϵ)	8 (+0.7ϵ)	17 (−0.1ϵ)	13 (−0.4ϵ)	44 (−0.2ϵ)
$\beta_{20}, T = 3.16, Z = 0.15$	27 (+1.1ϵ)	38 (−0.7ϵ)	66 (+0.4ϵ)	55 (−1.4ϵ)	>100
$\beta_{20}, T = 2, Z = 0.15$	25 (+1.3ϵ)	30 (+0.3ϵ)	51 (+0.9ϵ)	47 (−0.2ϵ)	5 (−1.0ϵ)
A1689 (MERGING/nCC; $z = 0.1810, f = 14.5, T = 10.1keV, n_{\rm H} = 1.8e20; R_{200} = 2.2$Mpc $= 12.2'$)					
$T = 5.05, Z = 0.15$	6 (−0.7ϵ)	23 (+0.5ϵ)	20 (−0.9ϵ)	27 (+1.1ϵ)	>100
$T = 2, Z = 0.15$	6 (+0.1ϵ)	7 (< 0.1ϵ)	13 (+0.2ϵ)	6 (−3.2ϵ)	35 (−1.3ϵ)
$\beta_{20}, T = 5.05, Z = 0.15$	>100	>100	>100	>100	>100
$\beta_{20}, T = 2, Z = 0.15$	55 (+0.2ϵ)	14 (−3.7ϵ)	>100	>100	>100

3.4. Detailed predictions

Our goal is to resolve the physical properties of the ICM in the virial regions making proper use of the *WFXT* (FOV with $R_{\rm WF} \approx 30'$).

Our strategy is to define a set of observations with reasonable exposure time ($\leq$ 50 ksec) that can allow the study of the virial regions through the spatial and spectral analysis with *WFXT*.

First, we select objects with known X-ray properties (flux, temperature, dynamical status) that can be good candidates for a single *WFXT* exposure, i.e. with an expected $R_{200} < R_{\rm WF} = 30'$. We can also relax a bit this assumption requiring however that a given exposure minimizes the risks in term of (i) problems of intercalibration with other X-ray observatories for measurements in known X-ray emitting regions, (ii) weak constraints on the X-ray properties at R_{200} due to the effect of unexpected large scale structures.

We estimate R_{200} from a given spectroscopic measurement of the gas temperature by using the best-fit results in Arnaud et al. (2005, cf. Table 2; similar results in Vikhlinin et al. 2006):

$$R_{200} = 1714 \times (T_{\rm gas}/5{\rm keV})^{0.5}\, E_z^{-1} h_{70}^{-1}\ {\rm kpc} \quad (1)$$

with $E_z = \left[\Omega_{\rm m}(1+z)^3 + \Omega_\Lambda\right]^{0.5}$ and $\Omega_{\rm m} = 1 - \Omega_\Lambda = 0.3$.

By applying the criterion $R_{200} < R_{\rm WF} = 30'$, we select 23 out of the 45 objects present in the flux-limited sample of the brightest clusters in Mohr et al. (1999; see Fig. 6)). More objects can be included if off-axis exposures are considered, as requested for the Perseus cluster with a R_{200} of $\sim$ 88 arcmin.

The response matrix used for our simulations is obtained by convolving the redistribution matrix with a mean effective area, $\overline{A(E)}$, constructed by averaging the vignetting over the whole field of view, i.e.

$$\overline{A(E)} = A_o(E) \cdot \frac{2\pi \int_0^{\theta_{max}} \theta\, d\theta\, V(E,\theta)}{\pi\theta_{max}^2},$$

where $A_o(E)$ is the energy dependent on-axis effective area, θ_{max} is maximum off-axis angle and $V(E,\theta)$ is the energy and off-axis dependent vignetting. The redistribution matrix,

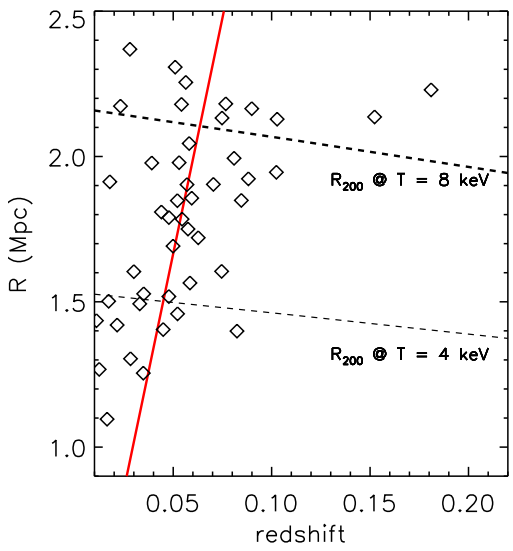

Fig. 6. Predicted R_{200} for the 45 objects in Mohr et al. (1999) compared to $R_{\rm WF} = 30'$ (red solid line) and the expected R_{200} for a typical cluster with a temperature of 4 and 8 keV (dashed lines). R_{200} are estimated from eq. 1.

the on-axis effective area and the vignetting were kindly provided by the *WFXT* team. We use our own script with the response matrix to simulate a *(source+background)* and a *(background only)* spectrum including in the latter one (i) a 1 per cent random fluctuation in absorbing $n_{\rm H}$ value and in the normalization of the instrumental background; (ii) a 5 per cent random fluctuation propagated to the normalization and temperature values of the two local background component (one absorbed, the other not), to the normalization and photon-index value of the CXB. The photon-index is allowed to vary between 1.4 and 1.6. We assume that 80 per cent of the CXB is resolved.

The spectra are integrated for 50 ksec over an area of 100 arcmin^2 and then jointly fitted in the range $0.3-6$ keV.

The surface brightness in the band $(0.5-2)$ keV are obtained from the best-fit values in Table 2 of Mohr et al. (1999) by evaluating the model prediction at R_{200} as estimated in equation 1. A more conservative estimate of the surface brightness is obtained by increasing the β value by 20 per cent, faking an expected steepening of the surface brightness profile in the cluster outskirts, as recent observations and simulations suggest (see Section 2). This correction reduces the predicted surface brightness by a factor of 7 on average.

All the simulated spectra assume a metallicity of $0.15Z_\odot$ and a temperature equal to 0.5 (see Roncarelli et al. 2006) times the quoted value in Table 1 of Mohr et al. (1999). We also consider the cases with metallicity equal to $0.05Z_\odot$ and temperature of about 0.25 times the quoted values (i.e. between 1 and 2 keV).

Our simulated spectra (e.g. Fig. 5) show that we can reach typical uncertainties (90% level of confidence) of $\leq 20\%$ on the normalization K and temperature T of the thermal spectra (see Tab. 1). Reasonable constraints ($\sim 40\%$) on the metallicity Z can be obtained in the case the surface brightness profile in the outskirts is still well reproduced from the models fitted to *ROSAT* PSPC data.

A steepening of the surface brightness profiles, as expected from the work discussed in Sect. 2 and modeled here by increasing the value of the outer slope β by 20 %, reduces significantly the level of accuracy to which we can constrain the physical parameters: about 60 per cent (relative error at 90% level of confidence) on K, 40 per cent on T, no constraints on Z.

4. Future missions & *WFXT*

In this section we provide an overview of missions under study or construction that may provide important contributions to the characterization of cluster outer regions. There are 3 such missions namely SRG, *XENIA* and *WFXT*. The eROSITA experiment Predehl et al. (2007) on board the Russian Spektrum Roentgen Gamma (SRG) satellite comprises 7 telescopes with a total on-axis effective area of 2000 cm^2, an on-axis angular resolution of 25 arcsec and will operate from an L2 orbit. *XENIA* Hartmann et al. (2009) carries an X-ray imager and spectrometer that would both be useful in characterizing cluster outskirts: the imager has an on-axis effective area of 600 cm^2 and an on-axis angular resolution of 15 arcsec; the spectrometer has an unprecedented spec-

tral resolution of a few eV, an on-axis effective area of about 1000 cm^2 and an angular resolution that is limited by the pixel size of a few arcmin. *WFXT* Murray et al. (2010) which, like *XENIA*, has been submitted to the *Astro2010: The Astronomy and Astrophysics Decadal Survey*, carries an X-ray imager comprising 3 telescopes for a total on-axis effective area of 6000 cm^2, and an on-axis angular resolution of 5 arcsec. A low earth equatorial orbit is forseen for both *XENIA* and *WFXT*.

Both the *XENIA* and *WFXT* imager have two considerable advantages over eROSITA, namely the low earth over the L2 orbit and the polynomial optics, which will result in a substantial reduction of the instrumental and cosmic X-ray background, respectively. In particular, the *WFXT* imager will provide the characterization of the cluster outer regions in about 1/10 of the time requested from *XENIA*, and will benefit from higher angular resolution. *XENIA* however, is in the unique position to complement the imager data with high spectral resolution data for relatively bright clusters. While eROSITA is scheduled for launch in 2012, *XENIA* and *WFXT* are both at an early stage of development and have to be considered as the next generation satellites for clusters studies.

5. Summary

Past and current X-ray mission allow us to observe only a fraction of the volume occupied by the ICM. Indeed, typical measures of the surface brightness, temperature and metal abundance extend out to a fraction of the virial radius. The coming into operation of the second generation of medium energy X-ray telescopes at the turn of the millennium, has resulted in relatively modest improvements in our ability to characterize cluster outskirts. Even though recent results from *Suzaku* show some improvement, the most sensitive instrument to low surface brightness to have flown thus far is quite possibly the *SWIFT* XRT which, ironically, never had cluster outer regions as one of its top scientific objectives.

The construction of an experiment capable of making measures out to R_{200} is well within the reach of currently available technology. What is required is an experiment design that will minimize the background, both instrumental and cosmic, and maximizes the grasp, i.e. the product of effective area and FOV. Since cluster emission in the outskirts will be background dominated, instrument design and observational strategy should also allow for a meticulous characterization of the background. Detailed simulations based on realistic estimates of the different spectral components and of the precision with which the may be determined shows that an experiments such as the one we envisage will allow a solid characterization of cluster outskirts. From what we can surmise *WFXT* is already designed to meet most of the requirements which are necessary to characterize cluster outskirts, and should have no major difficulty in accommodating the remaining few.

Acknowledgements. We acknowledge the financial contribution from contracts ASI-INAF I/023/05/0 and I/088/06/0.

References

Allen S.W., Schmidt R.W., Fabian A.C. 2001, MNRAS, 328, L37
Allen S.W., Schmidt R.W., Fabian A.C. 2001, MNRAS, 328, L37
Arnaud K.A. 1996, Astronomical Data Analysis Software and Systems V, eds. Jacoby G. and Barnes J., p17, ASP Conf. Series volume 101
Arnaud M., Pointecouteau E., Pratt G.W. 2005, A&A, 441, 893
Balestra I. et al. 2007, A&A, 462, 429
Baldi A. et al. 2007, ApJ, 666, 835
Bautz M.W. et al. 2009, PASJ, 61, 1117
Burrows et al. 1992, ApJ, 392,760
David L.P. et al. 1996, ApJ, 473, 692
De Grandi S., Molendi S. 2001, ApJ, 551, 153
De Grandi S., Molendi S. 2002, ApJ, 567, 163
De Grandi S. et al. 2004, A&A, 419, 7
De Luca A., Molendi S., 2004, A&A, 419, 837
Ettori S., Balestra I. 2009, A&A, 496, 343
Fabjan D. et al. 2010, MNRAS, 401, 1670
Finoguenov A., David L.P., Ponman T.J. 2000, ApJ, 544, 188
George M.R. et al. 2009, MNRAS, 395, 657

Giacconi et al. 2009, *Science White Paper* n.90, US Astro2010 Decadal Survey (arXiv:0902.4857)
Hall D. et al. 2008, *High Energy, Optical, and Infrared Detectors for Astronomy III*, ed. by Dorn D.A.; proceedings of the SPIE, Vol. 7021, p. 58
Hartmann et al. 2009, *Science White Paper* n.114, US Astro2010 Decadal Survey
Hickox R.C., Markevitch M. 2006, ApJ, 645, 95
Hoshino A. et al. 2010, PASJ, in press (arXiv:1001.5133)
Irwin J. A., Bregman J. N., Evrard A. E. 1999, ApJ, 519, 518
Leccardi A., Molendi S. 2008, A&A, 486, 359
Leccardi A., Molendi S. 2008, A&A, 487, 461
Leccardi A., Molendi S. 2007, A&A, 472, 21
Markevitch M. et al. 1998, ApJ, 503, 77
McCammon D. et al. 2002, ApJ, 576, 188
Moretti A. et al. 2003, ApJ, 588, 696
Moretti A. et al. 2010, in prep.
Murray et al. 2010, *AAS Meeting*, Bulletin of the American Astronomical Society, Vol. 41, p.520
Neumann D.M. 2005, A&A, 439, 465
Pratt G.W. et al. 2007, A&A, 461, 71
Predehl P. et al. 2007 SPIE, 6686, 36
Reiprich T.H. et al. 2009, A&A, 501, 899
Roncarelli M. et al. 2006, MNRAS, 373, 1339
Snowden S.L. et al. 2008, A&A, 478, 615
Vikhlinin A., Forman W., Jones C. 1999, ApJ, 525, 47
Vikhlinin A. et al. 2005, ApJ, 628, 655
Vikhlinin A. et al. 2006, ApJ, 640, 691
Voit G.M. 2005, AdSpR, 36, 701
White D.A. 2000, MNRAS, 312, 663

Mem. S.A.It. Suppl. Vol. 17, 60

Memorie della
Supplementi

Metal content in Galaxy Clusters cool-cores: an XMM-Newton study, and future prospects

S. De Grandi[1], S. Molendi[2] and F. Gastaldello[2]

[1] Istituto Nazionale di Astrofisica – Osservatorio Astronomico di Brera, Via E. Bianchi 46, e-mail: sabrina.degrandi@brera.inaf.it I-23807 Merate (LC), Italy
[2] Istituto Nazionale di Astrofisica – Istituto di Astrofisica Spaziale e Fisica Cosmica, Via Bassini 15, I-20133 Milano, Italy

Abstract.
We carried out a detailed study of the Si, Fe and Ni abundances in the cool cores of a representative sample of local galaxy clusters using *XMM-Newton* data. We first evaluated the systematic errors on the abundance measurements that are related to the instruments, the plasma codes and the spectral modeling. We then used the Si/Fe and Ni/Fe abundance ratios to revisit the relative contribution of type Ia and core-collapsed supernovae to the enrichment process taking into account the uncertainties on both the measured abundances and the current theoretical supernovae yields. *WFXT* will push forward sensibly abundance studies of the kind described in this paper: first by increasing dramatically the number of objects with adequate photon statistics and secondly, by means of an improved spatial resolution will allows us to study galaxy cluster cores at redshifts up to 1.

Key words. galaxies: cluster: general – galaxies: fundamental parameters – intergalactic medium – X-ray: galaxies: abundances – cosmology: observations – dark matter

1. Introduction

The detection of metal lines from X-ray observations of the intra-cluster medium (ICM) indicates that it does not have a primordial chemical composition but was enriched with material processed in stars. The measurement of heavy element abundances present in the ICM can provide important clues on the chemical evolution inside galaxy clusters.

The measurement of the abundance of an element from the X-ray spectrum is a conceptually simple process since the number of ions of the elements with respect to the number of protons is directly proportional to the equivalent width of the emission line produced by the element itself. This one-to-one correspondence is possible because the X-ray emitting plasma is optically thin and in collisional equilibrium. In practice, various sources of uncertainties are involved in the conversion process, such as the accuracy of the atomic physics, the moderate spectral resolution of the current imaging instruments which often results in line blending from both different ions of the same element or from different elements, and the presence of temperature gradients in the ICM, especially in cluster cores, that needs specific spectral modeling.

Send offprint requests to: S. De Grandi

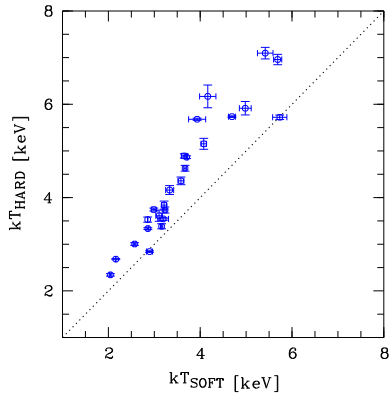

Fig. 1. ICM temperatures in the cool-core regions of the clusters in our sample measured with single-temperature models from the soft (0.7-3 keV) and the hard (2-10 keV) bands. As expected in case of multi-temperature ICM the two temperatures differ with the one derived from the hard band being higher with respect to the temperature derived from the soft band.

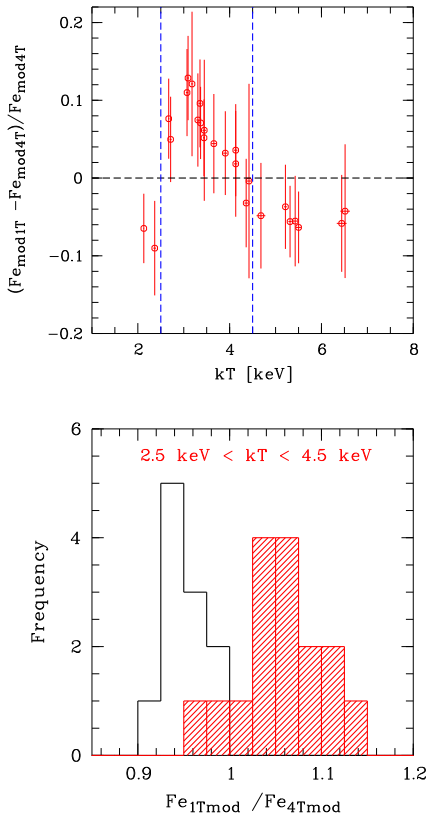

Fig. 2. Upper panel: relative differences between Iron measured in the cluster cool cores with a single temperature model and a multi-temperature model as a function of the temperature. The temperature in the x-axis is the one from the single temperature model measured in the broad band. The dashed lines highlighted the region between $\sim 2.5-4.5$ keV where the inverse Fe-bias is present, details on the iron biases are given in the text. **Lower panel**: histogram of the ratio between iron derived from single and multi-temperature models for the same clusters. The dashed region refers to clusters with temperatures in the 2.5 – 4.5 keV range.

With *Chandra* and *XMM-Newton* statistical errors on the derived abundances have greatly decreased, however only little attention was devoted to the characterization of systematic errors which, under some circumstances, are likely to play an important role.

The goal of this study was firstly to provide robust estimates of chemical elements, namely Si, Fe and Ni, in the cores of nearby and bright cool core clusters. In this context robust means the we included in the error budget also a careful evaluation of systematic uncertainties. Secondly, we used the derived metal abundances to study the abundance and abundance ratios (i.e Si/Fe and Ni/Fe) distributions for a well defined sample of clusters, and, finally, we provided a critical assessment of the relative role of SN types including uncertainties associated to current theoretical SN yields.

We decided to focus on the measurement of global abundances from the very central regions of cool core clusters since these regions provide us with the maximum photon statistic available due to their very intense surface brightness peaks. This allowed us to explore systematic uncertainties affecting the derived elements in great details (De Grandi & Molendi 2009).

We considered a subsample of 26 cool-core galaxy clusters from the B55 sample (Edge et al. 1990), and extracted spectra from the central regions within $0.5r_{cool}$ radius, where r_{cool} is the cooling radius taken for each cluster from the work of Peres et al. (1998). For our purposes half the cooling radius is a good sampling of the core region and has the advantage to be always within the EPIC field of view in all the clusters of our sample.

2. The systematic errors analysis

Details on the analysis can be found in (De Grandi & Molendi 2009). Here we report our main findings.

1. The cross-correlation between metal abundances acquired independently with the 3 EPIC detectors shows that to reconcile Si and Fe measurements we require a 3% systematic error.
2. Almost all core spectra show evidence of multi-temperature structure. For example applying a single temperature model on the two independent hard, 2-10 keV, and soft, 0.7-3 keV, energy bands gives significantly different temperatures for the ICM (with the temperature measured from the hard band larger than that measured from the soft one as expected in case of multi-temperature structure, see Fig. 1). We have therefore applied different multi-temperature models to the core spectra and investigated the systematic uncertainties due to the different modellization. We found that systematic uncertainties associated to the different spectral modeling, namely a 2 versus a 4 temperatures models, are below $2-3\%$.
3. In the *xspec* package there are two spectral codes, MEKAL and APEC. We have found that the two codes return somewhat different abundance values. We find that: Fe is almost unchanged, $\mathrm{Fe}_{apec}/\mathrm{Fe}_{mekal} = 1.05 \pm 0.01$; Si is somewhat higher, $\mathrm{Si}_{apec}/\mathrm{Si}_{mekal} = 1.11 \pm 0.02$ and Ni is lower, $\mathrm{Ni}_{apec}/\mathrm{Ni}_{mekal} = 0.82 \pm 0.04$. The Si/Fe ratio, as measured with *apec*, is slightly higher than that estimated with *mekal*, $(\mathrm{Si/Fe})_{apec}/(\mathrm{Si/Fe})_{mekal} = 1.06 \pm 0.02$, while Ni/Fe is substantially lower, $(\mathrm{Ni/Fe})_{apec}/(\mathrm{Ni/Fe})_{mekal} = 0.77 \pm 0.04$.
   In summary, we found that the systematic uncertainties related to the two emission codes are comparable to those associated to cross-calibration between EPIC detectors in the case of Fe (5%) and Si/Fe (6%), whereas they are the dominant source of uncertainties in the case of Si (10%), Ni (15%) and Ni/Fe (20%).
4. A single temperature analysis of a multi-temperature region, such as the one found in cool cores, leads to a biased Fe abundance (see Fig. 2). Below $\sim$ 2 keV and above $\sim$ 4 keV the measured Fe is *too low* with respect to a correct multi-temperature spectral analysis. This bias was already identified by Buote (2000a,b) for poor clusters and groups with ICM temperatures below $1-2$ keV. On the contrary, in the range between $\sim 2-4$ keV the measured Fe from a single temperature model is too high. This "inverse" Fe-bias was recently found both in a cluster simulation (Rasia et al. 2008), in the central regions of the Hydra A cluster (Simionescu et al. 2009) and A2028 (Gastaldello et al. 2009, 2010) clusters. In our sample we find that, although iron biases are present at any temperature above 2 keV, the total effect is always smaller than $10\%-15\%$, at any temperature (see Fig. 2).

2.1. Results on Abundance Measurements

The Si, Fe, Ni, Si/Fe and Ni/Fe distributions of the sample show moderate spreads (20%-30%) around their mean values (see Fig. 3) suggesting a similar ICM enrichment process at work in all cluster cores. Moreover, the mean Si, Fe and Si/Fe of our sample and their relative scatters are very similar to the values found for a sample of galaxy groups (Rasmussen & Ponman 2007) and a sample of X-ray luminous early type galaxies (Humphrey & Buote 2006). This suggests that, whatever the real proportion between different SNe types may be, the enrichment process of the hot gas associated to elliptical galaxies is likely the same in iso-

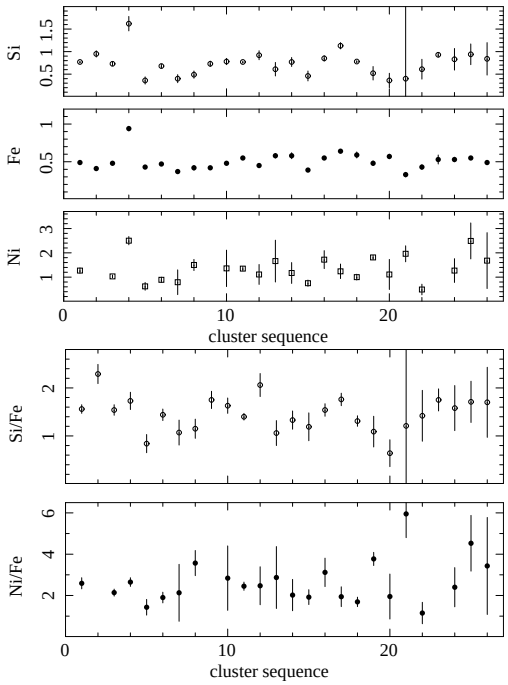

Fig. 3. Upper panel: Si, Fe, Ni abundance distributions within $r < r_{cool}/2$ for the sample. **Lower panel**: Si/Fe and Ni/Fe abundance ratio distributions within the same radius as above (abundances are all relative to Anders & Grevesse (1989) solar units).

lated ellipticals, dominant galaxies in groups and BCGs in clusters.

2.2. SN type Ia versus SN core-collapsed

We constrain the relative contribution of SNe using our observed Si/Fe, Ni/Fe and SN yields from theoretical works. We note that while errors on the observed abundance ratios are of the order of $\sim 5\%$, various sets of yields are reported in the literature, for both SN type Ia and SN core-collapsed (Woosley & Weaver 1995; Iwamoto et al. 1999; Chieffi & Limongi 2004; Nomoto et al. 2006) whose associated uncertainties are of the order of tens of % (Gibson et al. 1997; Young & Fryer 2007). We therefore estimate the relative contribution of SNe, including both uncertainties on the observed abundance ratios *and* on the theoretical yields. Assuming a 20% error on the yields we find that the SNIa Fe-mass-fraction overall permitted range is 0.48-0.79 and that the dominant source of uncertainty in the estimate of the SNIa Fe-mass-fraction are the errors on the yields.

From the SNIa Fe-mass-fraction we derived a SNIa number fraction, defined as the number of SNIa over the total number of SNe, which is between 0.10 and 0.38. This number fraction cannot be reconciled with 0 or 1, as we would need errors of 50% in the yields to reproduce 0 and errors up to 70% to have 1, which are both quite improbable.

Our conclusion is that the large uncertainties on the currently available yields prevent any precise estimate of the relative contribution of SNIa and SNcc, and that we can only say that they *both* concur to the enrichment process in cluster cool-cores.

We have shown how difficult is to determine the relative contribution of SNe to the ICM enrichment from global cool-core abundance measurements. An alternative approach is to consider radial profiles of metal abundance ratios, in this case variation of the Si/Fe ratio with the radius can be interpreted as evidence for variation of the relative contribution of the two SN types.

Unfortunately, recent works disagree in their conclusions. Finoguenov et al. (2000) using *ASCA* data for a sample of clusters and Rasmussen & Ponman (2007) using *Chandra* observations of a sample of groups found increasing Si/Fe with radius, that implies a radially increasing predominance of SNcc enrichment in the clusters outskirts. On the contrary, Tamura et al. (2004) with a sample of clusters observed with *XMM-Newton* and more recently *Suzaku* observations of various clusters and groups (collected in Fabjan et al. 2010 see their Fig. 13 and references therein) found flat Si/Fe profiles. Therefore this subject needs further investigation. This specific subject leaves space for great improvement with *WFXT* given its predicted high performances in observing the outermost cluster regions (see contribution of Ettori & Molendi in this Proceedings). *WFXT* will also allow to

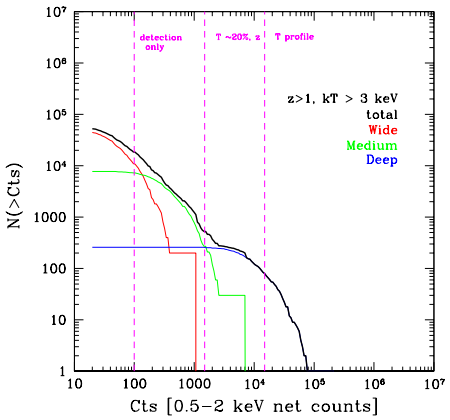

Fig. 4. Number of galaxy clusters (kT > 3 keV) that are at redshift larger than 1 in the three, wide (red line), medium (green line) and deep (blue line), surveys and their sum (black line) as a function of the total counts in the soft 0.5-2.0 keV band (P. Tozzi private comm.).

extend the study of abundance ratios to distant clusters.

2.3. A few quantitative estimates

In order to be more quantitative, we roughly estimate the number of clusters for which we can measure the temperature and abundances in one or two bins with the help of Fig. 4 (P. Tozzi private comm.). This Figure shows the expected number of clusters of galaxies (kT > 3 keV) and at $z > 1$ observed in the three surveys of *WFXT* as a function of the total source counts in the soft 0.5-2. keV band. We assume that a number of source counts between 2000 and 6000 are sufficient to achieve our scientific purpose. From Fig. 4 we estimate that 2000 counts can be collected for about 100 clusters in the medium survey and for about 300 clusters in the deep one, whereas 6000 counts can be acquired for 30 and 250 clusters in the medium and deep survey, respectively. We convert these counts (2000 and 6000 cts) in the corresponding fluxes by using the conversion factor for extended sources in the soft band computed by P. Tozzi in these same Proceedings, which is 2.22×10^{-13} (see Table 1 in P. Tozzi & the WFXT team: "*WFXT* simulations"). In the medium survey 2000 cts correspond to fluxes of $\sim 3.4 \times 10^{-14}$ erg s^{-1} cm^{-2} and 6000 cts to a flux of $\sim 1.0 \times 10^{-13}$ erg s^{-1} cm^{-2}, whereas in the deep survey 2000 cts correspond to a flux of $\sim 1.1 \times 10^{-15}$ erg s^{-1} cm^{-2} and 6000 cts to a flux of $\sim 3.3 \times 10^{-15}$ erg s^{-1} cm^{-2}. All these fluxes are well above the flux limit for extended sources of the medium (i.e., $\sim 1.44 \times 10^{-15}$ erg s^{-1} cm^{-2}) and deep ($\sim 0.2 \times 10^{-15}$ erg s^{-1} cm^{-2}) surveys (see Table 3 always in P. Tozzi & the WFXT team: "*WFXT* simulations"). Moreover, in the deep survey we will obtain a considerable sample of clusters, i.e. about hundred or more, with 10^4 net counts (see Fig. 4), corresponding to a soft band flux of 5.6×10^{-14} erg s^{-1} cm^{-2}, for which it will be possible to study temperature and abundances profiles in more than 2 bins. For comparison to the local sample of cluster cool-cores analyzed in our *XMM-Newton* work, we consider the average cool-core X-ray luminosity (1.5×10^{44} erg s^{-1} in the 2.-10. keV band), temperature (4 keV) and iron abundance (0.5 solar units) and then, by assuming a *mekal* spectral code, we estimate the expected flux for such a typical core shifted at $z = 1$ and in the soft 0.5-2. keV band. The expected flux is 2.6×10^{-14} erg s^{-1} cm^{-2} which roughly corresponds to 2000 cts in the medium survey and 6000 cts in the deep one.

From these estimates we conclude that the medium and deep *WFXT* surveys will allow us to measure the abundances of Fe and Si (Ni will always be outside the *WFXT* energy band at this high redshifts) for a large number of galaxy clusters at redshift around 1 and possibly beyond, this will allow us to extend to higher redshift the scientific topics addressed in the *XMM-Newton* work presented in this contribution.

References

Anders, E. & Grevesse, N. 1989, Geochim. Cosmochim. Acta, 53, 197
Buote, D. A. 2000a, ApJ, 539, 172
Buote, D. A. 2000b, MNRAS, 311, 176

Chieffi, A. & Limongi, M. 2004, ApJ, 608, 405
De Grandi, S. & Molendi, S. 2009, A&A, 508, 565
Edge, A. C., Stewart, G. C., Fabian, A. C., & Arnaud, K. A. 1990, MNRAS, 245, 559
Fabjan, D., Borgani, S., Tornatore, L., et al. 2010, MNRAS, 401, 1670
Finoguenov, A., David, L. P., & Ponman, T. J. 2000, ApJ, 544, 188
Gastaldello, F., Ettori, S., Balestra, I., et al. 2009, ArXiv e-prints
Gastaldello, F., Ettori, S., Balestra, I., et al. 2010, ArXiv e-prints
Gibson, B. K., Loewenstein, M., & Mushotzky, R. F. 1997, MNRAS, 290, 623
Humphrey, P. J. & Buote, D. A. 2006, ApJ, 639, 136
Iwamoto, K., Brachwitz, F., Nomoto, K., et al. 1999, ApJS, 125, 439
Nomoto, K., Tominaga, N., Umeda, H., Kobayashi, C., & Maeda, K. 2006, Nuclear Physics A, 777, 424
Peres, C. B., Fabian, A. C., Edge, A. C., et al. 1998, MNRAS, 298, 416
Rasia, E., Mazzotta, P., Bourdin, H., et al. 2008, ApJ, 674, 728
Rasmussen, J. & Ponman, T. J. 2007, MNRAS, 380, 1554
Simionescu, A., Werner, N., Böhringer, H., et al. 2009, A&A, 493, 409
Tamura, T., Kaastra, J. S., den Herder, J. W. A., Bleeker, J. A. M., & Peterson, J. R. 2004, A&A, 420, 135
Woosley, S. E. & Weaver, T. A. 1995, ApJS, 101, 181
Young, P. A. & Fryer, C. L. 2007, ApJ, 664, 1033

Mem. S.A.It. Suppl. Vol. 17, 66

Memorie della
Supplementi

Are there cool-core clusters at high-redshift? Chandra results and prospects with WFXT

J.S. Santos[1], P. Tozzi[1] and P. Rosati[2]

[1] INAF–Osservatorio Astronomico di Trieste, Via Tiepolo 11, I-34131 Trieste, Italy
e-mail: jsantos@oats.inaf.it
[2] European Southern Observatory

Abstract. Cool core clusters are characterized by strong surface brightness peaks in the X-ray emission from the Intra Cluster Medium (ICM). This phenomenon is associated with complex physics in the ICM and has been a subject of intense debate and investigation in recent years. The observational challenge of analyzing high redshift clusters and the small sample statistics have prevented an accurate assessment of the population of cool-cores at z >0.5. In this contribution we trace the evolution of cool-core clusters out to $z \sim 1.3$ using high-resolution *Chandra* data of three representative cluster samples spanning different redshift ranges. Our analysis is based on the measurement of the surface brightness (SB) concentration, c_{SB}, which strongly anti-correlates with the central cooling time and allows us to characterize the cool-core strength in low S/N data. We confirm a negative evolution in the fraction of cool-core clusters with redshift, in particular for very strong cool-cores. Still, we find evidence for a large population of well formed cool-cores at $z \sim 1$. This analysis is potentially very effective in constraining the nature and the evolution of the cool-cores, once large samples of high-z clusters will be available. In this respect, we explore the potential of the proposed mission Wide Field X-ray Telescope (WFXT) to address this science case. We conclude that WFXT provides the best trade-off of angular resolution, sensitivity and covered solid angle in order to discover and fully characterize the cool-core cluster population up to z=1.5.

Key words. Galaxy clusters - cosmology: Galaxy clusters - high redshift: observations - X-rays

1. Introduction

The majority of local X-ray clusters show a prominent central surface brightness peak in the intra cluster medium (ICM). The cluster core is also associated with a short cooling time, implying the presence of a cooling flow (Fabian et al. 1994), although the gas is not observed to cool below a minimum temperature of the order of 1/3 of the average value in the ICM, indicating that some heating mechanism counteracts the cooling process. The properties and the formation mechanism of these cool-cores (CC) are an open problem which forces one to consider complex non-gravitational physical processes able to provide smoothly distributed heating on scales of about 100 kpc. A successful model is expected to include phenomena such as removal of radiatively cooled gas, heating by a central radio

source, thermal conduction or other forms of feedback (see Peterson & Fabian 2006).

The impact of cool-cores on the local cluster population has been extensively studied for over a decade (Peres et al. 1998). X-ray observations have established that cool-cores dominate the local clusters, with an abundance of 50 to 70%, depending on the adopted definition of cool-core (e.g. Chen et al. 2007, Dunn & Fabian 2008, Hudson et al. 2009).

The evolution of cool-cores has been measured only up to redshift 0.4. Bauer et al. (2005) reported that the fraction of cool-cores does not significantly evolve up to $z \sim 0.4$, since clusters in this redshift range have the same temperature decrement (about one-third), as the nearby CC's, and their central cooling times are similar. The study of cool-cores at redshift greater than 0.5 is plagued by low statistics, and, so far, is limited to two works. Using the 400 Square Degree Survey (hereafter 400 SD, Burenin et al. 2007) which reaches $z = 0.9$, Vikhlinin et al. (2007) concluded, on the basis of a cuspiness parameter defined as the logarithmic derivative of the density profile, that there is a lack of cool-core clusters, with respect to the local cluster population. In Santos et al. (2008), we adopted a simple diagnostic based on the concentration of the surface brightness (which strongly anti-correlates with the central cooling time), and measured the fraction of cool-cores out to the current redshift limit ($z \sim 1.4$). At variance with previous results, we found a significant fraction of what we term moderate cool-cores.

In this contribution we present our results on the abundance of cool-cores across the entire cluster population, out $z \sim 1.3$, exploiting all the available data in the *Chandra* archive (Santos et al. 2010), and we assess the potential of the next-generation X-ray mission Wide Field X-ray Telescope (WFXT, Giacconi et al. 2009) in measuring the cool-core evolution.

2. Cluster samples

The local cluster sample used in this work is drawn form the catalog of the 400 Square Degree (SD) Survey (Burenin et al. 2007), an X-ray survey which detected 266 confirmed galaxy clusters, groups or individual elliptical galaxies out to $z \sim 1$ using archival ROSAT PSPC observations. The sample is complete down to a flux limit of 1.4×10^{-13} erg s^{-1} cm^{-2}. We extract a subsample of 26 clusters observed with Chandra with $z > 0.05$, in order to be able to sample the surface brightness profiles out to a radius of 400 kpc within the field of view. Hence, our local sample spans the redshift range [0.05 - 0.217].

X-ray images of distant clusters suffer a strong surface brightness dimming ($\propto (1+z)^{-4}$) and have a small angular size, thus the study of their central regions requires the sub-arcsecond resolution provided only by *Chandra*. Beyond redshift 0.5 there are only three X-ray complete cluster samples, all selected from ROSAT PSPC pointed observations. They are: (i) the 400 SD high-z sample which includes all clusters (20) from the 400 SD catalog with $z \geq 0.5$; (ii) the Rosat Deep Cluster Survey (RDCS, Rosati et al. 1998; and (iii) the Wide Angle ROSAT Pointed Survey (WARPS, Jones et al. 1998). While the distant 400 SD sample has been fully observed with Chandra, the RDCS and WARPS samples have been only partially observed with a Chandra follow up. For this reason, we merge them into the RDCS+WARPS sample, containing a total of 15 clusters.

3. Surface brightness concentration

The simplest observational signature of the presence of a cool-core is a central spike in the surface brightness profile. This is also the only possible diagnostic we can apply to high redshift clusters, given the difficulty in performing spectral analysis to detect the temperature decrease in the core region.

In Santos et al. (2008) we defined the phenomenological parameter c_{SB} that quantifies the excess emission in a cluster core by measuring the ratio of the surface brightness within a radius of 40 kpc with respect to the SB within a radius of 400 kpc: $c_{SB} = SB(r < 40kpc)/SB(r < 400kpc)$. This simple parameter has been shown to be robust and particularly useful when dealing with the low S/N data of distant clusters. We validated the red-

shift independence of c_{SB} (apart from possible K-corrections as described in Santos et al. 2010) by cloning low-z clusters to high redshift. After this detailed investigation, we propose the use of c_{SB} as the best proxy for the cool-core stength in the high-z range.

Before comparing the c_{SB} distribution of local and distant samples (400 SD high-z and RDCS+WARPS), we compare the two distant samples separately in Figure 1, top panel. Quite unexpectedly, the shape and range of the two high-z c_{SB} distributions are statistically different. We perform a K-S test and find a null hypothesis probability of 0.6%, implying that the two distant samples do have different distributions of cool-core strength. The 400 SD high-z reaches $c_{SB} = 0.10$, with median $c_{SB} = 0.043$, whereas the RDCS+WARPS reaches $c_{SB} = 0.15$, with a median c_{SB} value equal to 0.082. The RDCS+WARPS clusters have thus a significantly higher surface brightness concentration with respect to the 400 SD clusters.

Since both the RDCS+WARPS and the 400 SD are samples based on ROSAT data, we argue that this c_{SB} difference is likely due to different selection criteria used in the 400SD survey, resulting in a bias against compact clusters with a relatively high surface brightness. To check for these effects, we need to go through a detailed comparison of the selection criteria in the three surveys, a task that goes beyond the scope of this work. In order to investigate the evolution of the cool-cluster population, we decide to use the RDCS+WARPS only.

The c_{SB} distribution of the local sample (Figure 1, bottom) spans a broad range of values and reaches c_{SB}=0.315, with a significant peak at low c_{SB} and a median c_{SB} equal to 0.079. We performed a K-S test to the local and distant RDCS+WARPS samples and found a null hypothesis probability of 16%, implying that the two samples have a non-negligible probability to be statistically similar. Our findings are compatible with a significant population of cool-core clusters already well established at redshift $z \sim 1.3$ (5 Gyr after the Big Bang), while strong cool-cores ($c_{SB} > 0.150$) must wait for a longer time span before they can develop. To reinforce these results, it is necessary to use larger samples of high-z clusters.

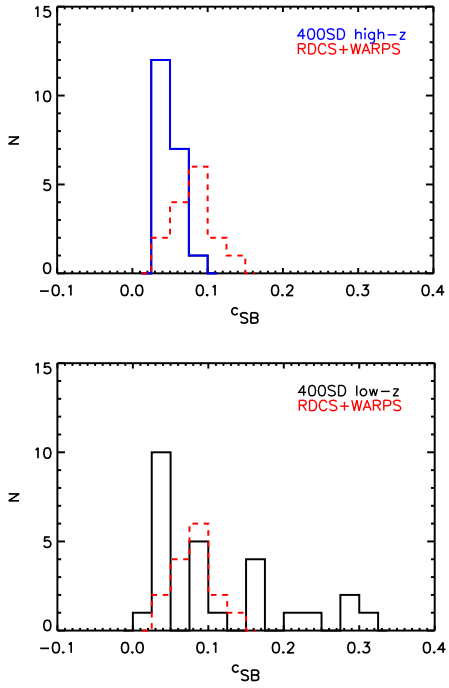

Fig. 1. Comparison of the distribution of c_{SB} of the distant samples (top) and of the local and RDCS+WARPS samples (bottom).

4. Central cooling time

The central cooling time is the measure most often used to quantify cool-cores, as it provides a time-frame for the evolutionary state of the gas. Adopting an isobaric cooling model for the central gas, t_{cool} can be computed as:

$$t_{cool} = \frac{2.5 n_g T}{n_e^2 \Lambda(T)}, \quad (1)$$

where $\Lambda(T)$, n_g, n_e and T are the cooling function, number density of ions and electrons, electron number density and temperature, respectively (Peterson & Fabian 2006). Using the global cluster temperature we obtained the central cooling time measured at a radius of 20 kpc. The local clusters span a

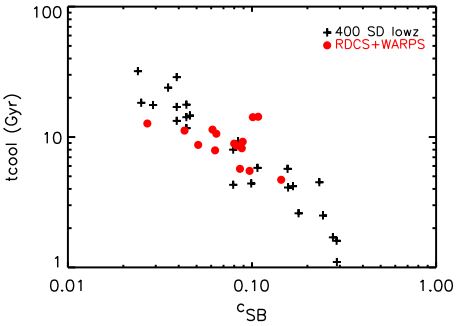

Fig. 2. Correlation between central cooling time and the phenomenological parameter c_{SB} for the local (crosses) and the high-z (filled cirles) samples.

wide range of ages [0.7 - 32.6] Gyr, whereas the RDCS+WARPS sample is limited to [4.7 - 14.3] Gyr.

The local clusters span the wide range of ages [0.7 - 32.6] Gyr, whereas the RDCS+WARPS sample is limited to [4.7 - 14.3] Gyr. The fraction of clusters with a central cooling time lower than the age of the Universe at the cluster redshift is: 58% in the local sample; 27% in the RDCS+WARPS, and 10% in the 400 SD high-z. However, a more meaningful quantity would be the cooling time normalized to the age of the cluster, defined as the time elapsed since the last major merger event. Considering the age of the Universe at z_{obs} is misleading, as this is a loose upper bound on the age of the cluster.

We confirm a strong anti-correlation between t_{cool} and c_{SB} (see Fig. 2), quantified by a Spearman rank test with coefficient ρ=-0.84.

5. The potential of WFXT to measure the evolution of cool-cores

With the present work we show that we can explore the population of cool-core clusters up to the highest redshift where X-ray clusters are selected, by exploiting the archive of *Chandra*. This is possible thanks to the exquisite angular resolution of *Chandra*, which allows us to sample the cool core region at any redshift with about 10 resolution elements. The only way to improve the present work is to add serendipitously discovered high-z clusters followed-up with deep *Chandra* observations. The number of $z > 1$ X-ray clusters is slowly increasing as a result of the ongoing surveys with *Chandra* and XMM-Newton. However, sample statistics is not expected to increase significantly without a dedicated wide area, deep X-ray survey. Hence, it is instructive to look into the future X-ray missions to investigate the capability of characterizing the cool-core strength of high-redshift clusters. Unfortunately, no proposed or planned future X-ray facility foresees an angular resolution comparable to that of *Chandra*. However, two future X-ray missions propose a PSF with a 5 arcsec half energy width (HEW) at 1 keV, the International X–ray Observatory and the Wide Field X–ray Telescope.

The International X-ray Observatory (IXO) (see e.g., Bookbinder 2010) is designed to have a great collecting power and high spectral resolution, therefore it will provide very detailed analysis of known or serendipitously discovered clusters, up to high-redshift. However, IXO will not be used in survey mode, but for a limited solid angle, and therefore it would not increase significantly the statistics of high-z cluster samples.

The Wide Field X-ray Telescope (WFXT) is one of the most promising proposed X-ray missions. The expected number of high-z clusters detected in WFXT surveys with signal to noise comparable to that of the cluster sample used in this work (conservatively expressed as a lower bound of 1500 net counts), is shown in Table 1. Simulations of realistic WFXT fields have been produced in order to investigate the accuracy of WFXT in characterizing cool core clusters. We used the cloning tech-

Table 1. Expected number of clusters sources with temperature >3 keV and minimum net counts 1500 in each of the three planned WFXT surveys in two redshift bins.

Survey	**0.5<z<1.0**	**1.0<z<1.5**
Shallow	200	0
Medium	2190	300
Deep	188	94

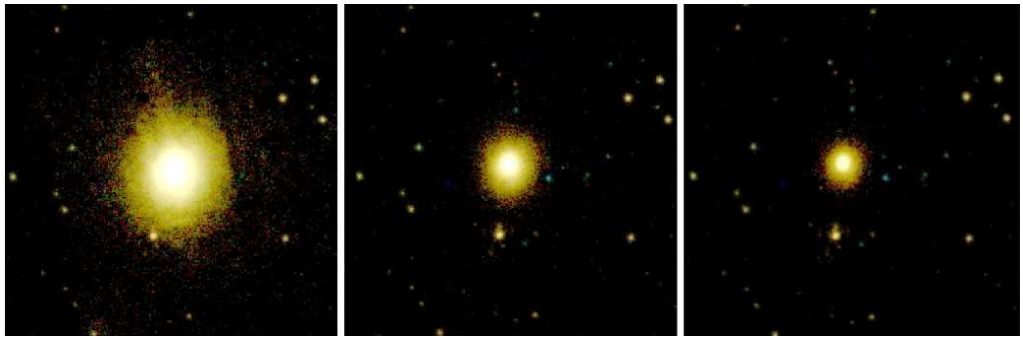

Fig. 3. Simulated WFXT images of the strong cool-core cluster A1835 in the medium survey (13.2 ksec), at redshifts 0.5 (left), 1.0 (middle) and 1.5 (right). The images are 10 arcmin across and are displayed in logarithmic scale.

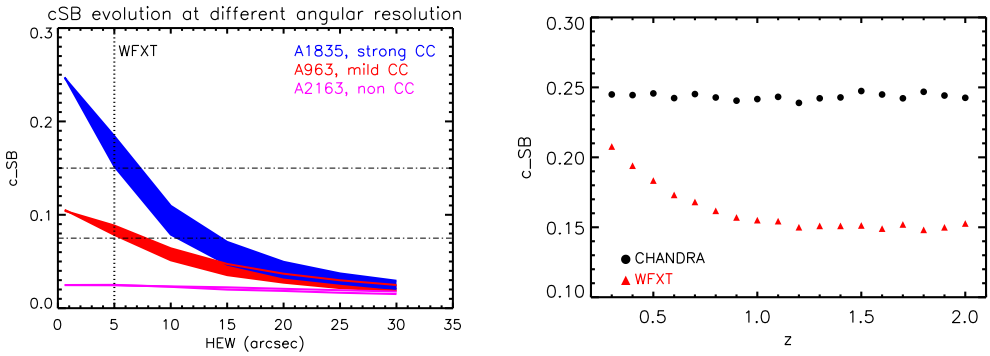

Fig. 4. (Left) Variation of the measured c_{SB} as a function of the telescope HEW for the three typical cases (strong-, moderate- and non-cool core). For each cluster the coloured area is bounded by the c_{SB} value at redshift 0.5 (higher bound) and 1.5 (lower bound). The two horizontal dash-dot lines represent the boundaries between strong CC and moderate CC (upper line, c_{SB}=0.15) and moderate-CC and non-CC (lower line, c_{SB}=0.075). (Right) Comparison between Chandra and WFXT measures of c_{SB} as a function of redshift, for a strong cool-core cluster.

nique (Santos et al. 2008) to simulate WFXT images of three canonical cluster types, corresponding to a typical strong-CC ($c_{SB} > 0.150$, A1835), a moderate-CC ($c_{SB} > 0.075$, A963) and a non-CC ($c_{SB} < 0.075$, A2163) (see Santos et al. 2008 for more details on these clusters), at redshifts 0.5, 1.0 and 1.5. To obtain a quantitative assessment of the cool-core properties of the simulated clusters, we measured c_{SB} in the simulated images.

We first investigated the effect of the angular resolution in the evaluation of the cool-core strength. The result clearly shows that the ability of an instrument to resolve the core and discriminate between a cool-core and non cool-core is compromised for HEW greater than 10″(see Figure 4, left panel). In more detail, the c_{SB} values for the strong cool-core cluster A1835 (Fig. 3) as measured by WFXT are shown in the right panel of Figure 4, in comparison with the values measured by *Chandra*. We notice an apparent evolution in c_{SB} due to the larger angular resolution of WFXT relative to *Chandra*, but we also confirm that the measure of c_{SB} at face-value allows us to assign the different clusters to their own cool-core class (i.e. strong, moderate or non cool-core) at any redshift, as already shown in Figure 4. In this

Fig. 5. The Bullet cluster as observed by WFXT in the deep (400 ksec) survey, at redshifts 0.5 (left), 1.0 (middle), 1.5 (right). Images sizes are 10x10 arcmin.

regime (i.e. HEW=5″), the degradation of the c_{SB} measurement due to the angular resolution is moderate and can be accounted for, while for angular resolution approaching 10″, this effect rapidly increases and make it impossible to measure the cool-core strength (see Fig. 4).

Besides detecting and characterizing distant cool cores, WFXT's angular resolution will also allow sharp features (such as cold front and shocks) to be detected at high-z. This is illustrated with simulations of the well-known Bullet cluster as it would appear in the WFXT deep survey, at redshifts 0.5, 1.0 and 1.5 (see Figure 5).

6. Conclusions

In this contribution we investigated the evolution of cool-core clusters across the entire redshift range currently available, i.e., out to z=1.3. Our analysis is based on the archival *Chandra* data of three cluster samples, and our results are derived mainly from the cluster X-ray surface brightness properties. The distributions of the surface brightness concentration c_{SB} (Fig. 1) show us that: (i) the 400SD and the RDCS+WARPS high-z samples are statistically different: the 400 SD high-z sample appears to miss concentrated clusters; (ii) the distribution of cool-core strength in the local and the RDCS+WARPS samples is rather similar, even though the distant sample lacks very peaked (or strong cool-core with c_{SB} >0.15) clusters.

The distribution of the central cooling time (Fig. 2) in the local sample spans a broad range, 0.7< t_{cool} <32.6 Gyr, where two-thirds of the sample have $t_{cool} < t_{Hubble}$. The RDCS+WARPS sample shows a somewhat different behaviour, displaying a narrower range of cooling times, ([4.7-14.3] Gyr), and a median $t_{cool} \sim$ of 8.9 Gyr. We confirm a strong anti-correlation between c_{SB} and t_{cool}, quantified by a Spearman rank coefficient of ρ=−0.84.

Our results extend the current knowledge of the cool-core population to the most distant X-ray clusters known to date, and show that even at such large lookback times, we detect a significant population of well developed cool cores. A significant advancement in this research can only be achieved when large samples will be available. This will be possible only with the next generation X-ray survey missions. In particular, we showed that WFXT will have the capacity to resolve the central regions of strong cool-cores up to redshifts $z \sim 1.5$. Since WFXT is expected to yield hundreds of new cluster detections at $z \sim 1$, it will add significant constraints to the formation and evolution of cool-cores in galaxy clusters.

References

Bauer, et al. 2005, MNRAS, 359, 1481
Böhringer, H., et al. 2005, ESO Messenger, 120, 33
Bookbinder, J. 2010, arXiv:1003.2847, submitted in response to Astro2010 Decadal Program Prioritization Panel

Burenin, R.A., et al. 2007, ApJS, 172, 561
Cavagnolo, K.W., et al. 2009, ApJS, 182, 12
Chen, Y., et al. 2007, A&A, 466, 805
Dunn, R.J.H. Dunn, & Fabian, A.C. 2008, MNRAS, 385, 757
Fabian, A.C., et al., 1994, MNRAS, 267, 779
Giacconi, R., et al. 2009, astro2010: The Astronomy and Astrophysics Decadal Survey, 2010, 90
Hudson, D.S., et al 2010, A&A 513, A37
Jones, L.R., et al. 1998, ApJ, 495, 100
Peres, C.B., et al. 1998, MNRAS, 298, 416
Peterson, J. R., & Fabian, A. C. 2006, Phys. Rep., 427, 1
Reiprich, T.H., & Boheringer, H. 2002, ApJ, 567, 716
Rosati, P., et al., 1998, ApJ, 492, 21
Santos, J.S., et al., 2008, A&A, 483, 35
Santos, J.S., Tozzi, P., Rosati, P., Böhringer, H., 2010, A&Ain press, arXiv1008.0754
Vikhlinin, A., et al., 2007, Heating versus Cooling in Galaxies and Clusters of Galaxies, 48
Vikhlinin, A., et al. 2009, ApJ, 692, 1033

Mem. S.A.It. Suppl. Vol. 17, 73

Memorie della
Supplementi

Probing the Development of Galaxy Clusters in X rays

A. Cavaliere[1], R. Fusco-Femiano[2], and A. Lapi[1,3]

[1] Dip. Fisica, Univ. 'Tor Vergata', Via Ricerca Scientifica 1, 00133 Roma, Italy.
[2] INAF-IASF, Via Fosso del Cavaliere, 00133 Roma, Italy
[3] SISSA, Via Bonomea 265, 34136 Trieste, Italy.

Abstract. The development of galaxy clusters is discussed basing on our Supermodel, that expresses in full the entropy-modulated, hydrostatic equilibrium of the intracluster plasma in the DM gravitational wells. We relate central entropy levels to energy injections by AGNs or deep mergers, and the outer entropy distribution to the accretion rates of DM and shocked intergalactic gas. We propose these to decline because of the cosmological slowdown in the outskirts growth at late cosmic times. Thus in addition to explaining the CC vs. NCC cores, we propose conditions leading to steep vs. shallow outer temperature declines, and outline related prospects for WFXT and IXO.

Key words. galaxies: clusters: general — X-rays: galaxies: clusters — methods: analytical.

1. Introduction

Galaxy clusters with their overall masses up to $M \sim 10^{15}\, M_\odot$ constitute the largest bound structures in the Universe. Their outskirts extend out to sizes $R \sim$ a few Mpcs, setting the *interface* between the intergalactic environment keyed to the cosmology at large, and the intracluster plasma (ICP; see Cavaliere et al. 2009, hereafter CLFF09). The ICP coexists with the gravitationally dominant dark matter (DM) halo in the baryonic fraction $m/M \sim 1/6$, and the two build up together from accretion across the cluster boundary.

In fact, the cluster buildup takes place in two stages; after an early collapse of the DM and gas to set the cluster body, a secular inside-out development of the outskirts follows (see Zhao et al. 2003; Diemand et al. 2007; Navarro et al. 2010). The body ranges out to radii comparable with r_{-2} where the slope of the DM density distribution equals -2; the adjoining outskirts extend out to the current virial radius R.

After the transition redshift z_t, secular accretion begins; then r_{-2} stays put while R grows larger in a quasi-static DM equilibrium (that may be described via the Jeans equation, see Lapi & Cavaliere 2009a). This implies for the concentration parameter $c \equiv R/r_{-2}$ present values $c \approx 3.5\, H(z_t)/H(z_{\rm obs}) \simeq (1+z_t)/(1+z_{\rm obs})$; these range from 3 to 10, and correspond to *young* or to *old* cluster ages marked by $z_t \sim 0.2 - 3$. The concentration can be directly probed not only with gravitational lensing observations (see Lapi & Cavaliere 2009b), but also in X rays as discussed below.

Send offprint requests to: lapi@roma2.infn.it

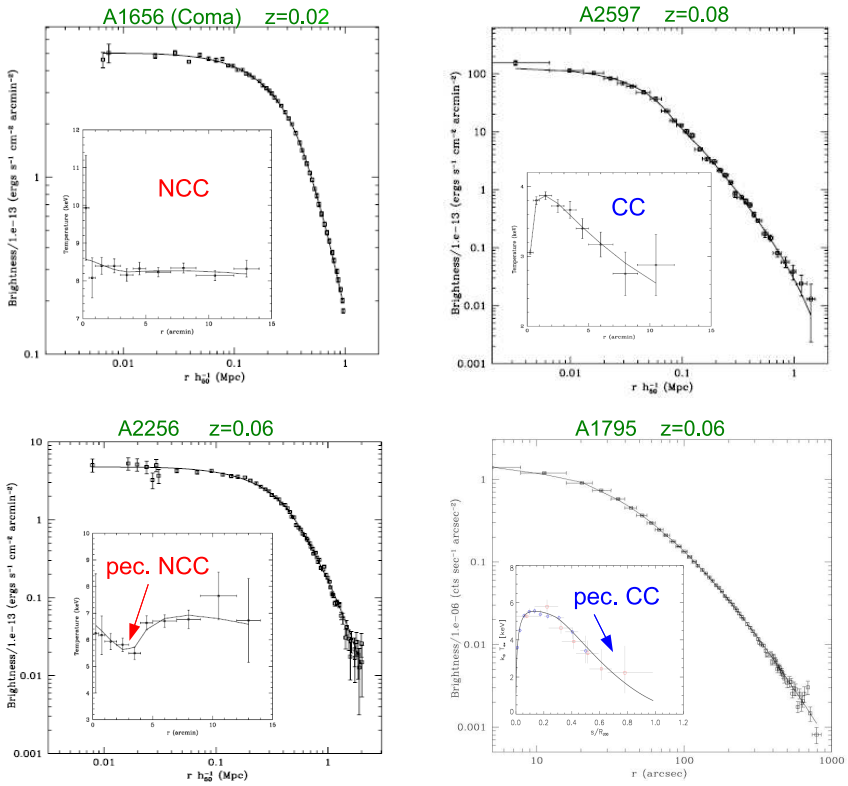

Fig. 1. The cluster Grand Design resulting from two-stage halo development and ICP analyses with the SM, is illustrated with examples of X-ray brightness profiles (projected temperatures in the insets) from Fusco-Femiano et al. (2009) and Lapi et al. (2010). Central entropy marks the CC/NCC dichotomy, while outer production modulates the outskirts.

2. An entropy primer

Secular accretion of intergalactic gas occurs along with DM's; the velocities are supersonic since the temperatures are as low as 10^{-1} keV. Thus much entropy is generated at a radius $r \approx R$ via accretion shocks which provide an effective bounding layer for the ICP (e.g., Lapi et al. 2005; Voit 2005). At the shock, gas inflowing with Mach number $\mathcal{M} \gtrsim 2$ undergoes a temperature jump to $T \propto \mathcal{M}^2$ and an enhancement of the number density n by a factor up to 4.

The ICP specific 'entropy' $k \equiv k_B T/n^{2/3}$ is correspondingly enhanced from intergalactic values of order 10^2 keV cm^2 by factors $\mathcal{M}^2/4^{2/3} \sim 10$. Moving toward the center, we expect the entropy to decrease to some 10^1 keV cm^2 as the temperature $k_B T \approx G m_p M(< r)/r$ goes up from R to $r_{-2} = R/c$ by factors $2-5$, while via adiabatic compression the density grows by several 10^2 to achieve equilibrium within the DM gravitational potential $\Delta\phi$ as outlined by the classic isothermal β-model $n \propto e^{\beta\,\Delta\phi}$, see Cavaliere & Fusco-Femiano (1976).

With such an inferred baseline, we expect significant or even overwhelming central entropy injections from blastwaves launched by AGN outbursts (up to several 10^1 keV cm^2, see Cavaliere et al. 2002; Valageas & Silk 1999; McNamara & Nulsen 2007), and even more by violent deep major mergers (up to several 10^2 keV cm^2, see McCarthy et al. 2007; Markevitch & Vikhlinin 2007). On the other hand, radiative cooling in hydrostatic equilib-

rium (HE) can erode k_c over timescales $t_c \approx 0.3\,(k_c/15\,\mathrm{keVcm}^2)^{1.2}$ Gyr. But AGNs recurring on similar scales may constitute an effective means to prevent a cooling catastrophe (e.g., Voit 2005; Vikhlinin et al. 2006).

3. Central classes and outer regions

To sharpen these estimates, we render the actual entropy run in the form

$$k(r) = k_c + (k_R - k_c)\,(r/R)^a\,, \qquad (1)$$

consistent with recent analyses of wide cluster samples (Cavagnolo et al. 2009; Pratt et al. 2010); this embodies two *specific* parameters: the central level k_c and the outer slope a.

To compute in full the equilibrium of the ICP within the DM gravitational well, we base on our Supermodel (SM; see Cavaliere et al. 2009). An IDL algorithm to implement it may be found at http://people.sissa.it/~lapi/supermodel/.

3.1. Cores, CC vs. NCC

From the latter we have found in CLFF09 that as k_c crosses a threshold around 20 keV cm^2 our temperature profiles *change* from a central drop typical of cool core (CC), to a plateau typical of non-cool core (NCC) clusters (see Molendi & Pizzolato 2001). We find that the latter feature a truly flat central brightness; in the temperatures some still bear the peculiar (if spherically averaged) imprint of a powerful, recently-driven blastwave that prevented or partially erased any cool core (see Fusco-Femiano et al. 2009; Rossetti & Molendi 2010). In addition, we have found that the NCCs are associated with low values of $c \sim 3-5$, and so by all accounts they must be *young*. CCs, on the other hand, generally feature higher concentrations $c \sim 6-10$ and smoother profiles, so they look *older* in age, beyond the cosmic variance.

The resulting Grand Design for galaxy clusters is presented with specific examples in Fig. 1 and caption. Next we focus on the outer structure.

3.2. Outskirts development

The slope a in Eq. (1) describes the powerlaw outward rise expected from the scale-free stratification of the entropy produced at the boundary shock as the cluster grows.

The slope a_R at $r \approx R$ has been derived by CLFF09 from the standard shock boundary conditions and the adjoining HE maintained by thermal pressure, to obtain

$$a_R = 2.4 - 0.47\,b_R\,. \qquad (2)$$

Here $b_R \equiv \mu m_p\, v_R^2/k_B T_R$ marks the ratio of the potential to the thermal energy of the ICP (see Lapi et al. 2005; Voit 2005). This reads $b_R \approx 3/2\,\Delta\phi$ when a strong shock efficiently thermalizes into 3 degrees of freedom the infall energy; the latter is expressed in terms of the potential drop $\Delta\phi$ experienced by successive shells of DM and gas that expand, and turn around at the radius $R_{\rm ta} \approx 2\,R$ to start their infall toward the shock located at R.

At any given cosmic time t, Eq. (2) holds at the current virial radius $R(t)$. On the other hand, the *specific* entropy deposited there is conserved during subsequent adiabatic compressions of the accreted gas into the DM gravitational well, while no other major sources or sinks of entropy occur down to central 10^2 kpc. So as the cluster outskirts develop out to the current $R(t)$, the inner entropy stratifies with a running slope $a(r) = a_{R(t)}$ that retains its original values at the times of deposition.

Standard values $a \approx 1$ (Tozzi & Norman 2001) are recovered on adopting the standard ratio $R/R_{\rm ta} \approx 0.5$, and the potential drop $\Delta\phi \approx 1 - (R/R_{\rm ta}) \approx 0.5$ associated to a top-hat initial mass perturbation $\delta M/M \propto M^{-1}$ that describes the collapse of the cluster *body* as a whole. From Eq. (2) this yields $b_R \approx 2.7$ and $a \approx 1.1$. However, we expect variations of $a(r)$ in the cluster outskirts.

3.3. Expected entropy runs

This is because during the outskirts development the accretion rates $\dot{M}/M \approx d/t\,\epsilon\ drop$, due to two concurring space-time effects: (i) the cosmological slowdown of structure development at late cosmic *times*, described by

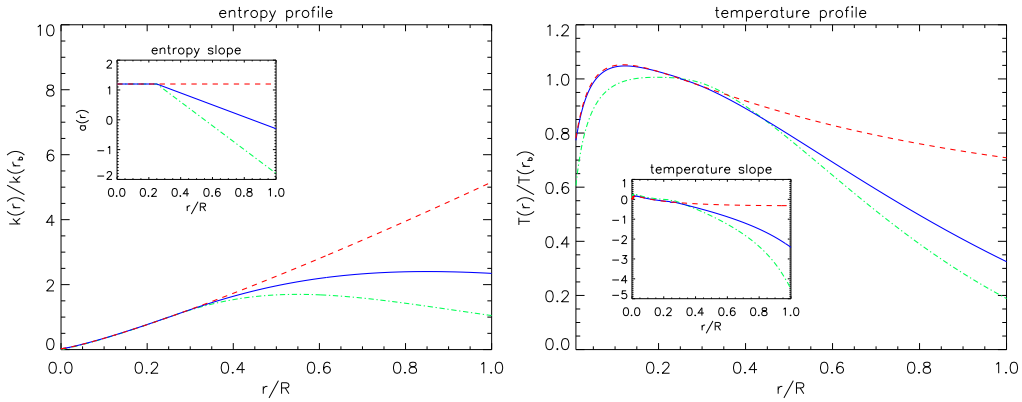

Fig. 2. Examples of entropy (left) and temperature (right) profiles computed with the SM: (red) dashed lines refer to Eq. (1) with $k_c = 0$ and $a = 1.2$; (blue) solid lines refer to Eq. (3) with $k_c = 0$, $a = 1.2$, $r_b = 0.25\,R$, and $a' = 0.5$; (green) dot-dashed line refer to Eq. (3) with $k_c = 0$, $a = 1.2$, $r_b = 0.25\,R$, and $a' = 1$. The insets illustrate the corresponding logarithmic slopes. All profiles are normalized to the values at $r = r_b$.

values of d decreasing from 2/3 to 1/2 (see Weinberg 2008); (ii) the *spatial* shape of the initial perturbations $\delta M/M \propto M^{-\epsilon}$ as described by the parameter ϵ taking on values > 1 in perturbation wings that scarcely feed the outskirts growth. The latter effect may be offset (and represented with a smaller effective ϵ) in biased environments, dense or adjacent to filamentary large-scale structures.

In average environs where $\epsilon > 1$ applies, the potential drop is shallower relative to the body value and reads $\Delta\phi = [1 - (R/R_{\rm ta})^{3\epsilon-2}]/(3\epsilon-2)$, so leading to larger values of b_R and *lower* values of a. Thus for r increasing towards the outskirts we expect the entropy profiles to deviate more and more downward from a simple powerlaw, see Fig. 2.

The decline of a from the body value will begin from a radius $r_b \sim r_{-2}$ where matter stratified just after the transition time z_t at the beginning of the outskirts growth. Such a radius is estimated in terms of the present concentration and radius R in the form $r_b/R \approx r_{-2}/R = 1/c$ that takes on values around 0.2 for a typical concentration $c \approx 6$ of CC clusters.

Thus under the *lower* accretion rates prevailing at *later* times in average environs, we expect the entropy slope $a(r)$ to decline toward smaller or even negative values; the corresponding entropy run will *flatten* out or even turn down into the cluster outskirts. This will imply a sharp *decline* of the outer temperatures $T(r) \propto k(r)\,n^{2/3}(r)$, as the overall density decline is insufficiently offset or is even reinforced by the entropy run.

4. A case study from current data

The above entropy behavior may be expressed in terms of a simple parametric form: a constant slope a applying in the cluster body for $r \le r_b$ to produce an inner shape like that in Eq. (1); a decline (e.g., a linear one) for $r > r_b$ with slope $a' \equiv (a - a_R)/(R/r_b - 1)$ toward the outer value $a_R < a$ at $r = R$, to produce the outer shape (see Fig. 2)

$$k(r) = k_R\,(r/R)^{a+a'}\,e^{a'\,(R-r)/r_b}\ . \qquad (3)$$

The ensuing temperature profiles provided by the SM are illustrated in Fig. 2. This shows that a flattening or even decreasing entropy run as in Eq. (3) produces in the cluster outskirts peculiarly *steep* temperature profiles. Next we focus on two clusters where temperature data have been recently obtained out to $r \approx R$; the uncertainties are quoted at the 68% level.

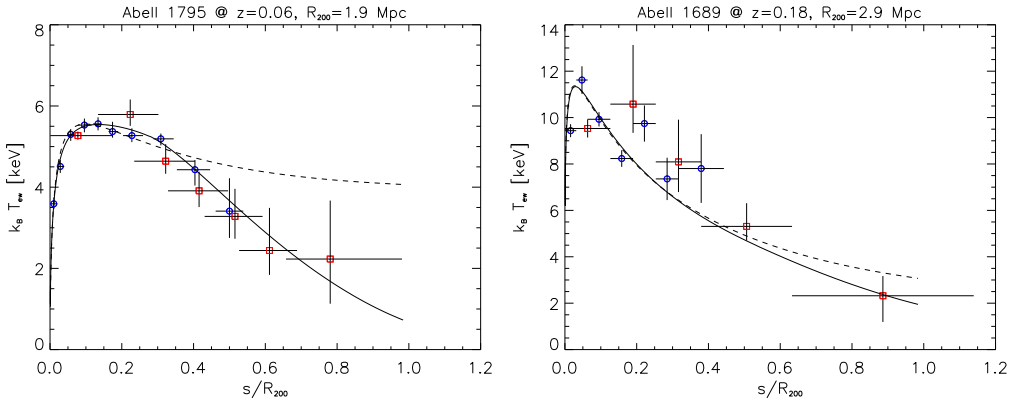

Fig. 3. Profiles of projected X-ray temperature for the CC clusters A1795 (left) and A1689 (right). Data from XMM-Newton (blue circles) and Suzaku (red squares), see refs. in the text. Our best-fits from the SM based on Eq. (3) are illustrated by the solid lines, while dashed lines refer to the fits based on Eq. (1). Temperature profiles with intermediate steepness hold for the CC clusters PKS0745-191 at $z \approx 0.1$ and A2204 at $z \approx 0.15$ (see Lapi et al. 2010).

For the CC cluster A1795 at $z = 0.063$, in Fig. 3 (left panel) we overplot on the temperature data from XMM-Newton and Suzaku (Snowden et al. 2008; Bautz et al. 2009) the best-fit (solid line) from the SM with the entropy profile in Eq. (3). The parameters read: $k_c < 10\,\mathrm{keV\,cm^2}$, $a = 1.2^{+0.3}_{-0.3}$, $r_b/R = 0.28^{+0.02}_{-0.02}$, and $a' = 1.8^{+1.3}_{-1.3}$, with a good value of the reduced $\chi^2 = 0.3$. We also evaluate the concentration $c = 8.5^{+1.9}_{-1.9}$. The simple entropy profile of Eq. (1) with $a' = 0$ would result in a worse best-fit (dashed line) with $\chi^2 = 2.6$.

As to the cluster A1689 at $z = 0.1832$, this is often classified as a CC although the temperature inner drop from its high peak is controversial to some extent (see Riemer-Sørensen et al. 2009). In Fig. 3 (right panel) we overplot on the temperature data averaged over 4 sectors from XMM-Newton and Suzaku (see Snowden et al. 2008; Kawaharada et al. 2010) the best-fit (solid line) from the SM with the entropy profile in Eq. (3). The parameters read: $k_c < 10\,\mathrm{keV\,cm^2}$, $a = 0.7^{+0.3}_{-0.3}$, $r_b/R = 0.5^{+0.1}_{-0.1}$, and $a' = 1.6^{+1.2}_{-1.2}$, with an acceptable values of the reduced $\chi^2 = 1.5$. We also estimate the concentration $c = 12.4^{+5.3}_{-5.3}$, consistent with gravitational lensing observations (see Broadhurst et al. 2008; Lapi & Cavaliere 2009b). The simple entropy profile of Eq. (1) with $a' = 0$ would result in a best-fit (dashed line) with $\chi^2 = 1.7$.

We have also computed the related brightness profiles, finding non-monotonic outer slopes; these first flatten where the entropy begins to deviate from a powerlaw, and then steepen where the entropy turns down. Such detailed features go beyond the resolution and/or the background-limited sensitivity of current instruments, but will be widely observed and easily pinpointed with WFXT (see http://wfxt.pha.jhu.edu/).

5. Summary and perspectives

These data support the view that outer entropy production is reduced especially at low $z_{\rm obs}$, as the inflows of DM and intergalactic gas peter out. This view stems from two concurring sources: (i) the *cosmological* slowdown in the growth of outskirts developing at late cosmic times; (ii) shallow perturbation wings scantily feeding the outskirts growth in average or poor environs.

Under such conditions, we expect the entropy profile to progressively flatten out or even decrease into the cluster outskirts as represented by Eq. (3). Whence the SM from

entropy-modulated equilibrium of the ICP and strong boundary shocks leads to envisage specifically steep outer temperatures.

On the other hand, we expect the accretion rates to be sustained in rich environs, or in cluster sectors adjacent to filamentary large-scale structures; shallower temperature runs are likely to prevail there. These can be effectively probed with a pointing instrument of high spectral sensitivity and resolution like IXO (see http://ixo.gsfc.nasa.gov/).

But from an adjacent filament blobs of DM and cold gas can easily fall into the cluster, leading to cold dense spots that may enforce a local breakdown of HE. The latter will fail anyway beyond R together with the DM equilibrium. In addition, as $\dot{M}$ decreases to the point that the infall velocities go down to transonic values, the shocks weaken, thermalization becomes inefficient (see CLFF09), the entropy production is terminated, and thermal pressure cannot support HE any longer.

To sum up, even on assuming standard boundary shocks with optimal energy conversion and HE, we find temperature profiles declining sharply outwards. We propose these to stem from progressive *exhaustion* of mass inflow, especially for young clusters in average or poor environments at lower $z_{\rm obs}$; such a trend is consistent with that looming out at decreasing redshifts for the clusters in Fig. 3 and caption. Conversely, at higher $z_{\rm obs}$ we expect sustained accretion, but also more frequent cold dense clumps infalling and departing from HE.

To conclude, we stress that with $\dot{M}$ decreasing rich astrophysics is likely to set in at the *interface* between the ICP and the intergalactic medium, including hydrodynamics in conditions of long mean free paths and slow/incomplete bulk motion conversion. As indicated above, such phenomena call for extensive probing even at $z \gtrsim 0.2$ with the next generation of X-ray telescopes planned to detect and resolve low-surface brightness features of the intracluster plasma (see Giacconi et al. 2009), like WFXT and IXO.

Acknowledgements. The material presented here is based upon the paper by Lapi et al. (2010).

References

Bautz, M.W., et al. 2009, PASJ, 61, 1117
Broadhurst, T., et al. 2008, ApJ, 685, L9
Cavagnolo, K. W., et al. 2009, ApJS, 182, 12
Cavaliere, A., Lapi, A., and Fusco-Femiano, R. 2009, ApJ, 698, 580 [CLFF09]
Cavaliere, A., Lapi, A., and Menci, N. 2002, ApJ, 581, L1
Cavaliere, A., and Fusco-Femiano, R. 1976, A&A, 49, 137
Diemand, J., Kuhlen, M., and Madau, P. 2007, ApJ, 667, 859
Fusco-Femiano, R., Cavaliere, A., and Lapi, A. 2009, ApJ, 705, 1019
George, M.R., et al. 2009, MNRAS, 395, 657
Giacconi, R., et al. 2009, in Astro2010: The Astronomy and Astrophysics Decadal Survey, Science White Papers, no. 90
Kawaharada, M., et al. 2010, ApJ, 714, 423
Lapi, A., Cavaliere, A., and Fusco-Femiano, R. 2010, A&A, 516, A34
Lapi, A., and Cavaliere, A. 2009a, ApJ, 692, 174
—— 2009b, ApJ, 695, L125
Lapi, A., Cavaliere, A., and Menci, N. 2005, ApJ, 619, 60
Leccardi, A., and Molendi, S. 2008, A&A, 486, 359
Markevitch, M., and Vikhlinin, A. 2007, Phys. Rep., 443, 1
McCarthy, I.G., et al. 2007, MNRAS, 376, 497
McNamara, B.R., and Nulsen, P.E.J. 2007, ARA&A, 45, 117
Molendi, S., and Pizzolato, F. 2001, ApJ, 560, 194
Navarro, J.F., et al. 2010, MNRAS, 402, 21
Pratt, G.W., et al. 2010, A&A, 511, 85
Riemer-Sørensen, S., et al. 2009, ApJ, 693, 1570
Rossetti, M., and Molendi, S. 2010, A&A, 510, 83
Snowden, S.L., et al. 2008, A&A, 478, 615
Tozzi, P., and Norman, C. 2001, ApJ, 546, 63
Valageas, P., and Silk, J. 1999, A&A, 350, 725
Vikhlinin, A., et al. 2006, ApJ, 640, 691
Voit, G. M. 2005, Rev. Mod. Phys., 77, 207
Weinberg, S. 2008, Cosmology (Oxford: Oxford Univ. Press)
Zhao, D.H., et al. 2003, MNRAS, 339, 12

Mem. S.A.It. Suppl. Vol. 17, 79

Memorie della
Supplementi

Non-thermal emission from galaxy clusters

C. Ferrari[1]

UNS, CNRS, OCA, Laboratoire Cassiopée, Nice, France
e-mail: chiara.ferrari@oca.eu

Abstract. The relevance of non-thermal cluster studies and the importance of combining observations of future radio surveys with *WFXT* data are discussed in this paper.

Key words. Cosmology: large-scale structure – Galaxies: clusters: general – Radiation mechanisms: non-thermal

1. Introduction

The discovery of diffuse radio sources in a few tens of merging galaxy clusters has pointed out the existence of a non-thermal component (i.e. relativistic particles with Lorentz factor γ >>1000 and magnetic fields of the order of μG) in the intracluster volume (e.g Ferrari et al. 2008). Through non-thermal studies of galaxy clusters we can estimate the cosmic-ray and magnetic field energy budget and pressure contribution to the intracluster medium (ICM), as well as get clues about the cluster dynamical state and energy redistribution during merging events. Non-thermal analyses can elucidate non-equilibrium physical processes whose deep understanding is essential to do high-precision cosmology using galaxy clusters (Pfrommer 2008).

In the following, we will give an overview of the main open questions about the non-thermal intracluster component (Sect. 2). The perspectives that will be opened in this field by a new generation of radio telescopes will also be addressed (Sect. 3.1). We will focus in particular on the study of clusters with similar X-ray and radio morphologies, i.e. clusters hosting diffuse radio sources that are called "radio halos". The importance of an X-ray facility such as *WFXT* will be discussed (Sect. 3.2). The ΛCDM model with H_0=70 km s^{-1}Mpc^{-1}, Ω_m = 0.3 and Ω_Λ = 0.7 has been adopted.

2. Open questions

The origin of intracluster cosmic rays (CRs) is matter of debate. CRs, gyrating around magnetic field lines which are frozen in the ICM, have typical diffusion velocity of the order of the Alfvén speed ($\sim$ 100 km/s). They thus need $\gtrsim$10 Gyr to propagate over radio halo extensions. Radiative timescales are longer than the Hubble time for CR protons (CR*p*s). They thus can be continuously accelerated (directly in the ICM or inside active galaxies and then ejected), resulting in an effective accumulation of relativistic and ultra-relativistic CR*p*s in clusters. Hadronic CRs can subsequently produce Gamma-rays and secondary relativistic electrons through inelastic collisions with the ions of the ICM (e.g. Aharonian et al. 2009).

The radiative lifetime of relativistic electrons (CR*e*s) is instead much shorter ($\lesssim$0.1 Gyr) than their cluster crossing time due to in-

Send offprint requests to: C. Ferrari

verse Compton (IC) and synchrotron energy losses. Therefore CR*e*s have to be continuously re-accelerated *in situ*. Two main classes of models have been proposed to explain intracluster electron acceleration: primary and secondary models. The former predict the acceleration of fossil radio plasma or directly of thermal electrons of the ICM through shocks and/or MHD turbulence generated by cluster mergers. Secondary models predict instead that non-thermal electrons in clusters are the secondary product of hadronic interactions between relativistic protons and the ions of the thermal ICM (e.g. Ferrari et al. 2008).

Current observational results are in favour of primary models. The very few detailed analyses of the radio spectral index α[1] distribution in radio halos show hints of a possible increase of α as a function of radius and of frequency (e.g Thierbach et al. 2003), as expected in the case of primary models. A possible anticorrelation between α and the ICM temperature (i.e. flatter spectra in hotter regions) has also been pointed out in a few cases (e.g. Orrú et al. 2007). The hottest ICM regions are usually associated to shock and/or turbulence induced by cluster collisions. The fact that these regions host younger CR*e*s is thus in agreement with primary models. A unique prediction of the turbulence re-acceleration models is the existence of ultra-steep radio halos, not associated to major cluster mergers, but to less energetic merging events. Recently Brunetti et al. (2008) claimed the detection of the first ultra-steep radio halo in the multiple merging cluster A521. At the moment, the most striking observational evidence in favour of primary models is the fact that diffuse cluster sources have been detected only in merging clusters.

Deeper statistical analyses of the correlation between diffuse radio sources and the physical properties of their host clusters are required to refine the physical models for CR acceleration. For instance, we know that diffuse radio sources have been detected in $\leq 10\%$ of known clusters, while about 40% of clusters show a disturbed dynamical state: why cluster mergers seem to be a necessary but not sufficient condition for the acceleration of intracluster relativistic particles? The answer could be related to the cluster mass, since a correlation between radio and X-ray cluster luminosity has been pointed out (e.g. Buote 2001). This suggests that only the most massive merging clusters are energetic enough to produce diffuse radio emission at power levels observable with current radio observations (see also the discussion in Sect. 3.1).

Even more debated are the origin and properties of intracluster magnetic fields (Dolag et al. 2008). The different methods available to measure intracluster magnetic fields (equipartition assumption, rotation measures, Compton scattering of CMB photons, X-ray study of cooling-cores in the ICM) show quite discrepant results (see Table 3 of Govoni & Feretti (2004)). Different reasons can explain this discrepancy (e.g. Ferrari 2010). Again, higher statistics is required for magnetic field measurements. For instance, we need deeper multiwavelength radio observations of radio galaxies per cluster for rotation measure (RM) estimates, combined to detailed modeling of the ICM X-ray brightness profile (Govoni et al. 2001b).

3. Perspectives

3.1. A new generation of radio telescopes

Huge perspectives in the study of the non-thermal intracluster component will be open by the Low Frequency Array (*LOFAR*, Röttgering et al. 2006). A steepening of the synchrotron spectrum of radio halos is expected in the framework of stochastic particle acceleration by MHD turbulence and it has been observed in several halos (e.g. Ferrari et al. 2008). Cassano et al. (2010) have introduced a characteristic frequency $\nu_s \sim 7\nu_b$ at which the steepening become extremely severe. Basically, surveys at frequency $\nu > \nu_s$ cannot detect radio halos. Since the lower is the radio luminosity of the halo, the lower is the expected break frequency, high-frequency ($\nu \approx 1.4$ GHz) surveys are sensitive only to high-luminosity halos, while most of the faint radio luminos-

[1] $S_\nu \propto \nu^{-\alpha}$

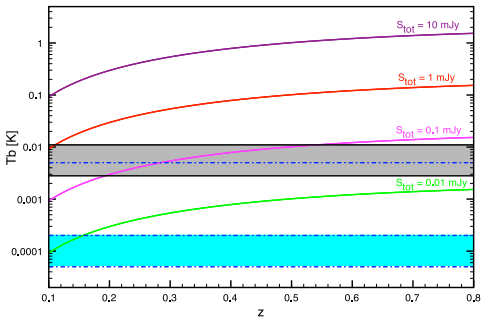

Fig. 1. Brightness temperature at ∼ 1.3 GHz as a function of redshift expected for radio halos of a given total flux and of 0.5 Mpc radius. Possible limits for the *ASKAP* EMU Survey and for 50% of the *SKA* with 1 hour integration time are indicated (shaded areas delimited by solid and dot-dashed lines respectively).

ity halo tail will appear at low-frequency radio observations. That's the huge potential of *LOFAR* in the study of diffuse cluster radio sources. Radio maps resulting from the *LOFAR* Surveys[2] (Tier-1 Wide, Tier-2 Deep, Tier-3 Ultra Deep) are expected to provide a catalog of several hundreds candidates of galaxy clusters hosting diffuse radio sources (e.g. Cassano et al. 2010).

The full international *LOFAR* telescope should be operational by early 2011. Other new generation radio telescopes will follow in the next few years, such as the Long Wavelength Array (*LWA*, 10–80 MHz)[3], the Australian Square Kilometre Array Pathfinder (*ASKAP*, 70–1800 MHz)[4], the Karoo Array Telescope (*MeerKAT*, 0.58–15 GHz)[5]. All these instruments will indeed play an important role for the study of non-thermal cluster physics and, more generally, will be crucial scientific and technical pathfinders for the Square Kilometre Array (*SKA*, 0.10 – 25 GHz)[6]. Multi-frequency radio surveys of the sky will be available that will unveil statistical samples of hundreds candidate diffuse cluster radio source (Feretti et al. 2004). As detailed above, wide and deep complementary cluster catalogs at other wavelengths will be necessary in order to answer the open questions about non-thermal cluster physics.

After *LOFAR*, the following survey project very important for non-thermal cluster studies will probably be EMU ("Evolutionary Map of the Universe", project leader: R. Norris). It will be a deep radio survey (∼ 10 μJy rms; 1130 – 1430 MHz) covering the entire Southern sky and part of the Northern sky ($\delta \lesssim 30°$) with the *ASKAP* telescope. Fig. 1 shows the brightness temperature at ≈ 1.3 GHz as a function of redshift expected for radio halos of a given total flux and of 0.5 Mpc radius. The shaded area delimited by solid lines indicates an approximate 3 σ sensitivity level of the EMU survey. We have taken into account that the exact observing strategy of EMU is under discussion. The best resolution of the survey will be of ∼10 arcsec, but lower resolutions radio maps will also be produced in order to increase the sensitivity to diffuse radio sources (see Sect. 3.5.1 in Johnston et al. (2008)). We have assumed here and in the following (see also Fig. 2) an rms sensitivity of 10-20 μJy/beam, with beam sizes variating from 40 to 80 arcsec. Our estimates for the EMU survey are here compared to the T_b ∼ 5mK sensitivity limit of 50% of the *SKA* collecting area. This 3σ sensitivity level (indicated by a dot-dashed line in Fig. 2) has been estimated by Feretti et al. (2004) assuming an integration time of 1 hour. The shaded area delimited by dot-dashed curves correspond to the 3 σ sensitivity limit of 50% *SKA* at the same resolution limits that we have adopted for EMU (from 40 to 80 arcsec).

Based on the results in Fig. 1 and on the radio halo luminosity function derived by Enßlin & Röttgering (2002) (see also Table 1 in Feretti et al. (2004)) we can expect to detect $\gtrsim$ 300 halos at any redshift with EMU (i.e. halos in $\gtrsim 2\pi$ sterad with $S_{tot} > 1$ mJy) and several thousands ($\gtrsim$ 6000) halos with the low-resolution 50% *SKA* observations (1h integration time), among which about one third at z >0.3. In such a case, in fact, our *SKA* estimates indicate that we can go down to $S_{tot} \approx 10\mu$Jy at any redshift. Note

[2] http://www.lofar.org/astronomy/surveys-ksp/surveys-ksp
[3] http://lwa.unm.edu/
[4] http://www.atnf.csiro.au/SKA/
[5] http://www.ska.ac.za/meerkat/
[6] http://www.skatelescope.org/

that, in addition, EMU could detect several tens higher redshift ($\gtrsim 0.3$) halos with $S_{tot} > 0.1$ mJy.

We have then refined our estimates to evaluate the evolution with redshift of the X-ray luminosity limit of clusters whose diffuse radio emission can be detected by the EMU Survey (shaded are delimited by solid curves in Fig. 2). We have considered radio halos of 1 Mpc size with radio luminosities $L_{1.4GHz} \gtrsim 5 \times 10^{20}$ W/Hz and a typical brightness profile as a function of radius has been adopted (Govoni et al. 2001a):

$$B_\nu(\eta R_h) = \xi \frac{L_{1.4GHz}(1400/\nu)^\alpha (1+z)^{-(3+\alpha)}}{1.5 \times 10^{31} (\eta R_h)^2}$$

where ξ indicates the fraction of the total flux of the source at $r = \eta R_h$ (thus $\xi \leq 1$ and $\eta \leq 1$), B_ν is in Jy/arcsec^2, $L_{1.4GHz}$ in W/Hz, ν in MHz and R_h (=0.5) in Mpc. In our estimates a radio halo is considered to be detected when $B_\nu(\eta R_h) \geq$ 5-10 rms_{EMU} and $\xi = 0.5$. The EMU detection limits for radio halo luminosities have finally be converted to X-ray luminosities of the host clusters following Eq. (1) in Cassano et al. (2006). Increased inverse Compton energy losses on the CMB at higher redshift and the consequent decrease in the intrinsic radio halo luminosity have also been taken into account (Enßlin & Röttgering 2002).

Note that the EMU limits shown in Fig. 2 concern the Wide EMU survey described above. The possibility to perform deeper *ASKAP* surveys, in particular at lower frequencies (~850 MHz) that are more favorable to radio halo detection, is currently considered within the EMU project (Johnston-Hollitt, private communication). In such a case, complementary cluster catalogs could provide excellent targets for deeper radio follow-ups, thus helping in selecting the regions of the sky to be observed with *ASKAP*, *MeerKAT* or any other radio facility. Fig. 2 also shows the detection limit expected with 50% of the *SKA* collecting area at a resolution of ~8, 40 and 80 arcsec, assuming a bandwidth of 0.5 GHz and an integration time of 1 hour. As before, a 3σ level brightness sensitivity of $T_b \sim 5$ mK has been adopted for these estimates (Feretti et al. 2004). We have converted this radio brightness sensitivity to X-ray luminosity limits as a function of redshift by adopting exactly the same method of our previous EMU estimates. The detection limits are here at 10 σ level. Much deeper sensitivity limits can of course be reached with the full *SKA* and longer integration times.

3.2. Importance of *WFXT* surveys

In order to be able to test current models about the origin of the non-thermal intracluster component we need both *statistical studies* of the fraction of observed clusters hosting diffuse radio sources as a function of the cluster mass and z, and *detailed analyses* of how the correlation between the radio emission and the physical properties of clusters (L_X, T_X, mass, dynamical state...) evolve with z. The newly identified candidates of radio emitting clusters described in Sect. 3.1 will thus have to be cross-matched with cluster catalogs in other wave bands, which will be needed for the cluster *identification* and *physical characterization*.

On short timescales, existing or incoming optical, IR, sub-mm and X-ray surveys will provide an important set of complementary data for the identification of potential clusters detected by *LOFAR* (among others: Ebeling et al. 1998; Böhringer et al. 2000; Ebeling et al. 2001; Böhringer et al. 2001; Goto et al. 2002; van Breukelen et al. 2006; Olsen et al. 2007). In Ferrari (2010) we have compared the cluster X-ray luminosity detection limits of *Planck* and *LOFAR*. Our estimates indicate that the Tier-1 Wide *LOFAR* survey will provide a galaxy cluster catalog through diffuse radio source detection that well match the expected *Planck* cluster detection at $z \lesssim 0.3$. At higher redshift, all the systems detected by *LOFAR* will have an X-ray luminosity above the *Planck* detection limit. Fig. 2 shows that the cluster detection limits of *Planck* will also be perfectly suited for the comparison with the list of diffuse radio surveys resulting from the EMU Wide survey. *eROSITA*[7] detection limits should

[7] http://www.mpe.mpg.de/heg/www/Projects/EROSITA/main.html

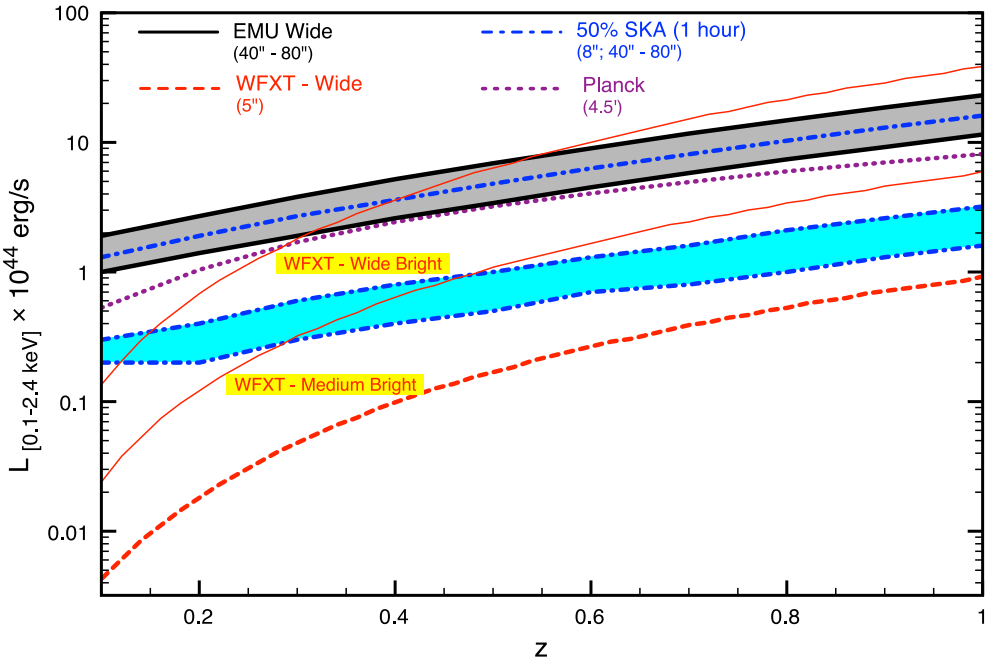

Fig. 2. Evolution with redshift of the X-ray luminosity limit of clusters whose diffuse radio emission can be detected: **a) (shaded area delimited by solid lines)** at 5-10 σ significance level with the *ASKAP* telescope down to the sensitivity limit of the EMU-Wide survey and at 40 to 80 arcsec resolution (Sect.3.1); **b) (dot-dahsed line)** at 10 σ significance level with 50% of the *SKA* collecting area assuming an integration time of 1 hour and a resolution of 8 arcsec (Feretti et al. 2004); c) **(shaded area delimited by dot-dashed lines)** at 10 σ significance level with 50% of the *SKA* collecting area assuming an integration time of 1 hour and 40 to 80 arcsec resolution. The cluster detection limits expected for the *Planck* (**dotted line**; courtesy of A. Chamballu and J. Bartlett) and *WFXT*-Wide (**dashed line**; courtesy of B. Sartoris) surveys are also shown. The thinner curves, finally, correspond to the bright sample limits of the *WFXT* Wide and Medium surveys (Sartoris et al. 2010).

match well the radio halo cluster detection limits with EMU presented here (Reiprich, private communication). Based on our estimates radio observations with the SKA will instead require deeper complementary surveys for cluster cross-identification.

The projected *WFXT* surveys will provide two kinds of cluster catalogs (Giacconi et al. 2009; Sartoris et al. 2010): $\sim 3 \times 10^6$ detected clusters (out of which $\approx 98\%$ at $z < 1$[8]), and $\sim 2 \times 10^4$ clusters (the so called "bright sample"), which, with a flux limit 30 times brighter than the detection flux limit, will have robust measures of mass proxies, as well as of ICM surface brightness and temperature profiles.

Most of the cluster detections will come from the all-sky *WFXT* Wide Survey, while the "bright sample" at $z < 1$ is mainly due to the Medium *WFXT* survey, which would cover 3000 square degrees (see Table 1 and Fig. 3 in Sartoris et al. (2010)). In Fig. 2 we have plotted the X-ray luminosity detection limits of the *WFXT* Wide survey as a function of z (red dashed curve), as well as the X-ray luminosity limits for the bright samples resulting from

[8] For $z \gtrsim 1$ the lifetime of CR*e*s whose synchrotron emission peaks at 1.4 GHz $\tau \lesssim 10$ Myr due to IC energy losses.

the Wide and Medium *WFXT* surveys (thin red curves). Fig. 2 shows that the comparison between possible *WFXT* and radio surveys could provide:

- an all-sky cluster catalog (*WFXT* Wide, dashed thick line in Fig. 2) deep enough for the identification of $\gtrsim$6000 candidate clusters hosting diffuse radio emission coming from *SKA* observations (see Sect. 3 and Fig. 1). This sample will offer the unique opportunity to study in a fully statistical way the cluster radio *vs.* X-ray luminosity correlation (Sect. 2);
- the possibility to compare radial profiles of the radio spectral index α and of the ICM brightness and temperature (Sect. 2). This could be done on several hundred clusters at z <0.5 by combinining radio surveys data (*LOFAR*, *ASKAP*, *SKA* in Fig. 2) with the bright samples deriving from *WFXT* Wide and Medium surveys (thin red lines in Fig. 2);
- interesting targets for deeper *LOFAR*, *ASKAP*, *MeerKAT* or *SKA* follow-ups.

WFXT will provide X-ray surveys with the necessary sensitivity to match those achievable in future radio surveys of galaxy clusters.

Acknowledgements. I am very grateful to M. Arnaud, S. Borgani, G. Giovannini, M. Johnston-Hollitt and the EMU cluster working group, P. Rosati and B. Sartoris for very useful discussions that helped to improve the paper. I acknowledge financial support by the Agence Nationale de la Recherche through grant ANR-09-JCJC-0001-01.

References

Aharonian, F., Akhperjanian, A. G., Anton, G., et al. 2009, A&A, 495, 27
Böhringer, H., Schuecker, P., Guzzo, L., et al. 2001, A&A, 369, 826
Böhringer, H., Voges, W., Huchra, J. P., et al. 2000, ApJS, 129, 435
Brunetti, G., Giacintucci, S., Cassano, R., et al. 2008, Nature, 455, 944
Buote, D. A. 2001, ApJ, 553, L15
Cassano, R., Brunetti, G., Röttgering, H. J. A., & Brüggen, M. 2010, A&A, 509, A68+
Cassano, R., Brunetti, G., & Setti, G. 2006, MNRAS, 369, 1577
Dolag, K., Bykov, A. M., & Diaferio, A. 2008, Space Science Reviews, 134, 311
Ebeling, H., Edge, A. C., Bohringer, H., et al. 1998, MNRAS, 301, 881
Ebeling, H., Edge, A. C., & Henry, J. P. 2001, ApJ, 553, 668
Enßlin, T. A. & Röttgering, H. 2002, A&A, 396, 83
Feretti, L., Burigana, C., & Enßlin, T. A. 2004, New Astronomy Review, 48, 1137
Ferrari, C. 2010, ArXiv e-prints
Ferrari, C., Govoni, F., Schindler, S., Bykov, A. M., & Rephaeli, Y. 2008, Space Science Reviews, 134, 93
Giacconi, R., Borgani, S., Rosati, P., et al. 2009, in ArXiv Astrophysics e-prints, Vol. 2010, astro2010: The Astronomy and Astrophysics Decadal Survey, 90–+
Goto, T., Sekiguchi, M., Nichol, R. C., et al. 2002, AJ, 123, 1807
Govoni, F., Enßlin, T. A., Feretti, L., & Giovannini, G. 2001a, A&A, 369, 441
Govoni, F. & Feretti, L. 2004, International Journal of Modern Physics D, 13, 1549
Govoni, F., Taylor, G. B., Dallacasa, D., Feretti, L., & Giovannini, G. 2001b, A&A, 379, 807
Johnston, S., Taylor, R., Bailes, M., et al. 2008, Experimental Astronomy, 22, 151
Olsen, L. F., Benoist, C., Cappi, A., et al. 2007, A&A, 461, 81
Orrú, E., Murgia, M., Feretti, L., et al. 2007, A&A, 467, 943
Pfrommer, C. 2008, MNRAS, 385, 1242
Röttgering, H. J. A., Braun, R., Barthel, P. D., et al. 2006, ArXiv Astrophysics e-prints
Sartoris, B., Borgani, S., Fedeli, C., et al. 2010, ArXiv e-prints
Thierbach, M., Klein, U., & Wielebinski, R. 2003, A&A, 397, 53
van Breukelen, C., Clewley, L., Bonfield, D. G., et al. 2006, MNRAS, 373, L26

Mem. S.A.It. Suppl. Vol. 17, 85

Memorie della
Supplementi

Demography of obscured and unobscured AGN: prospects for a Wide Field X-ray Telescope

R. Gilli[1], P. Tozzi[2], P. Rosati[3], M. Paolillo[4], S. Borgani[2,5], M. Brusa[6], A. Comastri[1], E. Lusso[7], F. Marulli[7], C. Vignali[7], and the WFXT team

[1] INAF – Osservatorio Astronomico di Bologna, Via Ranzani 1, I-40127 Bologna, Italy
e-mail: roberto.gilli@oabo.inaf.it
[2] INAF – Osservatorio Astronomico di Trieste, Via Tiepolo 11, I-34131 Trieste, Italy
[3] ESO, Karl Schwarzschild Strasse 2, 85748 Garching bei Muenchen, Germany
[4] Università Federico II, Dip. di Scienze Fisiche C.U. Monte S.Angelo, ed.6, via Cintia 80126, Napoli
[5] Dip. di Astronomia dell'Università di Trieste, Via G.B. Tiepolo 11, I-34131 Trieste, Italy
[6] MPE, Giessenbachstrasse, 1, 85748 Garching bei Muenchen, Germany
[7] Dip. di Astronomia, Università di Bologna, Via Ranzani 1, 40127 Bologna, Italy

Abstract. We discuss some of the main open issues in the evolution of Active Galactic Nuclei which can be solved by the sensitive, wide area surveys to be performed by the proposed Wide Field X-ray Telescope mission.

Key words. Galaxies: active – X-rays; Active Galactic Nuclei – galaxies: high-redshift

1. Introduction

The observed scaling relations between the structural properties of massive galaxies (bulge mass, luminosity, and stellar velocity dispersion) and the mass of the black holes (BHs) at their centers suggest that galaxy assembly and black hole growth are closely related phenomena. This is often referred to as BH/galaxy co-evolution. The BH growth is thought to happen primarily through efficient accretion phases accompanied by the release of kinetic and radiative energy, part of which can be deposited into the galaxy interstellar medium. Active Galactic Nuclei (AGN) are then believed to represent a key phase across a galaxy's lifetime. Support for this hypothesis comes from several lines of evidence such as i) the match between the mass function of BHs grown through AGN phases and that observed in local galaxies (Marconi et al. 2004; Shankar et al. 2004); ii) the cosmological "downsizing" of both nuclear activity and star formation (Ueda et al. 2003; Cowie et al. 1996); iii) the feedback produced by the AGN onto the galaxy interstellar medium through giant molecular outflows (Feruglio et al. 2010). A number of semi-analytic models (SAMs) have been proposed over about the past decade to explain the BH/galaxy co-evolution (Kauffmann & Haehnelt 2000; Monaco et al. 2007; Menci et al. 2008; Marulli et al. 2008; Lamastra et al. 2010). These models follow the evolution and growth of dark matter structures

Send offprint requests to: R. Gilli

across cosmic time, either through the Press-Schechter formalism or through N-body simulations, and use analytic recipes to treat the baryon physics within the dark matter halos. A common assumption of these models is that mergers between gas-rich galaxies trigger nuclear activity and star formation. Recently, a BH/galaxy evolutionary sequence associated to "wet" galaxy mergers has been proposed (Hopkins et al. 2008), in which an initial phase of vigorous star formation and obscured, possibly Eddington limited, accretion is followed by a phase in which the nucleus first gets rid of the obscuring gas shining as an unobscured QSO, then quenches star formation, and eventually fades, leaving a passively evolving galaxy.

While being successful in many respects, this picture is still very partial and many fundamental pieces are missing to get a satisfactory understanding of BH/galaxy co-evolution, such as the very first stages of this joint evolution (e.g. at redshifts $z > 6$), the cosmological evolution of nuclear obscuration, the triggering mechanisms and environmental effects of nuclear activity. In this contribution it will be shown how the proposed Wide Field X-ray Telescope mission (WFXT) can effectively address some of these fundamental issues through sensitive, large area X-ray surveys.

2. The WFXT surveys at a glance

As detailed in Rosati et al. (2010, this volume), WFXT is a mission thought and designed to perform X-ray surveys, featuring a large (1 deg^2) field-of-view (FOV), large (1 m^2 at 1 keV) effective area, and sharp (5" HEW) resolution, constant across the FOV (the quoted values refer to the goal mission design). The observational survey strategy with WFXT will consist of three main X-ray surveys with different area and depth to sample objects in a wide range of redshifts and luminosities. To illustrate the power of the WFXT surveys, a simple excercise can be performed by rescaling the number of X-ray sources obtained from well-known X-ray surveys of similar sensitivity. The 20000 deg^2 WFXT-Wide survey will cover about 2000 times the area of the XBootes survey (Murray et al. 2005), in which more than 3000 X-ray sources have been detected, with the same depth. Similarly, the 3000 deg^2 WFXT-Medium and 100 deg^2 WFXT-Deep surveys will cover 3000 times the area of the C-COSMOS survey (Elvis et al. 2009) and 1000 times the area of the 2Ms CDFS survey (Luo et al. 2008), in which 1700 and 450 objects have been detected, respectively. By summing these numbers it is easy to see that the total source sample obtained by WFXT, mainly composed by AGN, will contain more than 10 million objects.

A more precise estimate of the number of AGN to be detected is obtained by considering the logN-logS relationships in the soft, 0.5-2 keV, and hard, 2-7 keV, bands. About 15 millions AGN detections are expected in the soft band up to $z > 6$ and about 4 millions in the hard band. Remarkably, for a very large number of objects it would be possible to obtain an accurate spectral characterization over the 0.5-7 keV WFXT band pass and derive physical properties such as the X-ray absorption (see Section 4 and Matt & Bianchi, 2010, this volume). Indeed, it is worth noting that, while being most effective at 1 keV, the WFXT collecting area at > 4 keV is still significantly large: in the goal design, the effective area at 5 keV is equal to that of XMM (pn+2MOS combined) at the same energy.

In the following Sections we will present a few unique science cases which can be addressed only with wide area and sensitive X-ray surveys.

3. Supermassive Black Holes in the early Universe

Most stars formed at $0.5 < z < 3$, when SMBHs were also growing most of their mass, but the assembly of the first organized structures started at earlier epochs, as soon as baryons were able to cool within dark matter halos. Discovering the first galaxies and black holes ever formed and understanding how their (concurrent?) formation takes place is a fascinating subject to which more and more efforts will be devoted in the next decade. To date, several tens of galaxies and about 20 QSOs

have been confirmed spectroscopically at redshifts above 6 (e.g. Taniguchi 2008; Fan 2006; Willott et al. 2009). Besides a GRB discovered at $z \sim 8.2$ (Salvaterra et al. 2009; Tanvir et al. 2009) and a galaxy at $z = 8.6$ (Lehnert et al. 2010), no other object is known spectroscopically at $z > 7$, although more than 100 galaxy candidates have been recently isolated through deep near-IR imaging with WFC3 (Oesch et al. 2010; Wilkins et al. 2010). The most distant SMBHs known to date are three QSOs at $z \sim 6.4$ discovered through the SDSS (Fan 2006) and the CFHQS survey (Willott et al. 2009, 2010). These two surveys have been the main resource for investigating the most distant QSOs in the past decade. About 20 QSOs at $z > 5.7$ have been detected in the SDSS main survey, which represent the brightest tail of the early QSO population ($\log L_x \sim 45.5$; $\log L_{bol} \sim 47$). Less luminous objects have been detected in the SDSS deep stripe (Jiang et al. 2009) and CFHQS. The BH masses measured for the SDSS bright objects are of the order of 10^9 $M_\odot$ (Kurk et al. 2007, 2009), which must have been built in less than 1 Gyr, i.e. the age of the Universe at $z = 6$. These giant black holes are thought to have formed through mass accretion onto smaller seeds with mass ranging from $10^2 M_\odot$, as proposed for the remnants of massive, PopIII stars (Madau & Rees 2001), to $10^4 M_\odot$, as proposed for the products of direct collapse of large molecular clouds (Volonteri et al. 2008). Whatever the seed origin is, to account for the observed BH mass distribution at $z \sim 6$, BH growth must have proceeded almost continuously at (or even above) the Eddington limit for a time interval of about 1 Gyr. Recent hydrodynamical simulations have shown that, within large dark matter halos, merging between proto-galaxies at $z \sim 14$ with seed BH masses of $10^4 M_\odot$ may trigger Eddington limited nuclear activity to produce a 10^9 solar mass BH by $z \sim 6$ (Li et al. 2007). The overall frequency and efficiency by which this merging and fueling mechanism can work is however unknown.

Because of the paucity of observational constraints, the study of BH and galaxy formation at early epochs remained speculative. For example, the relation between the BH mass and the galaxy gas mass has been measured for a few bright QSOs at $z \sim 5-6$, in which the ratio between the BH mass and the dynamical mass within a few kpc radius, as measured from CO line observations, is of the order of 0.02-0.1 (Walter et al. 2004). This is more than one order of magnitude larger than the ratio between the BH mass and stellar bulge mass measured in local galaxies. Despite the uncertainties on these measurements (see e.g. Narayanan et al. 2008), the possibility that SMBHs are leading the formation of the bulge in proto-galaxies, poses severe constraints to galaxy formation models. Large statistical samples of $z > 6$ AGN are needed to understand the relation between the BH growth and formation of stars in galaxies at their birth. Based on SAMs (see e.g. Hopkins et al. 2008 and Marulli et al. 2008 for recent works), the luminosity function and spatial distribution (clustering) of AGN at $z > 6$ would constrain: i) where, i.e. in which dark matter halos, they form; ii) what their average accretion rate is; iii) what the triggering mechanism (e.g. galaxy interactions vs secular processes) is.

The accreting SMBHs at $z > 6$ known to date have been all selected as *i*-band dropouts ($i - z \gtrsim 2$) in optical surveys. The sky density of the bright ($z_{AB} < 20.2$) QSOs at $z > 6$ in the SDSS main survey is 1/470 deg^2. Fainter objects ($z_{AB} \sim 21 - 22$) have densities of 1 every ∼30-40 deg^2 (Jiang et al. 2009; Willott et al. 2009). The discovery of significant samples of objects therefore relies on the large areas covered by these surveys (>8000 deg^2 for the SDSS, ∼900 deg^2 for the CFHQS). Based on the SDSS and CFHQS samples, a few attempts to measure the luminosity function of $z \sim 6$ QSOs have been performed, the most recent of which are those by Jiang et al. (2009) and Willott et al. (2010). While the uncertainties at low luminosities ($M_{1450} > -25$) are still substantial, the space density of luminous QSOs ($M_{1450} < -26.5$; $L_{bol} > 10^{47}$ erg s^{-1}) is relatively well constrained, decreasing exponentially from $z \sim 3$ to $z \sim 6$ (see Fig. 1). Furthermore, multiwavelength studies of SDSS QSOs at $z \sim 6$ showed that these objects have metallicities and spectral energy distributions pretty similar to those of lower red-

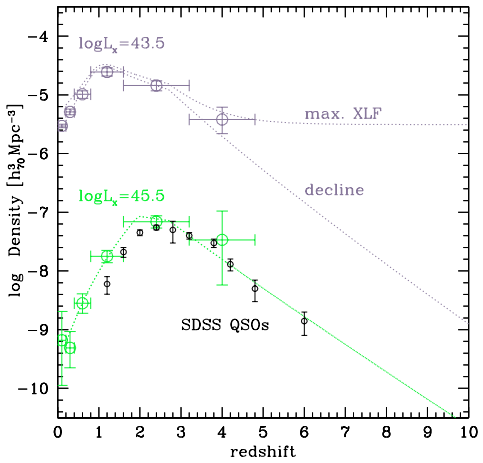

Fig. 1. The space density of unabsorbed AGN with $\log L_x = 43.5$ and $\log L_x = 45.5$. Big open circles are from Hasinger et al. (2005). Small black symbols have been obtained from the space density of optically luminous SDSS QSOs (Richards et al. 2006) by assuming $\alpha_{ox} = -1.5$. The space density of luminous QSOs is found to decrease from $z \sim 3$ to $z \sim 6$ and is well fitted by an exponential decline curve (dotted line from Gilli et al. 2007). The space density of lower luminosity objects is unconstrained for $z > 4$, and we show two alternative working hypotheses: either a "decline" scenario, as observed for luminous QSOs, or a constant density model, which is referred to as "maximum XLF".

shifts QSOs, suggesting their are already mature objects in a young Universe (see however Jiang et al. 2010 for two counter-examples).

Most of the multiwavelength studies mentioned above refer to optical QSOs above the knee of the luminosity function. These likely represent a minor fraction of the active BH population at $z > 6$, which is expected to be made primarily by less massive, $\approx 10^6\ M_\odot$, and less luminous, 10^{44} erg s^{-1}, objects.

When compared with optically selected objects at the same redshift, X-ray selected AGN are on average less luminous, either intrinsically or because of obscuration effects. Therefore X-ray selection might be the key to sample the bulk of the high-z AGN population. Several arguments indeed suggest that obscured AGN should be abundant even at very high redshift. First, observations and modeling showed that obscured AGN outnumber unobscured ones by a significant factor up to $z \lesssim 4$ and it is then reasonable to extrapolate that even at $z > 6$. Second, most current models of galaxy formation postulate that the early phases of accretion onto seed black holes are obscured (e.g. Menci et al. 2008). Third, optical/near-IR spectroscopy and IR/sub-mm imaging of $z \sim 6$ QSOs showed that dust and metals are abundant in their inner regions (Juarez et al. 2009; Beelen et al. 2006). Dust and metals must have then formed in large quantities at $z > 6$ and can effectively absorb the nuclear radiation from the optical regime to the soft X-rays.

Among the objects discovered so far at $z > 6$ no one is obscured, since these have been selected only through optical color selection criteria. The most distant object discovered to date through X-ray selection is an AGN at $z = 5.4$ in the COSMOS field (Civano et al. in preparation) and only a few are known at $z > 4$. The lack of sufficient sky area covered to deep sensitivities is the reason behind that. The discovery space for early obscured AGN is therefore huge, and can have a significant impact on our understanding of BH and galaxy formation.

Different routes can be tried to estimate the space and surface density of X-ray emitting high-z AGN and hence make forecasts for the samples to be observed in the WFXT surveys. As a first step, we considered extrapolations based on our current knowledge of the AGN X-ray luminosity function (XLF) and evolution. As shown in Fig. 1, the space density of luminous, unobscured QSOs with $M_{1450} < -26.5$ has been determined to steadily decrease from $z \sim 3$ to $z \sim 6$ (Richards et al. 2006). When their optical luminosity is converted to the X-rays (using $\alpha_{ox} = -1.5$), there is a good match between their space density and that determined by Hasinger et al. (2005) for soft X-ray selected QSOs in the overlapping redshift range. The behaviour of lower luminosity sources, $\log L_x = 43.5$, is instead known only up to $z \sim 4$ (Yencho et al. 2009; Aird et al. 2010) and extrapolations to higher redshifts are highly uncertain (see Brusa et al. 2010, this

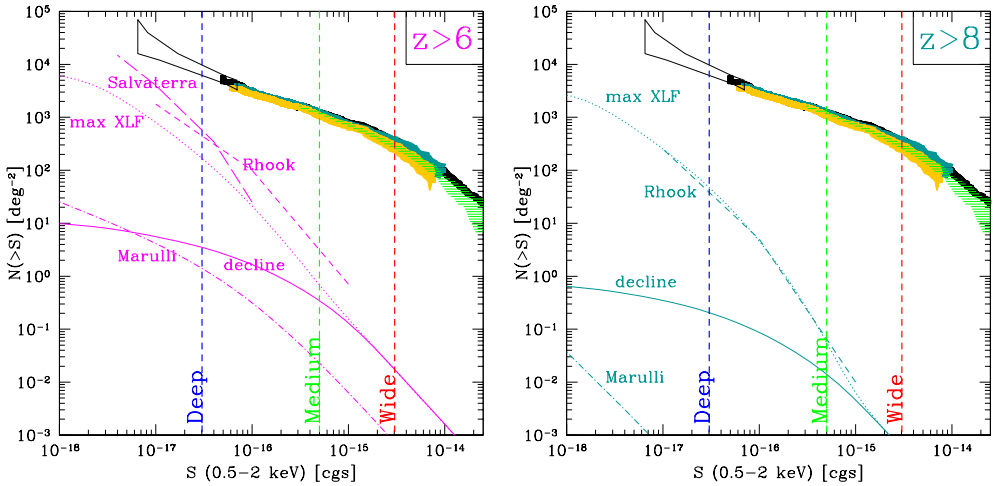

Fig. 2. *Left:* Expected number counts in the 0.5-2 keV band for $z > 6$ AGN according to different models as labeled (see text for details). The datapoints and shaded regions show the observed, total logN-logS of X-ray sources. The sensitivity limits of the three WFXT surveys are shown as vertical dashed lines. *Right*: As in the *left* panel but for $z > 8$ AGN.

volume). Starting from the X-ray background synthesis model by Gilli et al. (2007), we considered a first scenario in which the space density of AGN with $\log L_x < 44$ undergoes the same exponential decline as observed for luminous QSOs - which we will call the "decline" scenario - and a second, perhaps extreme, scenario in which it stays constant above a redshift of ~ 4, which will be referred to as the "maximum XLF" scenario (see Fig. 1). The 0.5-2 keV logN-logS of $z > 6$ AGN expected in the two above mentioned scenarios is shown in Fig. 2, where we also show a range of predictions based on different SAMs of BH/galaxy coevolution (Salvaterra et al. 2007; Rhook & Haehnelt 2008; Marulli et al. 2008). The limiting fluxes of the three WFXT surveys are also shown. It is clear how the $z > 6$ AGN Universe is a completely uncharted territory, the various predictions differing by a few orders of magnitude already at fluxes around 10^{-16} cgs. The predictions by the SAMs of Salvaterra et al. (2007) and Rhook & Haehnelt (2008) are even more optimistic than the "maximum XLF" scenario, predicting about 500-600 $z > 6$ AGN deg^{-2} at the WFXT-Deep limiting flux. The model by Marulli et al. (2008) is instead the most pessimitic, with 15 $z > 6$ AGN deg^{-2} at the same limiting flux. The predictions by SAMs depend on a pretty large number of parameters such as the mass of seed BHs, their location in the density field (i.e. the abundance of the dark matter halos hosting them), the recipes used for accretion, the AGN lightcurve. Although different assumptions are made by different models, the ~ 3 orders-of-magnitude difference at faint X-ray fluxes between the predictions by Marulli et al. (2008) on the one hand, and Salvaterra et al. (2007) and Rhook & Haehnelt (2008) on the other hand, seems to be primarily related to the assumed space density of seed black holes. In the Marulli et al. (2008) model, seed BHs are placed in each halo that can be resolved by the Millennium simulation, i.e. in those halos with mass above $\sim 10^{10}$ $M_\odot$, while in Salvaterra et al. (2007) BHs populate mini-halos with mass as low as $\sim 10^{7-8}$ $M_\odot$, which are therefore much more abundant. In Rhook & Haehnelt (2008) BHs are assumed to radiate at the Eddington limit and their mass to be proportional to that of the hosting halos. This implies that, if small mass seed are assumed, these populate low mass, abundant halos. If large mass seeds are assumed, these pop-

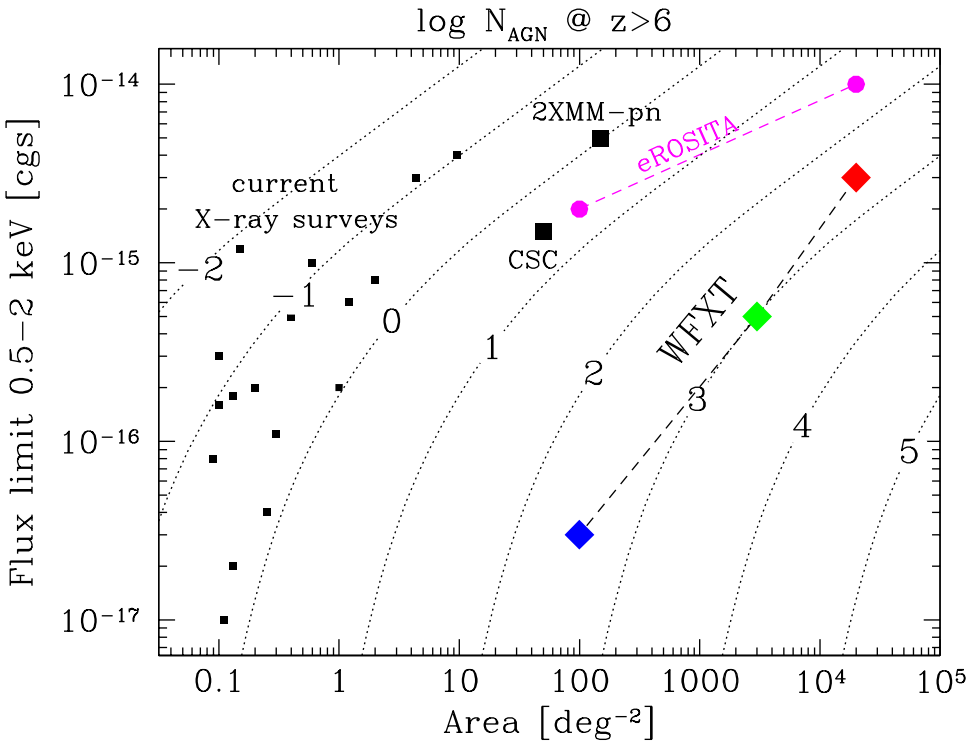

Fig. 3. Number of AGN at $z > 6$ expected from the "decline" model (see text) for different combination of survey area vs 0.5-2 keV limiting flux. Dotted lines are the locii of equal AGN number as labeled (labels are in log units). Small black squares show the major Chandra and XMM surveys (either performed or ongoing, including the 4Ms CDFS, the 2Ms CDFN, C-COSMOS, AEGIS, XBootes and many others). Big black squares show the current coverage of the Chandra (CSC) and XMM (2XMM-pn) archives. The deep and wide surveys to be performed with eROSITA in 4 years are shown as magenta circles (based on Cappelluti et al. 2010, this volume). The three WFXT surveys (5 year program) are shown as rotated squares. Less than one $z > 6$ AGN is expected in each of the current X-ray surveys. eROSITA will return about 40 objects with the current design. WFXT will detect about 1600 objects.

ulate less abundant halos but their luminosity, and hence detectability, is higher. In each case, surface densities as high as 500 deg^{-2} at the WFXT-Deep limiting flux are reached.

Observations of significant samples at $z > 6$ would constrain the physics of early BH formation disentangling between these scenarios. The surveys performed by WFXT have the power to provide such large statistical samples. As a reference model, we will consider the "decline" model outlined above, which is found to be in excellent agreement with the 0.5-2 keV logN-logS of AGN at $z > 3, 4, 5$ (Brusa et al. 2009, Civano et al. in prep.). About 1600 AGN at $z > 6$ are expected to be detected by WFXT, and about 70 ot them should be at $z > 8$. A summary of the predictions for AGN at $z > 6$ and $z > 8$ in the three WFXT surveys for the decline and maximum XLF scenarios is shown in Table 1. In the WFXT-Deep survey it will be possible to detect in significant numbers $z > 6$ AGN down to $\log L_x = 43.1$ and $z > 8$ AGN down to $\log L_x = 43.4$, making possible to determine the shape of the high-z XLF. To compare the high-z AGN yields from WFXT surveys with what is expected from major current X-ray surveys and with other X-ray missions which are either proposed or planned, we

Table 1. Number and minimum 0.5-2 keV luminosity of high-z AGN expected in the WFXT surveys according to the two evolution models ("decline" and "max LF") described in the text.

Quantity	Survey		
	Deep	Medium	Wide
$z > 6$			
$\log L^{min}$(0.5-2 keV)	43.1	44.3	45.1
N. AGN (decline)	300	1000	300
N. AGN (max LF)	15000	2300	300
$z > 8$			
$\log L^{min}$(0.5-2 keV)	43.4	44.6	45.4
N. AGN (decline)	20	45	10
N. AGN (max LF)	4300	210	10

show in Fig. 3 the number of $z > 6$ AGN to be detected with different combination of surveyed sky area and soft limiting flux according to the "decline" scenario. It is evident that even the major current X-ray surveys (e.g. CDFS, CDFN, COSMOS, AEGIS, X-Bootes) should return less than one object per field. In the full Chandra and XMM archives (labeled as CSC and 2XMM-pn, respectively) one would expect less than 10 objects in total. With the current mission design and survey strategy (Cappelluti et al. 2010, this volume), the eROSITA satellite, planned for launch in 2012, is expected to return about 40 $z > 6$ AGN, most of them at the luminosities of bright SDSS QSOs. The big leap is clearly expected to be performed by WFXT. The mission design and observing strategy studied for the Internation X-ray Observatory (IXO) are still uncertain: IXO will probably return a sample of $z > 6$ AGN with size in between those by eROSITA and WFXT (see Comastri et al. 2010, this volume).

The identification of these objects will clearly require wide area surveys with deep multiband optical and near-IR imaging like e.g. the LSST surveys (Brusa et al. 2010, this volume). On the other hand, the WFXT surveys will represent a perfect complement for all optical and near-IR campaigns that search the unobscured part of the high-z AGN population as image dropouts. Late type brown dwarfs are the main contaminants in optically selected samples, being 15 times more abundant than high-z QSOs of comparable magnitudes (Fan et al. 2001). Even when using near-IR colors to separate them from high-z QSO candidates, the success rate of optical spectroscopy is only 20-30% (Jiang et al. 2009). If sensitive X-ray images were available underneath each optical dropout, a detection in the X-rays would almost automatically ensure that the object is an AGN, since brown dwarfs of comparable optical magnitudes are $\sim$ 300 times fainter in the X-rays. LSST and WFXT surveys will then reinforce each other in the search of $z > 6$ AGN.

4. Evolution of the obscuration

A built-in feature of the BH/galaxy evolutionary sequence described in the Introduction is that an obscured accretion phase preceeds a clean accretion phase, at least in powerful, QSO-like objects. One may therefore wonder whether the fraction of obscured AGN was higher in the past. This indeed depends on many parameters such as i) the physical scale of the absorbing gas and how this is driven towards the BH; ii) the relative timescales of the obscured and unobscured phases; iii) whether the absorbed-to-unabsorbed AGN transition occurs also in low-mass/low-luminosity objects (i.e. Seyfert galaxies). Not many theoretical predictions on the evolution of the obscured AGN fraction are available in the literature. Models that relate the obscuration on nuclear scales to the availability of gas in the host galaxy generally predict an increase of the obscured AGN fraction with redshift (e.g Menci et al. 2008) since the gas mass in galaxies was larger in the past. Some others models, which anti-correlate the covering factor of the obscuring medium to the BH mass and then follow the evolution of the BH mass function using empirical relations (Lamastra et al. 2008), however do not predict such an increase. The situation is also debated from an observational point of view. An increase of the obscured AGN fraction with redshift among X-ray selected AGN has been observed by La Franca et al. (2005); Treister & Urry (2006); Hasinger (2008); Trump et al. (2009), but other works did not find any evidence of this trend (Ueda et al. 2003; Dwelly & Page 2006; Gilli et al.

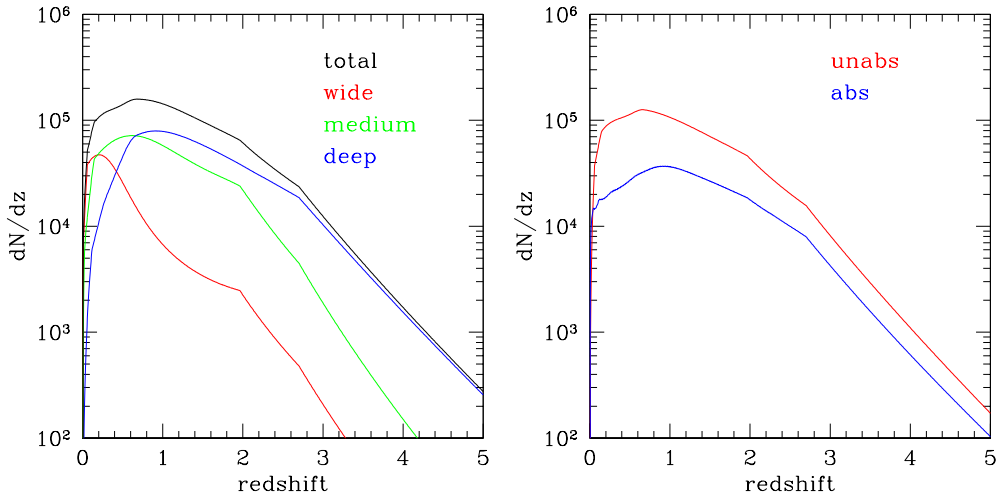

Fig. 4. *Left*: Redshift distribution of the 300,000 AGN with good X-ray spectra (i.e. with more than 1000 photons) in the three WFXT surveys. The Deep survey is providing most of the good X-ray spectra at $z > 1$. *Right*: As in the *left* panel but splitting the total sample of 300,000 AGN into unabsorbed ($\log N_H < 22$) and absorbed ($\log N_H \geq 22$) objects.

2007). Selection effects in these computations are very important and could mimic a spurious evolution of the obscured AGN fraction (see e.g. Gilli et al. 2010a).

Much of this uncertainty can be related to the lack of large statistical samples of AGN with high-quality X-ray spectra. Using samples of limited size, which cannot be split into narrow luminosity and redshift bins, it is often complicated to disentangle any redshift-dependent from luminosity-dependent effects (it is generally agreed that the obscured AGN fraction decreases with luminosity, but the slope and normalization of this relation differ from paper to paper). Furthermore, the absorption column density is often estimated either from the X-ray hardness ratio, or from the absence of broad emission lines in the optical spectrum. Both methods suffer from caveats and limitations (Brusa et al. 2010), and ideally the absorbing column should be measured through X-ray spectra with good photon statistics. The most recent XLF determinations contain $\lesssim$ 2000 AGN (Hasinger 2008; Silverman et al. 2008; Yencho et al. 2009; Ebrero et al. 2009; Aird et al. 2010), most of which are just slightly more than simple X-ray detections. With WFXT one would expect to detect about 300,000 AGN with good X-ray spectra, i.e. with more than 1000 photons each, in a broad redshift range ($z \sim 0-5$). As shown in Fig. 4 *left*, the WFXT-Deep survey is providing most of the good X-ray spectra at $z > 1$, while the Medium and Wide surveys provide the largest contribution at lower redshifts. About 1/3 of the detected objects with good X-ray spectra are expected to be absorbed by column densities above 10^{22} cm^{-2} (see Fig.4 *right*). Future wide area optical and near-IR surveys should provide redshifts, either spectroscopic or photometric, for a significant fraction of these sources, making possible to divide the sample into fine redshift, luminosity and obscuration bins and therefore map the cosmological evolution of nuclear obscuration.

5. The most obscured AGN

If the overall evolution of obscured AGN is uncertain, the evolution of the most heavily obscured and elusive ones, the so-called Compton-Thick AGN ($N_H > 10^{24}$cm^{-2}; hereafter CT AGN), is completely unknown, mak-

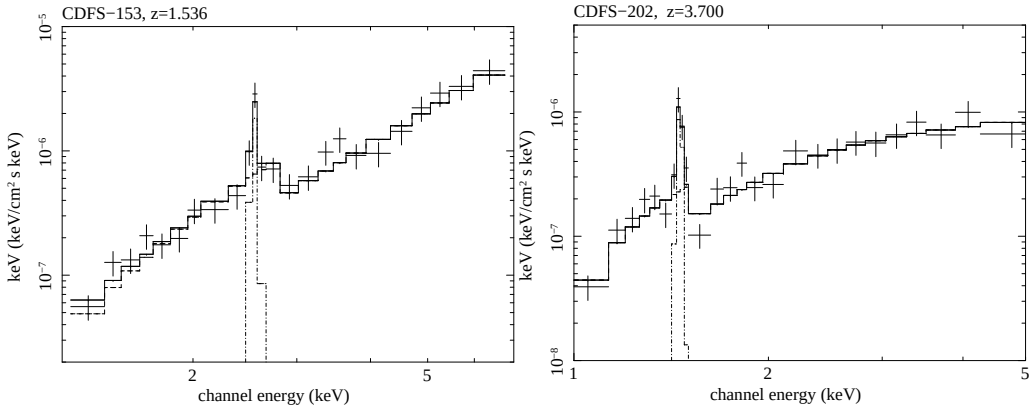

Fig. 5. Simulated WFXT spectra of CDFS-202 and CDFS-153, two high-z CT AGN with $f_{2-10} > 10^{-15}$ erg cm^{-2} s^{-1} observed in the XMM-CDFS: the goal effective area and an exposure time of 400 ks were assumed. No background is included, which however is not expected to alter significantly the S/N ratio (see text).The 100 deg^2 WFXT-Deep survey (Murray et al. 2008, Rosati et al. 2010, this volume) is expected to reveal about 500 objects like these at $z > 1$ in terms of obscuration and photon statistics.

ing the census of accreting black holes largely incomplete.

Only ∼50 *bona-fide* CT AGN, i.e. certified by X-ray spectral analysis, are known in the local Universe (Comastri 2004; Della Ceca et al. 2008), but their abundance has nonetheless been estimated to be comparable to that of less obscured ones (Risaliti et al. 1999). At higher redshifts, an integrated constrain to the space density of CT AGN can be obtained from the spectrum of the X-ray background. Depending on the assumptions, synthesis models of the XRB predict that from ∼10 to ∼30% of the XRB peak emission at 30 keV is produced by the emission of CT AGN integrated over all redshifts (Gilli et al. 2007; Treister et al. 2009), but the main contribution likely arises at $z \sim 1$. In the absence of any information, the luminosity function and evolution of CT AGN in XRB synthesis models have been usually assumed to be equal to those of less obscured ones. Because of the uncertainties in the average spectrum of CT AGN and in their evolution, however, the constraints to the CT space density from the XRB spectrum remain rather loose.

In recent years there have been many attempts to constrain the space density of CT AGN in different luminosity and redshift intervals exploiting different selection techniques. Very hard (> 10 keV) X-ray surveys are still limited in sensitivity and are just sampling the local Universe (Malizia et al. 2009). To sample AGN at higher redshifts, and in particular at $z \sim 1$, one needs to rely on deep X-ray surveys in the 2-10 keV band and try to select CT AGN either directly from X-ray spectroscopy, or by comparing the measured, obscured X-ray emission (if any) with some other indicator of the intrinsic nuclear power: IR selection can track the nuclear emission as reprocessed by the dusty absorber; narrow optical emission lines can sample the gas ionized by the nucleus on scales free from obscuration. X-ray stacking of IR-selected sources not individually detected in the X-rays has been used to estimate the space density of CT AGN at $z \sim 1-2$ (Daddi et al. 2007; Alexander et al. 2008; Fiore et al. 2009; Bauer et al. 2010). The comparison between the [O III]5007 and X-ray flux has been used to select X-ray underluminous QSOs and then estimate the density of CT QSOs at $z = 0.5$ (Vignali et al. 2010). To sample the population of CT around $z \sim 1$, Gilli et al. (2010b) recently devised a selection method based on the [Ne V]3426 emission line, which can be applied to optical spectroscopic surveys with deep X-ray cover-

age and seems to deliver clean, albeit not complete, samples of CT objects at $z > 0.8$, i.e. at redshifts not reachable with [O III]5007 selection. Despite these numerous efforts, [Ne V], [O III], and IR selection are all indirect ways to select CT AGN, since the CT nature of an object is simply inferred from the faintness of its X-ray emission relative to an indicator of the intrinsic power, and therefore may suffer from severe systematic uncertainties.

To unambiguously obtain samples of *bona-fide* CT AGN over a broad redshift range, very deep X-ray exposures are needed such as the 2.5 Ms XMM survey in the CDFS (Comastri et al. 2010, in prep.). A number of CT candidates, identified in the 1 Ms CDFS catalog on the basis of their flat (low quality) spectrum (Tozzi et al. 2006), are indeed being confirmed as such by the higher quality XMM spectra (Comastri et al. 2010, in prep.), including the well-known CT candidate CDFS-202 at $z = 3.7$ (Norman et al. 2002). Because of their limited sky coverage, however, only a few tens of *bona-fide* high-z CT AGN are expected to be detected in current deep X-ray surveys, making population studies of CT AGN problematic.

The WFXT surveys are expected to determine the cosmological evolution of *bona-fide* CT AGN up to $z \sim 3$. Based on the synthesis model by Gilli et al. (2007), the WFXT-Deep survey will return a sample of ~ 500 objects at $z > 1$ which are *bona-fide* CT AGN, i.e. with more than 500 net counts in the 0.5-7 keV band (the number of simple detections of CT objects will be obviously much larger). In Fig. 5 we show two such objects (CDF-202 and CDFS-153, another CT AGN, at $z = 1.53$, found in the XMM-CDFS) simulated using the WFXT response matrices for the goal design. No background is assumed in the simulation, but, based on the level estimated for low-earth orbits (see Ettori & Molendi 2010, this volume), only about 20 background photons are expected above 1 keV, which would therefore not alter significantly the spectral quality. It is evident that 500 X-ray photons are sufficient to unambiguously reveal their CT nature: in principle, based on the iron Kα line, it would be possible to determine also their redshift without the need of optical spectroscopy. In total, 500, 270, 60 and 12 *bona-fide* CT AGN at redshifts above 1, 2, 3 and 4, respectively, are expected in the WFXT-Deep survey. Future missions sensitive to energies above 10 keV, such as NuSTAR and ASTRO-H (approved by NASA and JAXA, respectively) or EXIST and NHXM (proposed to NASA and ASI, respectively) are expected to allow population studies of CT AGN at $z < 1$, with a peak in the redshift distribution at $z \sim 0.3 - 0.4$. The WFXT mission appears to uniquely complement these and extend them to $z > 1$. Only IXO, on a longer timescale and depending on the adopted survey strategy and mission design, could possibly provide samples of distant CT objects matching in size those expected from WFXT.

6. Conclusions

About 15 millions of AGN in a very broad redshift and luminosity range will be detected by the WFXT surveys. Some of the major issues related to the evolution of accreting SMBHs are expected to be solved by this sample as detailed below.

• WFXT will break through the high-z Universe: more than 1600 AGN will be observed at $z > 6$, allowing population studies at these redshifts and providing an unvaluable complement for future wide area optical and near-IR surveys searching for black holes at the highest redshifts. Such a large sample is a unique feature of the WFXT surveys and cannot be matched by any other planned or proposed X-ray mission.

• Good X-ray spectra, with more than 1000 photons, will be obtained for 300,000 AGN allowing accurate measurements of their absorbing column density. This will make possible for the first time to measure the evolution of nuclear obscuration with cosmic time up to $z \sim 5$ and verify its connection with e.g. star formation.

• About 500 *bona fide*, i.e. certified by X-ray spectral analysis, CT AGN at $z > 1$ will be found in the WFXT-Deep survey. This will complement population studies at lower red-

shifts obtained by future high-energy surveys such as those performed by the approved missions NuSTAR and Astro-H and will make possible to detemine the abundance and evolution of this still missing BH population. Performing population studies of distant heavily obscured objects, and determining their relevance in the census of accreting black holes and evolutionaly path of galaxies is another unique science case to be carried out by WFXT.

Acknowledgements. We thank all the members of the WFXT collaboration. RG acknowledges stimulating discussions with R. Salvaterra. We acknowledge partial support from ASI-INAF and PRIN/MIUR under grants I/023/05/00, I/088/06/00 and 2006-02-5203.

References

Aird, J., Nandra, K., Laird, E. S., et al. 2010, MNRAS, 401, 2531
Alexander, D. M., Chary, R., Pope, A., et al. 2008, ApJ, 687, 835
Bauer, F. E., Yan, L., Sajina, A., & Alexander, D. M. 2010, ApJ, 710, 212
Beelen, A., Cox, P., Benford, D. J., et al. 2006, ApJ, 642, 694
Brusa, M., Civano, F., Comastri, A., et al. 2010, ApJ, 716, 348
Brusa, M., Comastri, A., Gilli, R., et al. 2009, ApJ, 693, 8
Comastri, A. 2004, in Astrophysics and Space Science Library, Vol. 308, Supermassive Black Holes in the Distant Universe, ed. A. J. Barger, 245–+
Cowie, L. L., Songaila, A., Hu, E. M., & Cohen, J. G. 1996, AJ, 112, 839
Daddi, E., Alexander, D. M., Dickinson, M., et al. 2007, ApJ, 670, 173
Della Ceca, R., Severgnini, P., Caccianiga, A., et al. 2008, Memorie della Societa Astronomica Italiana, 79, 65
Dwelly, T. & Page, M. J. 2006, MNRAS, 372, 1755
Ebrero, J., Carrera, F. J., Page, M. J., et al. 2009, A&A, 493, 55
Elvis, M., Civano, F., Vignali, C., et al. 2009, ApJS, 184, 158
Fan, X. 2006, New Astronomy Review, 50, 665
Fan, X., Narayanan, V. K., Lupton, R. H., et al. 2001, AJ, 122, 2833
Feruglio, C., Maiolino, R., Piconcelli, E., et al. 2010, A&A, 518, L155+
Fiore, F., Puccetti, S., Brusa, M., et al. 2009, ApJ, 693, 447
Gilli, R., Comastri, A., & Hasinger, G. 2007, A&A, 463, 79
Gilli, R., Comastri, A., Vignali, C., Ranalli, P., & Iwasawa, K. 2010a, in American Institute of Physics Conference Series, Vol. 1248, American Institute of Physics Conference Series, ed. A. Comastri, L. Angelini, & M. Cappi, 359–364
Gilli, R., Vignali, C., Mignoli, M., et al. 2010b, A&A, 519, A92+
Hasinger, G. 2008, A&A, 490, 905
Hasinger, G., Miyaji, T., & Schmidt, M. 2005, A&A, 441, 417
Hopkins, P. F., Hernquist, L., Cox, T. J., & Kereš, D. 2008, ApJS, 175, 356
Jiang, L., Fan, X., Bian, F., et al. 2009, AJ, 138, 305
Jiang, L., Fan, X., Brandt, W. N., et al. 2010, Nature, 464, 380
Juarez, Y., Maiolino, R., Mujica, R., et al. 2009, A&A, 494, L25
Kauffmann, G. & Haehnelt, M. 2000, MNRAS, 311, 576
Kurk, J. D., Walter, F., Fan, X., et al. 2009, ApJ, 702, 833
Kurk, J. D., Walter, F., Fan, X., et al. 2007, ApJ, 669, 32
La Franca, F., Fiore, F., Comastri, A., et al. 2005, ApJ, 635, 864
Lamastra, A., Menci, N., Maiolino, R., Fiore, F., & Merloni, A. 2010, MNRAS, 405, 29
Lamastra, A., Perola, G. C., & Matt, G. 2008, A&A, 487, 109
Lehnert, M. D., Nesvadba, N. P. H., Cuby, J., et al. 2010, Nature, 467, 940
Li, Y., Hernquist, L., Robertson, B., et al. 2007, ApJ, 665, 187
Luo, B., Bauer, F. E., Brandt, W. N., et al. 2008, ApJS, 179, 19
Madau, P. & Rees, M. J. 2001, ApJ, 551, L27
Malizia, A., Stephen, J. B., Bassani, L., et al. 2009, MNRAS, 399, 944
Marconi, A., Risaliti, G., Gilli, R., et al. 2004, MNRAS, 351, 169

Marulli, F., Bonoli, S., Branchini, E., Moscardini, L., & Springel, V. 2008, MNRAS, 385, 1846
Menci, N., Fiore, F., Puccetti, S., & Cavaliere, A. 2008, ApJ, 686, 219
Monaco, P., Fontanot, F., & Taffoni, G. 2007, MNRAS, 375, 1189
Murray, S. S., Kenter, A., Forman, W. R., et al. 2005, ApJS, 161, 1
Murray, S. S., Norman, C., Ptak, A., et al. 2008, in Society of Photo-Optical Instrumentation Engineers (SPIE) Conference Series, Vol. 7011, Society of Photo-Optical Instrumentation Engineers (SPIE) Conference Series
Narayanan, D., Li, Y., Cox, T. J., et al. 2008, ApJS, 174, 13
Norman, C., Hasinger, G., Giacconi, R., et al. 2002, ApJ, 571, 218
Oesch, P. A., Bouwens, R. J., Illingworth, G. D., et al. 2010, ApJ, 709, L16
Rhook, K. J. & Haehnelt, M. G. 2008, MNRAS, 389, 270
Richards, G. T., Strauss, M. A., Fan, X., et al. 2006, AJ, 131, 2766
Risaliti, G., Maiolino, R., & Salvati, M. 1999, ApJ, 522, 157
Salvaterra, R., Della Valle, M., Campana, S., et al. 2009, Nature, 461, 1258
Salvaterra, R., Haardt, F., & Volonteri, M. 2007, MNRAS, 374, 761
Shankar, F., Salucci, P., Granato, G. L., De Zotti, G., & Danese, L. 2004, MNRAS, 354, 1020
Silverman, J. D., Green, P. J., Barkhouse, W. A., et al. 2008, ApJ, 679, 118
Taniguchi, Y. 2008, in IAU Symposium, Vol. 250, IAU Symposium, ed. F. Bresolin, P. A. Crowther, & J. Puls, 429–436
Tanvir, N. R., Fox, D. B., Levan, A. J., et al. 2009, Nature, 461, 1254
Tozzi, P., Gilli, R., Mainieri, V., et al. 2006, A&A, 451, 457
Treister, E. & Urry, C. M. 2006, ApJ, 652, L79
Treister, E., Urry, C. M., & Virani, S. 2009, ApJ, 696, 110
Trump, J. R., Impey, C. D., Elvis, M., et al. 2009, ApJ, 696, 1195
Ueda, Y., Akiyama, M., Ohta, K., & Miyaji, T. 2003, ApJ, 598, 886
Vignali, C., Alexander, D. M., Gilli, R., & Pozzi, F. 2010, MNRAS, 404, 48 (V10)
Volonteri, M., Lodato, G., & Natarajan, P. 2008, MNRAS, 383, 1079
Walter, F., Carilli, C., Bertoldi, F., et al. 2004, ApJ, 615, L17
Wilkins, S. M., Bunker, A. J., Ellis, R. S., et al. 2010, MNRAS, 403, 938
Willott, C. J., Delorme, P., Reylé, C., et al. 2009, AJ, 137, 3541
Willott, C. J., Delorme, P., Reylé, C., et al. 2010, AJ, 139, 906
Yencho, B., Barger, A. J., Trouille, L., & Winter, L. M. 2009, ApJ, 698, 380

Mem. S.A.It. Suppl. Vol. 17, 97

Memorie della
Supplementi

X-ray variability with WFXT

AGNs, transients and more

M. Paolillo[1,8], C. Pinto[2,1], V. Allevato[3,1], D. de Martino[4], M. della Valle[4], I. Papadakis[5], R. Gilli[6], P. Tozzi[7], and the WFXT collaboration

[1] Università Federico II, Dip. di Scienze Fisiche C.U. Monte S.Angelo, Napoli, Italy e-mail: paolillo@na.infn.it
[2] SRON, Sorbonnelaan 2, 3584 CA Utrecht, the Netherlands
[3] Max-Planck-Institut für Plasmaphysik, Boltzmannstrasse 2, D-85748 Garching, Germany
[4] Istituto Nazionale di Astrofisica – OAC, Napoli, Italy
[5] University of Crete Dept Physics, P.O. Box 2208, GR 710 03 Heraklion, Greece
[6] Istituto Nazionale di Astrofisica – OABo, Bologna, Italy
[7] Istituto Nazionale di Astrofisica – OATs, Trieste, Italy
[8] Istituto Nazionale di Fisica Nucleare, Napoli, Italy

Abstract. The Wide Field X-ray Telescope (WFXT) is a proposed mission with a high survey speed, due to the combination of large field of view (FOV) and effective area, i.e. grasp, and sharp PSF across the whole FOV. These characteristics make it suitable to detect a large number of variable and transient X-ray sources during its operating lifetime. Here we present estimates of the WFXT capabilities in the time domain, allowing to study the variability of thousands of AGNs with significant detail, as well as to constrain the rates and properties of hundreds of distant, faint and/or rare objects such as XRF/faint GRBs, Tidal Disruption Events, ULXs, Type-I bursts etc. The planned WFXT extragalactic surveys will thus allow to trace variable and transient X-ray populations over large cosmological volumes.

Key words. Galaxies: active – X-rays: bursts – Gamma-ray burst: general – supernovae: general – X-rays: binaries – novae, cataclysmic variables – Surveys – Telescopes

1. Introduction

The ability to conduct timing studies has always characterized X-ray astronomy, but so far, due to the limited sensitivity and field-of-view (FOV) of the instruments on board of X-ray satellited, studies were concentrated on individual and relatively nearby and bright sources.

The Wide Field X-ray Telescope (WFXT) is a proposed X-ray mission characterized by a wide field (1 square degree), a large effective area ($1m^2$ @ 1 keV) and a costant PSF across the entire FOV (goal design, see Rosati et al. in this volume). While not designed to be a monitoring mission, its capabilities and the proposed observing strategy, make it suit-

Send offprint requests to: M. Paolillo

able to conduct timing studies for an unprecedented number of moderate and high redshift AGNs, as well as to discover and constrain rates and properties of distant, faint and rare X-ray populations such as X-ray Flashes/faint GRBs, Tidal Disruption Events, ULXs, Type-I bursts etc.

In this work we present estimates of the WFXT monitoring capabilities for AGNs and other variable/transient sources, that can be detected in the 3 main extragalactic surveys planned for the mission. In this respect the work presented here represents the minimum achievements expected by WFXT in the time domain, since more specific and/or dedicated studies (e.g. galactic surveys, nearby galaxies monitoring etc.) will certainly increase the WFXT impact in the field.

2. Monitoring SMBH accretion with WFXT

Monitoring campaigns on nearby galaxies have shown that intense variability on all timescales, from hours to years, is a common property of all AGNs. This variability increases with energy, and is very intense in the X-ray regime, in close resemblance with the one observed in galactic accreting Black Holes (BH) (see McHardy 2010, for a comprehensive review). Long observations, as those required to conduct deep surveys (*Chandra* Deep Fields, Lockmann Hole), allowed to study variability also in higher redshift sources, confirming that variability is common to all AGNs over cosmological volumes, and that it reflects the details of the accretion process and the properties of the system (mass, accretion rate, obscuration) (Almaini et al. 2000; Paolillo et al. 2004). X-ray variability can thus be used as a tool to trace the accretion history of SMBH across cosmic time (Papadakis et al. 2008; Allevato et al. 2009). Such attempts however have been hampered by the random sampling pattern and small number of sources accessible with the present generation of X-ray satellites.

The study of AGN populations is one of the primary objectives of the WFXT missions. In its first 5 years WFXT will conduct 3 extragalactic surveys that are predicted to detect an unprecedented number of AGNs ($> 10^7$, see Gilli et al. and Matt & Bianchi contributions in this volume). While a large number of these sources will be close to the detection limit, the WFXT grasp (Rosati et al., this volume) ensures that a considerable fraction will be detected with several thousand photons, thus allowing to perform variability studies on the temporal baselines sampled by the different surveys.

2.1. Predicting the number of variable AGNs

In order to evaluate the WFXT monitoring capabilities for AGNs, we initially assumed that each field in the 3 planned surveys will be observed continuously. While this is feasible for the *Wide* and *Medium* survey due to its short exposure time per field (2 ks and 13 ks), it is unrealistic for the *Deep* survey due to the long exposure times (400 ks) and the visibility constraints for a low-orbit mission; we will discuss how to relax these constraints in 2.2. To simulate the intrinsic AGN variability we adopted a template X-ray Power Density Spectrum (PDS) observed in nearby AGNs (e.g. NGC 4051) displaying the characteristic power-law shape with a high-frequency break (e.g. Uttley et al. 2002). We further required at least 10 bins of equal duration in the X-ray lightcurve, and that the average signal-to-noise ratio (S/N) per bin in the satellite band, due to the intrinsic variability, is larger than a fixed threshold ($S/N = 3$ in Figure 1). Note that these requirements are much more stringent than a simple variability detection, allowing to derive constraints on the underlying physical processes. We adopted the background estimates of Tozzi et al. (this volume) which include particle contribution, galactic ISM and unresolved AGNs/galaxy clusters. The expected number of variable AGNs was finally derived from AGN number counts (Hasinger et al. 1995; Giacconi et al. 2002; Luo et al. 2008), after converting the S/N limit into a flux limit, and multiplying for the total angular coverage of each survey (20000, 3000 and 100 sq.deg. for the Wide, Medium and Deep survey respectively).

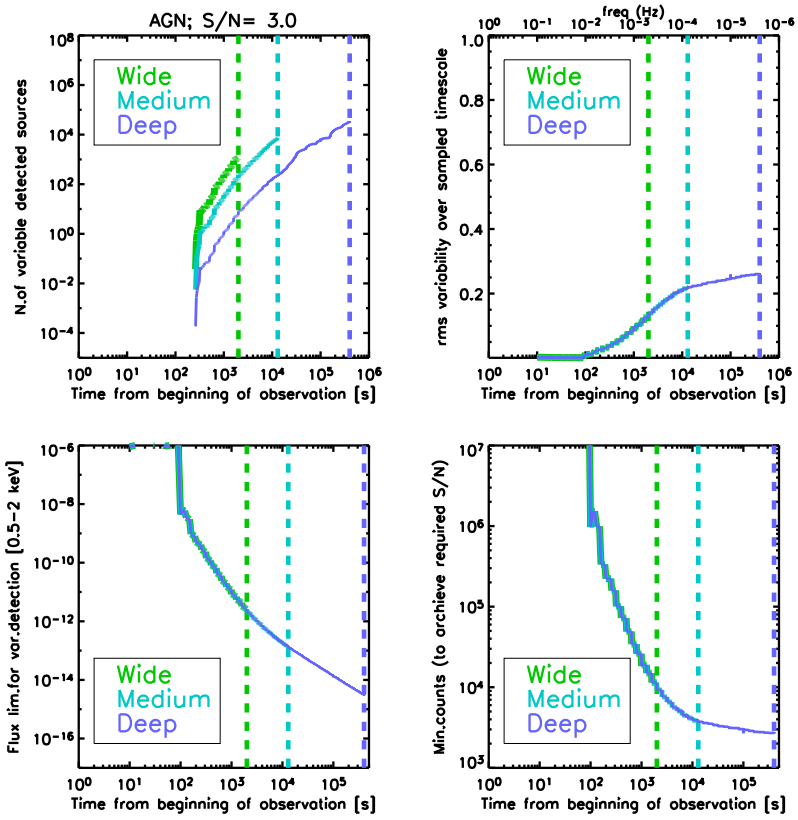

Fig. 1. AGN variability estimates for the WFXT extragalactic surveys as a function of the sampled timescale: *Top panels*) Number of sources for which variability is detected with the required S/N (left) and average rms variability detected at every timescale (right); *Bottom panels*) Flux limit for variability detection within the assumed S/N threshold (left) and corresponding total counts (right). The vertical dashed lines represent the duration limit of each survey, assuming continuous monitoring.

The results of the simulations are shown in Figure 1. As the sampled timescale increases, the flux and count limits for a sound variability detection decrease, due to a combination of longer integration time and a larger intrinsic rms variability produced by the power-law behavior of the AGN PDS. The three surveys will reach limiting (variability) sensitivities, for $S/N > 3$, of $\sim 2 \times 10^{-12}$, 1×10^{-13} and 5×10^{-15} erg/s for the Wide, Medium and Deep survey respectively in the 0.5-2 keV band. With several thousand of counts in each source this sample largely overlaps with the one suited for spectroscopic studies (Gilli et al., this volume), allowing a detailed characterization of these AGNs. The predicted rms range between 10% and 25%, in good agreement with the values reported for deep extragalactic surveys (see e.g. Paolillo et al. 2004). While the Wide survey covers a much larger sky area, the longer integration will favour the Medium and Deep surveys, both in terms of accessible flux range and variability timescales.

These results are summarized in Figure 2, where we present the WFXT performance in terms of the number of AGNs with variability detected at the $> 3\sigma$ level, over the whole lightcurve. In this respect the WFXT capabilities appear comparable to other planned missions with a more stringent monitoring charac-

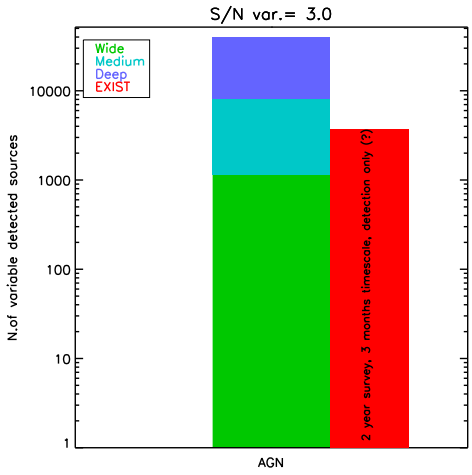

Fig. 2. Number of AGNs for which WFXT is expected to detect variability with $S/N > 3$, in each of the 3 planned extragalactic surveys. For comparison we show an estimate of the number of AGNs that will be detected by the EXIST mission, during the 2 years survey phase, with > 10 data points, as extrapolated from Della Ceca et al. (2009).

ter: for instance the wide field EXIST mission (Grindlay 2007) will also monitor thousands of AGNs but, due to the different energy band, spatial resolution, sensitivity and sampling pattern, will offer a complementary view of more nearby AGNs (Della Ceca et al. 2009).

2.2. Constraining the observing strategy

The study of X-ray variability in nearby AGNs has shown that the AGN PDS depends most likely on the mass of and accretion rate onto the central supermassive BH (McHardy et al. 2006). The expectations based on the template PDS spectrum used in §2.1 may not be realistic when we assume a wide range of masses and accretion rates: for more massive/lower accreting sources the expected variability will be lower than assumed so far. On the other hand the continuous monitoring hypothesis must also be relaxed, thus compensating the reduced variability with longer temporal baselines. To investigate the impact that a sparse sampling pattern may have on the final variability measurements, we performed a set of Monte Carlo simulations of AGNs lightcurves in order to quantify the bias of the variability estimator. To this end we modified the original Timmer & Koenig (1995) algorithm that generates red-noise data with a power-law density spectrum, to reproduce the sampling pattern, background and sensitivities expected by WFXT. Figure 3 (left panel) presents an example of a possible observing scheme for a single field in the Deep survey, where observations of 50 ks each are spread evenly over ~ 6 months. Such scheme would allow to derive AGNs lightcurves with gaps of a few weeks, thus sampling both high and low frequencies in the PDS. Additionally such pattern could be useful to discover and trace transients with long decay timescales such as Tidal Disruption Events which are believed to be due to stellar disruptions near quiescent SMBH (see §3). In Figure 3 (right panel) we show the excess variance (i.e. the fractional variability) distribution for 5000 simulations of the sparsely sampled lightcurve compared to the input value. The retrieved mean excess variance agrees well with the input value, while the uncertainty on the single measurements is of the order of 20%. The large AGN samples provided by WFXT will allow to further reduce the statistical uncertainties on each of the studied subsamples. Finally this observing pattern will allow to extend the sampled frequency range, thus making the observation suitable to study the bulk of the AGN population down to low accretion/higher mass SMBHs.

3. Transient and variable sources

Other than AGNs, a large variety of variable and transient sources can be predicted to be observed by WFXT during its operating lifetime. To provide some quantitative estimates of the WFXT capabilities in this field, we took into consideration a few of the most likely variable objects that will be observed during the WFXT main surveys: Tidal Disruption Events (TDEs), Low Luminosity GRBs/X-ray flashes (LL-GRB, XRF), Super Soft Sources (SSS), Ultraluminous X-ray binaries (ULX), Type I bursts etc.

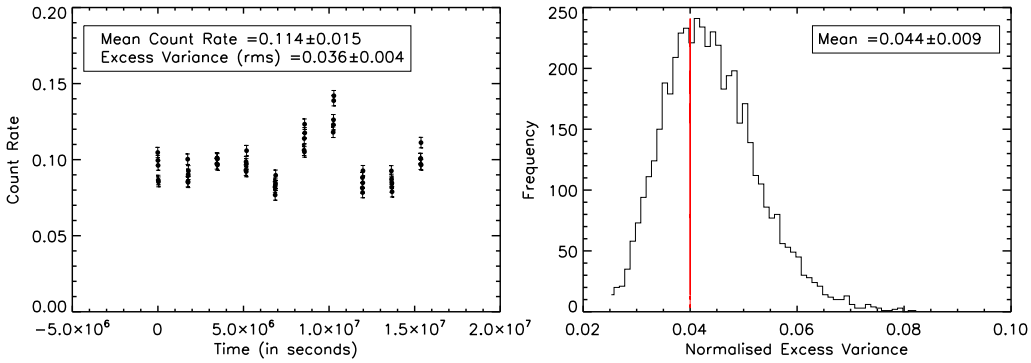

Fig. 3. *Left:* One example of a simulated WFXT AGN lightcurve for the Deep survey, reproducing flux and variability of one of the CDFS sources (Allevato et al. 2009), sampled in 50 ks observations spread uniformly over ∼ 6 months. *Right:* The *excess variance* distribution of 5000 simulated lightcurves, such as the one shown in the left panel, compared to the input value (vertical line) fixed at 0.04, i.e. 20% rms. This observing strategy will be able to retrieve the intrinsic variance with a 1σ uncertainty of 21%.

TDE: are believed to occur when a star is disrupted in the proximity of a quiescent SMBH, fueling the BH and revealing itself through the UV and X-ray emission due to the gravitational energy release of the accreted material. TDE are one of the few means to detect quiescent SMBH in distant galaxies. So far however only a handful of events have been serendipitously observed (e.g. Gezari et al. 2009). The large area covered by WFXT will make the detection of such events very likely, especially since their emission is expected to peak in the FUV/soft X-ray bands.

LL-GRBs/XRF: X-ray bursts have been detected in coincidence with SN explosions and/or GRBs. The fenomenology of such events is still poorly understood and both precursor type and rates are very debated in the literature, due to the small number of serendipitous detections observed so far. In this work we took into consideration two possible types of X-ray transients associated with SN events: XRF and LL-GRBs. The first class has its template in XRF 080109 observed by the Swift satellite without an associated GRB, and its origin can be due to the breakout of either the SN shock (Soderberg et al. 2008) or a mildly relativistic jet (Mazzali et al. 2008). On the other end LL-GRB, such as GRB 060218 (Campana et al. 2006), could represent the X-ray counterpart of many associated GRB-SNe. The number of future detections (see Table 1) depends on both the intrinsic SN rates (e.g. Cappellaro et al. 1999) and the opening angle of the associated jet (Guetta & Della Valle 2007).

SSS: Supersoft sources are X-ray emitters detected at energies below 1 keV, with X-ray luminosities of $10^{36\div38}$ erg s^{-1}, and characterized by blackbody-like spectra with temperatures of 15−80 keV (Kahabka & van den Heuvel 2006). Believed to be mostly hydrogen-burning white dwarfs, they are found both in early and late-type galaxies. SSS have complex time variability which is irregular over hours to years.

ULX: Ultraluminous X-ray binaries are variable accreting systems whth luminosities $> 10^{39}$ erg/s, i.e. larger than the Eddington luminosity for a neutron star or $5M_{\odot}$ BH, which display both long-term (days-months) variability and X-ray flares on timescales of hours. They tend to be associated to star forming regions, and proposed as candidates for intermediate ($> 100M_{\odot}$) mass BHs (Fabbiano 2006). The interest in such objects is due to the difficulties in explaining their formation in standard star-formation scenarios.

Type I bursts: these are accreting neutron stars (NS) in low-mass X-ray binaries (LMXB) displaying rapid (tens to hundreds of seconds) bursts with X-ray intensity many times brighter than the persistent level. The burst X-ray spec-

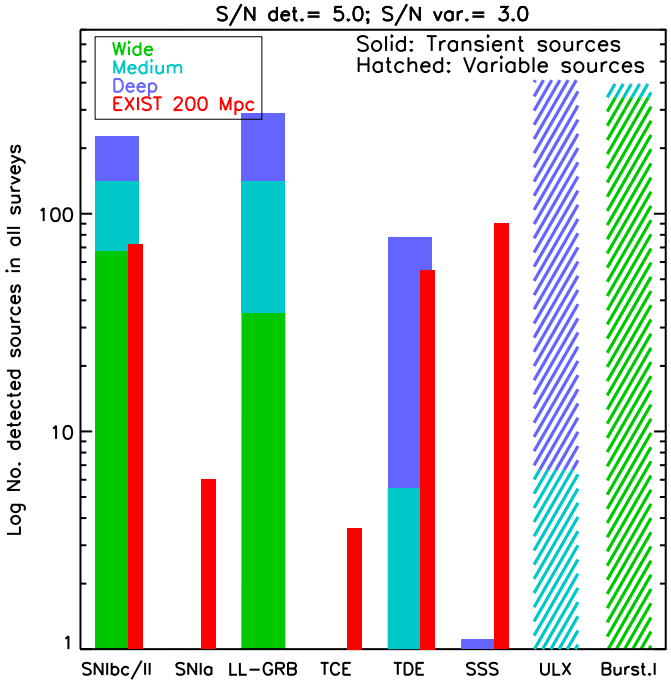

Fig. 4. Number of transient/variable sources expected in the WFXT extragalactic surveys. Recurring bursters are reported as hatched bars. For comparison we show the expected numbers within 200 Mpc from the EXIST mission over a comparable mission lifetime (Soderberg et al. 2009).

trum is generally consistent with a blackbody with color temperature of 2-3 keV, reaching X-ray luminosities up to 10^{38} erg s^{-1}. These events are caused by unstable nuclear burning on the surface of the NS (Galloway 2008). The X-ray bursts are often recurrent on timescales from 30 min to a few hours.

Other: many more types of rare and/or faint variable and transient sources are not discussed here in detail. For instance a breakout X-ray flash is predicted in SNIa events, while flares due to tidal compression (TCE) in stars accreted by a SMBH could mark the onset of the disruption process, triggering prompt followups. We included these in our simulations in order to cover the plausible parameter space, and highlight the WFXT capabilities as a function of the properties of the transient event.

We simulated the WFXT performance for variable and transient sources, other than AGNs, assuming a simplified burst model where a source of luminosity L_X^{quiesc} in the pre-burst phase, undergoes a burst of constant luminosity L_X^{burst} for a duration equal to the characteristic timescale of the actual X-ray lightcurve. We computed the number of expected detections, requiring that a source is detected with $S/N > 5$ and that its variable nature is ascertained with significance $S/N > 3$ with respect to the pre-burst phase, i.e. the burst starts during the observation. This simplified scheme allowed us to derive detection rates without the need of a specific knowledge of the characteristic of each source; obviously a more sophisticated approach is desirable and shall be implemented for each source separately in the future. The number of objects is calculated integrating over the cosmological volume accessible by WFXT for each source, given the parameters and constraints discussed above, and assuming an average volume density for the whole population. We did not ex-

Table 1. Number of transients expected in the WFXT extragalactic surveys, along with the physical parameters used in the simulations and the calculated distance limits.

Type	N.sources	L_X^{burst} (10^{40} erg/s)	$L_X^{quiescent}$ (10^{40} erg/s)	characteristic timescale (s)	Rate (Mpc^{-3} yr^{-1})	Dist.limit (Mpc, z)
SNIbc/II	226	10^3	1.0	500	10^{-3}	2.8×10^3, **0.50**
SNIa	2.1×10^{-5}	10^2	0.0	0.01	10^{-2}	3.8, **0.0009**
LL-GRB	290	10^4	0.0	10^4	3×10^{-5}	3.8×10^4, **4.2**
TCE	0.0062	10^2	0.0	10	10^{-4}	120, **0.028**
TDE	77.6	10^2	0.0	5×10^5	5×10^{-5}	1.8×10^4, **2.3**
SSS	1.1	10^{-4}	0.0	5×10^5	30	18, **0.004**
ULX	411	1	0.5	10^5	0.1	920, **0.19**
Type I bursts	395	10^{-2}	0.0	100	30	3.8, **0.0009**

plicitly include any evolutionary term, which is appropriate for most sources that will be observable only in the local Universe.

Figure 4 shows the number of detections in all surveys for the different classes discussed above: in particular hundred of LL-GRBs, XRF, TDE are expected over cosmological distances, mainly from the Deep survey. Recurrent bursters (ULX, Type I bursts) on the other hand will be mainly observable in the nearby Universe. For comparison we also show the predictions for the EXIST mission within 200 Mpc, as reported in Soderberg et al. (2009), even though it must be kept in mind that this mission will be using different energy bands and sampling patterns. In Table 1 we report the input parameters and the numbers derived from our simulations. It must be stressed however that the properties of most sources considered here may span a wide range and/or be affected by large uncertainties. The values presented in this work are mainly intended to highlight the mission capabilities as a function of the observational parameters. An online version of the *WFXT transient simulator* is available at `http://wfxt.na.infn.it/`, allowing the interested user to test additional type of source and/or parameter combinations.

The number of expected transients in each survey varies greatly depending both on the involved luminosities, volumetric rates and timescales. For instance frequent bursters (e.g. type I bursts) are likely to be observed mainly in the Wide survey, due to the greater area covered and despite the shorter exposure times. The interplay between these parameters can be observed in Figure 5, where we show the number of detections, flux limit and minimum counts for TDEs and LLGRBs. The different behavior of the two classes is caused by the different luminosities and timescales, since the volumetric rates are comparable. In particular the duration of the burst, compared with the survey duration, affects the shape of the curves because it reflects our ability to verify the source variability, especially close to the flux limit. Also note that the WFXT low background allows to detect transients down to $\sim$ 25 counts, but transients appearing early during the survey will end up having several thousand counts, thus allowing a good characterization of the lightcurve and of the spectral properties of the event.

4. Conclusions

The time domain is rapidly opening up for astronomical studies, at all wavelengths. For instance in the near future a number of optical facilities, such as Pann-STARR and LSST, will allow to monitor the whole sky with unprecedented speed. While not a monitoring missions WFXT, with its large effective area, wide FOV and stable PSF, promises to offer a complementary view of the variable high-energy Universe. WFXT will allow to study thousand of variable AGNs, and hundred of other transient and variable sources. The study of such populations has been mostly limited to the local Universe so far, while WFXT will be able

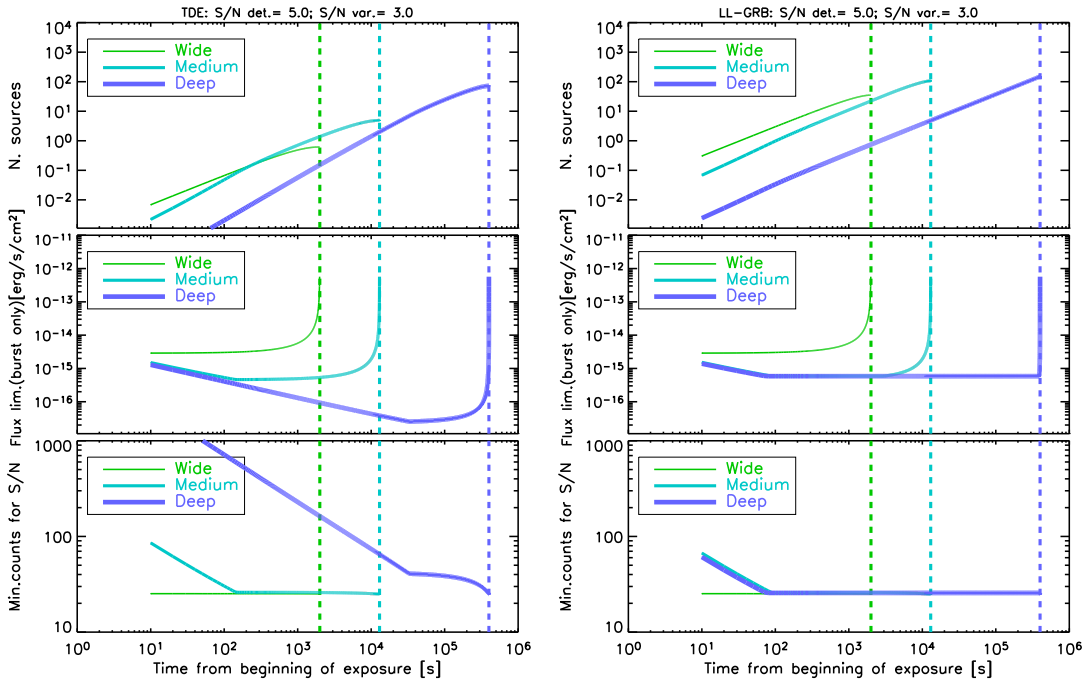

Fig. 5. Detection number and limiting fluxes and counts (tob, middle and bottom) for TDE (left panels) and LL-GRB (right panels) as a function of the sampled timescale.

to sample cosmologically relevant volumes, thus constraining their rates, evolution and the underlying physical processes. Finally, recent studies suggest that the X-ray band could be the optimal energy range to use in order to identify triggers and/or counterparts for next generation Gravitational Wave and Neutrino experiments (see, e.g. Guetta & Eichler 2010); WFXT thus would prove extremely valuable in validating and characterizing the astronomical events detected by these facilities.

Acknowledgements. We wish to thank S. Gezari, L. Stella, P. Giommi, A. Cavaliere and A. Paggi for helpful discussions and comments. MP and DdM acknowledge ASI financial support through contract I/088/06/0.

References

Allevato, V., Pinto, C., Paolillo, M., et al. 2010, AIP Conference Series, 1248, 491
Almaini, O., et al. 2000, MNRAS, 315, 325
Campana, S., et al. 2006, Nature, 442, 1008
Cappellaro, E., Evans, R., & Turatto, M. 1999, A&A, 351, 459
Della Ceca, R., et al. 2009 "The Extreme Sky: Sampling the Universe above 10 keV"; arXiv:0912.3096
Fabbiano, G. 2006, ARA&A, 44, 323
Galloway, D.K., et al. 2008, ApJS, 179,360
Gezari, S., et al. 2009, astro2010: The Astronomy and Astrophysics Decadal Survey, 2010, 88
Giacconi, R., et al. 2002, ApJS, 139, 369
Grindlay, J. 2007, in AIP Conf. Proc. 921, The First GLAST Symposium (New York: AIP), 211
Guetta, D., & Della Valle, M. 2007, ApJ, 657, L73
Guetta, D., & Eichler, D. 2010, ApJ, 712, 392
Hasinger, G., et al. 1993, A&A, 26, 275
Kahabka, P., & van den Heuvel, E. P. J. 2006, Compact stellar X-ray sources, 461
Luo B., et al. 2008, ApJS, 179, 19
Mazzali, P.A., et al. 2008, Science, 321, 1185
McHardy, I.M., et al. 2006, Nature, 444, 730
McHardy, I. 2010, Lecture Notes in Physics, Berlin Springer Verlag, 794, 203
Paolillo M., et al. 2004, ApJ, 611, 93
Papadakis, I. E., et al. 2008, A&A, 487, 475
Soderberg, A. M., et al. 2008, Nature, 453, 469

Soderberg, A., et al. 2009, 'The Astronomy and Astrophysics Decadal Survey', 2010, 278
Timmer, J. & Koenig, M. A&A, 1995, 300, 707
Uttley, P., McHardy, I. M., & Papadakis, I. E. 2002, MNRAS, 332, 231

Mem. S.A.It. Suppl. Vol. 17, 106

Memorie della
Supplementi

Identification of (high-redshift) AGN with WFXT: lessons from COSMOS and CDFS

M. Brusa[1], R. Gilli[2], F. Civano[3], A. Comastri[2], R. Fiore[4], and C. Vignali[5]

[1] Max Planck Institut für Extraterrestrische Physik, Giessenbachstrasse 1, D-85748 Garching by München, Germany e-mail: marcella@mpe.mpg.de
[2] Istituto Nazionale di Astrofisica – Osservatorio Astronomico di Bologna, Via Ranzani 1, I-40127 Bologna, Italy
[3] Harvard-Smithsonian Center for Astrophysics, 60 Garden Street, Cambridge, MA 02138
[4] Istituto Nazionale di Astrofisica – Osservatorio Astronomico di Monteporzio Catone, Via Frascati 33, I-00044 Monte Porzio Catone, Italy
[5] Dipartimento di Astronomia – Università di Bologna, Via Ranzani 1, I-40127 Bologna, Italy

Abstract. The Wide Field X–ray Telescope (WFXT) will provide tens of millions of AGN, with more than 4×10^5 expected at z> 3. Here we review the issues present in the identification of (large) samples of faint and high-redshift X–ray sources, and describe a statistical, powerful tool that can be applied to WFXT catalogs. The depth of associated optical and near infrared catalogs, needed for a reliable and as much complete as possible identification, are also discussed, along with the combined synergies with existing or planned facilities.

Key words. Galaxies: active – X-rays: Active Galactic Nuclei – galaxies: high-redshift

1. Scientific drivers

One of the main aims in extragalactic astronomy for the next decade is the study of the co-evolution of galaxies and the Super Massive Black Holes (SMBH) residing in their centre, out to the very first epochs of galaxy formation. In this respect, deep and sensitive X–ray observations will be the *unique* instrument to reveal the accretion light from SMBH in galactic nuclei at high-z, which are often invisible at longer wavelengths because of intergalactic absorption and dilution by the host galaxy.

The study of Active Galactic Nuclei (AGN) demography at z> 3 is one of the key science drivers for the Wide Field X–ray Telescope (WFXT, e.g. Forman et al. 2010). In the past decade, the characterization of the early phase of SMBH growth has been limited to the study of optically selected QSOs detected mostly in the SDSS survey, i.e. sampling only the unobscured and most luminous tail of the AGN population. Deep and medium deep *Chandra* and XMM-*Newton* surveys have allowed the study of X–ray selected QSOs up to relatively high redshifts, z$\sim$ 3 – 4. At higher redshifts, present X–ray surveys are highly incomplete and strongly limited by the small area sampled. As an example, there are only a few X–ray selected QSO with confirmed spectroscopic redshifts at z> 5 (see Barger et al. 2005) Moreover, the extrapolations of the X–ray lu-

Send offprint requests to: M. Brusa

minosity function (LF) as obtained combining various XMM and Chandra surveys differ by up an order of magnitude (see Figure 1, and reference therein, adapted from Brusa et al. 2010). As a comparison, the number of optically selected QSOs revealed up to z$\sim$ 6 is approaching 50, i.e. large enough to determine their LF which encodes the information about the history of SMBH build up and the integrated flux of UV ionizing radiation (e.g. Fan et al. 2006; Jiang et al. 2009; Willott et al. 2010, and reference therein). An unbiased search of X–ray selected z$\sim$ 5 – 6 QSOs would require to survey several hundreds of square degrees to a depth of the order of $\sim 10^{-15}$ erg cm^{-2} s^{-1} and thus beyond the capabilities of current X–ray telescopes. WFXT will offer the unique opportunity to explore the high-redshift universe, providing *about two order of magnitudes* larger samples with respect to the current SDSS samples ($\sim$ 2000 z$>$ 6 AGN vs. $\sim$ 50), opening a completely new, unexplored window for LF analysis. (see Gilli et al. 2010, this volume, for a full description of the high-redshift AGN demography with WFXT).

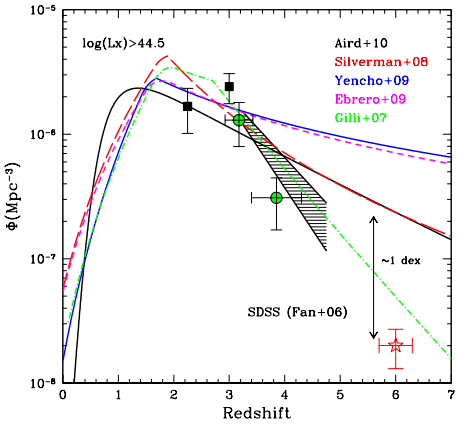

Fig. 1. The number density of $\log L_{2-10keV} > 44.5$ erg s^{-1} X–ray selected AGN vs. redshift as obtained from published LF, as labeled (Gilli, Comastri & Hasinger 2007; Silverman et al. 2008; Ebrero et al. 2009; Yencho et al. 2009; Aird et al. 2010) along with datapoints from the XMM–COSMOS surveys (green circles, Brusa et al. 2009a) and from Aird et al. (2010, black squares). The red star at $z = 6$ represents a conservative estimate of the z$\sim$ 6 QSO space density computed from the optical one assuming no evolution of the α_{ox}. For comparison (black shaded area) we plot the results for very bright QSOs ($M_{1450} < -27$, Fan et al. 2006), rescaled by an arbitrary factor.

2. Identification issues

The identification of the correct counterparts of both obscured and unobscured AGN is the first, crucial step for a full characterization of the physical and evolutionary properties of the entire population. At high redshifts, this process is further complicated by the fact that 1) z$>$ 3 sources constitute only a tiny fraction ($\sim$ 1%) of the entire X–ray population ($<$ 0.1% for z$>$ 6 sources) and 2) these objects are usually faint in the optical band, because the emission would be strongly reduced by cosmological dimming, and/or, for obscured sources, the intrinsic AGN emission is absorbed by the surrounding material. As a result, the probability of finding by chance a galaxy of R$>$ 24 in the X–ray error box is not negligible even with Chandra given the high surface density of background galaxies (see extensive discussions in, e.g., Luo et al. 2010). The identification process is made easier by using deep near infrared images given that AGN are strong IR emitters and the K-band flux is more tightly correlated with the X-ray flux than the optical (obscured) one (see Brusa et al. 2009b).

2.1. The likelihood ratio technique

A statistical, powerful method extensively exploited in deep XMM-Newton and Chandra surveys in the past years to look for the correct counterparts of X–ray sources is the "likelihood ratio" (*LR*) technique (Sutherland & Saunders 1992; Brusa et al. 2005). The method calculates the probability that a source is the correct association by weighting the information on the X–ray to optical distance, the surface density of (possible) false coincidence background objects and the brightness of the chosen counterpart:

$$LR = \frac{q(m)f(r)}{n(m)}$$

The object with the highest LR value[1] (above a certain threshold; see Sutherland & Saunders 1992 for details) is the most likely counterpart; when two or more sources have comparable LR values, a unique identification is not possible and both sources have a similar probability of being the correct identification ("ambiguous" sources). Using catalogs extracted from different bands (e.g., optical and infrared) may lead to different choices of the correct counterparts, and this information should be taken into account, too. In the following we will show the potentiality (and the challenges) on the use of the LR technique applied to WFXT data and the multiwavelength datasets available. We will make the case separately for the Wide ($F_{0.5-2} \gtrsim 3 \times 10^{-15}$ erg cm^{-2} s^{-1}), Medium ($F_{0.5-2} \gtrsim 5 \times 10^{-16}$ erg cm^{-2} s^{-1}), and Deep ($F_{0.5-2} \gtrsim 3 \times 10^{-17}$ erg cm^{-2} s^{-1}) parts of the WFXT survey (Rosati et al. 2010, this volume), based on the experience developed in the framework of the XMM-COSMOS (Hasinger et al. 2007), C-COSMOS (Elvis et al. 2009) and CDFS (Luo et al. 2008) surveys, where *multiwavelength* catalogs (e.g. optical to mid-infrared) resulted crucial to keep the fraction of ambiguous or false identification at minimim.

2.2. Wide and Medium survey: COSMOS lessons

To quantify the expected efficiency of the LR technique on the sources detected in the WFXT Wide survey, we first limited the XMM-COSMOS sample (Cappelluti et al. 2009) at fluxes larger than the expected limiting flux of the WFXT Wide survey ($F_{0.5-2keV} > 3 \times 10^{-15}$ erg cm^{-2} s^{-1}) and comparable to those expected for the eROSITA deep survey (Predehl et al. 2010, see also Cappelluti et al. 2010, this volume). Then we looked at the breakdown of the combined optical and IR identifications from the LR technique: 95% of the sources have been provided "secure" associations, while the remaining 5% show ambiguous counterparts in the Brusa et al. (2010) catalog. The reliability of the method has been tested a posteriori using Chandra, and turned out to be 99.6%: only one of the 245 unique/reliable XMM-COSMOS sources at fluxes larger than the WFXT Wide survey resulted associated to the wrong optical counterpart. Moreover, the statistical properties (such as redshifts, magnitudes, colors etc.) of the primary and secondary counterpart within the ambiguous sources are almost *indistinguishable*, and therefore the choice of the counterpart among the two does not in principle affect the characterization of the full X–ray population.

The WFXT Medium survey has been designed to cover ~ 3000 deg^2 at fluxes of the order of $\sim 5 \times 10^{-16}$ erg cm^{-2} s^{-1}, i.e. comparable to the depth reached by the C-COSMOS survey (Elvis et al. 2009). Following a procedure similar to that applied to XMM-COSMOS data (see above), and thanks to the smaller (< 1") angular resolution of *Chandra* with respect to XMM-*Newton*, Civano et al. (2010) were able to provide secure associations for more than 95% of the sources detected above the expected WFXT Medium survey limit. The fraction of ambiguous sources in this sample is reduced to ~ 2%, only 1.4% of the X–ray sources are not identified.

Taking into account that the WFXT positional accuracy is expected to be better than that of XMM-*Newton* (HEW=5" – 10" for WFXT vs. HEW $\sim$ 15" for XMM-*Newton*), and only slightly worse than the *Chandra* one (HEW $\sim$ 2" when averaged across the FOV), we can safely conclude that counterpart identification would not be an issue for the WFXT Wide and Medium surveys, provided that the depth of the optical and IR ancillary data is enough to match the X–ray fluxes (see Section 2.4).

2.3. Deep survey: CDFS lessons

The WFXT deep survey ($F_{0.5-2keV} > 3 \times 10^{-17}$ erg cm^{-2} s^{-1} in the soft X–ray band) would be almost as deep as the CDFS 2Ms survey

[1] *q(m)* is the expected probability distribution, as a function of magnitude, of the true counterparts, *f(r)* is the probability distribution function of the positional errors of the X–ray sources assumed to be a two–dimensional Gaussian, and *n(m)* is the surface density of background objects with magnitude *m*.

Table 1. Optical and IR ideal coverage depth for WFXT AGN surveys

Survey	$F^{lim}_{0.5-2}$ cgs	I	K
Wide	4×10^{-15}	23.0	21.5
Medium	5×10^{-16}	25.0	23.0
Deep	3×10^{-17}	25.5	23.5

(Luo et al. 2008), over an area that is a factor of ∼ 1000 larger. The detailed identification analyses for the 2Ms CDFS sources (Luo et al. 2010), implementing likelihood ratio matching accross five bands (R, z, K, 3.6μm and 1.4 GHz) have shown the power of this approach while also quantifying the significant challenges in source identification at faint magnitudes (R> 25). Indeed, it was possible to provide identifications for 96% of the X–ray sources; among them, 90% have been classified as unique/secure, and 10% as ambiguous. At these deep X–ray fluxes, the statistical properties of primary and secondary counterparts between the ambiguous sources are often *different*. Moreover, 4% of the sources, despite the excellent quality and depth of the multiwavelength information available, were not associated to any counterpart, i.e. the correct counterpart is most likely fainter than the image depth. This exercise shows that the identification of the faintest among the WFXT counterparts in the deep survey may be challenging; In this respect, the HEW goal of 5" is a crucial requirement to keep at acceptable values the (already not negligible) identifications issues and to fully characterize the multiwavelength properties of the X–ray sources at the highest redshifts.

2.4. Depth of optical infrared images

The power of the LR technique described in the previous subsections is strongly related to the depth of the optical and infrared images and catalogs that will be used to identify the X-ray sources. The challenge will be to provide a homogeneous and (enough) deep coverage for the different WFXT surveys. At the limiting flux of the WFXT wide survey an optical coverage to I∼ 23 and K∼ 21.5 would be enough to identify ∼ 90% of the X–ray sources (see Figure 2, upper panels, and Table 1), but this should be on the *entire* surveyed area. At the time WFXT will be launched, PanSTARRS[2] will have surveyed ∼ 30.000 deg^2 to I∼ 24.2, and will provide imaging in at least 5 bands, needed to characterize the SED of the X–ray sources and isolate high-z candidates (see next Section). On a longer timescale, Euclid[3] will cover the entire extragalactic sky in the IR down to H∼ 24 (roughly corresponding to K∼ 23), and will provide also spectra. The LOw Frequency ARray (LOFAR, Morganti et al. 2010), that will survey the northern sky down to a flux of 0.8 mJy at 120 MHz (see Fig. 2 in Morganti et al. 2010), may be crucial to correctly identify radio emitters X–ray sources (radio AGN and starbursts).

PanSTARRS will also provide identification for a substantial fraction (> 50%) of the sources detected in the WFXT Medium and Deep surveys. In order to identify a fraction as large as 90% of the sources in these surveys, a coverage in the optical and near–infrared down to I∼ 25.5 and K∼ 23.5 is needed (see Figure 2, middle and lower panels, and Table 1). LSST is a proposed facility expected to cover the southern sky down to I∼ 27 (Abell et al. 2010); similarly to PanSTARRS, LSST will also provide multiband photometry at a depth comparable to the I-band limit. The coordination with present and next generation facilities is mandatory, in order to choose the areas for the deep surveys which maximize the availability of the deepest multiwavelength coverage, in particular: JWST[4], the PanSTARRS deep survey (I∼ 28 over 28 deg^2), the LSST deep survey (I∼ 28 on a few hundreds deg^2), Euclid (K∼ 25.5 on 40 deg^2), the VISTA VIDEO survey (down to K=23.5 over 15 deg^2).

[2] http://pan-starrs.ifa.hawaii.edu
[3] http://sci.esa.int/euclid
[4] http://www.jwst.nasa.gov

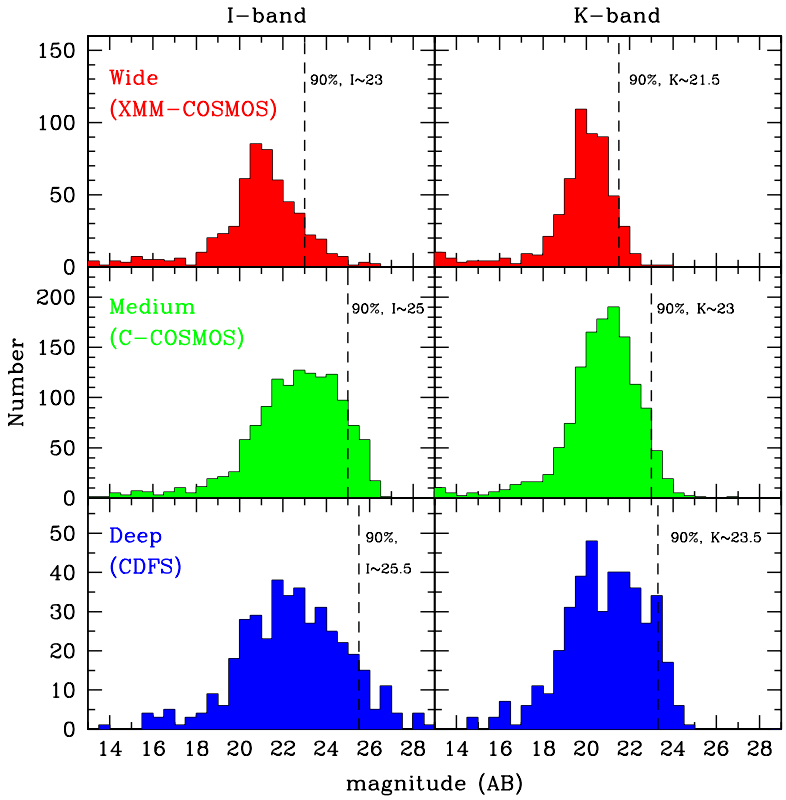

Fig. 2. I-band (left panels) and K-band (right panel) magnitude distributions expected in the three different WFXT surveys (Wide, Medium and Deep, from top to bottom). The expected magnitude distributions have been extracted from the XMM-COSMOS (Brusa et al. 2010), C-COSMOS (Civano et al. 2010), and CDFS (Luo et al. 2010) samples limited to fluxes $F_{0.5-2} > 3 \times 10^{-15}$ erg cm^{-2} s^{-1}, $F_{0.5-2} > 5 \times 10^{-16}$ erg cm^{-2} s^{-1} and $F_{0.5-2} > 3 \times 10^{-17}$ erg cm^{-2} s^{-1} in order to match the Wide, Medium and Deep limiting fluxes, respectively. The dashed lines mark the magnitudes at which most of the sources (90%) are identified.

3. Selecting z> 3 (or z> 6) AGN

Photometric redshifts of X–ray selected faint sources (R= 24 – 27) are essential for enabling science analyses and planning deep spectroscopy, and resulted *crucial* in isolating the high-z population in, e.g., XMM-COSMOS and CDFS. A similar, detailed source characterization requiring *multiband* imaging may be feasible only for small samples of WFXT sources. In this context, key resources will be again the upcoming LSST, PanSTARRS, Euclid, and (as far as spectroscopy for the Wide survey is concerned) the SDSSIII-BOSS[5] project. However, the high-z population shows on average fainter magnitudes than the overall X–ray source population (see Figure 3 in Brusa et al. 2009a), and therefore may remain among the unidentified population, if deep enough optical and near infrared coverage is not provided over the full area Another possibility is to search for X–ray counterparts on preselected high-z QSO on the basis of optical colours and/or dropouts techniques (e.g. Casey et al. 2008; Steidel et al. 2003), extended including the

[5] http://www.sdss3.org/boss.php

near-infrared bands in order to sample the z> 6 population (e.g. Willott et al. 2010). In this respect, the unprecedent combination of depth and area of WFXT will result in a much better characterization of the physical properties (such as bolometric luminosity and accretion rate) of the first accreting supermassive black holes. Moreover, z> 6 color selections suffer from significant contamination stellar objects (brown dwarfs are overwhelmingly more abundant and the spectroscopy success rate for z> 6 QSOs is only $\sim$ 20%). The complete SED characterization from NIR to X–ray will be able to resolve issues on contamination and completeness. For a non negligible fraction of the high-z candidates (a few out of a few hundreds, see also Matt et al. 2010, this volume), redshifts may be directly measured from the FeKα line (see examples in Civano, Comastri & Brusa 2005).

4. Conclusions

- WFXT will provide orders of magnitudes *larger* samples of high-redshift (z> 6) AGN compared to current (e.g. SDSS) optical surveys;
- the counterpart identification for WFXT sources selected in the Wide survey will be relatively easy, *if* synergies with present and future large area / all sky facilities (e.g. PanSTARRs, LSST, Euclid) are pursued;
- the secure identification of the counterparts detected in the WFXT Medium and Deep surveys would greatly benefit of the *smallest possible angular resolution* (the 5" HEW goal is really auspicable) and should heavily rely in the coordination with the future optical and NIR deep survey area (e.g. LSST, JWST);
- multiwavelength information is *mandatory* in order to get the redshift and the physical properties of the high-z AGN in the WFXT surveys.

Acknowledgements. We gratefully acknowledge the essential contribution from the COSMOS and CDFS teams, and in particular Bin Luo. RG acknoweledges support from the ASI grant I/088/06/00.

References

Abell et al., 2010, LSST White Book v.2.0, arXiv:0912.0201
Aird, J., et al., 2010, MNRAS, 401, 2531
Barger, A.J., et al., 2005, AJ, 129, 578
Brusa, M., et al., 2005, A&A, 432, 69
Brusa, M., et al., 2009a, ApJ, 693, 8
Brusa, M., et al., 2009b, A&A, 507, 1277
Brusa, M., et al., 2010, ApJ, 716, 348
Cappelluti, N., et al., 2009, A&A, 497, 635
Casey, C., et al., 2008, ApJS, 177, 131
Civano, F., Comastri, A., & Brusa, M., 2005, MNRAS, 358, 693
Civano, F., et al., 2010, ApJ submitted
Ebrero, J., et al. 2009, A&A, 493, 55
Elvis, M., et al., 2009, ApJS, 184, 158
Fan, X., et al. 2006, AJ, 132, 117
Fiore, F., et al., 2010, Proceedings of the conference "X-ray Astronomy 2009", arXiv:1002.3538
Forman, W., et al., 2010, Proceedings of the conference "X-ray Astronomy 2009", arXiv:
Gilli, R., Comastri, A., & Hasinger, G. 2007, A&A, 463, 79
Hasinger, G., et al., 2007, ApJS, 172, 29
Jiang, et al., 2009, AJ 138, 305
Luo, B., et al., 2008, ApJS, 179, 19
Luo, B., et al., 2010, ApJS, 187, 560
Morganti, R., et al., 2010, proceedings of "Panoramic Radio Astronomy: Wide-field 1-2 GHz research on galaxy evolution", arXiv:1001.2384
Predehl, P., et al., 2010, Proceedings of the conference "X-ray Astronomy 2009", arXiv:1001.2502
Silverman, J.D., et al., 2008, ApJ, 679, 118
Steidel, C., et al., 2003, ApJ, 592, 728
Sutherland, W. & Saunders, W. 1992, MNRAS, 259, 413
Yencho, B., et al., 2009, ApJ, 698, 380
Willott, C., et al. 2010, AJ, 139, 906

Mem. S.A.It. Suppl. Vol. 17, 112

Memorie della
Supplementi

X-ray spectroscopy of bright AGN

G. Matt and S. Bianchi

Dipartimento di Fisica, Università degli Studi Roma Tre, Via della Vasca Navale 84, I-00146 Roma, Italy
e-mail: matt@fis.uniroma3.it; bianchi@fis.uniroma3.it

Abstract. WFXT will observe tens of thousands of AGN with at least a few thousands counts each, so allowing for a detailed spectral analysis and providing a great leap forward in population studies. In this paper we review the present status of spectroscopic studies of samples of AGN, and discuss a few open issues, to the solution of which WFXT will contribute significantly.

Key words. X-rays: Active Galactic Nuclei

1. Introduction

In this paper we will try to assess the relevance of WFXT to the study of "bright" AGN. First of all, let us clarify what we mean with "bright" in this context. We mean a source detected with enough counts to permit a decent spectral analysis. Based on experience, one can (conservatively) put the number of counts needed to characterize and model the main spectral components to 5000, even if about 1000 counts may be sufficient if the spectrum is not too complex. Figure 1 shows the logN-log (Counts) in the 0.5-2 keV energy range for the three surveys (wide, medium and deep) which are the backbone of the WFXT observational program. All together, about 60000 (300000) AGN with more than 5000 (1000) counts are expected. This is a really impressive number when compared with what we have today (hundreds of sources, see below).

With so many sources available for a detailed spectral analysis, and even if WFXT has been mainly conceived and designed for cosmological purposes, studies of bright AGN - with the main emphasis to population studies - promise to be extremely rewarding.

Send offprint requests to: G. Matt

2. Where we are now

Spectroscopic studies of AGN populations are largely based on XMM-Newton observations. The largest sample is that derived from the BSS (Bright Serendipitous Survey: Della Ceca et al. 2004, Caccianiga et al 2008). It is a flux limited sample (flux limit of 7×10^{-14} erg cm^{-2} s^{-1} in the 0.5-4.5 keV energy range), extracted from the XMM Serendipitous Survey based on sources found serendipitously in the field of pointed targets. The sample comprises 400 sources, 80% of which are AGN. The X-ray selection guarantees the detection of sources like e.g. elusive AGN (Maiolino et al. 2003) which are very difficult to find at longer wavelengths.

A different approach to population studies is to collect all the pointing observations of AGN which have a sufficient number of counts for a detailed spectral analysis. We built

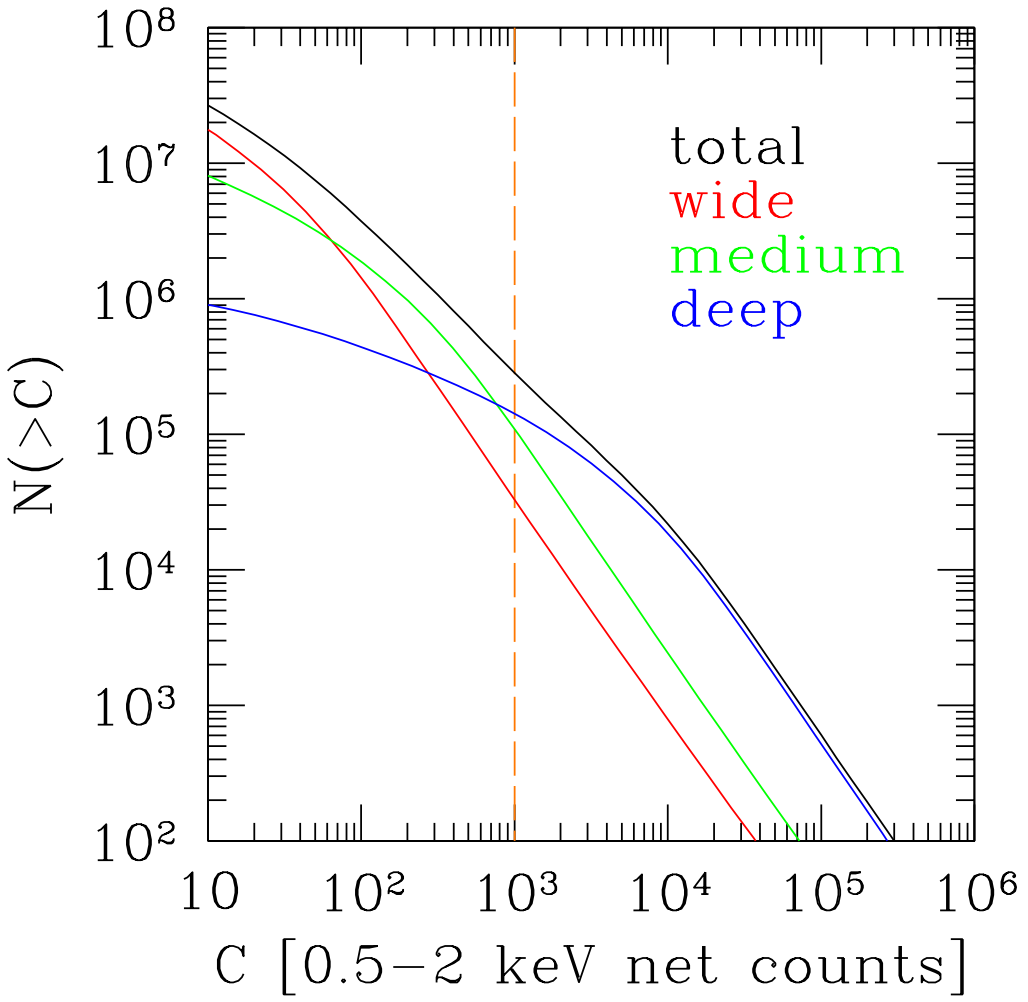

Fig. 1. The logN-log(Counts) in the 0.5-2 keV energy range for the three WFXT surveys (wide, medium and deep). The dashed vertical line indicates the number of sources with more than 1000 counts. Courtesy of Roberto Gilli.

such a sample by requiring at least 200 counts in both the 0.5-2 keV and 2-10 keV energy bands (most sources actually have more than a thousand counts). Further constraints are pile-up less than 1% and absorbing column density less than 10^{22} cm^{-2}. We selected only radio-quiet sources. The resulting sample of Seyfert 1/QSO, called CAIXA (Catalogue of AGN in the XMM-Newton Archive; Bianchi et al 2009a,b) is composed of 156 objects. All sources have 6 and 20 cm fluxes measured, while for 64% of them the Hβ FWHM from the Broad Line Region is known. The mass of the black hole is known for 52% of the sample.

The main results from CAIXA can be summarized as follows.

– The 2-10 keV power law index is harder in Broad Lines Seyfert 1s (BLS1; Γ=1.62±0.04) than in Narrow Lines Seyfert 1s, (NLS1; Γ=1.94±0.07) as shown in Figure 2. The two populations

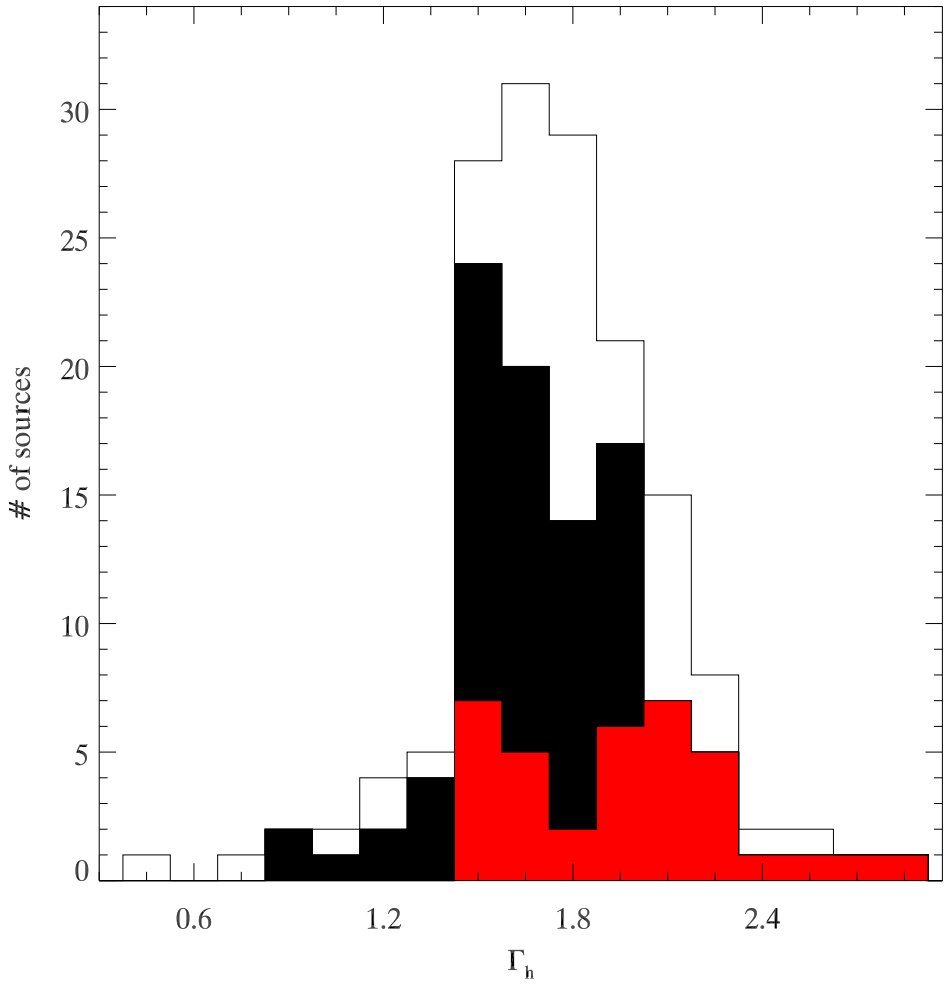

Fig. 2. The histogram of the 2-10 keV power law indices for NLS1 (red), BLS1 (black) and unclassified objects (white). From Bianchi et al. (2009a).

are different at more than 99.99% confidence level. (Here BLS1/NLS1 are defined as having the FWHM of the Hβ line larger/smaller than 2000 ks/s). This result confirms previous findings (Brandt et al. 1997).

– The Hβ FWHM is anticorrelated with the ratio between the soft and hard X-ray luminosities, and with the ratio between the optical and the X-ray flux. NLS1 seem to be X-ray weaker than BLS1.

– 123 out of 156 sources need a second and steeper power law to model the soft X-ray emission. If the second power law is replaced by a thermal model, the soft excess is characterized by a temperature which is constant across the range of luminosities and black hole masses, as already found by several authors (Gierlinski & Done 2004; Crummy et al. 2006). More on the soft excess issue in the next section.

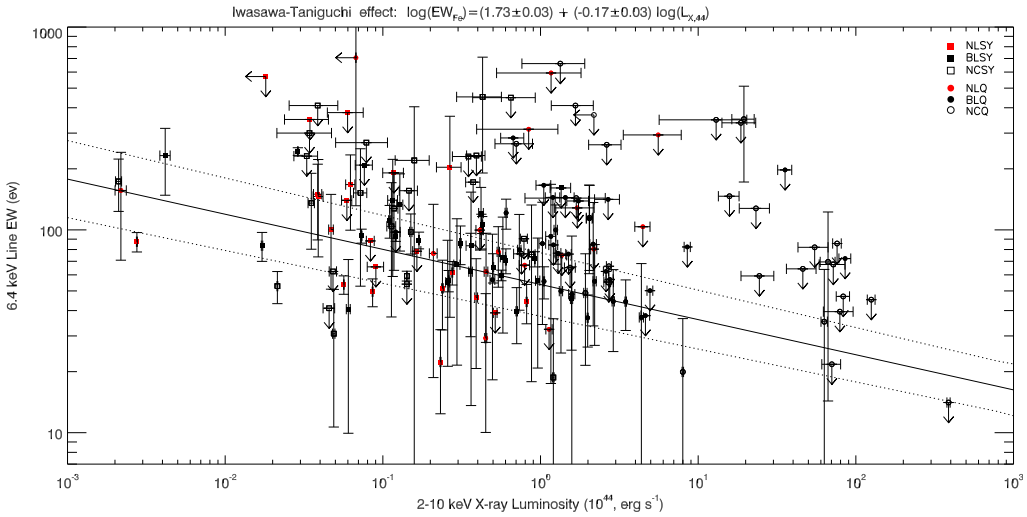

Fig. 3. The IT effect: the neutral iron line EW against 2-10 keV X-ray luminosity. See Bianchi et al. (2007) for details.

– A strong correlation between the X-ray luminosity and the BH mass is found. The slope is flatter than 1, suggesting that high-luminosity objects may be X-ray weak. A luminosity dependent bolometric correction could explain this result, but the one proposed by Marconi et al. (2004) leads to a more-than-linear relation. A linear relation is instead recovered using a bolometric correction based on the accretion rate (Vasudevan & Fabian 2007) or using the radio luminosity.
– The Iwasawa-Taniguchi effect is definitely confirmed (see next section).
– Fe XXV and Fe XXVI lines are detected in 24 sources, indicating that the presence of highly ionized matter is not uncommon. Their absolute and relative EWs are consistent with a production in distant matter which is photoionised by the AGN, with large ionization parameters and large column densities (up to 10^{23} cm^{-2} for Fe XXV, even larger for FeXXVI).

3. The WFXT contribution

A number of currently open problems (part of them already mentioned in the previous section) may be addressed - and hopefully solved - by WFXT thanks to the very large number of AGN which will be characterized spectroscopically.

– The nature of the soft X-ray emission in type 1 AGN. Soft X-ray emission in excess to the extrapolation of the hard X-ray power law was first discovered by EXOSAT in the Seyfert 1 galaxy Mkn 841 (Arnaud et al. 1985), and then observed to be common in type 1 AGN. Its origin, however, is still unknown. An interpretation in term of thermal disc emission - possibly Comptonized by a scattering layer - was first suggested, and remained the most popular one for many years. However, it was recently realized that the temperature which results from fitting the spectrum with a thermal emission is always around 0.1-0.2 keV, independently of the mass of the black hole. In the standard accretion disc model, instead, the temperature should scale with $M_{BH}^{-\frac{1}{4}}$. Alternative models have been proposed, which assume that the almost constant temperature is actually an artifact due to emission related to atomic physics transitions. The two most popular models are the relativistically broadened wind (Gierlinski & Done 2004, Middleton

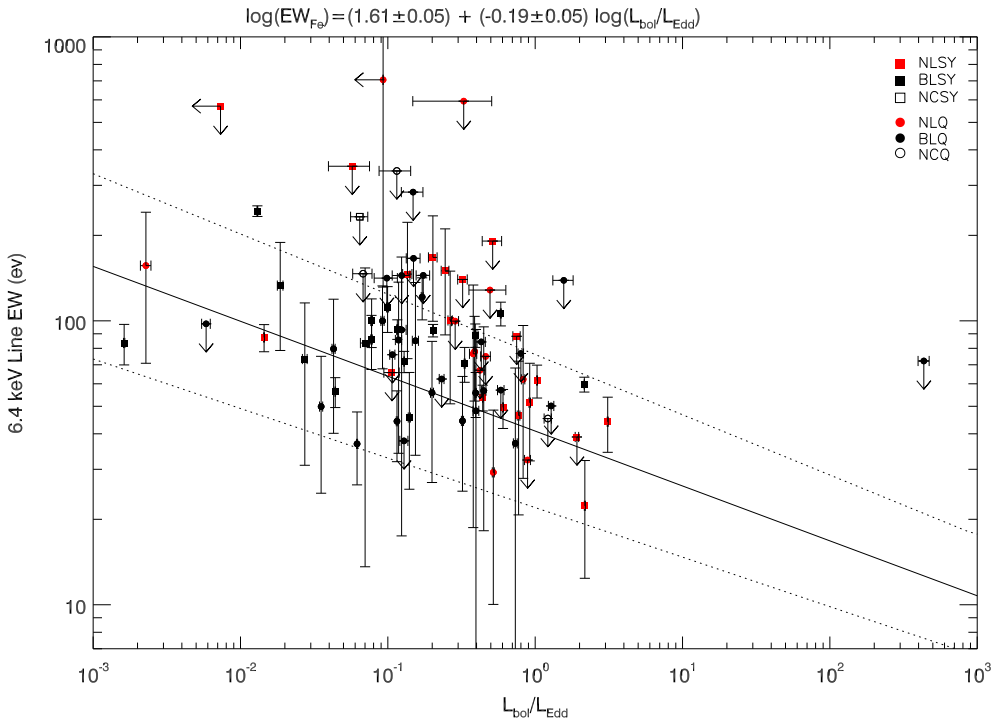

Fig. 4. The IT effect as a function of the Eddington ratio. See Bianchi et al. (2007) for details.

et al 2007) and the reflection model (Ross & Fabian 1993, Crummy et al. 2006). Both models, however, have serious problems. The wind model requires very large outflow velocities, while the reflection model requires - at least in some sources - very large reflection components.
WFXT will enlarge tremendously the number of sources where the soft X-ray excess can be studied, in so doing stretching considerably the range of masses probed. Its soft X-ray response is very well suited to this purpose. While at the moment no clear-cut measurement to solve the soft X-ray problem has been proposed, it is very likely that WFXT will contribute significantly to the understanding of the soft X-ray excess.

– The properties of the Warm Absorber beyond the local Universe. In about half of Seyfert 1s in the local Universe, absorption by moderately ionized matter (the so-called "Warm Absorber") is present (e.g. Reynolds 1997). The absorbing matter is usually outflowing with velocities of the order of hundreds of km/s, even if higher velocities have also been found, but in more ionized matter (Risaliti et al. 2005). The location of the Warm Absorber is still uncertain, even if Blustin et al. (2005) suggest that this matter is related to the obscuring pc-scale torus required in unification models. Mass and energetics are consequently also largely unknown.
Possible dependencies of the presence of the Warm Absorber and its physical properties on luminosity and redshift are basically unexplored. WFXT will provide such an exploration, helping to understand the nature and the physical and morphological properties of the Warm Absorber.

– The IT effect at high redshifts and luminosities. The Iwasawa-Taniguchi (IT) effect (Iwasawa & Taniguchi 1993) is the anticorrelation between the equivalent width

(EW) of the narrow core of the iron line and the X-ray luminosity, and for this reason it is also known as "X-ray Baldwin effect". The reality of this effect has been disputed for a long time, but now it is established beyond doubt (Bianchi et al. 2007; see Figure 3). While part of this effect may be due to variability (Jiang et al. 2006) - if the line is emitted in distant matter, and is therefore not variable on short time scale, an increase in the primary flux results inevitably in a decrease of the line EW - the presence of the anticorrelation over several decades in luminosity indicates a different, more fundamentale cause. The anticorrelation seems to be driven by the Eddington ratio (see Figure 4), rather than the mass of the black hole.

The most likely explanation of the IT effect is an anticorrelation between the covering factor of the line emitting matter (possibly the torus) and the X-ray luminosity, as also suggested by IR observations (Maiolino et al. 2007). Unfortunately, the limited energy band of WFXT prevents a study of the IT effect in the local Universe; a much larger sample, to confirm the relation with the Eddington ratio and to search for the effect in separate subclasses would be highly desirable. On the other hand, WFXT will offer the opportunity to search for this effect beyond the local Universe, in so doing significantly populating the - now severely underpopulated - high luminosity part of the anticorrelation.

4. Conclusions

Samples based on XMM-Newton consist of a few hundreds of sources with enough counts for a detailed spectral analysis. WFXT will increase this number by 2-3 orders of magnitude, providing an analogue in the X-ray domain of the SDSS in the optical band. Extensive population studies over a large range of luminosities and redshifts will then become, for the first time in X-rays, a reality.

References

Arnaud, K. A., Branduardi-Raymont, G., Culhane, J. L., et al., 1985, MNRAS, 217, 105

Bianchi, S., Guainazzi, M., Matt, G., Bonilla, N.F., 2007, A&A, 467, L19

Bianchi, S., Guainazzi, M., Matt, G., Bonilla, N.F., Ponti, G., 2009a, A&A, 495, 421

Bianchi, S., Bonilla, N.F., Guainazzi, M., Matt, G., Ponti, G., 2009b, A&A, 501, 915

Blustin, A.J., et al., 2005, A&A, 431, 111

Brandt, W.N., Mathur, S., Elvis M., 1997, MNRAS, 285, L25

Caccianiga, A., et al., 2008, A&A, 477, 735

Crummy, J., Fabian, A. C., Gallo, L., Ross, R. R., 2006, MNRAS, 365, 1067

Della Ceca, R., et al., 2004, A&A, 428, 383

Gierlinski, M., Done C., 2004, MNRAS, 349, L7

Iwasawa, K., Taniguchi, Y., 1993, ApJ, 413, L15

Jiang, P., Wang, J.X., Wang, T.G., 2006, ApJ, 644, 725

Maiolino, R., et al., 2003, MNRAS, 344, L59

Maiolino, R., et al., 2007, A&A, 468, 979

Marconi, A., et al., 2004, MNRAS, 351, 169

Middleton, M., Done, C., Gierlinski, M., 2007, MNRAS, 381, 1426

Reynolds, C.S., 1997, MNRAS, 286, 51

Risaliti, G., et al., 2005, ApJ, 630, L129

Ross, R.R., Fabian, A.C., 1993, MNRAS, 261, 74

Vasudevan, R.V., Fabian, A.C, 2007, MNRAS, 381, 1235

Mem. S.A.It. Suppl. Vol. 17, 118

Memorie della
Supplementi

X-ray absorption variability in AGN

Guido Risaliti[1,2]

[1] Istituto Nazionale di Astrofisica – Osservatorio Astrofisico di Arcetri, Largo E. Fermi 5, 50125 Firenze (Italy)
[2] Harvard-Smithsonian Center for Astrophysics, 60 Garden Street, Cambridge, MA 02138 (USA) e-mail: risaliti@arcetri.astro.it

Abstract. X-ray absorption variability is a common feature in Active Galactic Nuclei (AGN). Recent works of our group demonstrated that X-ray eclipses, on time scales of a few hours, occurred during several observations of local bright AGNs, without being spotted with traditional, time-averaged spectral analysis. These eclipses are remarkable events in themselves, but, more importantly, are a powerful way to investigate the inner structure of AGNs: they allow to measure the size of the X-ray source and the size, density and geometrical shape of the obscuring clouds. We show that WFXT would provide a real breakthrough in this field, allowing a systematic study of X-ray eclipses on hundreds of sources.

Key words. Galaxies: active

1. Introduction

X-ray absorption variability is common among Active Galactic Nuclei (AGN). Considering local bright obscured AGN with multiple hard X-ray observations, we found that N_H variations on time scales from months to a few years are almost ubiquitous (Risaliti et al. 2002).

More recently, such variability has been found at much shorter time scales, form a few hours to a few days, through campaigns of multiple observations within days/weeks, and detailed, time-resolved studies of long single observations.

In particular, in the case of the AGN in NGC 1365 we revealed extreme spectral changes, from Compton-thin (N_H in the range 10^{23} cm^{-2}) to reflection-dominated (N_H>10^{24} cm^{-2}) in time scales from a couple of days to ∼10 hours (Risaliti et al. 2007, 2009). Such rapid events imply that the absorption is due to clouds with velocity v>10^3 km s^{-1}, at distances of the order of 10^4 gravitational radii (assuming that they are moving with Keplerian velocity around the central black hole). The physical size and density of the clouds are of the order of 10^{13} cm and 10^{10}-10^{11} cm^{-3}, respectively.

All these physical parameters are typical for Broad Line Region (BLR) clouds, strongly suggesting that the X-ray absorber and the clouds responsible for broad emission lines in the optical/UV are one and the same.

Although NGC 1365 remains the most extreme case of X-ray eclipses, similar occultation events have now been found in several more sources (about 10, including both type 1 and type 2 sources, see Risaliti (2009) for an updated list). These results prove that X-ray absorption variability within single observations is common in local AGNs. Therefore, it

Send offprint requests to: G. Risaliti

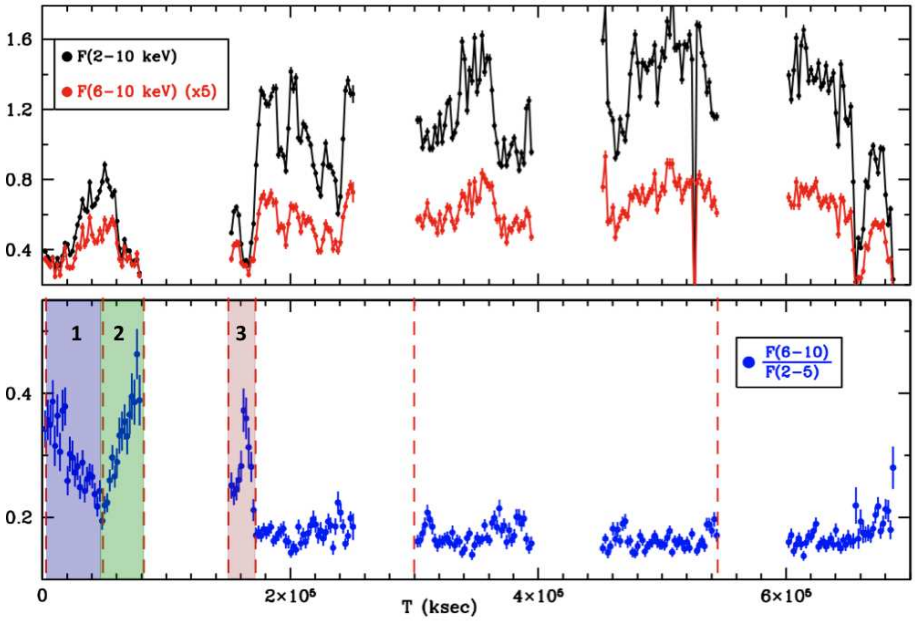

Fig. 1. Flux (top) and hardness ratio (bottom) light curves from the *XMM-Newton* long observation of Mrk 766. The observation is made in five consecutive *XMM-Newton* orbits.

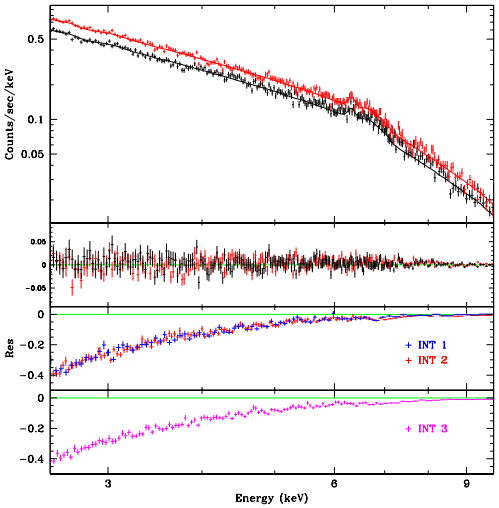

Fig. 2. Results from the spectral analysis of the eclipses observed in Mrk 766. Top two panels: spectra, best fit model and residuals from the third and fourh orbit (Fig. 1), where no spectral changes are observed. Bottom panels: difference between the spectra in the three intervals with spectral variations (Fig. 1) and the best fit model for the third and fouth orbit.

can be used as a tool to measure the properties of the X-ray absorbing clouds and, therefore, of the broad line region.

For this reason, a systematic study of X-ray eclipses in AGN would be invaluable to investigate the structure of the circumnuclear medium in AGN. Current observatories allow this kind of study only for a few bright sources with long *Suzaku* or *XMM-Newton* observations. In the future, new observatories with small fields of view, such as IXO, will be useful to better study single events, but only an observatory with both large efefctive area and large field of view, like WFXT, will be able to understand the relevance of this phenomenon in the general population of AGNs.

2. X-ray eclipses of AGNs

The method to search for X-ray eclipses in AGNs consists of a two-phase analysis: we first use the hardness-ratio light curve to select the time intervals where strong spectral variations occurred; we then perform a complete analysis of the spectra obtained from these intervals, in

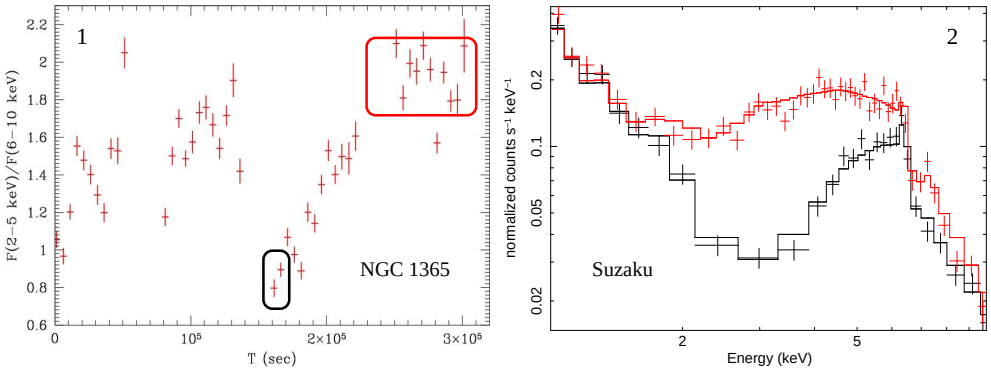

Fig. 3. Panel 1: Hardness ratio light curve form a *Suzaku* long observation of NGC 1365. Panel 2: Spectra obtained from the two intervals highlighted in the 1st panel.

order to measure possible N_H variations (and to check if the spectral changes are due to other effects, such as variations of the slope of the continuum emission).

As an example, this approach is illustrated in Fig. 1 for the long *XMM-Newton* observation of Mrk 766. We note that Mrk 766 is a Narrow Line Seyfert 1, so on average we do not expect to observe complete X-ray absorption of the X-ray source. However, as we show below, isolated clouds occasionally cross the line of sight, producing measurable absorption in the X-ray spectrum. The upper panel of Fig. 1 shows the standard 2-10 keV flux light curve for this observation, with the well known strong variability on time scales of thousands of seconds, or even shorter. The lower panel shows the light curve of the (6-10 keV)/(2-5 keV) flux ratio. In general, this light curve shows much smaller variations, indicating that the continuum shape remains the same during most of the luminosity variations. However, clear exceptions are observed in at least three intervals, highlighted in Fig. 1. During these intervals it is possible that a cloud with N_H of the order of 10^{23} cm^{-2} has covered the central source, strongly decreasing the observed flux in the soft band, without affecting the hard band, and therefore increasing the observed hardness ratio.

In order to check this scenario, we performed a complete analysis of the spectra obtained from the three highlighted intervals, and of those obtained from the third and fourth orbit, representing the standard spectral state of the source. In this analysis we allowed all the main spectral parameters of the model to vary among the different intervals. The results of the this study, illustrated in Fig. 2 are the following:
1) the 2-10 keV spectrum obtained from the third and fourth orbit (the "standard" state) is well reproduced by a typical model for type 1 AGNs, consisting of a power law, a reflection component and an iron emission line;
2) the spectral variations observed in the three intervals discussed above are completely reproduced by three absorption components with column densities in the range 1-3 10^{23} cm^{-2}.

As mentioned above, this analysis is at present possible one for a handful, very bright sources. In the following Section we show how WFXT can expand this kind of analysis on fainter/more rapidly variable sources.

3. WFXT observations of AGN eclipses

In order to show the capabilities of WFXT in detecting X-ray eclipses, we start from an already observed event in the "best" source for this kind of studies, i.e. NGC 1365.

In Fig. 3 we show the results of a long *Suzaku* observation of NGC 1365 (Maiolino et al. 2010, subm.). The hardness ratio light curve shows strong variations (1st panel). A complete spectral analysis of several intervals, chosen following the hardness ratio variations,

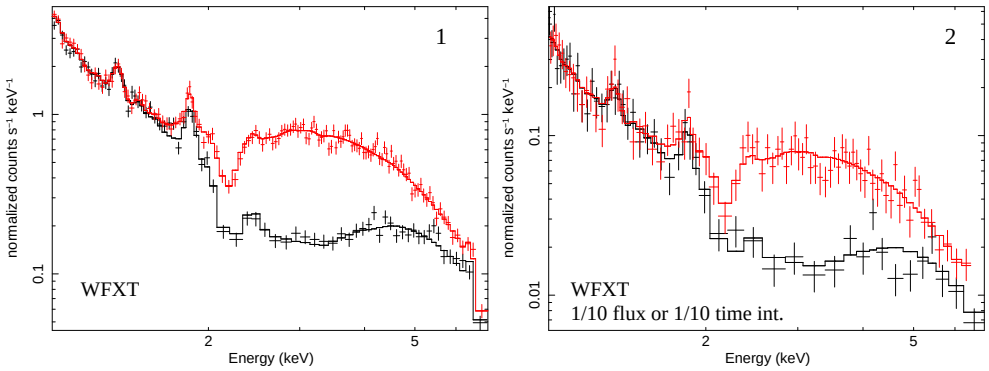

Fig. 4. WFXT simulations. Panel 1: simulation of the same events shown in Fig. 3, as observed with WFXT. Panel 1: same simulation, for a 10 times fainter source, or for the same source, but with spectra extracted from 10 times shorter intervals.

revealed that the whole observed variability can be reproduced with a constant continuum model, and a variable partial covering component. Two spectra obtained from two states with different hardness ratio are shown in the second panel.

Fig. 4 reveals the capabilities of WFXT to perform this kind of analysis: the same event observed with WFXT would produce the spectra in Panel 1, with a much higher S/N, and therefore with a more precise determination of the physical parameters of the obscuring cloud. The real possible breakthrough is however shown in Panel 2: this simulation show the same analysis performed with WFXT on a 10 times fainter source or, equivalently, on the same source, but selecting 10 times shorter time intervals. This imply that (1) the detection of X-ray eclipses will be possible for hundreds of sources, especially in the planned WFXT medium-depth survey; (2) in a few cases of very bright sources, it will be possible to investigate absorption variations on much shorter time scales than those accessible with currently available instruments.

Acknowledgements. This work has been partly supported by NASA grants GO8-9107X and NNX08AX78G.

References

Risaliti, G., Elvis, M., & Nicastro, F. 2002, *ApJ*, 571, 234
G. Risaliti, M. Elvis, G. Fabbiano, A. Baldi, A. Zezas, & M. Salvati, 2007, *ApJ*, 659, L111
G. Risaliti, G., et al. 2009,*ApJ*, 696, 160
Risaliti, G. 2009, arXiv:0912.2118

Mem. S.A.It. Suppl. Vol. 17, 122

Memorie della
Supplementi

The evolution of star forming galaxies with the Wide Field X-ray Telescope

P. Ranalli

Università di Bologna – Dipartimento di Astronomia, via Ranzani 1, 40127 Bologna, Italy
e-mail: piero.ranalli@oabo.inaf.it

Abstract. Star forming galaxies represent a small yet sizable fraction of the X-ray sky (1%–20%, depending on the flux). X-ray surveys allow to derive their luminosity function and evolution, free from uncertainties due to absorption. However, much care must be put in the selection criteria to build samples clean from contamination by AGN. Here we review the possibilities offered by the proposed WFXT mission for their study. We analyze the expected luminosity and redshift distributions of star forming galaxies in the proposed WFXT surveys. We discuss the impact of such a mission on the knowledge of the cosmic star formation history, and provide a few suggestions.

Key words. X-rays: galaxies – galaxies: luminosity function – galaxies: evolution – galaxies: high-redshift – galaxies: spiral

1. Introduction

The X-ray luminosity of star forming galaxies (SFG; they usually are spiral galaxies without AGN activity) appears to be a reliable, absorption-free estimator of star formation (Ranalli et al. 2003). This is justified on the basis that the X-ray luminosities are linearly and tightly correlated with the radio and FIR ones, which in turn are commonly used as star formation rate (SFR) indicators. Thus, the X-ray emission of SFG may be considered as a tool to investigate the cosmic star formation history. To this end, the study of the X-ray luminosity function (XLF) of galaxies and of its evolution represents a necessary step. Ranalli et al. (2005, hereafter RCS05) built a local ($z = 0$) XLF of SFG and investigated the possibilities for evolution. In this paper, we build on the RCS05 XLF and methods to explore the possible contribution of the Wide Field X-ray Telescope (WFXT) mission to our understanding of the SFG content of the universe, by analyzing the expected luminosity and redshift distributions.

The WFXT is a proposed mission which aims to perform very wide and moderately deep X-ray surveys. By taking a different approach to mirror design than the classical Wolter type-1 (Burrows et al. 1992), it could achieve a very large field of view ($\sim$ 1 deg^2) while maintaining a good angular resolution ($\sim 5''$) and a large effective area ($\sim$ 1 m^2) in the 0.1-7 keV band (Conconi et al. 2010).

Such a telescope would be able to observe a number of X-ray sources far exceeding all those known today. While X-ray surveys mainly detect AGN, star-forming galaxies (SFG) are also present, comprising a frac-

Send offprint requests to: P. Ranalli

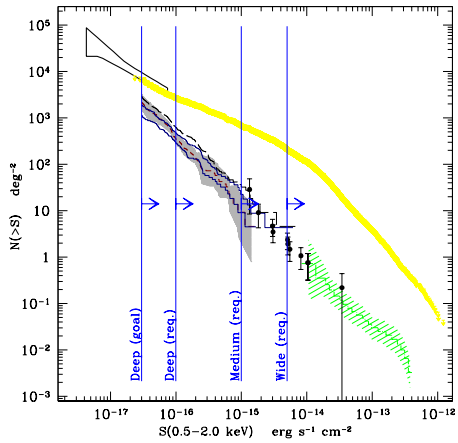

Fig. 1. Observed X-ray number counts in today's surveys, and planned WFXT limiting fluxes. The thick upper line and the horn show the observed Log N–Log S for all X-ray sources in the *Chandra* Deep Fields (Moretti et al. 2003) and the limits from the fluctuation analysis (Miyaji & Griffiths 2002). The bundle of histograms and data points shows several determinations of the star-forming galaxies Log N–Log S (see text). The vertical lines illustrate the limiting fluxes of the planned surveys.

Table 1. Covered area (deg^2) and limiting fluxes (erg s^{-1} cm^{-2} in the 0.5–2.0 keV band) of the proposed WFXT surveys.

	wide	medium	deep
area	20000	3000	100
flux (req.)	$5 \cdot 10^{-15}$	10^{-15}	10^{-16}
flux (goal)	$3 \cdot 10^{-15}$	$5 \cdot 10^{-16}$	$3 \cdot 10^{-17}$

tion in the range 1%–20% (depending on the flux) of all the sources detected in the 0.5–2.0 keV band. Three major surveys are envisaged with the WFXT, covering different amounts of the sky at different limiting fluxes and named *wide*, *medium* and *deep* (Fig 1). Their limiting soft X-ray fluxes correspond broadly to those probed in ROSAT (Tajer et al. 2005), XMM-*Newton* (Georgakakis et al. 2004) and deep *Chandra* (Bauer et al. 2004; Norman et al. 2004, RCS05) surveys of SFG. In Fig. 1 we show the total Log N–Log S from X-ray surveys, and different estimates of the SFG number counts.

Depending on technological developments, both a *requirement* and a *goal* value for the limiting fluxes can be quoted. Reaching the goals could extend the number of detected objects by a factor ~ 5. However, given the early stage of the mission, here we will consider only the requirements, and regard the goal flux limit for the *deep* survey only.

We assume $H_0 = 70$ km s^{-1} Mpc^{-1}, $\Omega_{\rm M} = 0.3$ and $\Omega_\Lambda = 0.7$.

2. The LF and evolution of star-forming galaxies

The local differential luminosity function

$$\varphi(\mathrm{Log}L)\,\mathrm{dLog}L \tag{1}$$

is defined as the comoving number density of sources per logarithmic luminosity interval. The evolution can be described as pure luminosity with the form (Schmidt 1972)

$$L(z) \propto (1+z)^{\eta_{\rm l}}. \tag{2}$$

Infrared surveys provide a powerful method to select SFG, since the bulk of the far and near IR emission is due to reprocessed light from star formation, with AGN representing only a minor population (de Jong et al. 1984; Franceschini et al. 2001; Elbaz et al. 2002). The FIR LFs may be assumed to be essentially unaffected by a contribution from Seyfert galaxies, as the fraction of Seyferts is about $\sim$ 5–10% (RCS05). While many determinations of IR LFs exist (see references in RCS05), here we take Takeuchi et al. (2003, 2004, hereafter T03) as reference. This is a 60μ LF derived from the IRAS Point Source Catalog Redshift (Saunders et al. 2000) (PSCz). It includes 15,411 galaxies with $z \lesssim 0.07$, covering 84% of the sky with a flux limit of 0.6 mJy at 60μ. While T03 reports pure-density evolution for their LF, pure-luminosity may provide an equally good fit to the data (T. Takeuchi, priv. comm.).

Other determinations of the SFG LF have been derived by the cross correlation of radio surveys with optical ones (see references in RCS05). The redshifts covered in these surveys are similar to those of the T03 galaxies,

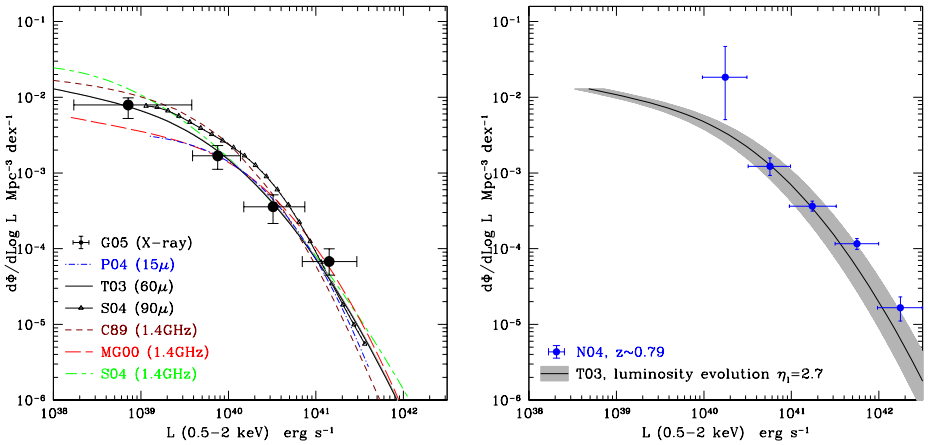

Fig. 2. *Left:* IRAS, ISO, and radio local luminosity functions of SFG converted to the X-rays (see RCS05 for references to the individual LFs). All the LFs converge to the same location. The large data points with error bars show an observational determination of the local XLF, based on XMM-*Newton* data by Georgantopoulos et al. (2005). *Right:* Comparison of the XLF derived from IRAS data (solid curve; the grey area shows the uncertainty on the evolution) with the XLF derived by Norman et al. (2004) in the *Chandra* Deep Field (data points with error bars).

but the number of objects is smaller due to a smaller sky coverage, so reliable estimates of the evolution may not be derived.

The local IR or radio LFs may be converted to X-ray ones by using the approach first developed in Avni & Tananbaum (1986) (see also: Georgantopoulos et al. 1999; Norman et al. 2004), which may be summarised as follows. Given a galaxy with IR or radio luminosity L, let $P(L_{\rm X}|L)$ be the probability distribution of the possible values of the galaxy's X-ray luminosity $L_{\rm X}$, as given by the optical/IR/radio vs. X-ray correlations. Thus, the X-ray LF may be otained by the convolution of an optical/IR/radio LF with $P(L_{\rm X}|L)$. In Ranalli et al. (2003) it was reported that the X-ray luminosity is tightly correlated with radio and FIR luminosities. By assuming a Gaussian probability distribution for these correlations, one has for example

$$P(\mathrm{Log}\, L_{0.5-2\mathrm{keV}}|\, \mathrm{Log}\, L_{60\mu}) = \\ = \frac{1}{\sqrt{2\pi}\sigma}\, \mathrm{e}^{-\frac{\mathrm{Log}\, L_{60\mu}+9.05-\mathrm{Log}\, L_{0.5-2}}{2\sigma^2}} \qquad (3)$$

with $\sigma \sim 0.30$.

A clear prediction for a $z = 0$ XLF emerges from the comparison of the infrared and radio LFs (Fig. 2, left panel): the derived XLFs agree within a factor of 2 in the luminosity interval 10^{40}–10^{41} erg s^{-1}, encompassing the knee region after which all XLFs steepen toward higher luminosities; although departures at lower and higher luminosities are present, the average local X-ray luminosity density, $\sim (3 \cdot 10^{37} \pm 30\%)$ erg s^{-1} Mpc^{-1}, appears to be well defined.

Norman et al. (2004) derived an XLF at higher redshifts (two bins: $\bar{z} \sim 0.27$ and $\bar{z} \sim 0.79$; Fig. 2, right panel) than those probed by the IR and radio surveys discussed above. Other strong constraints at high redshift come from the COMBO-17 survey (Wolf et al. 2003), and from the comparison of the observed X-ray Log N–Log S with that derived by integrating the XLF. This work has been done in detail in RCS05, and here we just quote the results: the evolution is well described as pure-luminosity with an exponent $\eta_{\rm l} \sim 2.7$, with possibly an hint that the evolution could be stopped at $z \sim 1$ (Fig. 2, right panel).

3. Expected luminosity and redshift distributions with the WFXT

The XLF derived in the previous section can be integrated in the volume of space probed by the surveys to obtain luminosity distributions

$$\frac{\mathrm{d}N}{\mathrm{dLog}L} = \int_0^{z_{\max}} \varphi(\mathrm{Log}L, z')\ \min[V(z), V(\mathrm{Log}L, F_{\lim})]\ \mathrm{d}z \qquad (4)$$

and redshift distributions

$$\frac{\mathrm{d}N}{\mathrm{d}z} = \int_{\mathrm{Log}L_{\min}}^{\mathrm{Log}L_{\max}(z')} \varphi(\mathrm{Log}L, z')\ \min[V(z), V(\mathrm{Log}L, F_{\lim})]\ \mathrm{dLog}L \qquad (5)$$

where $z' = \min(z, z_{\mathrm{stop}})$; $F_{\lim}$ is the limiting flux of the survey; $V(z)$ is the comoving volume at redshift z; and $V(L, F)$ is the comoving volume at the redshift at which a source with luminosity L is observed with flux F. All fluxes are considered in the 0.5–2.0 keV band.

For the following calculations, we take $z_{\max} = 4$, $z_{\mathrm{stop}} = 1$, $L_{\min} = \max[10^{39}, 4\pi \mathrm{D}_{\mathrm{lum}}(z)^2 F_{\lim}]$ erg s^{-1} and $L_{\max} = 10^{42}(1 + z')^{\eta_{\mathrm{l}}}$ erg s^{-1}. In words, this means that we integrate on the luminosity range (at $z = 0$) 10^{39}–10^{42} erg s^{-1}, that we allow the maximum luminosity to evolve with redshift, that we exclude luminosities lower than what could visible given the redshift and limiting flux, and that the integration is done up to $z = 4$ but stopping the evolution at $z_{\mathrm{stop}} = 1$. The evolution is pure-luminosity as in Eq. (2) with $\eta_{\mathrm{l}} = 2.7$.

The luminosity distribution is shown in Fig. 3, both in cumulative (left panel) and differential form (right panel). The cumulative form immediately shows the total number of SFG which are expected to be detected in the WFXT surveys ($2 \cdot 10^4$–$4 \cdot 10^4$ objects per survey). Reaching the development goal would enhance the number of SFG by a factor of ~ 5, up to $2 \cdot 10^5$ objects in the *deep* survey.

It is important to check that the SFG XLF will be well sampled at all luminosities. From Fig. 3 it is evident that at least 10^3 SFG with $L < 2 \cdot 10^{39}$ erg s^{-1} should be detected in the *medium* and *deep* surveys, and that the "knee" region of the XLF (the range 10^{40}–10^{41} erg s^{-1} at $z = 0$, compare with Fig. 2) will be very well sampled with around $1.6 \cdot 10^4$ objects in each of the *medium* and *deep* surveys. Similarly, the high luminosity tail ($L > 10^{42}$ erg s^{-1}) will also be well sampled with around $7 \cdot 10^3$ objects in the *medium* survey. This part of the XLF is especially important because objects in this luminosity range are quite rare, and generally suspected of having a substantial part of their emission due to an AGN. Refined classification criteria, and the possibility of doing spectral analysis will clearly be essential.

Reaching the development goal will enlarge the sample of SFG with $L < 10^{42}$ erg s^{-1} by a factor of ~ 5, while it should not make much difference for brighter objects.

The expected redshift distribution is shown in Fig. 4 (left panel). The *wide* and *medium* surveys should have redshift peaks around 0.02 and 0.05, respectively. Both will provide sizable samples at larger redshift: ~ 1000 in the range $0.2 < z < 0.3$ for the *wide* survey, and ~ 900 in the range $0.6 < z < 0.7$ for the *medium*. The *deep* survey will probe much higher redshifts: ~ 900 objects with $1.2 < z < 1.3$, and other ~ 900 with $1.5 < z < 2.0$; these numbers would also be larger by a factor of ~ 5, if the development goal is reached. The uncertainties on the SFG evolution are illustrated by the grey area in Fig. 4 (left panel), whose upper and lower edges correspond to evolution with $\eta_{\mathrm{l}} = 3.4$ and 2.0, respectively.

However, it is likely that the highest redshift objects will also have the larger luminosities. Thus it is reasonable to ask *up to which redshift will the knee of the XLF be probed*. The local XLF exhibits its knee in the range 10^{40}–10^{41} erg s^{-1} (Fig. 2), thus we repeated the integration in Eq. (5) taking $L_{\max} = 3 \cdot 10^{40}(1+z')^{\eta_{\mathrm{l}}}$ erg s^{-1}. The result is shown in Fig. 4 (right panel). The *wide* and *medium* surveys will not probe the knee of the XLF at redshift larger than $z \sim 0.1$ and $z \sim 0.2$, respectively. The *deep* survey will extend the probed redshift range up to $z \sim 0.5$, while if the development goal is reached, redshifts as large as ~ 1.1 could be observed.

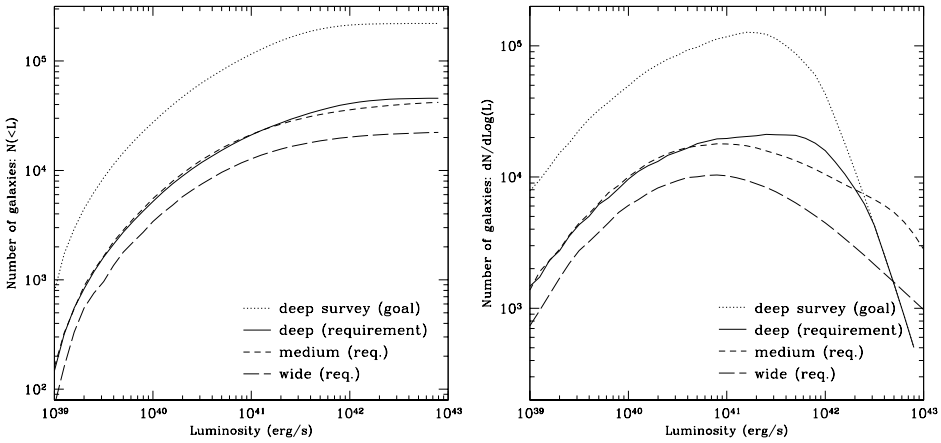

Fig. 3. *Left:* Expected cumulative luminosity distributions for SFG in the WFXT surveys. *Right:* Differential luminosity distributions. Since the knee of the SFG XLF is comprised (at $z = 0$) in the range 10^{40}–10^{41} erg s^{-1}, it appears that the XLF will be well sampled by the WFXT.

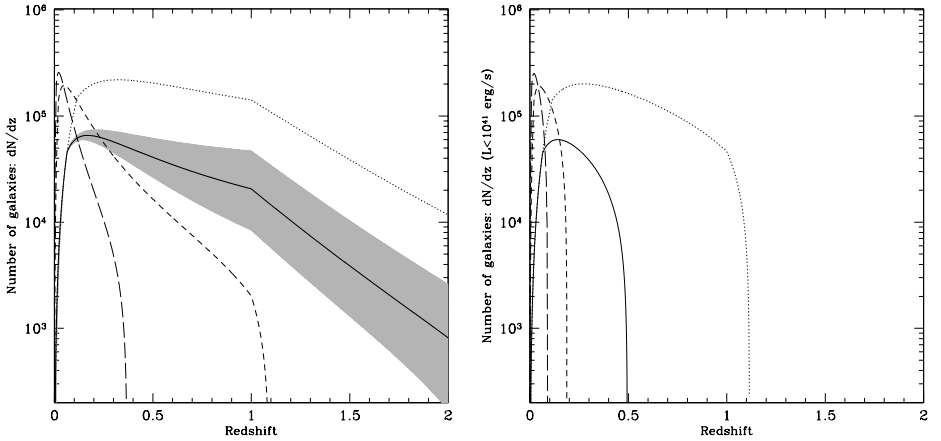

Fig. 4. *Left:* Expected differential redshift distributions for SFG in the WFXT surveys. The grey area illustrates how the uncertainties about the XLF evolution could affect the *deep* survey. *Right:* Same as left, but only considering galaxies with luminosity $L \leq 3 \cdot 10^{40}(1 + z')^{\eta}$ erg s^{-1}: the knee region of the XLF will be probed up to $z \sim 0.5$–1.1. *Both:* Line styles as in Fig. 3.

4. Discussion

From the expected luminosity and redshift distributions, it is evident that the WFXT will be able to determine the SFG XLF with an accuracy comparable to that of IRAS or optical surveys. Thus there will be many new possibilities to study how the X-ray emission depends on other parameters, such as morphology, colours, redshift, etc. However, such a work could only be made if multiwavelength information is available. In fact, the first and most important task will be the selection of the SFG, which are a minor fraction of the total of X-ray surveys. Several different combinations of the same basic parameters (X-ray lu-

minosity, X-ray/optical flux ratio, hardness ratio, amount of absorption, presence of broad lines in optical spectra, etc.) have been explored by different authors in deep *Chandra* surveys (RCS05, and references therein). All the determinations differ by up to a factor of $\sim$ 2; this scatter can be reduced only with a better understanding of how these parameters are linked to each other, and how they affect the selection (and the completeness of samples) of SFG. This only gets more difficult for wide-and-shallow surveys (respect to deep pencil-beam ones) because the SFG/AGN fraction in X-ray surveys depends on the limiting flux (Fig. 1). An attempt to investigate this problem for a sample of SFG in the *Chandra*-COSMOS survey (Elvis et al. 2009) may be found in Ranalli et al. (2010, to be submitted). One of its main results is that no rigid boundaries on the selection parameters can be put; a sensible approach should build on statistical methods for object classification.

The need for the most complete multiwavelength coverage also requires that the choice of the sky areas covered by the WFXT surveys be coordinated with (or follow, if not possible otherwise) other present and future survey facilities (Pan-Starrs, the Large Synoptical Survey Telescope, ALMA, LOFAR, E-VLA, etc.).

The planned WFXT surveys will be able to derive the SFG XLF and determine its evolution with unprecedented accuracy up to $z \sim 0.5$ (1.1 if the development goals are reached) in the knee region, and up to $z \sim 2$ (2.5) for the high-luminosity tail. Since the cosmic star formation history as a peak in the range $1 \lesssim z \lesssim 2$, it is evident that the goals should be pursued with strong commitment. The cosmic accretion history has a peak at a similar redshift, and the two phenomena seem to have shared a very similar trend. Thus, the larger the probed redshift range, the more impact the WFXT will have for studies of SFG and AGN coevolution.

Finally, were the goals reached, and the numbers still on the safe side of the confusion limit, some ultra-deep pointings should be considered as very profitable. E.g., observing an area of 10 deg^2 with a limiting flux of 10^{-17} erg s^{-1} cm^{-2} would extend the coverage of the knee of the XLF up to $z \sim 1.7$, and of the high-luminosity tail up to redshifts well beyond the peak of the cosmic star formation history.

Acknowledgements. We thank Roberto Gilli and Andrea Comastri for stimulating discussions.

References

Avni, Y. & Tananbaum, H. 1986, ApJ, 305, 83
Bauer, F. E., Alexander, D. M., Brandt, W. N., et al. 2004, AJ, 128, 2048
Burrows, C. J., Burg, R., & Giacconi, R. 1992, ApJ, 392, 760
Conconi, P., Campana, S., Tagliaferri, G., et al. 2010, MNRAS, 509
de Jong, T., Clegg, P. E., Rowan-Robinson, M., et al. 1984, ApJ, 278, L67
Elbaz, D., Cesarsky, C. J., Chanial, P., et al. 2002, A&A, 384, 848
Elvis, M., Civano, F., Vignali, C., et al. 2009, ApJS, 184, 158
Franceschini, A., Aussel, H., Cesarsky, C. J., Elbaz, D., & Fadda, D. 2001, A&A, 378, 1
Georgakakis, A. E., Georgantopoulos, I., Basilakos, S., Plionis, M., & Kolokotronis, V. 2004, MNRAS, 354, 123
Georgantopoulos, I., Basilakos, S., & Plionis, M. 1999, MNRAS, 305, L31
Georgantopoulos, I., Georgakakis, A., & Koulouridis, E. 2005, MNRAS, 360, 782
Miyaji, T. & Griffiths, R. E. 2002, ApJ, 564, L5
Moretti, A., Campana, S., Lazzati, D., & Tagliaferri, G. 2003, ApJ, 588, 696
Norman, C., Ptak, A., Hornschemeier, A., et al. 2004, ApJ, 607, 721
Ranalli, P., Comastri, A., & Setti, G. 2003, A&A, 399, 39
Ranalli, P., Comastri, A., & Setti, G. 2005, A&A, 440, 23
Saunders, W., Sutherland, W. J., Maddox, S. J., et al. 2000, MNRAS, 317, 55
Schmidt, M. 1972, ApJ, 176, 273
Tajer, M., Trinchieri, G., Wolter, A., et al. 2005, A&A, 435, 799
Takeuchi, T. T., Yoshikawa, K., & Ishii, T. T. 2003, ApJ, 587, L89
Takeuchi, T. T., Yoshikawa, K., & Ishii, T. T. 2004, ApJ, 606, L171
Wolf, C., Meisenheimer, K., Rix, H.-W., et al. 2003, A&A, 401, 73

Mem. S.A.It. Suppl. Vol. 17, 128

Memorie della
Supplementi

X-ray emission from early-type galaxies

S. Pellegrini

Dipartimento di Astronomia, Università di Bologna, via Ranzani 1, I-40127 Bologna, Italy
e-mail: silvia.pellegrini@unibo.it

Abstract.
The last ∼10 years have seen a large progress in the X-ray investigation of early-type galaxies of the local universe, and first attempts have been made to reach redshifts $z > 0$ for these objects, thanks to the high angular resolution and sensitivity of the satellites *Chandra* and *XMM*−Newton. Major advances have been obtained in our knowledge of the three separate contributors to the X-ray emission, that are the stellar sources, the hot gas and the galactic nucleus. Here a brief outline of the main results is presented, pointing out the questions that remain open, and finally discussing the prospects to solve them with a wide area X-ray survey mission such as *WFXT*.

Key words. Galaxies: elliptical and lenticular, cD – Galaxies: evolution – Galaxies: ISM – Galaxies: nuclei – X-rays: binaries – X-rays: galaxies

1. Introduction

X-ray investigations of early-type galaxies[1] (hereafter ETGs) of the local universe began in the 1980s with the *Einstein* satellite, and revealed that the total X-ray luminosity originates from a combination of hot interstellar gas and low-mass X-ray binaries (LMXBs; Fabbiano 1989). With the advent of the *ROSAT*, *ASCA* and then *Chandra* and XMM-Newton eras, our knowledge of all the components of the X-ray emission has deepened considerably: among stellar sources by far the largest contribution comes from LMXBs, and it has been quantified; a hot gaseous halo (with a temperature of ∼few million degrees) can be present with largely varying amounts; another important galactic component, a supermassive black hole (MBH) believed to be common at the center of ETGs and a relic of the past quasar activity, showed luminosities ranging continuously from the lowest detectable levels (e.g., that of a bright LMXB in Virgo) to values typical of Seyferts. The combined study of the hot gas and low luminosity nuclei turned out to be a crucial tool to build our understanding of MBH accretion and feedback in the local universe.

The results above are based on few tens of ETGs accurately studied with *Chandra* and *XMM*-Newton, whose archives contain at present roughly two hundreds ETGs with a specific pointing, located within a distance of ∼ 100 Mpc. In this work I review briefly the main advances concerning the three major emission components (the stellar emission in Sect. 2, the hot gas in Sect. 3 and the galactic nuclei in Sect. 4), indicating also the needs for further

Send offprint requests to: S. Pellegrini

[1] This work is devoted to "normal" early-type galaxies, where the X-ray emission is not dominated by an AGN, and keeps below $\sim 10^{42}$ erg s^{-1}.

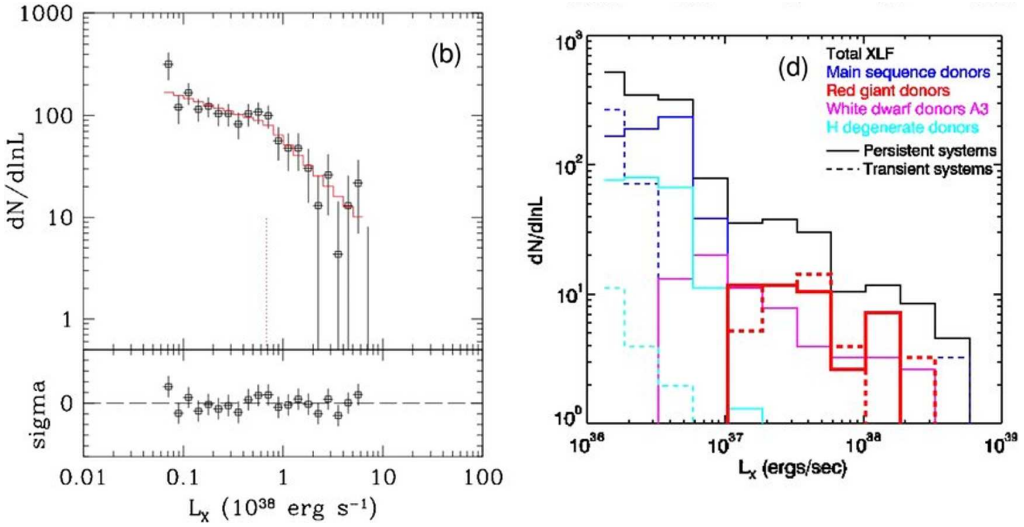

Fig. 1. The 0.3–8 keV luminosity function of LMXBs for three hot gas poor ETGs with deep *Chandra* pointings (Sect. 2) on the left, and the theoretical prediction of Fragos et al. (2008) on the right (from Kim et al. 2009).

investigation; in Sect. 5 I summarize the current scant and sparse knowledge of the X-ray properties of ETGs beyond the local universe; in Sect. 6 I discuss the prospects to address a few important science goals with *WFXT*.

2. Stellar sources

The stellar X-ray emission of ETGs is contributed by a population of weak sources ($L_X < 10^{34}$ erg s^{-1}) as late type stellar coronae, cataclismic variables, and coronally active binaries (Pellegrini & Fabbiano 1994), and by the more luminous LMXBs, associated with an old stellar population and powered by accretion from a low-mass late-type star onto a compact stellar remnant, a neutron star or a black hole. The origin and evolution of the collective LMXB population of ETGs is the subject of much discussion (Fabbiano 2006); LMXBs are found in both the stellar field and globular clusters, but their incidence per unit stellar mass is much higher in the latter, suggesting the importance of a dynamical formation mechanism.

Exploiting the sub-arcsecond angular resolution provided by *Chandra* the nature of the stellar contribution to the X-ray emission could be better constrained, especially with deep pointings at ETGs (almost) devoid of an important contaminant such as the hot gas (Brassington et al. 2008, 2009). In this way the collective contribution of the weak population could be estimated in NGC3379 (Revnivtsev et al. 2008). Luminous ($L_X > 10^{36}$ erg s^{-1}) pointlike sources could instead be individually detected and their X-ray luminosity function (XLF) be built in a number of galaxies, the deepest studies being those for NGC3379, NGC4278 and NGC4697 (Kim et al. 2009, see Fig. 1), and NGC5128 (Voss et al. 2009). One major goal is to calibrate the dependence of the collective X-ray emission from LMXBs on the galaxy stellar mass or luminosity, age and globular cluster specific frequency. The high luminosity end of the XLF (L_X >several$\times 10^{37}$ erg s^{-1}) and the collective luminosity of the whole LMXB population as a function of the galactic luminosity are now reasonably known, with a possible dependence also on the globular cluster specific frequency still to be evaluated (Kim & Fabbiano 2004; Gilfanov 2004; Kim et al. 2009). The features in the observed XLFs that are being discovered (as breaks at high and low luminosities, possible bumps, dif-

ferences for field and globular cluster sources) represent important inputs to theoretical models for LMXB formation and evolution, as those built with the advanced population synthesis code StarTrack (Fragos et al. 2008, 2009). These models also predict the evolution of the XLF with galaxy age, and then the collective (hard) emission from LMXBs; such predictions are useful for investigations of ETGs at higher redshift that are attempted currently (Sect. 5) and will flourish with *WFXT* (Sect. 6).

3. Hot interstellar medium

Chandra observations allowed to separate the contribution of stellar sources and hot gas, as well as emission coming from different spatial regions within galaxies, obtaining the best definition ever for the hot gas properties (e.g., Kim & Fabbiano 2003; Humphrey & Buote 2006). It is now proven that in optically luminous ETGs the soft interstellar gas can be present with largely varying amounts (Fabbiano 1989; Pellegrini & Ciotti 1998; Sarazin et al. 2001), producing a scatter in L_X up to a factor of 100 at fixed galactic optical luminosity (Fig. 2); in optically faint ETGs instead the X-ray emission is always dominated by LMXBs (David et al. 2006; Pellegrini et al. 2007; Trinchieri et al. 2008).

The hot ISM provides fuel for the central MBH and absorbs energy from nuclear outbursts, in a complex cycle whose mechanism is not yet fully understood (e.g., Forman et al. 2005; Baldi et al. 2009; Ciotti et al. 2010). A compilation of radial temperature profiles for the hot gas shows that the radio luminosity decreases continuously as gradients in the profiles change from positive to negative, as if the profiles were reversing the temperature gradient over time following an activity cycle (Diehl & Statler 2008). Also the environment in which ETGs reside can influence the hot gas coronae, having an effective impact on their outer temperature gradient (Diehl & Statler 2008), and on their size and luminosity via stripping, sloshing, compression, conduction (Sun et al. 2007); the environment is also important for the injection of metals

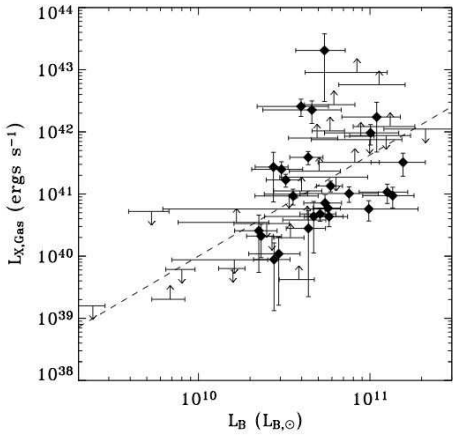

Fig. 2. The 0.3–5 keV luminosity of the hot gas as a function of absolute blue galactic luminosity, for a sample of ETGs of the local universe in the *Chandra* archive (from Diehl & Statler 2007).

from ETGs in the intracluster medium (e.g., Kim et al. 2008a). The sample of ETGs for which all these phenomena have been investigated is however limited, and real samples in a statistical sense (i.e., made of thousands of objects) are needed to establish clearly the effects of a surrounding medium, of the interactions with neighbours, of feedback, possibly dividing galaxies based on mass, age, and kinds of environment.

4. Low luminosity MBHs

Thanks to *Chandra*'s angular resolution, for the first time measurement of the nuclear X-ray emission down to values as low as 10^{39} erg s^{-1} and out to distances of $\sim$ 60 Mpc were obtained. MBHs of the local universe turned out to be typically very sub-Eddington emitters (Pellegrini 2005; Gallo et al. 2008) and their radiative quiescence was interpreted in terms of radiatively inefficient accretion (RIAF; Narayan & Yi 1994), possibly with the mechanical power dominating the total energy output of accretion (e.g., Allen et al. 2006). From the sample available, there appears to be only a weak relation of the nuclear luminosity with the MBH mass or with the galactic hot gas content, with a very large disper-

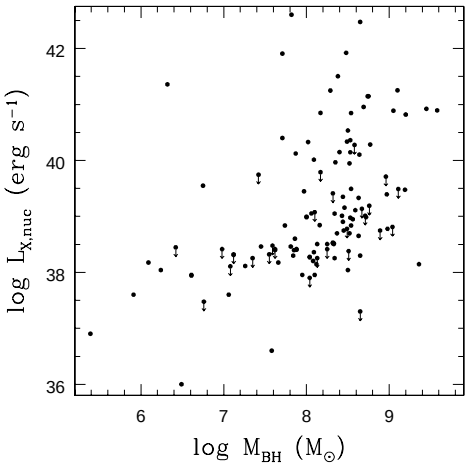

Fig. 3. The 2–10 keV nuclear luminosity as a function of the MBH mass for a sample of ETGs of the local universe in the *Chandra* archive (Pellegrini 2010).

sion dominating the two relations (Pellegrini 2010; Fig. 3). The modeling of the observables (mainly the nuclear spectral energy distribution from radio to X-rays, and the mass accretion rate derived from the gas density and temperature close to the accretion radius) allows to establish the origin of the nuclear X-rays (standard disk plus hot corona, RIAF, jet, or a combination of them; e.g., Fabbiano et al. 2003; Ptak et al. 2004), and derive important clues on the modality of the MBH feeding, or the kinetic feedback from jets, and then on the co-existence of MBHs and host galaxies. Despite many efforts applied to observational data, accretion in the local universe remains poorly known, while its knowledge is important for a complete understanding of the MBH-host galaxy coevolution process. Current believes are that MBHs spend most of their life in the RIAF regime (Hopkins et al. 2006; Ciotti et al. 2010), an accretion state expected to be efficient in producing outflows and jets, and then to correspond to the "radio-mode" of MBH feedback invoked in semi-analytic studies and hydrodynamic simulations of galaxy formation (e.g., Croton et al. 2006).

5. Beyond the local universe

Many surveys with different depths and fields of view have been performed so far with *Chandra* and *XMM*−Newton; for each of them typically a sample of only <∼ 100 ETGs could be built, so that only few results could be obtained about the evolution with redshift of ETGs. The deepest study was conducted in the GOODS fields, where 40 ETGs divided in two redshift bins, of $z < 0.5$ and $0.5 < z < 1.2$, showed luminosity evolution, by which ETGs were brighter in the past; this could be due to passive evolution of LMXBs (Ptak et al. 2007, Sect. 2). In the ECDF-S regions, 539 optically selected ETGs with $0.1 < z < 0.7$ and $R < 24$ corresponded to the detection of 13 luminous ETGs plus 32 AGNs, and the characterization via the stacking procedure of the others (Lehmer et al. 2007). When divided in four z-bins from $z = 0.25$ to $z = 0.66$, and two luminosity bins separated at $L_B \sim 10^{10} L_{B\odot}$, the optically faint samples seem to show an increase in L_X with z, while the brighter ones keep within the range of values observed locally, as due to a long-lasting (∼ 6 Gyr) balance between heating and cooling of the hot gas coronae. The wide area (∼ 30 deg^2) ChaMP survey based on archival *Chandra* fields (Kim et al. 2008b) for a sample of <∼ 100 ETGs at $0.01 < z < 0.3$ finds the minimum X-ray–to–optical ratio (likely the baseline contributed by LMXBs) to be constant with redshift. In the wide area (9.3 deg^2) XBoötes survey studied with a mosaic of 5 ks pointings, the hardness ratio of 2968 stacked ETGs evolves from $z = 0.2$ to $z = 0.4$, i.e., the average spectrum becomes harder with increasing z, which could be due to an increasing AGN contribution (Watson et al. 2009). A collection of data from the *Chandra* Deep Fields to XBoötes, the shallowest survey, produced a sample of 101 ETGs up to $z \sim 1.4$, that show no significant luminosity evolution when divided in two z-bins centered at 0.17 and 0.67 (Tzanavaris & Georgantopoulos 2008). Overall these investigations are heterogeneous, based on different selection criteria, and plagued by the limited numbers of ETGs in the samples, so that the results can be considered only preliminary.

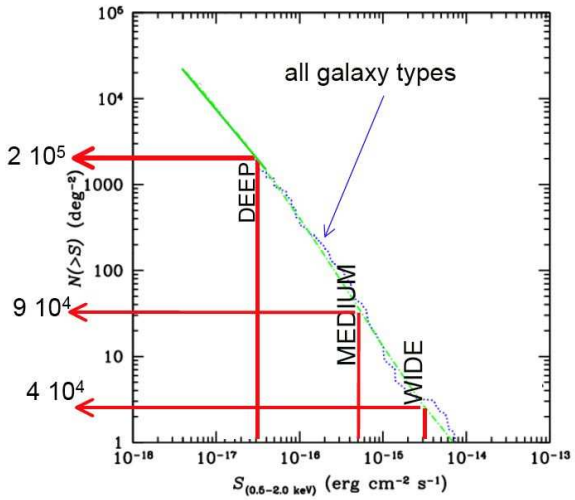

Fig. 4. The number of galaxies to be detected in the three *WFXT* surveys (indicated by the arrows), based on a recent estimate extrapolated to low fluxes (green line) of the number $N(>S)$ of galaxies with 0.5–2 keV flux S larger than the value on the x-axis (Tzanavaris & Georgantopoulos 2008). The green line referes to both late and early types, with the galaxies in the sample roughly equally divided between the two types.

6. WFXT

As discussed in the previous Sections, X-ray information about ETGs in the local universe (distance $<$ 100 Mpc) is mostly based on a number of $<\sim$ 200 galaxies that benefitted of pointed observations with *Chandra* and *XMM*-Newton. Beyond the local universe, only samples with $<$ 100 objects could be built, with very limited information on them; future extensions of the surveys performed so far are not likely to produce substantial improvements. Statistical studies, as the building of the ETG's LF and the search for its possible evolution, or the study of the dependence of the X-ray emission on different kinds of environment, require far larger samples. *WFXT* is designed to produce a dramatic advance over existing or planned missions in combined solid angle and sensitivity, keeping a good angular resolution of 5″ (see, e.g., Rosati in these proceedings); the energy band (0.4–7 keV) is sensitive to both the soft hot gaseous emission and the hard stellar/AGN contribution. With the three surveys (wide of 20000 deg^2, medium of 3000 deg^2 and deep of 100 deg^2) *WFXT* could drastically increase the number of detected ETGs and revolutionize the field (see Fig. 4, based on the flux limits indicated by Rosati). For example, the deep survey is expected to produce $\sim 10^3$ times the solid angle of the *Chandra* Deep Fields at the same sensitivity. An ETG with a (conservative) size of $\sim$ 20 kpc will have an angular dimension of 10″ at $z = 0.1$ and 5″ at $z = 0.3$, beyond which it will appear as a pointlike source for *WFXT*. Using flux limits for point sources, an average ETG X-ray luminosity of 10^{41} erg s^{-1} will be detected out to $z = 1$, 0.3 and 0.1 respectively in the deep, medium and wide surveys. The combination of the X-ray data with photometric and spectroscopic information at other wavelengths like those provided by current and planned surveys (as 2MASS, SDSS, Galex, LSST, SDSSIII/BOSS, ...) should give distances and the main galactic parameters.

The wide survey then could detect ~few10^4 ETGs mostly within $z = 0.1$, and allow to build the first really large sample of ETGs in the local universe. More than $\sim 10^3$ objects could be studied with enough detail to measure gas properties, and distinguish stellar and nuclear luminosities; angular resolution could enable to detect sharp features in the hot gas as shocks,

holes, rims. This could make up a baseline for medium/high z studies. Sample questions to be tackled with a large database include: how is feedback working at all galactic luminosities? with what duty cycle? is the large dispersion in hot gas content (Fig. 2) related to nuclear activity, galaxy structure, or environment?

At $z > 0.1$ (a lookback time larger than 1.3 Gyr for standard cosmological parameters), instead, the three main components (LMXBs, hot gas and nuclei) should be revealed mostly from their integrated contribution to the X-ray spectra, and their evolution could be studied. For example, the LMXB's contribution, determined at $z = 0$ as described in Sect. 2, at $z > 0$ should be higher than in local ETGs, depending on epoch of major star formation (Sect. 2). The evolution of hot gas and nuclear activity (respectively contributing to the soft and hard bands) should give important insights on the feedback process, revealing for example whether the hot gas content and temperature evolve with time, and the nuclear luminosity increases. In the deep survey there will be detections of ETGs out to $z \sim 1$, to study the transition of accretion in the radio mode and its evolution in this state (Sect. 4).

References

Allen, S. W., Dunn, R. J. H., Fabian, A. C., et al. 2006, MNRAS, 372, 21

Baldi, A., Forman, W., Jones, C., et al. 2009, ApJ, 707, 1034

Brassington, N. J., Fabbiano, G., Kim, D.-W., et al. 2008, ApJS, 179, 142

Brassington, N. J., Fabbiano, G., Kim, D.-W., et al. 2009, ApJS, 181, 605

Ciotti, L., Ostriker, J.P., Proga, D. 2010, ApJ, in press (arXiv:1003.0578)

Croton, D.J., Springel, V., White, S.D.M. et al. 2006, MNRAS, 365, 11

David, L.P., Jones, C., Forman, W., Vargas, I.M., Nulsen, P. 2006, ApJ, 653, 207

Diehl, S., Statler, T. 2007, ApJ, 668, 250

Diehl, S., Statler, T. 2008, ApJ, 687, 986

Fabbiano, G. 1989, ARAA, 27, 87

Fabbiano, G., Elvis, M., Markoff, S., et al. 2003, ApJ, 588, 175

Fabbiano, G. 2006, ARAA, 44, 323

Forman, W., Nulsen, P., Heinz, S., et al. 2005, ApJ, 635, 894

Fragos, T., Kalogera, V., Belczynski, K., et al. 2008, ApJ, 683, 346

Fragos, T., et al. 2009, ApJ, 702, L143

Gallo, E., Treu, T., Jacob, J., et al. 2008, ApJ, 680, 154

Gilfanov, M. 2004, MNRAS, 349, 146

Hopkins, P.F., Narayan, R., Hernquist, L. 2006, ApJ, 643, 641

Humphrey, P.J., Buote, D.A. 2006, ApJ, 639, 136

Kim, D.W., Fabbiano, G. 2003, ApJ, 586, 826

Kim, D.W., Fabbiano, G. 2004, ApJ, 613, 933

Kim, D.-W., Kim, E., Fabbiano, G., Trinchieri, G. 2008a, ApJ, 688, 931

Kim, D.-W., Green, P. J., Barkhouse, W. A., et al. 2008b, ChJAS, vol. 8, p. 138

Kim, D.-W., Fabbiano, G., Brassington, N. J., et al. 2009, ApJ, 703, 829

Lehmer, B.D., et al. 2007, ApJ, 657, 681

Narayan, R., Yi, I. 1994, ApJ, 428, L13

Pellegrini, S., Fabbiano, G. 1994, ApJ, 429, 105

Pellegrini, S., Ciotti, L. 1998, A&A, 333, 433

Pellegrini, S. 2005, ApJ, 624, 155

Pellegrini, S., Baldi, A., Kim, D. W., et al. 2007, ApJ, 667, 731

Pellegrini, S. 2010, ApJ, 717, 640

Ptak, A., Terashima, Y., Ho, L.C., Quataert, E. 2004, ApJ, 606, 173

Ptak, A., et al. 2007, ApJ, 667, 826

Revnivtsev, M., et al. 2008, A&A, 490, 37

Sarazin, C.L., Irwin, J.A., Bregman, J. 2001, ApJ, 556, 533

Sun, M., et al. 2007, ApJ, 657, 197

Trinchieri, G., Pellegrini, S., Fabbiano, G., et al. 2008, ApJ, 688, 1000

Tzanavaris, P., Georgantopoulos, I. 2008, A&A, 480, 663

Voss, R., et al. 2009, ApJ, 701, 471

Watson, C.R., et al. 2009, ApJ, 696, 2206

Mem. S.A.It. Suppl. Vol. 17, 134

Memorie della
Supplementi

Galaxies and the Local Universe with WFXT

G. Trinchieri and A. Wolter

INAF – Osservatorio Astronomico di Brera, Via Brera 28, I-20121 Milano, Italy
e-mail: ginevra.trinchieri@brera.inaf.it

Abstract. Galaxies are essential building blocks in the Universe. However they are faint and complex X-ray sources and require high performance instrumentation to be properly studied. Yet they are fundamental for our understanding of the Universe, and a detailed knowledge of the local structures is mandatory to explain the deep and far Universe. We make a few examples, and discuss how well suited WFXT is to address this issue.

Key words. X-ray: galaxies – galaxies: spiral – galaxies: general – galaxies: ISM

1. Introduction

Galaxies are relatively faint and complex X-ray sources: their luminosities range between $L_X \sim 10^{39}$ erg/s and $L_X \sim 10^{41}$ erg s^{-1}, and their emission is due to several distinct components, whose relative importance is related to galaxy parameters such as morphology and evolutionary stage. Due to their complexity, our understanding of their X-ray properties is not as advanced as for other astronomical objects, and is limited to systems in the local universe. Nonetheless, they are fundamental if we aim at understanding the Universe at large, for no other reason that they have been recognized as the dominant component in the extragalactic sky at very low fluxes (see Georgakakis et al. 2006, for a recent review). Therefore, only a precise determination of the key components in local galaxies allows us to predict their behaviour at high redshifts and/or to study their evolution.

The advantages in a detailed study of local galaxies are manifold:
a) The "same" distance to all sources in a galaxy allows an investigation of specific source classes more homogeneously. b) A few source classes can **only** be studied outside Milky Way (e.g. ULXs, SSS, hot halos). c) It returns a better understanding of population of the Milky Way where sources can be studied in more detail. d) It represents a baseline for comparison with the more distant universe: today's galaxies are the end product of evolution and as such are important traces of the distant Universe that we can investigate in detail. Only a precise knowledge of their properties will allow us to properly interpret the "unresolved" emission from distant objects.

In spite of the efforts to understand local Universe objects, a real break-through requires instruments with the following characteristics:
• Large field of view: local objects have large angular size. Given their complexity, it is important also to be able to determine the background locally, to avoid normalization and spectrum issues.
• Very good spatial resolution. This is required to separate different components, to minimize reciprocal contamination, and to study individual sources in detail.

Send offprint requests to: G. Trinchieri

• Sensitivity. Given their faint nature, galaxies are at low fluxes: at the limit of the Medium Survey, $f_x \sim 10^{-15}$ erg cm^{-2} s^{-1}, they will all be detected out to D=90 Mpc. Only the brightest ones ($\sim 10^{41}$ erg s^{-1}) out to z$\sim$0.2.
• Broad energy band. Different components have significantly different spectral characteristics, and their contributions dominate different regions of the spectrum. In order to be able to separate them spectrally, a broad band is essential.
• "Reasonable" spectral resolution. While a superb spectral resolution would be desirable, all other constraints would make this too demanding. Nonetheless, spectral analysis is needed to characterize different components and provides an excellent alternative in separating contributions from different sources when the spatial resolution is not adequate.

Most of the above requirement are indeed met by WFXT, at least to a reasonable compromise to be useful for detailed studies of the local Universe. The spatial resolution (required or goal) would not allow us to address some of the outstanding issues outlined below (Chandra resolution or better would be required), but a resolving power of 1-2″ would be enough to tackle many of them.

2. Outstanding issues where WFXT can contribute

Several questions related to our understanding of the X-ray properties of galaxies still need to be addressed and properly studied. We list some here, and discuss a few in detail below, in context with WFXT characteristics.

Luminosity Function of normal galaxies. This has never properly been done on large enough samples to be able to distinguish them in different classes that reflect intrinsic characteristics. We discuss this better in § 4.1

What is the nature of ULXs? This extreme class of sources can only be studied in external galaxies. Current samples are limited, but WFXT will provide a reasonably large sample of sources in diverse galaxies (see § 4.2).

Dwarf galaxies This class has been so far neglected, largely due to the difficulty related to their observation. A survey mode at reasonable depth is the ideal tool to collect enough examples, and the large FoV will allow us to examine those around bigger galaxies.

Hot gas in early type galaxies: how much and why only in some of them? A large spread in the $L_{X-gas} - L_B$ plane is observed, and attempts at interpreting it in light of intrinsic galaxy properties have been so far only partially successful. Emission of galaxies located at group centers is hard to separate from that of the environment and requires special attention in the interpretation in the context of galaxy properties. Even a careful selection of galaxies as a function of environment has not led to conclusive results (Memola et al. 2009; Mulchaey & Jeltema 2010). Investigating this with larger and well studied samples might help to better assess what the relevant parameters are (see Pellegrini, this conference).

Hot gas in the local universe: how much? and what physical state? We have seen the presence of instabilities such as hot/cold bubbles and cavities in clusters and now also around bright or central group galaxies. Large halos have been detected around spiral galaxies, and in the intergalactic space. Studying these phenomena on a large number of galaxies will allow us to put the presence and frequencies of these effects on a statistical ground and to correlate them with intrinsic properties (see § 5)

Young spiral-dominated groups. As part of our understanding of the presence and amount of hot gas in the local universe, a new and largely unexplored field is that of poor groups, in particular those at a young dynamical age. As a whole, groups could be regarded as the fainter end of the cluster class, and their properties interpreted in this context. However, so far very little is known about the X-ray properties of spiral-only compact groups, which could represent the beginning of an evolutionary sequence that would lead them into more relaxed systems, dominated by an early-type galaxy population, through a multiplicity of mechanisms such as mergers of member galaxies, accretion of new gas from external reservoirs, infall of new galaxies and heating of the intra-group medium through dynamical friction and AGN feedback. A hot ISM in these

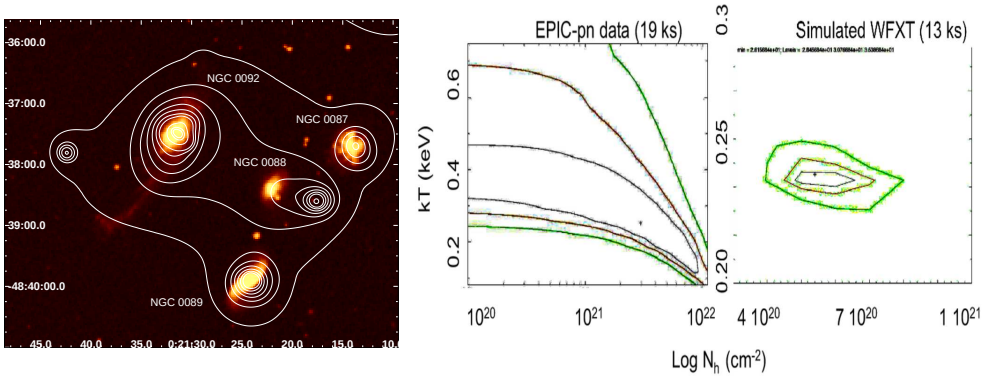

Fig. 1. EPIC-pn observations of SCG0018-4854 (Trinchieri et al. 2008) have identified a hot ISM in this spiral-dominated system (*left panel*). However, its spectral properties are poorly determined. A WFXT observation of similar duration would significantly reduce the parameter space (*middle and right panels*). Credit: Trincheri et al. A&A 467,195, 2008, reproduced with permission ©ESO.

systems is very hard to observe because it appears to be significantly fainter and possibly cooler than in more evolved systems (Belsole et al. 2003; Trinchieri et al. 2008). However determining its presence could have a significant impact on our understanding of these early stages of group evolution. Moreover we expect to encounter more at higher z, therefore making their interpretation more challenging if we lack a good knowledge of their properties locally. Fig. 1 demonstrates the improvement we can expect on determining the presence and the characteristics of a hot ISM in these systems.

3. WFXT and the local Universe: how good a match is it?

The field of view provided by WFXT has the fundamental advantage over current instruments that it can cover the large angular size of nearby galaxies with a limited number of separate pointings, providing at the same time enough space for a proper sampling of the immediate neighbouring environment. For example M31, the nearest spiral to us, would need $\sim$ 10 pointings, compared to $\sim$ 30 needed with XMM-Newton to cover it out to D25 only. The observations will include also at least two of its satellites -M32 and NGC 205- and enough area outside the disk to study the outer halo regions and the local environment. M33, NGC 253, NGC 300 (see Fig. 2), NGC 1291, M106 are all examples of galaxies with sizable angular sizes, that can be covered in a single field together with enough area for a local determination of the background.

As shown by the example in Fig. 2, bright sources can be easily resolved and studied individually. The depth at which they will be resolved will depend upon the final spatial resolution reached for WFXT, since crowding will be a real issue even in nearby systems, and will be different in different environments. Being able to observe the entire system and its surrounding in each observation will have a significant impact e.g. in building long-term light curves of all sources in a given galaxy for variability studies, which in turns has an impact on our understanding of their nature, when spectral or spatial information are not sufficient.

However, to exploit the advantages of WFXT will require careful considerations of the strategy of the observations, both to study individual sources (spectral studies, XLF, time variability, source classification, etc) and to detect and characterize the unresolved emission and the galaxy outskirts and environment. In particular, in order to be able to exploit the ad-

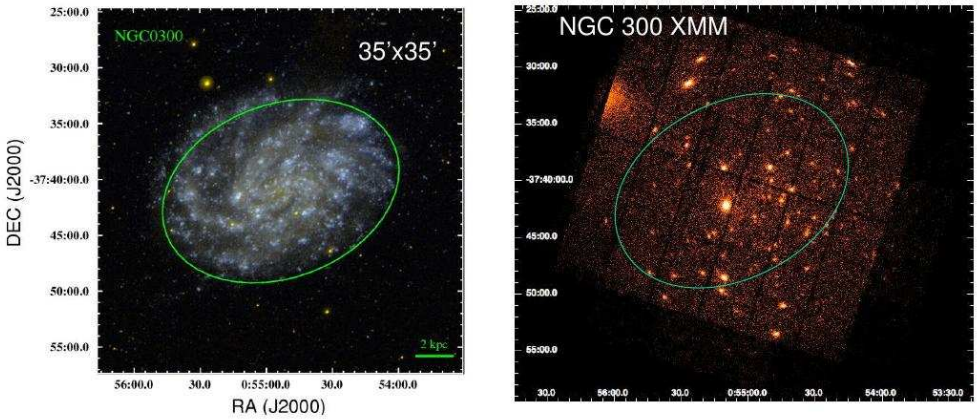

Fig. 2. An example of a face-on galaxy, NGC 300 (*left panel*, green ellipse marking D_{25}), and its observation with XMM-Newton (EPIC-pn, *right panel*). While the whole galaxy is contained in the FoV, there is little left to explore the area outside D_{25}.

vantage of a large FoV and use a local determination of the background, one major requirement is that we know the instrumental response *very well*, as a function of energy and position on the detector.

One didactic example is given by the extremely elaborate analysis that was required to measure the characteristics of the halo in NGC 253 (see Bauer et al. 2008, for details of the analysis required). The size of the halo and its low surface brightness posed a real challenge to the available XMM-Newton data, both because the source almost fills the FoV, making a local determination of the intensity and spectral shape of the background quite difficult, and because the calibration of the instrument response, required to extrapolate the background values to the area covered by the emission, was not accurate enough. If we want to fully exploit the potential of WFXT to measure low surface brightness extended features, proper calibration issues must be considered.

4. Large samples

Current studies of galaxies suffer from small sample statistics, since only a few normal galaxies are typically detected in X-ray surveys (Tajer et al. 2007; Georgantpoulos et al. 2005; Hornschemeier et al. 2005; Brusa et al. 2010). The huge increment in the number of sources which will be possible with WFXT has incredible potential in improving our knowledge in many areas, provided that the identification of the X-ray sources is done in an automated but secure way. One of the main issues will be to be able to resolve the small fraction of normal galaxies from the much larger populations of AGNs. Although some discrimination can be made on the basis of the X/O ratios (e.g., as done since Maccacaro et al. 1988), low redshift galaxies have the advantage that their X-ray extent can be used as a classification tool: at $z \leq 0.2$ the WFXT PSF should still be able to show them as extended sources, and might allow us to distinguish those dominated by a bright nuclear source. We also expect them to be optically bright, thus easily recognizable on most plates.

4.1. X-ray luminosity functions

As discussed in Ranalli (this conference) the number of objects in the three WFXT surveys will be so large that we can derive a logN-logS and a XLF (after identification!!) for different types of galaxies and at different redshifts. This

will allow us to put a more firm base for cosmological studies. Based on our current knowledge of the XLF of normal galaxies, we expect that the density of galaxies, at the medium survey flux, is almost 10/deg^2, for a grand total of about 30 000 galaxies at the end of the survey!

4.2. ULX

Provided they are covered, we will be able to count on a very large number of photons for sources already known and studied. This will allow a precise determination of their spectral shape, which in some cases cannot be determined with current data. With the large statistics we can study their temporal behaviour, to better assess their nature, and investigate the presence of characteristic variability patterns (QPOs, PSD etc) which might help in determining the mass of the compact object.

We also expect to be able to discover many more of these sources, and to extend their detection and characterization to objects at much larger z, to study them in different contexts. It is well known that ULXs are invariably associated with star formation activity and young population of stars. However, we need to quantify what percentage of ULX can be associated with compact objects in binary systems and what other phenomena might give rise to the extreme luminosities observed. At the present time, we expect that about a quarter of ULXs are SNR, but this is based on a very scanty statistics (Swartz et al. 2004). Possibly the different species of ULXs can be discriminated on the basis of their spectral shape. For instance a thermal model would be preferentially associated to a SN, while classical binary are mostly defined by power laws, modified by a disk and/or corona in a few cases. If covered at the sensitivity of the medium survey, WFXT will provide enough photons to distinguish spectra of many ULXs up to the distance for example of the Cartwheel, which hosts a large population of ULXs and one of the brightest known to date (Wolter & Trinchieri 2004; Wolter, Trinchieri & Colpi 2006). The lack of a well determined spectral shape is hampering our understanding of the nature of even the brightest one, which can be interpreted as a compact, $\sim$100 M$_\odot$ BH binary or a SN (Pizzolato, Wolter & Trinchieri 2010).

5. Hot gas in the local universe

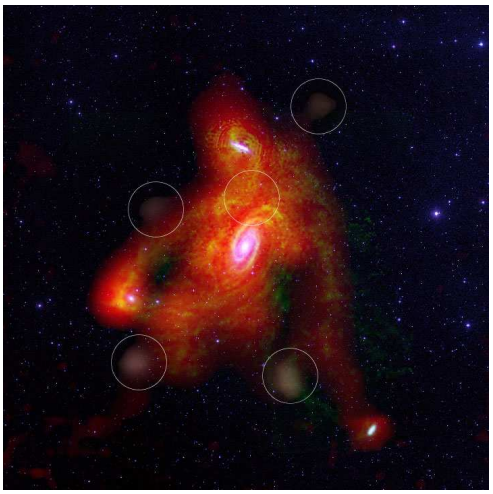

Fig. 3. Composite radio optical image of the M81/M82 galaxy group, covering an area of $\sim 3^o \times 3^o$ (from Chynoweth et al. 2008). Reproduced by permission of the AAS.

HI envelops and high velocity cloud systems (HVC) are observed around spiral galaxies (e.g. M83, NGC 2403) and between objects (NGC4631 connecting to its companions, Rand 1994; M81 connecting to NGC3077/M82, Yun et al. 1994). These HI halos extend over large angular scales and appear to be dominated by filamentary structures (see e.g. Fig 3) clearly demonstrating disruption of the system by tidal interactions. Some HVCs may be the remnants of galaxy formation currently being accreted or may be associated to current episodes of vigorous star formation like supernovae explosions. A hot halo is also detected in these same objects, so we need to understand whether both come from the same source. The presence of extend halos could also indicate the existence of large reservoirs of gas at low surface brightness and large size that could go undetected.

Similarly, a connection is expected between early type galaxies and their surround-

ings. The evidence of cavities in the diffuse X-ray surface brightness in clusters of galaxies points to a close connection with a central AGN radio outbursts. In X-ray bright clusters, cavities are prominent and can be easily identified. This phenomenon is now beginning to emerge at all scales, down to bright central group galaxies and normal galaxies (see Diehl et al. 2008, for a recent discussion of this topic). However, due to the smaller scale and the lower luminosities expected, detections of cavities is increasingly more difficult in groups and galaxies. And yet they are expected to play a more prominent role in the evolution of the host structure, given the shallower potential and the faster dynamical time-scales than in clusters.

We can benefit from observations of nearby objects, such as Centaurus A, which exhibits complex morphology on spatial scales from milliarcseconds to degrees (Fig 4), to understand the relation and the interference between jets and environment, feedback etc. Observing the local universe, where powerful radio sources exist, allows us to obtain details and relatively large fluxes — but the angular sizes require the large and effective FoV that WFXT can provide.

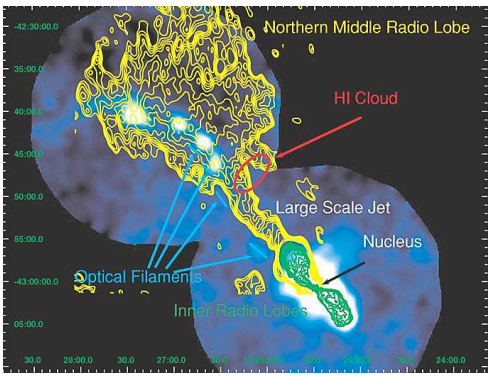

Fig. 4. Exposure corrected, Gaussian smoothed XMM-Newton image of Cen A in the 0.3-1.0 keV band pass (from Kraft et al. 2009). The field displayed is 40′ in size and does not include all of the diffuse emission of CenA and its interesting features. Reproduced by permission of the AAS.

6. Conclusions

Although not in the primary science, the exploration of the local universe is possible and in fact almost mandatory to fully exploit the WFXT performance. We have shown a few cases in which just the large focused area of WFXT would greatly improve our knowledge. The size of the samples of all kinds of galaxies and of individual sources will be much larger than has been possible so far, opening new areas of exploration and allowing us to confirm tentative results based on small number statistics. It is important to focus on the observation strategy, in order to include nearby objects of crucial interest, on the identification procedure, to rapidly have a list of candidates, and on proper calibration of the whole FoV, to fully exploit it. Repeated observations of the same area of sky will yield also a base for variability studies, which can be vital for the identification and classification of many sources.

References

Bauer, M., et al. 2008 A&A 489 1029
Belsole, E., et al. 2003 A&A 398 1
Brusa, M., at al. 2010 ApJ in press
Chynoweth, K. M., et al. 2008 AJ 135 1983
Diehl, S. et al. 2008 ApJ 687 173
Georgakakis, A.E., et al. 2006 MNRAS 367 1017
Georgantopoulos, I., et al. 2005 MNRAS 360 782
Hornschemeier, A.E., et al. 2005 ApJ 129 86
Kraft, R., et al. 2009 ApJ 698 2036
Maccacaro, T., et al. 1988 ApJ 326 680
Memola, E., et al. 2009 A&A 497 359
Mulcahey, J.S., Jeltema, T.E. 2010 ApJL 715 1
Pizzolato, F., Wolter, A. Trinchieri, G. 2010 MNRAS in press
Rand, R.J. 1994 A&A 285 833
Tajer, M., et al. 2007 A&A 467 73
Trinchieri, G., et al. 2008 A&A 484 195
Swartz, D.A., et al. 2004 ApJS 154 519
Yun, M.S., et al. 1994 Nature 372 530
Wolter, A., Trinchieri, G., 2004 A&A 426 787
Wolter, A., Trinchieri, G., & Colpi, M., 2006 MNRAS 373 1672

Mem. S.A.It. Suppl. Vol. 17, 140

Memorie della
Supplementi

WFXT studies of the stellar populations in the Galaxy

S. Sciortino

INAF-Osservatorio Astronomico di Palermo Giuseppe S. Vaiana, Piazza del Parlamento 1, 90138 Palermo, Italy, e-mail: sciorti@astropa.inaf.it

Abstract. I will highlight and discuss some of the studies of the stellar population in the Galaxy that will become possible with or will greatly advantage of the capability of a Wide Field of view X-ray Telescope (WFXT) mission. This mission concept, that was been around for more than 15 years, recently has been re-proposed with renovated interest as part of the US Decadal Astronomy Survey.

Key words. Open Cluster and Association – IMF – Star Formation – X-rays – Wide Area Survey – Stellar Populations

1. Introduction

The idea of a Wide Field X-ray Telescope mission as one key step for the advancement of today astrophysics has been around from nearly 20 years. Such a mission, conceived by R. Giacconi, has as its main driver the investigation of the large scale structure of the Universe, by tracing the hot X-ray emitting plasma in the clusters of galaxies (cf. Borgani et al., this volume) and the population of the farthest AGN (cf. Gilli et al., this volume). A key element of such a mission is a "new-technology" X-ray mirror in which we trade angular resolution near the fov center improving the PSF shape (and resolution) at large off-axis angles over a wide field of view. (see the Pareschi et al. contribution in this volume for a detailed discussion). The concrete realizability of a WFXT[1] has been demonstrated by Citterio et al. (1999) as part of the study phase of an Italy-USA WFXT mission proposed for the ASI small satellite program (Chincarini et al. 1998).

It was clear, since the beginning, that a WFXT mission is a terrific machine for a very ample variety of astrophysical investigations. The key characteristics of the mission that has been proposed to the US Decadal Survey are summarized in Table 1. In the following I will try to briefly show the WFXT role for studies of stellar populations in the Galaxy. In all the cases that I will consider – a highly selected, personal taste, choice – a multiwavelength approach is crucial where key WFXT data need to be complemented with optical, IR, etc. observations. Apart the many possible stellar studies in the Galaxy one can think of, I predict that WFXT observations will results in

Send offprint requests to: S. Sciortino, sciorti@astropa.inaf.it

[1] In 1998 it was realized a mirror shell prototype with an almost uniform 10" angular resolution over a ∼ 1 sq.deg. fov

Table 1. WFXT Planned Survey Sensitivity

Survey		S_{min} (0.5 - 2 keV) point-like at 5σ erg s^{-1} cm^{-2}	
Area (sq. deg.)	Exposure (ksec)	Performance Goal	Baseline
20000	2	3 x 10^{-15}	5 x 10^{-15}
3000	13	5 x 10^{-16}	1 x 10^{-15}
100	400	3 x 10^{-17}	1 x 10^{-16}

The values, taken from Rosati et al. (this volume), refer to goal performances (A_{eff} = 1 m^2, HEW = 5"), and to minimal requirements (A_{eff} = 0.6 m^2, HEW = 10").

many new serendipitous exciting discoveries. In this respect let me just mention, as an example, the very recent XMM-Newton discovery of very intense (100 times higher than expected) X-ray emission from a young brown dwarf (Stelzer et al. 2010) that is urging us to somehow reconsider the X-ray emission mechanism possibly at work in the very low-mass objects.

2. The young stellar population and the recent star formation history in the Galaxy

The reason why X-ray observations are crucial for the study of the nearby, less than 10^9 yr old, stellar populations is the well known fact that the X-ray luminosity decays by 1000-10000 times evolving from the PMS to the solar age; this decay occurs mainly during the main sequence phase. Such a behaviour is due to the decrease of angular momentum and rotational velocity with age. The younger, faster rotating, stars have a stronger magnetic field resulting in a higher X-ray coronal emission. For the sake of the reader let me remember that due to their fast rotation the older synchronized, so called active, binaries are also characterized by an intense coronal emission. While the age decay is the major observable effect we have also observed a softening of emitted X-ray spectrum with stellar age (cf. Micela (2003) and reference therein cited).

Since the stellar X-ray (coronal) emission depends strongly on age, X-ray surveys play a key role in deriving i) the spatial distribution, in particular the densities and scale heights, of the young ($< 10^9$ yr) stellar populations as well as ii) the star formation rate in the last billion year. Indeed in this age range optical photometric surveys are blind since there are no discernible color changes in stellar luminosity and one has to resort to spectroscopically discernible changes (i.e. the intensity of Lithium line) observed in dG-dK stars. Moreover, for dG stars this change mainly occurs after the first $\sim$ 5 x 10^7 yr.

In the "soft" ($\sim$ 0.2-10 keV range) X-rays we can observe young stars at much larger distances than old stars; hence young stars dominate shallow stellar X-ray selected sample while old stars dominate deep high latitude X-ray selected stellar samples (cf. Fig. 1). Active binaries, with their high X-ray luminosities, are selected as well, so companion optical data can be required to disentangle the case. Starting from a "classical" model (Bahcall & Soneira 1980; Bahcall 1986) for the stellar counts in the Galaxy Favata et al. (1992) have build a model, X-COUNT, that provides stellar counts in the X-ray band-pass. The model is based on i) average stellar spatial distributions for various age ranges, ii) an average spatial model of interstellar gas (and resulting extinction in X-rays), and Maximum Likelihood X-ray luminosity distribution functions from age-selected well studied open clusters and stellar samples. Using X-COUNT (or a similar model developed by Guillout et al. 1996) it is possible to compare observed and predicted X-ray stellar counts and, as a result, to derive the spatial distributions of stellar populations in the Galaxy. Following a seminal paper (Favata et al. 1988) on the stellar content of the *Einstein* Medium Sensitivity Survey (Gioia et al. 1990; Stocke et al. 1991), a detailed investigation of the stellar content of the *Einstein* EMSS (215 stars at a limiting $f_X \sim 2$ x 10^{-13} erg/sec/cm^2 over about $\sim$ 778 sq. deg.) has shown the presence of an excess of yellow (dG-dK) stars with respect to predictions (Sciortino, Favata, & Micela 1995). This excess can be either young star or active binaries;

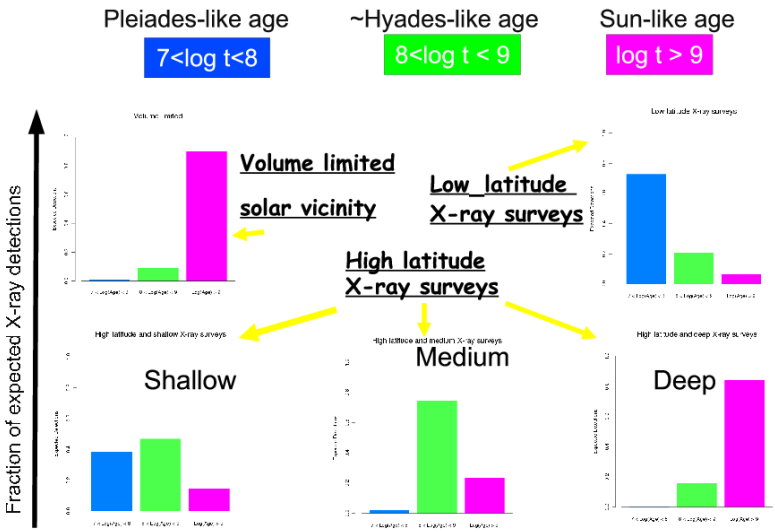

Fig. 1. A schematic representation of the fraction of predicted X-ray normal star counts for various directions and limiting flux for 3 distinct stellar age ranges (identified by distinct colours). In this illustrative calculation the X-ray luminosity of all stars for each given age range has been taken equal to the median L_X of the corresponding sample. The absolute number of predicted stellar counts is different in each of the 5 panels.

an extensive optical campaign has shown that most of them are indeed young stars (Favata et al. 1993, 1995). By comparing the observed and predicted stellar logN - LogS it is possible to infer the behaviour of the recent star formation rate in the Galaxy. This has been firstly demonstrated by Micela, Sciortino, & Favata (1993) who, using the EMSS data, have been able to show that some hypothetical temporal behaviours of the recent star formation rate are not consistent with available data (cf. Fig. 2).

The EMSS is by construction an high (b > 20 deg) latitude survey, while the stellar density in the Galaxy is higher near the plane. In order to study the Galactic Plane content at a limiting flux, $f_X \sim 10^{-14}$ erg/sec/cm^2, 10 times deeper than the RASS, a ROSAT pointed Galactic Plane survey covering ~ 2.5 sq. deg. was performed. The analysis of the 93 stars found in this survey (Morley et al. 2001) has allowed us to conclude that the density of active stars in the Galactic Plane is larger than assumed in X-COUNT; henceforth either the star formation rate is increased in the last billion year or the young population scale heights are smaller than assumed in X-COUNT.

Coming back to high latitude surveys, the analysis of the stellar content (152 stars over 9 sq. deg.) of the ROSAT NEP survey ($f_X \sim 10^{-14}$ erg/sec/cm^2) has confirmed, but at one dex deeper limiting flux, the EMMS results, namely: for dA-dF and for dM X-COUNT predictions agree well with the observations, while a significant excess of yellow (dG-dK) stars is present (Micela et al. 2007). López-Santiago et al. (2007) have analyzed the stellar content of the XBSS (XMM-Newton Bright Serendipitous Survey) confirming an excess of yellow (G+K) stars. A model calculation with a decreasing stellar birthrate is ruled out by observations. A constant SFR can reproduce the number of A and M stars, but underestimates the total number of observed stars. An increasing birthrate seems to work better: the total number of predicted sources agrees with the observations although it overestimates the total number of M stars. Those however can be hidden in some "yellow" binary. The FGK

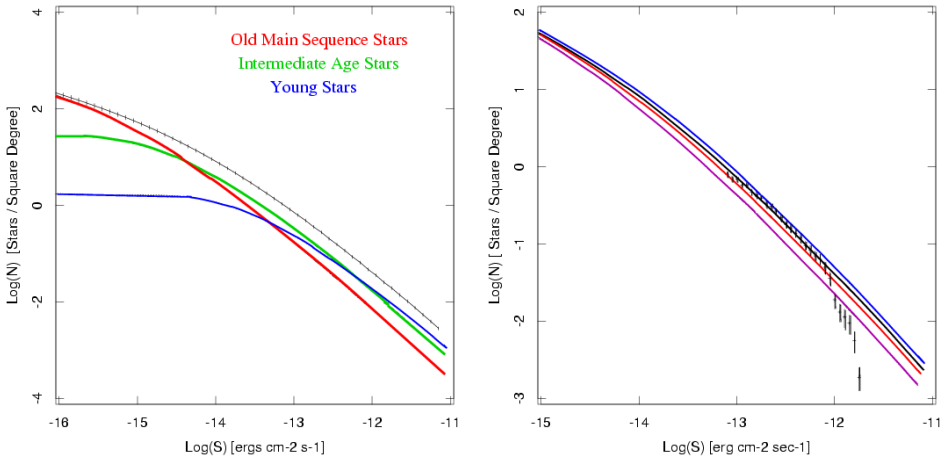

Fig. 2. Left panel: X-COUNT predicted stellar number counts at high galactic latitude assuming a constant stellar birthrate for 3 distinct age ranges: young stars (blue line), intermediate age stars (green line), and old stars (red line), summed over ages (black line). Right panel: observed (points & error bar from EMSS data) and predicted Log(N)-Log(S_x) toward the direction $l = 90°$ and $b = 90°$ assuming $\tau = \infty$ (black line), $\tau = 15\ Gyr$ (red line), $\tau = -15\ Gyr$ (blue line), and $\tau = 5\ Gyr$ (magenta line), [figures adapted from Micela, Sciortino, & Favata (1993)].

star excess cannot be reproduced by using only a smooth stellar birthrate, unless the discrepancy between observations and predictions is due to a stellar population not (yet) included in the X-COUNT model. In summary the discrepancy between predicted and observed spectral type distributions could either be due to an "additional" population of young stars with small scale height or to a number of M dwarfs in binary systems with a yellow primary.

A contribution to this studies has been provided by the analysis of the stellar content of the Chandra Deep Field North (Feigelson et al. 2004). With a quite small sample consisting of 11 stars with V < 22.5, it has been possible to derive strong evidence of a decrease of X-ray luminosities over the 1Gyr <t<11Gyr age interval. With no decrease 39 rather than 11 stars should have been detected. The deduced "best fit" model has $L_X \sim age^{-2}$ ergs s^{-1}, which is faster than the age^{-1} behaviour expected on the basis of known rotational spin-down rates and X-ray-activity relations (cf. Fig. 3).

However larger stellar samples (and deeper surveys) are required to firmly derive the recent star formation history, and specifically, the alternation of peaks and lulls of the star formation rate. This is an area in which WFXT can provide the still lacking data.

3. The Gould Belt (or Disk?) nature

Guillout et al. (1998) have performed the positional cross-identification between the RASS source list (at the limiting count rate of S = 0.03 PSPC c/s) and the stars listed in the Tycho catalog. The large scale sky distribution of the X-ray emitting Tycho stars (cf. Fig. 5) shows an enhancement (apart around the Galactic Plane) that has been interpreted as a structure of young nearby stars, likely, coincident with the so called Gould Belt. The available data have still left open various questions: i) Is this enhancement due to a real, recently formed, physical structure? ii) Is this structure a Belt or instead is more similar to a Disk? iii)

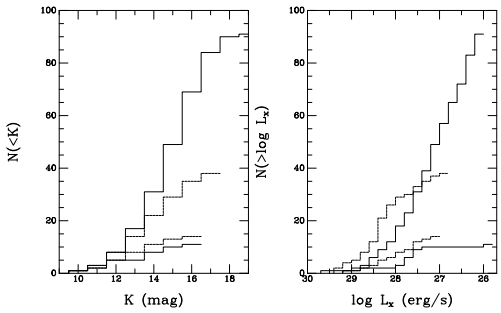

Fig. 3. Left panel: Comparison of cumulative distributions of stellar parameters for XCOUNT models of the CDF-N stellar population. Left: K-band magnitude. Right: X-ray luminosity. In each panel, histograms from top to bottom are as follows: total stellar population in the CDF-N field with V < 22.5 and without X-ray selection (thin solid line), XCOUNT model prediction with standard settings including X-ray selection and no age > 1 Gyr magnetic activity evolution (thin dashed line), XCOUNT model with rapid age^{-2} X-ray decay (thick dashed line), and the observed distributions (thick solid line (figures from Feigelson et al. 2004).

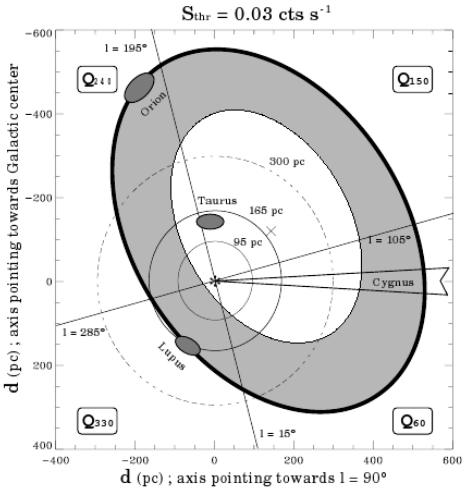

Fig. 4. A sketch of the Gould Belt geometry projected on the Galactic plane. The Gould Belt is assumed to be an ellipsoidal shaped ring with semi-major and minor axes equal to 500 and 340 pc, respectively. The members are assumed to be located near the outer edge of belt (solid thick curve). The asterisk marks the Sun position. The depicted circles of radius 95, 165 and 300 pc centered on the Sun show the X-ray horizon, at a PSPC limiting count-rate of 0.03 cts s^{-1} ($\sim$ 3 x 10^{-13} erg/s/cm^2), for stars with log(L_X [erg/s]) = 29.5, 30.0 and 30.5, respectively. The horizon for a G5 ZAMS star at the Tycho completeness threshold (10.5 mag) is 160 pc. The grey shaded area illustrates the alternative picture of the Gould Disk whose members are spatially distributed between the inner and outer rings (figure from Guillout et al. 1998).

Is this structure related to nearby star formation processes and some "local" triggering mechanism(s)? With the RASS we have been able just to see the side of a hypothetical belt/disk structure nearest to the Sun, while the farthest side is beyond the RASS horizon (cf. Fig. 4). To answer those and other connected questions we definitively need a much deeper large area X-ray survey with a spatial resolution better than XMM-Newton (to select the possible members of such a structure) and we need the GAIA data to derive distances and 3-d space velocities to discriminate the very likely members. A joint WFXT/GAIA investigation will provide an invaluable contributions to assess the nature of the Gould Belt/Disk and more generally of the star formation process in the solar neighborhood. This is clearly shown in pictorial form by the simulation (cf. Fig. 5) of the outcome of a 30-50 times deeper than the RASS X-ray survey with an angular resolution of 10". The nature of the Gould Belt (or Disk) will clearly be derived from a properly selected survey of a (large) sky area, without the need to an all sky coverage. With an efficency of 80% a dedicated medium depth survey (cf. 1) of about 200 sq. deg. will require about 1-2 months.

4. Formation and evolution of Young Stellar Clusters (YSC) and their IMFs

The study of the formation and evolution of the YSC (Young Stellar Clusters) and of their IMF's (Initial Mass Function) is another wide research theme on which a mission like WFXT will provide otherwise impossible to obtain data. For a thorough discussion of this theme I point the reader to a recent white paper by

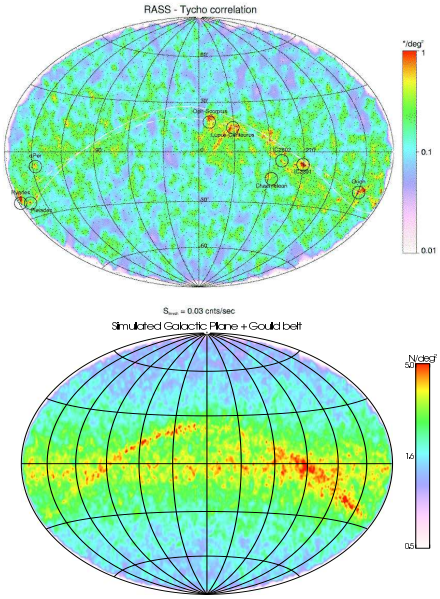

Fig. 5. Top panel: All sky distribution in galactic coordinates of RASS-Tycho stars (black dot) at a PSPC count-rate threshold S = 0.03 cts s^{-1} (~ 3 x 10^{-13} erg/s/cm^2). Color codes the surface density, the enhancement at low galactic latitude is clearly visible. The dashed line indicates Gould belt. Black circles indicate young clusters and star forming regions that show up in the RASS-Tycho sample. Bottom Panel: A simulated all sky distribution in galactic coordinates of X-ray emitting stars at a limiting flux of 5 10^{-14} erg s^{-1} cm^{-2}, 30-50 times deeper than the RASS. Color codes the surface density. At this deeper flux the Gould Belt, if a physical structure, will clearly be discernible (Simulation courtesy of P. Guillout).

Feigelson et al. (2009) submitted to the US Decadal Committee lead by R. Blanford.

Let me just recall the major open issues and related questions: th

Do clusters form rapidly during a single collapse event or slowly over many crossing times ? Why are massive stars rare ? Do they form via accretion disks or stellar mergers ? How does the feedback from OB stars both halt and promote further star formation? Is the stellar IMF truly universal over a wide range of cloud conditions, and what produces its distinctive shape ? When and why does primordial mass segregation (if any) occur ? What effect do shocked OB winds have on the physics of the HII region and the confining GMC ? What fraction of stars in the Galaxy form from triggered processes? What determines whether a YSC survives the dispersal of its parental molecular gas and becomes a bound open or globular cluster? How does the cluster environment influence the evolution of protoplanetary disks and subsequent formation of planetary systems?

Such a research theme definitively requires panchromatic studies: optical, infrared (from ground and space), millimeter (ALMA), as well as X-rays observations are needed. Given the typical extent of relevant targets (that often cover up to tens of square degrees) a WFXT is a key element of the needed instrumental suite. While there are many reasons for the key role played by X-ray observations, let me remember a very basic one: IRAC Spitzer data as well as the new data from Herschel are having an impressive impact in the field, but a reliable IMF can hardly be derived from Spitzer data alone since one will very likely miss a large fraction of WTTs. For example, the identification of a complete sample of members (both Classical T Tauri and Weak Line T Tauri) has proven to be a very crucial point in the investigations of the "environmental" effects on disk evolution (cf. Guarcello et al. 2007, 2009).

5. Continuous monitoring: Variability of Class I e Class II emission

Recently Favata and collaborators have obtained a 23-days long uninterrupted COROT observation of the Young Cluster/SFR NGC 2264 (with an age of ~ 3 Myr). This was a specific additional program aimed to study the variability phenomena of a large sample of NGC 2264 members. The long photometric series are allowing many investigations, in particular to look for light curve variability of the same nature as that observed in the classical T Tauri star AA Tau (Alencar et al. 2010). This variability was interpreted as due to inner warp dynamic associated to and controlled by the interaction between stellar magnetic field and the inner disk region . The classification purely

based on the analysis of light curves is in good agreement with the Spitzer IRAC classification systems, about 40% of of NGC 2264 members show warped disks, i.e. evidence of an intense accretion process mediated by a highly dynamical star-disk magnetospheric interaction. If this picture is correct then we should expect evidence of time correlation between optical and X-ray variability among the sample of AA Tau-like PMS stars; in particular, we should see variability in the emitted intensity as well as in the emitted spectrum (mostly related to a time variable absorption).

Dedicated long observations, such as those of the Chameleon SFR that will be possible with the ESA CV proposed PLATO mission, together with simultaneous (week) long continuous observations with WFXT will definitively provide a big step forward in our understanding of the disk-star interaction and on the role of magnetic field. This would require a couple months of dedicated WFXT observations.

6. Long Term Programs: X-ray Cycles of late-type stars

Currently the WFXT mission concept that has been proposed to the US Decadal Survey considers a mission lifetime of 5 years. However based on the experience of other highly successful X-ray observatories (like Chandra and XMM-Newton), whose lifetime has been extended to more than a decade, I think that we have to consider from the beginning the possibility to include few selected long-term plan investigations that ask for repeated observations over a decade. As an example, let me focus on the case of X-ray cycles of quiet late-type stars, whose X-ray luminosity is similar to that of our Sun, $L_X \sim 10^{27}$ erg/sec. While for our Sun the evidence of a long term (11 years) cycles of the emission in many bands including the X-ray one is based on firm observational evidence, a similar evidence was completely lacking in the case of other X-ray quiet stars; indeed the spotted nature of the available observations had been a serious observational limitation. It has been only for the perseverance of some of us (and good will of many TAC members) that, thanks to a decennial campaign of XMM-Newton repeated observations, we have been able to provide in a couple of cases clear observational evidence of X-ray cycles: probably the best case, HD 81809 (Favata et al. 2008) is shown in Fig. 6. I guess that a proper planned campaign of WFXT observations can enlarge this very small sample and allow us to verify if X-ray cycle and CaII periods do, in general, agree or not and, more generally, what are the conditions under which X-ray cycles may occur. While this is just an example, I feel it contains a lesson: even if formally a mission, WFXT in such a case, has a nominal lifetime too short for a decade-long investigation (this was indeed the case of XMM-Newton), it is definitively worth to start few selected of such long-term investigations, since they can provide scientific returns otherwise impossible.

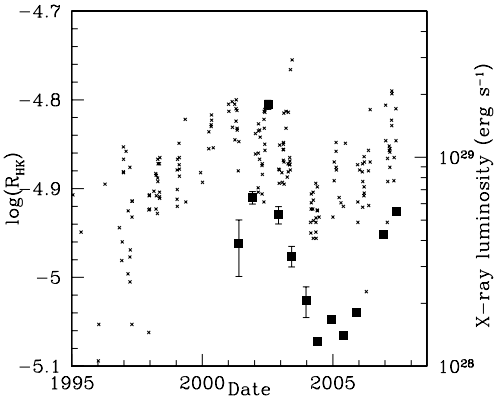

Fig. 6. The variation of the X-ray luminosity for HD 81809 as observed by XMM-Newton since 2001 plotted together with the CaII data available until 2007.

7. Concluding Remarks

WFXT surveys will allow deriving the properties of $< 10^9$ yr old population in the Galaxy. Properly planned follow-up optical observations are needed. The shallow, medium and deep planned high latitude WFXT surveys will allow determining densities and scale heights of young, intermediate and old stellar populations and the history of the star formation rate in the last billion year, a period of time that

optical surveys alone cannot explore. A properly planned, dedicated survey at low-galactic latitude will allow investigating the nature and origin of the Gould Belt/Disk and of its low-mass stellar population, i.e. the nature of one of the recent episodes of star formation occurred in the solar neighborhood. A WFXT mission can step forward our knowledge on many open issues on the physics and process at work in Young Stellar Clusters (and associated proto-planetary systems) formation and early evolution. Key laboratories are the nearby (< 1 kpc) SFRs dispersed on a large area of sky. Such investigation will greatly take advantage of the ∼ 5" angular resolution, the current WFXT goal. More in general stellar studies will require that some time will be devoted to surveying properly selected regions: medium and medium/deep observations are required in order not only to find the sources, but to ease the identification process by using the collected X-ray spectra.

Acknowledgements. I acknowledge many enlightening discussions with G. Micela, E. Feigelson, E. Flaccomio and F. Damiani and the material they have kindly provided. This work was partially supported from ASI/INAF Contracts I/088/06/00 and I/023/05/0.

References

Alencar, S.H.P., et al. 2010, A&A, in press, arXiv 1005.4384

Bahcall, J. N. and Soneira, R. M. 1980, ApJS, 44, 73.

Bahcall, J. N. 1986, Ann. Rev. Astron. Astrophys., 24, 577.

Chincarini, G., Murray, S., Trüemper, J., Wells, A., Citterio, O., Tagliaferri, G., Sciortino, S., 1998, WFXT Proposal to ASI Small Mission Program.

Citterio O., Campana S., Conconi P., Ghigo M., Mazzoleni F., Braeuninger H. W., Burkert W., Oppitz A., 1999, SPIE, 3766, 198

Favata F., Sciortino S., Rosner R., Vaiana G. S., 1988, ApJ, 324, 1010

Favata F., Micela G., Sciortino S., Vaiana G. S., 1992, A&A, 256, 86

Favata F., Barbera M., Micela G., Sciortino S., 1993, A&A, 277, 428

Favata F., Barbera M., Micela G., Sciortino S., 1995, A&A, 295, 147

Favata F., Micela G., Orlando S., Schmitt J. H. M. M., Sciortino S., Hall J., 2008, A&A, 490, 1121

Feigelson, E. D., et al. 2004, ApJ, 611, 1107

Feigelson E., et al., 2009, astro, 2010, 77

Gioia, I. M., Maccacaro, T., Schild, R. E., Wolter, A., Stocke, J., Morris, S ., and Henry, J. P. 1990, ApJS, 72, 567.

Guarcello, M. G., Prisinzano, L., Micela, G., Damiani, F., Peres, G., & Sciortino, S. 2007, A&A, 462, 245

Guarcello, M. G., Micela, G., Damiani, F., Peres, G., Prisinzano, L., & Sciortino, S. 2009, A&A, 496, 453

Guillout P., Haywood M., Motch C., Robin A. C., 1996, A&A, 316, 89

Guillout P., Sterzik M. F., Schmitt J. H. M. M., Motch C., Egret D., Voges W., Neuhaeuser R., 1998, A&A, 334, 540

Guillout P., Sterzik M. F., Schmitt J. H. M. M., Motch C., Neuhaeuser R., 1998, A&A, 337, 113

López-Santiago, J., Micela, G., Sciortino, S., Favata, F., Caccianiga, A., Della Ceca, R., Severgnini, P., & Braito, V. 2007, A&A, 463, 165

Micela G., 2003, AN, 324, 77

Micela G., Sciortino S., Favata F., 1993, ApJ, 412, 618

Micela G., Affer L., Favata F., Henry J. P., Gioia I., Mullis C. R., Sanz Forcada J., Sciortino S., 2007, A&A, 461, 977

Morley J. E., Briggs K. R., Pye J. P., Favata F., Micela G., Sciortino S., 2001, MNRAS, 326, 1161

Sciortino S., Favata F., Micela G., 1995, A&A, 296, 370

Stelzer, B., et al. 2010, MNRAS, in press, arXiv/1006.2717.

Stocke, J. T. et al. 1991, ApJS, 76, 813.

Mem. S.A.It. Suppl. Vol. 17, 148

Memorie della
Supplementi

Neutron star observations with WFXT

S. Campana

Istituto Nazionale di Astrofisica – Osservatorio astronomico di Brera, Via E. Bianchi, I-23807, Merate (LC), Italy e-mail: sergio.campana@brera.inaf.it

Abstract. The Wide-Field X-ray Telescope (WFXT, see Rosati et al. in this volume) is a proposed NASA mission dedicated to performing surveys of the sky in the soft X-ray band (0.3 – 6 keV). The key characteristics of this missions are a constant point spead function with Half Energy Width of ∼ 5 arcsec over ∼ 1 degree fielf of view as well as an effective area ∼ 10 times larger than the one of Chandra. Despite the fact tjat the mission is tailored for extragalactic purposes, we show here that extremely inetersting results can also be obtained on the study of neutron stars.

Key words. Neutron: stars – X-rays

1. Introduction: status

Neutron stars are formed in supernova explosions and live their early life as rotationally powered emitters, shining mainly in the high energy band. A small fraction of the neutron star spin-down power goes in the radio band in the form of pulsed emission, making their discovery possible. As newborn objects, neutron stars are also very hot (millions of degrees) and emit in the soft X–ray band thanks to the cooling of the compact object. As the neutron star ages its spin-down power and internal heat decreases and it becomes readily unobservable. Only for compact objects in close binary systems there is an additional way to power their emission thanks to the exchange of mass from the companion to the neutron star. Accretion of matter onto a compact object naturally leads to emission in the X–ray band, powering the so-called X–ray binaries.

Stable mass transfer onto compact objects produces the brightest objects in the X–ray sky. For this reason our knowledge of the population of X–ray binaries in the Galaxy started with the first all-sky hard-band survey from the Uhuru satellite. Monitoring instruments such as the RossiXTE ASM and now INTEGRAL, Swift BAT and MAXI provide a nearly real-time census of the population of bright X–ray binaries in our Galaxy and in our closeby neighboorhood. With these instruments we have access, however, only to the brightest tip of the population. It was clear from the first X–ray missions that, together with persistent sources, there is a large population of transient X–ray binaries which spend most of their time (90 – 99%) in quiescence and show signs of X–ray activity only for very limited periods of time (during which they share the same properties of persistently bright sources). With the coming of new facilities such as XMM-Newton and Chandra it became clear that intermediate luminosity X–ray binaries are also present, but difficult to discover and, in turn, difficult to study.

Send offprint requests to: S. Campana

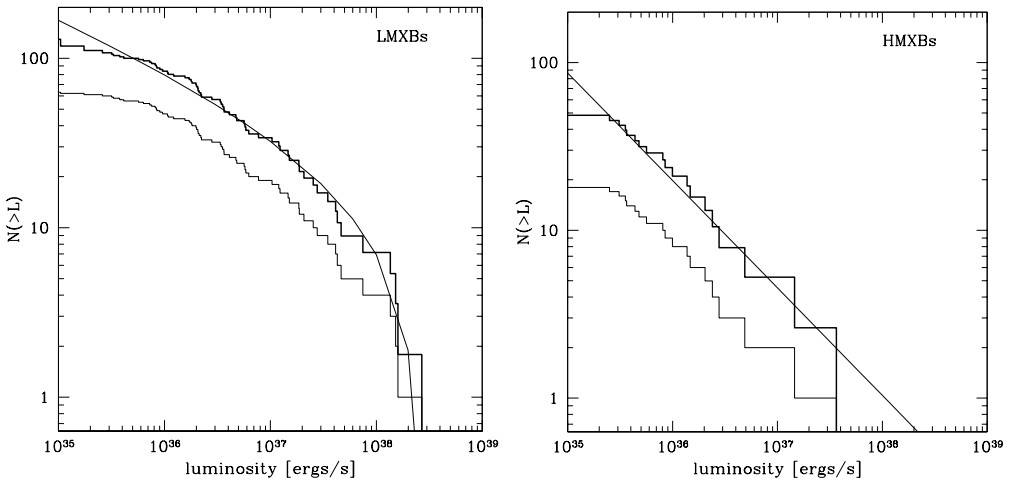

Fig. 1. The apparent (thin histogram) and volume corrected (thick histogram) cumulative luminosity function for Low Mass X–ray Binaries and High Mass X–ray Binaries. The solid lines are the best fits to the data (from (Grimm et al. 2002)). Credit: Grimm et al., A&A, 391, 923, 2002, reproduced with permission © ESO.

Our present view on quiescent and intermediate luminosity X–ray binaries comes from the ROSAT All Sky Survey (RASS) in the soft band only and from partial or limited serendipitous surveys carried out with imaging satellites like XMM-Newton and Chandra.

2. A WFXT survey of the Galactic plane: neutron stars

Actually our knowledge of X–ray binaries as a population relies only on studies with the RossiXTE ASM, providing luminosity function of high-mass and low-mass X–ray binaries (depending on the mass of the companion) down to luminosities of the order of $10^{35} - 10^{36}$ erg s^{-1} (Grimm et al. 2002, see also Fig. 1). This clearly provides only a biased view of the population missing the great majority of faint objects. In addition, below this limiting luminosity level accretion onto neutron stars in high mass (magnetic field $B \sim 10^{12}$ G and spin periods in the few seconds range for the fastest pulsators) and low mass (magnetic field $B \sim 10^{8-9}$ G and spin periods of a few milliseconds) X–ray binary transients might enter in accretion regimes different from the direct fall of matter onto the neutron star surface (e.g. Campana et al. 1998). These regimes (e.g. propeller, reactivation of a radio pulsar) are basically unexplored as a population. In quiescence X–ray binary transients are observationally in the $\sim 5 \times 10^{31} - 10^{33}$ erg s^{-1} range (e.g. Campana 2004).

A WFXT survey of the Galactic plane comparable in depth with the 'wide' survey (i.e. reaching a flux limit of $\sim 3 \times 10^{-15}$ erg cm^{-2} s^{-1} will reach a luminosity limit of $\sim 10^{32}$ erg s^{-1} throughout the Galaxy, providing a complete census of the X–ray binary population. A complete census of the X–ray binary population will help constraining the formation and evolutionary models.

A similar mapping can be achieved on the Magellanic Clouds with a survey comparable in depth to the 'medium' survey. Studying the properties of X–ray binary sources in the Magellanic Clouds rather than in our own Galaxy presents several advantages: *i*) the distance of all sources are well known; *ii*) the much lower column density allows us to investigate a much wider spectral range than it is possible in the Galactic plane. The importance of this low column density is highlighted by

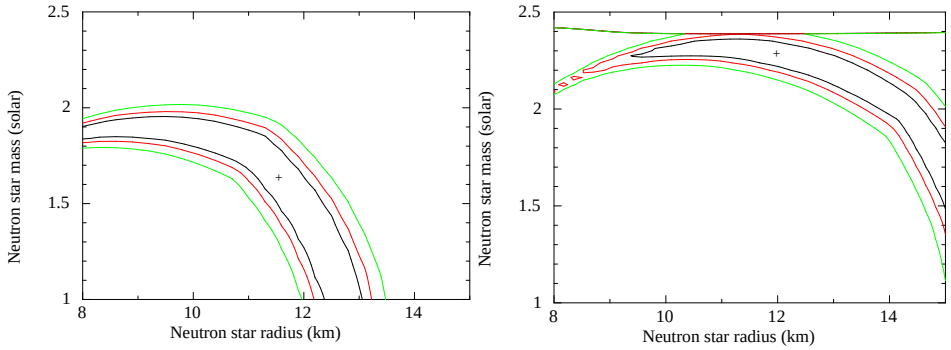

Fig. 2. Typical mass-radius relation that can be obtained with WFXT observing for 100 ks a neutron star low mass transient in quiescence. Simulations were carried out taking the quiescent transient in Omega Cen as a template. In the left panel a mass and radius of 1.66 $M_{\odot}$ and 11.6 km were selected, respectively; in the right panel 2.25 $M_{\odot}$ and 12 km.

e.g. the large number of supersoft sources discovered in the Magellanic Clouds; *iii*) since the metallicities of the Magellanic Clouds differ from that of our Galaxy, a comparison of their X–ray population will help us understanding the role of abundances in their properties.

2.1. Globular Clusters

Globular clusters contain a large number of X–ray binaries, that are formed thanks to close encounters (Heinke et al. 2003) and the large majority of them are quiescent. The X–ray spectrum of a transient low mass X-ray binary in quiescence comprises two spectral components: one hard usually modelled with a power law (with variable importance of a source-by-source basis, from $\lesssim 3\%$ to $\sim 50\%$) and the other soft modelled with a black body emission. The soft component is also consistent with emission coming from the cooling of the entire neutron star surface that has been heated during (transient) accretion episodes (Brown et al. 1998). This emission is well understood and, if data of very good quality are gathered, in principle, it can provide a tool to disentangle the small spectral differences induced by different neutron star masses and radii. Given the large area of WFXT, 100 ks observation will allow to set strong constraints on the neutron star equation of state through observations of transient low mass X-ray binaries in quiescence (see Fig. 2).

In addition, globular clusters contain also a large number of recycled millisecond pulsars (Bogdanov et al. 2006). A statistical study of millisecond radio pulsars can provide insight on the energy conversion mechanism of spin down power into high energy photons.

2.2. Galactic Center

Thanks to the Chandra observatory the Galactic center region has been mapped in exquisite details (Wang et al. 2002; Muno et al. 2009). A scan of two degree across the Galactic center has been carried out (with 2 Ms exposure) reaching a completeness 0.5–8 keV flux limit of 4×10^{32} erg s^{-1} and up to an order of magnitude more sensitive in the deepest exposure around Sgr A (see Fig. 3). 9017 X–ray sources were detected. The majority of the absorbed sources ($N_H > 4 \times 10^{22}$ cm^{-2}) are made by cataclysmic variables, even if a number of transients have been discovered. WFXT can cover the same area more deeply by an order of magnitude in in 200 ks. This opens the possibility of variability studies either temporal and spectral. Monitoring programs can be very effective in discovery faint or very faint transients ($L \sim 10^{34} - 10^{36}$ erg s^{-1}) that cannot be detected and followed by all-sky monitor instruments. Explorative campaigns have

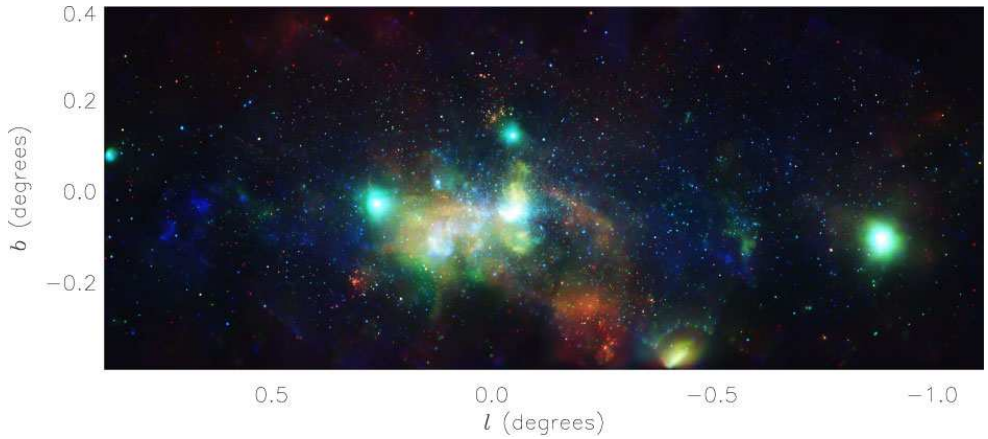

Fig. 3. Three-color image of the Galactic center region. Red is 1–3 keV, green is 3–5 keV, and blue is 5–8 keV, from Muno et al. (2009). Reproduced by permission of the AAS.

been carried out in the Galactic center region with Chandra and XMM-Newton (Wijnands et al. 2006). These systems are poorly studied and only focussing telescope surveys can reveal and study their population (Campana 2009).

2.3. Old neutron stars

About 10^9 neutron stars are thought to populate our Galaxy, but only $\sim 2 \times 10^3$ are directly observed as radio pulsars or as accretion-powered X–ray binaries (see Fig. 4). In principle also the accretion of the interstellar medium material may make isolated neutron stars shine, and their weak luminosity could be detected in soft X–rays. Recent ROSAT observations have convincingly shown that neutron stars accreting from the interstellar medium are extremely rare, if observed at all, in contrast with earlier theoretical predictions. In addition, accreting objects can be confused with much younger, cooling neutron stars. However, a combination of observations and theoretical modeling may help in discriminating between the two classes (Treves et al. 2000).

Clearly also isolated cooling neutron stars are extremely important targets since they can shed light on the supernova explosion rate in the Galaxy and chemical evolution. The ROSAT All-Sky-Survey is the only available survey for this kind of studies. Turner et al. (2010), using new and archival observations made with the Swift satellite and other facilities, examined 147 X–ray sources selected from the RASS Bright Source Catalog (BSC) searching for isolated neutron stars (INS). Independent of X–ray spectrum and variability, the number of INSs is $\lesssim 48$ (90% confidence). Restricting attention to soft ($T < 200$ eV), non-variable X–ray sources they put an all-sky limit of $\lesssim 31$ INSs. Five new objects were also detected. A future (nearly) all-sky X–ray survey with WFXT can be expected to increase the detected population of X–ray-discovered INSs from the 8 to 50 in the BSC, to (for a disk population) 240 to 1500, which will enable a more detailed study of neutron star population models.

3. Conclusions

The Wide Field X-Ray Telescope (WFXT) is a medium-class mission designed to be 2-orders-of-magnitude more sensitive than any previous or planned X–ray mission for large area surveys and to match in sensitivity the next generation of wide-area optical, IR, and radio surveys. The WFXT mission is scientifically broad. The main focus of the mission is on extragalactic science but, as shown above, many important topics can be covered by WFXT concerning neutron stars.

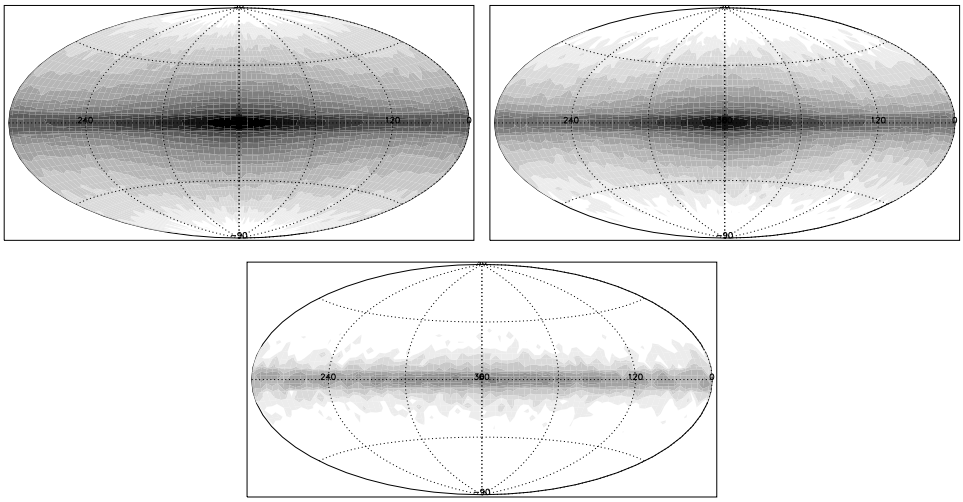

Fig. 4. Sky maps of the projected density of neutron star ($N_{star} = 10^9$) - The cut-off distances are 30 kpc (upper panel), 10 kpc (central panel) and 3 kpc (lower panel) respectively. The density scale is normalized to the maximum density at 30 kpc, from (Sartone et al. 2010). Credit: Sartone et al., A&A, 510, A23, 2010, reproduced with permission © ESO.

References

Bogdanov, S., et al., 2006, ApJ, 646, 1104
Brown, E. F., Bildsten L. & Rutledge R. E., 1998, ApJ, 504, L95
Campana, S., et al., 1998, A&ARv, 8, 279
Campana, S., 2004, AIPC, 703, 260
Campana, S., 2009, ApJ, 699, 1144
Grimm, H.-J., Gilfanov, M., Sunyaev, 2002, A&A, 391, 923
Heinke, C. O., et al., 2003, ApJ, 598, 501
Muno, M. P., et al., 2009, ApJS, 181, 110
Sartore, N., Ripamonti, E., Treves, A., Turolla, R., 2010, A&A, 510, A23
Treves, A., Turolla, R., Zane, S., Colpi, M., 2000, PASP, 112, 297
Turner, M. L. et al., 2010, ApJS in press (arXiv1003.3955)
Wang, Q. D., Gotthelf, E. V., & Lang, C. C., 2002, Nature, 415, 148
Wijnands, R., et al., 2006, A&A, 449, 1117

Mem. S.A.It. Suppl. Vol. 17, 153

Memorie della
Supplementi

WFXT synergies with next generation radio surveys

P. Padovani

European Southern Observatory, Karl-Schwarzschild-Str. 2, D-85748 Garching bei München, Germany e-mail: ppadovan@eso.org

Abstract. I highlight the synergies of the Wide Field X-ray Telescope (WFXT) with the next generation radio surveys, including those to be obtained with the Australian Square Kilometre Array Pathfinder and the Square Kilometre Array, and discuss the overlap between the X-ray and radio source populations. WFXT will benefit greatly from the availability of deep radio catalogues with very high astrometric precision, while on the other hand WFXT data will be vital for the identification of faint radio sources down to $\approx 50\ \mu$Jy.

Key words. galaxies: active — galaxies: starburst — radio continuum: galaxies — X-rays: galaxies — surveys — telescopes

1. Introduction

The Wide Field X-Ray Telescope (WFXT)[1] is a medium-class mission designed to be about two orders of magnitude more sensitive than any previous or planned X-ray mission for large area surveys and to match in sensitivity the next generation of wide-area optical, infrared, and radio surveys (see Giacconi et al. 2009; Murray et al. 2009, and Rosati et al. this volume for details)

I explore here the possible WFXT synergies with future radio surveys. Sect. 2 describes the current status of radio surveys, while a selection of up-coming and future radio projects is described in Sect. 3. Sect. 4 deals with the source population in deep radio and X-ray surveys, while the X-ray/radio synergy is discussed in Sect. 5. My conclusions are summarised in Sect. 6 As this is *not* a review of future radio projects, only basic information on them will be provided. Readers wanting to know more should consult the relevant references and World Wide Web pages.

Send offprint requests to: P. Padovani

[1] http://www.wfxt.eu

2. Current radio surveys

Currently available radio surveys can be divided, as it is the case for most observational bands, into two main categories: shallow/large area and deep/small area (see, e.g., Fig. 1 of Norris et al. 2009). The first group includes, above 0.5 GHz: the NRAO VLA Sky Survey (NVSS; Condon et al. 1998), which covers 82% of the sky ($\delta > -40°$) at 1.4 GHz down to 2.5 mJy, with a 45" resolution; the Faint Images of the Radio Sky at Twenty centimeters (FIRST; Becker et al. 1995), covering 22% of the sky (the North Galactic Cap) at 1.4 GHz down to 1 mJy, with a 5" resolution; the Sydney University Molonglo Sky Survey (SUMSS; Mauch et al. 2003), which maps

63% of the sky ($\delta < -30^\circ$ and $|b_{II}| > 10^\circ$) at 843 MHz down to $\sim$ 10 mJy, with a resolution similar to that of the NVSS. The second category includes a number of Very Large Array (VLA) small area surveys below 0.1 mJy at a few GHz, reaching a maximum area of ~ 2 deg^2 (VLA-COSMOS; Bondi et al. 2008) and a minimum flux density ~ 15 μJy at 1.4 GHz (SWIRE; Owen & Morrison 2008) and ~ 7.5 μJy at 8.4 GHz (SA 13; Fomalont et al. 2002).

3. Up-coming and future radio surveys

Radio astronomy is at the verge of a revolution, which will produce large area surveys reaching flux density limits way below current ones. I highlight here some of projects, which are being planned.

3.1. LOw Frequency ARray

The LOw Frequency ARray (LOFAR)[2] is a new radio telescope designed and built by ASTRON (the Netherlands Institute for Radio Astronomy) in collaboration with Dutch universities and other European partners. LOFAR operates in a largely unexplored region of the electro-magnetic spectrum (from below 20 up to $\sim$ 240 MHz), and consists of a distributed interferometric array of dipole antenna stations that permit large areas of the sky to be imaged simultaneously.

LOFAR will carry out large area surveys at 15, 30, 60, 120 and 200 MHz reaching different flux density limits (see Morganti et al. 2009, for details). For the largest area planned the 120 MHz survey will reach $\approx$ 0.5 mJy, which is equivalent to $\approx$ 0.1 mJy at 1.4 GHz for a power-law $\alpha_r = 0.7$ ($S \propto \nu^{-\alpha}$). The resolution is obviously dependent on the longest baseline and on the observing frequency, and will at best be $\sim$ 3" at 240 MHz. LOFAR has started operations in 2010.

LOFAR will open up a whole new region of parameter space at low radio frequencies. Based on our knowledge of the spectra of the various classes of radio sources and LOFAR's sensitivity, the large majority of detections should be radio- and star-forming galaxies, in contrast with X-ray surveys, which include mostly radio-quiet AGN (see Sect. 4). However, the deeper surveys will reach fainter radio sources and should have a larger overlap with the type of objects detected in the X-ray band by WFXT.

3.2. Expanded VLA

The Expanded VLA (EVLA)[3] Project will modernise and extend the existing VLA. When completed in 2012, the EVLA will provide the following capabilities: observing frequency between 1 and 50 GHz, reaching as low as 1 μJy r.m.s. in 6 hours (i.e., between 5 and 20 times better than the VLA), and resolution as good as $\sim$ 1" at 1.5 GHz and 0.03" at 45 GHz. To the best of my knowledge no large area surveys are being planned at present but some surveys will be obviously carried out by individual teams.

3.3. Evolutionary Map of the Universe

The Australian Square Kilometre Array [SKA] Pathfinder (ASKAP) will produce wide-deep radio surveys of the sky at 1.4 GHz. The highest ranked ASKAP continuum project is the Evolutionary Map of the Universe (EMU)[4].

The primary goal of EMU is to make a deep survey of the entire southern sky, extending as far north as $\delta = +30^\circ$. By reaching a flux density limit $\approx$ 50 μJy EMU will have $\sim$ 50 times more sensitivity than NVSS, whilst covering a similar area (75% of the sky) with a five times better angular resolution (10"). EMU will then provide a similar gain with respect to previous surveys as WFXT in the X-ray band (see, e.g., Fig. 1 of Norris et al. 2009).

With a likely start of operations in 2013, the EMU catalogue, which will include around 70 million sources, should be available to the astronomical community by around 2015.

[2] http://www.astron.nl/radio-observatory/astronomers/lofar-astronomers

[3] http://science.nrao.edu/evla

[4] http://www.atnf.csiro.au/people/rnorris/emu

Besides ASKAP, other radio telescopes currently under construction in the lead-up to the SKA include the Allen Telescope Array[5] (ATA), Apertif[6], and Meerkat[7].

3.4. Square Kilometre Array

The Square Kilometre Array (SKA)[8] will represent a true revolution in radio astronomy by combining unprecedented versatility and sensitivity. It will provide an observing window between 70 MHz and 10 GHz reaching flux density limits well into the *nanoJy* regime. Resolution will likely need to be < 1" around GHz frequencies to avoid confusion, with a baseline extending to at least 3,000 km. The field of view will be large, up to ~ 200 deg^2 below 0.3 GHz and possibly reaching ~ 25 deg^2 at 1.4 GHz. Timeline for completion is 2020, with first science with 10% SKA around 2015 - 2016. Location will be in the southern hemisphere, either Australia or South Africa.

Many surveys are being planned with the SKA, possibly including an "all-sky" 1 μJy survey at 1.4 GHz and an HI survey out to redshift ~ 1.5, which should consist of $\sim 10^9$ galaxies.

4. The deep radio and X-ray skies

Before discussing the X-ray/radio synergy it is important to have a look first at the types of sources that are being detected in the two bands, as current deep radio and X-ray surveys are sampling somewhat different populations. For example, the X-ray selected sample of Polletta et al. (2007), with an X-ray flux limit $f(2-10\,\mathrm{keV}) > 10^{-14}$ erg cm^{-2} s^{-1} contains $\sim$ 97% Active Galactic Nuclei (AGN), $\approx$ 10% of them radio-loud (as derived from the radio data provided in their paper). Similarly, the 1 Ms observations of the Chandra Deep Field South (CDFS) have shown that, amongst the optically brightest sources, 75% are AGN and only 22% are associated with galaxies [Szokoly et al. (2004); see also, e.g., Feruglio et al. (2008) and references therein]. On the other hand, deep ($S_{1.4\,\mathrm{GHz}} \geq 42$ μJy) radio observations of the VLA-CDFS have identified $\gtrsim$ 40% AGN (about half of them radio-loud) and $\lesssim$ 60% star-forming galaxies (SFG) (Padovani et al. 2009). Therefore, while faint X-ray sources are mostly radio-quiet AGN, deep radio surveys are revealing SFG and AGN in almost equal numbers, with only about half of the latter, or $\approx 1/5$ of the total, being radio-quiet.

This small population overlap is corroborated by the fractions of sources detected in one band with counterparts in the other one. Of the radio sources in the VLA-Extended CDFS (ECDFS) sample of Miller et al. (2008) ($S_{1.4\,\mathrm{GHz}} \geq 32$ μJy) only $\sim$ 34% are found in the 2 Ms X-ray catalogue of Luo et al. (2008). And only $\sim$ 20% of the X-ray sources in 2 Ms catalogue have a radio counterpart in the VLA-ECDFS survey (Vattakunnel & Tozzi, private communication).

It is important to note that X-ray data, including upper limits, play a very important role in the identification of faint (sub-mJy) radio sources, as shown by Padovani et al. (2009). In fact, the radio-to-optical flux density ratio is not a very good discriminant between SFG and AGN. Radio power fares somewhat better but is not helpful in separating SFG from radio-quiet AGN. On the other hand, high X-ray powers ($L_\mathrm{x} > 10^{42}$ erg/s) can only be reached by AGN.

5. The X-ray/radio synergy

Figure 1 plots 0.5 – 2 keV X-ray flux vs. 1.4 GHz radio flux density and includes the limits of the WFXT, EMU, and SKA 1 μJy surveys (I am considering here only high-frequency radio surveys for the reasons discussed in Sect. 3.1.). Note that, confusion aside, SKA should be able to detect sources as faint as a few tens of nanoJy.

The loci of SFG, X-ray selected, and radio-quiet, radio-selected AGN are also shown. These give only order of magnitude estimates as the dispersion around the mean value can be quite large. For instance, AGN will span

[5] http://ral.berkeley.edu/ata
[6] http://www.astron.nl/general/apertif/apertif
[7] http://www.ska.ac.za/meerkat
[8] http://www.skatelescope.org

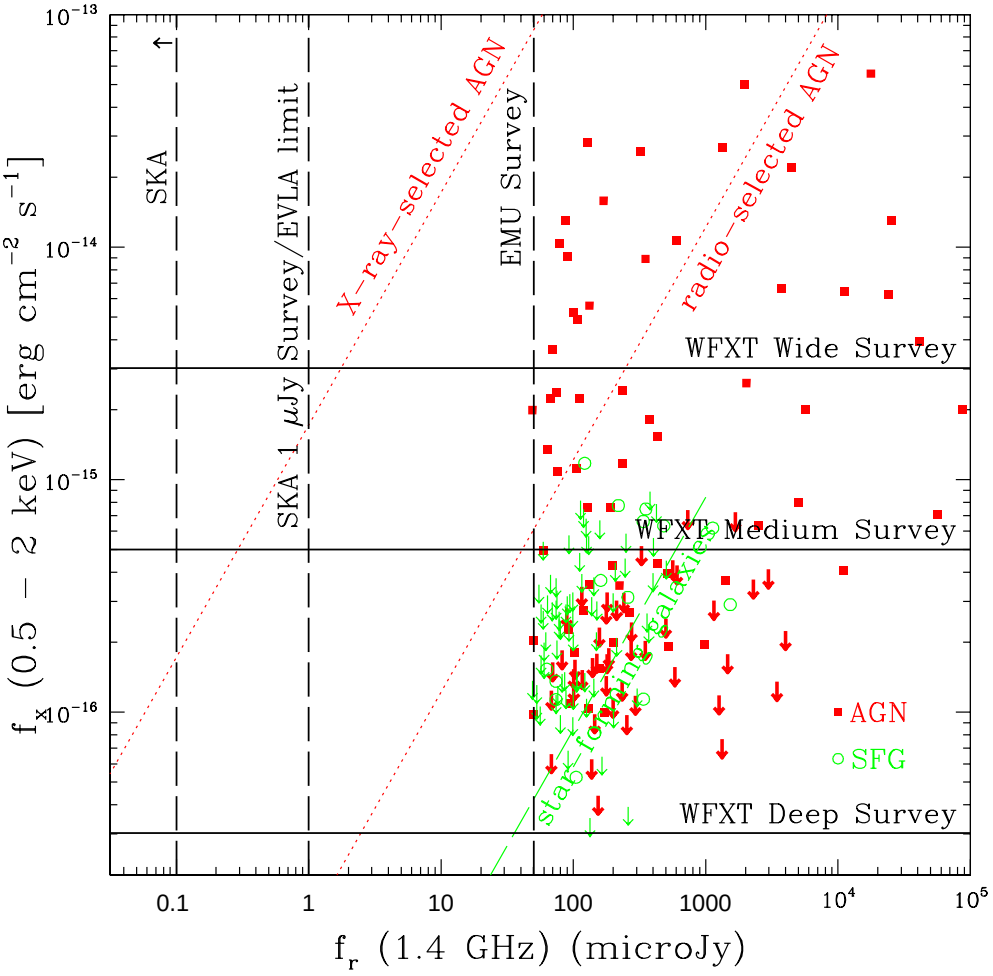

Fig. 1. The 0.5 – 2 keV X-ray flux vs. 1.4 GHz radio flux density for the AGN (filled squares) and star-forming galaxies (SFG; empty circles) in the VLA-CDFS sample (Padovani et al. 2009). Upper limits are also indicated (AGN: thick lines; SFG: thin lines). The loci of SFG (slanted dashed line; Ranalli et al. 2003), X-ray selected (mostly radio-quiet) (leftmost dotted line, from data in Polletta et al. 2007, converted to the 0.5 – 2 keV band) and radio-quiet, radio-selected AGN (rightmost dotted line from data in Padovani et al. 2009) are also shown. The position of these loci with respect to the survey limits determines the fraction of sources of a given class detected in one band with counterparts in the other. The horizontal solid lines indicate the limits of the WFXT Wide, Medium, and Deep surveys, while the two rightmost vertical dashed lines denote the limits of the Evolutionary Map of the Universe (EMU) and SKA 1 μJy surveys, both of which will cover a large fraction of the sky. The latter represents also the approximate EVLA r.m.s. level. The leftmost vertical dashed line at 0.1 μJy represents the upper limit for other smaller area SKA surveys, which will likely be conducted.

the full range between the two dotted lines in Fig. 1, with X-ray (radio) selection favouring sources with high (low) X-ray-to-radio flux density ratios. The position of these loci with

respect to the survey limits determines the fraction of sources of a given class detected in one band with counterparts in the other. For example, very few AGN in the WFXT Wide survey will have a radio counterpart in the EMU survey because the locus of X-ray selected AGN (leftmost dotted line in Fig. 1) is to the left of the EMU limit for $f(0.5-2\ \mathrm{keV}) \lesssim 10^{-13}$ erg cm^{-2} s^{-1}.

For illustration purposes the fluxes of the AGN and SFG VLA-CDFS sources are also shown (Padovani et al. 2009). The AGN below the radio-quiet AGN locus are identified with radio-galaxies.

5.1. The X-ray survey perspective

Figure 1 shows that the bulk of the X-ray sources in the WFXT Wide survey will have a radio counterpart in a possible SKA 1 μJy survey. This should help in the identification work of the 10 million or so expected objects by also providing very accurate positions. Similarly, most objects belonging to the Medium survey will be detected in SKA surveys at, or below, the ≈ 0.3 μJy level.

Finally, most SFG in the Deep survey will have a radio counterpart already at the EMU levels, while they will all be detected in an SKA 1 μJy survey. Radio detection of the bulk of the AGN will need much fainter (< 0.1 μJy) radio flux limits. This might be accomplished by the SKA given also the small area of the WFXT Deep survey (~ 100 deg^2). All of this, and what follows below (Sect. 5.2), obviously requires that WFXT surveys are carried out in the southern sky.

5.2. The radio survey perspective

Figure 1 shows that the bulk of the radio-quiet AGN in the EMU survey will have an X-ray counterpart in the WFXT Medium Survey, which should greatly facilitate their optical identification. Overall, one expects $< 34\%$ X-ray detections, based on the CDFS, which goes deeper in the X-rays. However, most EMU sources, including SFG, should be detected by the WFXT Deep survey. The EMU/WFXT combination will provide in this case a better sample than the VLA-CDFS one on an area ~ 500 times larger, for a total of $> 100,000$ sources.

The bulk of radio-quiet AGN in an SKA 1 μJy survey will have an X-ray counterpart in the WFXT Deep survey. However, at these flux density levels most objects are expected to be of the SFG type (see, e.g., Padovani et al. 2009), which means that the majority of these radio sources will not be detected in the X-rays even at the deepest WFXT limit.

Finally, a fraction of the radio-quiet AGN in SKA surveys reaching below 0.1 μJy should have an X-ray counterpart in the WFXT Deep survey. Since at these levels the expected optical magnitudes are very faint even for unabsorbed sources ($\gtrsim 26$), X-ray information is going to be vital for source identification.

6. Conclusions

Radio astronomy is at the verge of revolutionary advances, which over the next ten years or so will allow the detection of radio sources as much as $\gtrsim 100$ times fainter than currently available.

Although at present X-ray and radio surveys detect somewhat different sources, with AGN making up most of the deep X-ray sky while sharing this role with star-forming galaxies in the radio band, synergy between the two bands is already required since, for example, X-ray information is vital to establish the nature of faint radio sources.

The availability of deep radio catalogues with very accurate source positions will be a huge asset to WFXT. Similarly, WFXT data will provide vital help with the identification of faint radio sources down to ≈ 50 μJy. At lower flux densities the X-ray counterparts of most radio sources are expected to be fainter than the WFXT deepest limit.

In summary, the combination of future deep radio surveys with WFXT will shed light on the nature of very faint X-ray and radio sources.

Acknowledgements. I thank Ken Kellermann and Raffaella Morganti for reading the manuscript and Piero Rosati for useful discussions.

References

Becker, R. H., White, R. L., & Helfand, D. J. 1995, ApJ, 450, 559
Bondi, M., et al. 2008, ApJ, 681, 1129
Condon, J. J., et al. 1998, AJ, 115, 169
Feruglio, C., et al. 2008, A&A, 488, 417
Fomalont, E. et al. 2002, AJ, 123, 2402
Giacconi, R., et al. 2009, Astro2010: The Astronomy and Astrophysics Decadal Survey, Science White Papers (arXiv:0902.4857)
Luo, B., et al. 2008, ApJS, 179, 19
Mauch, T., et al. 2003, MNRAS, 343, 1117
Miller, N. A., et al. 2008, ApJS, 179, 114
Morganti, R., et al. 2009, in Panoramic Radio Astronomy: Wide-field 1-2 GHz research on galaxy evolution, Gröningen, The Netherlands, June 2009, (arXiv:1001.2384)
Murray, S., et al. 2009, Astro2010: The Astronomy and Astrophysics Decadal Survey, Science White Papers (arXiv:0903.5272)
Norris, R. P. et al. 2009, in Panoramic Radio Astronomy: Wide-field 1-2 GHz research on galaxy evolution, Gröningen, The Netherlands, June 2009, (arXiv:0909.3666)
Owen, F. N., & Morrison, G. E. 2008, AJ, 136, 1889
Padovani, P., et al. 2009, ApJ, 694, 235
Polletta, M. et al. 2007, ApJ, 663, 81
Ranalli, P., Comastri, A., & Setti, G. 2003, A&A, 399, 39
Szokoly, G. P., et al. 2004, ApJS, 155, 271

Mem. S.A.It. Suppl. Vol. 17, 159

Memorie della
Supplementi

eROSITA on SRG

A X-ray all-sky survey mission

N. Cappelluti [1], P. Predehl[1], H. Böhringer[1], H. Brunner[1], M. Brusa[1], V. Burwitz[1], E. Churazov[2], K. Dennerl[1], A. Finoguenov[1], M. Freyberg[1], P. Friedrich[1], G. Hasinger[3], E. Kenziorra[4], I. Kreykenbohm[5], G. Lamer[6], N. Meidinger[1], M. Mühlegger[1], M. Pavlinsky[7], J. Robrade[8], A. Santangelo[4], J. Schmitt[8], A. Schwope[6], M. Steinmitz[6], L. Strüder[1], R. Sunyaev[1], and C. Tenzer[4]

[1] Max-Planck-Institut für extraterrestrische Physik, D-85741 Garching, Germany
[2] Max-Planck-Institut für Astrophysik, D-85741 Garching, Germany
[3] Max-Planck-Institut für Plasma Physik, D-85741 Garching, Germany
[4] Institut für Astronomie und Astrophysik, Abteilung Astronomie, Universität Tübingen, Sand 1, 72076 Tübingen, Germany
[5] Universit"at Erlangen/Nürnberg, Dr.-Remeis-Sternwarte Bamberg, Sternwartstrasse 7, D-Bamberg
[6] Astrophysikalisches Institut Potsdam, An der Sternwarte 16, D-14482 Potsdam, Germany
[7] Space Research Institute Moscow, Russian Federation
[8] Universität Hamburg, Hamburger Sternwarte, Gojenbergsweg 112, 21029 Hamburg, Germany e-mail: cap@mpe.mpg.de

Abstract. eROSITA (extended ROentgen Survey with an Imaging Telescope Array) is the core instrument on the Russian Spektrum-Roentgen-Gamma (SRG) mission which is scheduled for launch in late 2012. eROSITA is fully approved and funded by the German Space Agency DLR and the Max-Planck-Society. The design driving science is the detection of 50 - 100 thousands Clusters of Galaxies up to redshift z 1.3 in order to study the large scale structure in the Universe and test cosmological models, especially Dark Energy. This will be accomplished by an all-sky survey lasting for four years plus a phase of pointed observations. At the time of writing the instrument development is currently in phase C/D.

Key words. Stars: abundances – Stars: atmospheres – Stars: Population II – Galaxy: globular clusters – Galaxy: abundances – Cosmology: observations

1. Mission overview

The Russian Spectrum-Roentgen-Gamma (SRG) satellite will fly on a medium class platform ("Navigator", Lavochkin Association, Russia). The launch will be in 2012 using a Soyuz-2 rocket from Bajkonur into an orbit around L2. The payload consists of the X-ray instruments eROSITA (extended ROentgen

Send offprint requests to: N. Cappelluti

Survey with an Imaging Telescope Array) and ART-XC (Astronomical Roentgen Telescope – X-ray Concentrator).

The seven eROSITA telescopes are based on the existing design launched on the ABRIXAS mission plus an advanced version of the pnCCD camera successfully flying on XMM-Newton. In order to optimize eROSITA for the Dark Energy studies, the effective area is increased by a factor of five, the angular resolution is improved by a factor of two, and the field of view is also increased by a factor of two with respect to ABRIXAS. Such a design has been drawn to match the outcome of the most recent calls for ideas on Dark Energy observations (like e.g. by NASA, DOE, ESA, ESO and others).

Similarly to eROSITA ART-XC contains 7 telescopes working in the energy range between 6 and 30 keV. The telescopes are conical approximations of the Wolter-I geometry with CdTe detectors in their focal planes (Pavlinsky et al., 2010, this Volume)

2. Design Driving Science

2.1. Dark Energy

One way to test cosmological models and to assess the origin, geometry, and dynamics of the Universe is through the study of the large-scale structures Indeed galaxy clusters are strongly correlated and thus they are good tracers of the large-scale structure on very large scales by sampling the most massive congregates of matter. The galaxy cluster population provides information on the cosmological parameters in several complementary ways:

1. The cluster mass function in the local Universe mainly depends on the matter density Ω_m and the amplitude of the primordial power spectrum σ_8.
2. The evolution of the mass function f(M,z) is directly determined by the growth of structure in the Universe and therefore gives at the same time sensitive constraints on Dark Matter and Dark Energy.
3. The amplitude and shape of the cluster power spectrum , P(k) and its growth with time, depend sensitively on Dark Matter and Dark Energy.
4. Baryonic wiggles due to the acoustic oscillations at the time of recombination are still imprinted on the large scale distribution of clusters (i.e. in their P(k) and the Autocorrelation function) and thus can give tight constraints on the curvature of space at different epochs.

The constraints provided by the different cosmological tests with clusters are complementary in such a way, that degeneracies in the parameter constraints in any of the tests can be broken by combinations. The simultaneous constraint of Ω_m and σ_8 by combining method 1 and 3 above is one such example Schuecker et al. (2003). In addition the combination of several tests provides important consistency checks as explained below. In addition to the above applications, galaxy clusters have been used as cosmological standard candles to probe absolute distances, analogous to the cosmological tests with supernovae type Ia. The assumption that the cluster baryon fraction is constant with time combined with observations of this quantity provides constraints on Dark Matter and Dark Energy, e.g. Allen et al. (2004)). In a very similar way, combined X-ray and Sunyaev-Zeldovich-measurements provide a mean for absolute distance measurements and constraints of the geometry of the Universe, e.g. Molnar et al. (2004).
Large, well defined and statistically complete samples of galaxy clusters (which are dynamically well evolved and for which masses are approximately known) are obvious prerequisites for such studies. A substantial progress in the field requires samples of tens to hundreds of thousands of clusters. Surveys at several wavelengths are used or planned to be used to achieve this goal. More in general, in X-ray surveys, galaxy clusters are detected by the radiation of the hot intracluster medium and X-ray observations are still the most efficient tools to select clean cluster samples. In addition X-ray observations provide accurate estimates of the cluster physical parameters. Indeed the X-ray luminosity is tightly correlated to the gravitational mass, temper-

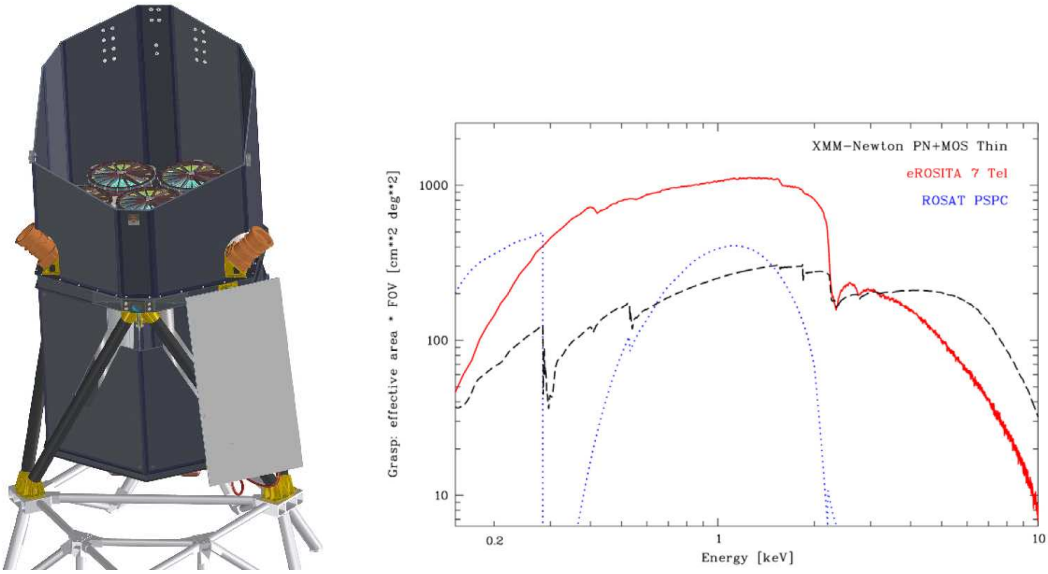

Fig. 1. *Left Panel* : The eROSITA telescope on board SRG. *Right Panel* : The grasp of eROSITA compared with ROSAT-PSPC and XMM-Newton.

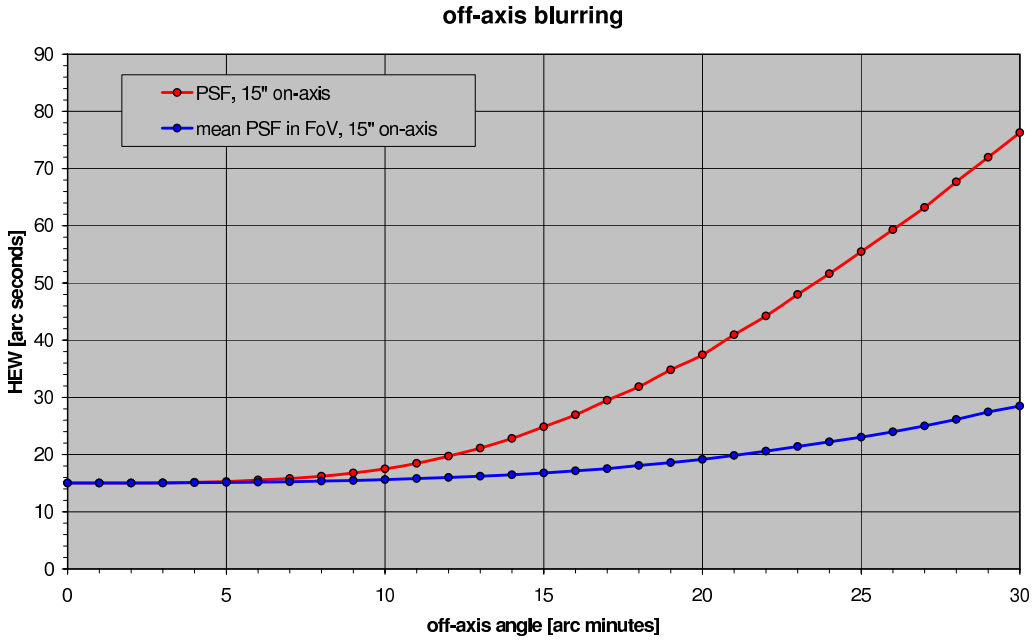

Fig. 2. *Red Curve*: the PSF HEW as function of the offaxis angle in pointing mode. *Blue Curve*: the PSF HEW within an encircled off-axis angle during a scan. Basically the value at 30′, is the cumulative PSF in the survey.

ature and core radius Reiprich et al. (2002). Therefore most cosmological studies involving galaxy clusters are based on X-ray surveys (e.g. Henry (2000), Henry (2004), Böhringer et al. (2000), Vikhlinin et al. (2003).

3. Instrument

The mirror replication technique was developed for XMM-Newton and has then been applied to the small satellite mission ABRIXAS, which had scaled the XMM-Newton telescopes down by a factor of about 4. The ABRIXAS optical design and manufacturing process are adopted for eROSITA partially because the inner 27 mirror shells and therefore the focal length are kept the same. The mirror system consists of 7 mirror modules with 54 mirror shells each and a X-ray baffle in front of each module. Unlike on ABRIXAS, the seven optical axes are co-aligned. Compared to a large single mirror system, the advantages of a multiple mirror system are: shorter focal length (reduced instrumental background) and reduced pileup when observing bright sources. This configuration allows a more compact telescope and multiple but identical cameras which automatically provides a 7-fold redundancy. The capabilities of the X-ray mirror system are described by effective area, vignetting function, and PSF. The production of the flight mirrors has already started. The eROSITA-CCD Meidinger et al. (2009) have 384 × 384 pixels or an image area of 28.8 mm × 28.8 mm, respectively, for a field of view of 1.03° diameter. The 384 channels are read out in parallel. The nominal integration time for eROSITA will be 50 msec. The integrated image can be shifted into the frame store area by less than 100 msec before it is read out within about 5 msec. CCD together with the two CAMEX and the (passive) front-end electronics are integrated on a ceramic printed circuit board (CCD-module) and is connected to the "outer world" by a flexlead. The flight-CCDs have already been fabricated. For operation the CCDs have to be cooled down to -80 °C by means of passive elements (heatpipes and radiator). Fluorescence X-ray radiation generated by cosmic particles is minimized by a graded shield consisting of aluminum and boron carbide. For calibration purposes, each camera housing contains a radioactive Fe^{55} source and an aluminum target providing two spectral lines at 5.9 keV (Mn-K_α) and 1.5 keV (Al-K_α). The mechanism ("Filter Wheel") for moving the calibration source into and out of the field of view is designed and qualified. Also the telescope structure is qualified. The optical bench connects the mirror system and the baffles on one side with the focal plane instrumentation on the other side. Additionally, it forms the mechanical interface to the S/C bus. The flight model manufacturing is on-going. The dimensions of the telescope structure is of the order 1.9 m diameter x 3.2 m height. The total weight of eROSITA is 735 kg Predehl et al. (2007). The instrument design is shown in Figure 1.

4. Sensitivity

Figure 1 shows the grasp of eROSITA, i.e. the product of effective area and solid angle of the field of view. The effective area of eROSITA is about twice that of one XMM-Newton telescope in the energy band below 2keV, whereas it is three times less at higher energies. This is a consequence of the small f-ratio (focal length vs. aperture) of the eROSITA mirrors. An advantage of the short focal length is also larger field of view. The eROSITA angular resolution is 15 arcsec on-axis. Due to the unavoidable off-axis degradation of a Wolter-I telescope, the angular resolution averaged over the field of view is of the order of 28″ (Fig. 2). We will scan the entire sky for four years (ROSAT 1/2 year). Therefore the eROSITA sensitivity during this all-sky survey will be approximately 30 times ROSAT. With the current scanning strategy, we expect an average exposure of ∼3 ks in the all-sky survey, with two deep fields at the ecliptic poles with an exposure of the order of 20-40 ks, depending on the actual mission strategy.

We have performed simulations of the radiation environment in L2 and determined, by including the cosmic components, a background intensity of 5.63 cts s^{-1} deg^{-2} and 3.15 cts s^{-1} deg^{-2} in the 0.5–2 keV and 2–10 keV energy bands, respectively.

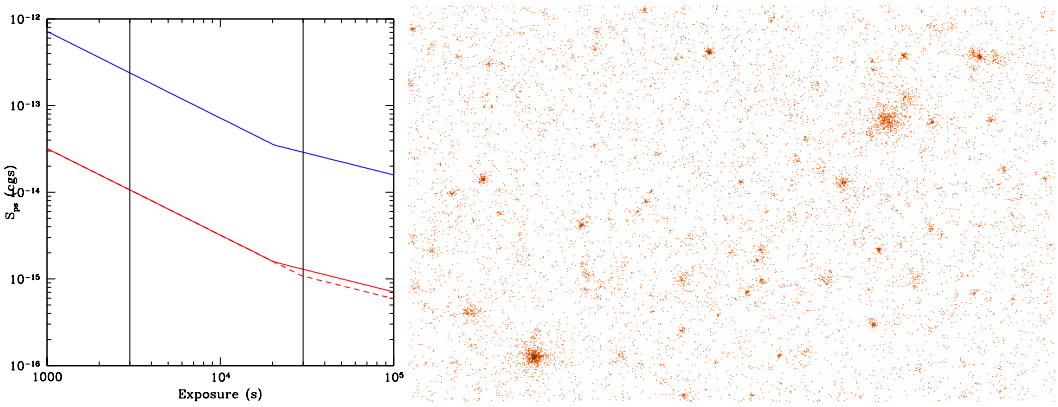

Fig. 3. *Left Panel* : the 5σ point-source sensitivity vs. exposure in the 0.5–2 keV (*red*) and 2–10 keV (*blue*) energy bands by assuming a PSF HEW of 30″ and 40″, respectively. The dashed lines is the sensitivity achieved with an average PSF-HEW of 25″. *Right Panel* : A simulation of a 3ks observation of a 1°×1.6° of eROSITA in survey mode. The simulations includes cosmis+particle background, randomly distributed AGN and clusters extracted from Hydrodinamical simulations.

The 0.5-2 keV flux limit for clusters will be, on average, of the order of 3×10^{-14} erg cm^{-2} s^{-1} and 5×10^{-15} erg cm^{-2} s^{-1} in the all-sky survey and in the ecliptic poles, respectively. In Figure 3 we plot the eROSITA 5σ point source flux limit of the survey in the 0.5–2 keV and 2–10 keV energy bands as function of the exposure time. In the all-sky survey the typical flux limit will be $\sim10^{-14}$ erg cm^{-2} s^{-1} and $\sim3\times10^{-13}$ erg cm^{-2} s^{-1} in the 0.5-2 keV and 2–10 keV energy band, respectively. At the poles we expect to reach flux limits of the order of $\sim2\times10^{-15}$ erg cm^{-2} s^{-1} and $\sim3\times10^{-14}$ erg cm^{-2} s^{-1} in the 0.5-2 keV and 2–10 keV energy band, respectively. Note that the observation will be photon limited up to exposures of ∼20 ks. In the 0.5–2 keV band, the confusion limits of 1 source every 10 beams will be reached in about 20-30 ks. At this fluxes the X-ray sky is dominated by clusters and AGN, which can be separated with an angular resolution of 25″–30″. The logN-logS of clusters is well known to the proposed depth (Gioia et al. (2001), Rosati et al. (2002), Finoguenov et al. (2007)). The proposed survey will identify 50,000 100,000 clusters depending on the capabilities in disentangle moderately-low extended sources from AGN. Concerning the number of AGN we can use the logN-logS measurement in moderately wide field surveys, like XMM-COSMOS Cappelluti et al. (2007), Cappelluti et al. (2009), to predict the detection 3-10×10^6 sources, up to z∼7-8, depending on the detection threshold. A simulation of a 3 ks eROSITA observation of a typical extragalactic field is shown in Figure 3. Multi-band optical surveys to provide the required photometric and spectroscopic redshifts are already in the planning stages, and will be contemporaneous with or precede our survey. The cluster population will essentially cover the redshift range z = 0 - 1.3 and will reveal all evolved galaxy clusters with masses above $3.5 \times 10^{14} h^{-1} M_{\odot}$ up to redshifts of 2. Above this mass threshold the tight correlations between X-ray observables and mass allow direct interpretation of the data.This sample size is necessary for example to precisely characterize the cluster mass function and power spectrum in at least ten redshift bins, to follow the growth of structure with time.

References

Allen, S. W., Schmidt, R. W., Ebeling, H., Fabian, A. C., & van Speybroeck, L. 2004,MNRAS, 353, 457

Böhringer, H., et al. 2000, ApJS, 129, 435

Cappelluti, N., et al. 2007, ApJS, 172, 341
Cappelluti, N., et al. 2009, A&A, 497, 635
Finoguenov, A., et al. 2007, ApJS, 172, 182
Gioia I. M., Henry J. P., Mullis C. R., Voges W., Briel U. G., Böhringer H., Huchra, ApJ 533, 105 (2001)
Henry, P., ApJ 534, 565 (2000)
Henry, P., ApJ 609, 603 (2004)
Schuecker, P., Böhringer H., Collins C. A., Guzzo L., A&A 398, 867 (2003)
Meidinger, N., Andritschke, R., Ebermayer, S., Elbs, J., Hälker, O., Hartmann, R., Herrmann, S., Kimmel, N., Predehl, P., Schächner, G., Soltau, H., Strüder, L., Tiedemann, L., "UV, X-Ray, and Gamma-Ray Space Instrumentation for Astronomy XVI". Ed. Siegmund, O.H. Proc. of the SPIE 7435, pp. 743502 (2009)
Molnar, S., Haiman, Z., Birkinshaw, M., Mushotzky, R.F., ApJ 601, 22 (2004)
Predehl, P., Andritschke, R., Bornemann, W., Bräuninger, H., Briel, U., Brunner, H., Burkert, W., Dennerl, K., Eder, J., Freyberg, M., Friedrich, P., F?rmetz, M., Hartmann, R., Hartner, G., Hasinger, G., Herrmann, S., Holl, P., Huber, H., Kendziorra, E., Kink, W., Meidinger, N., Müller, S., Pavlinsky, M., Pfeffermann, E., Roh?, C., Santangelo, A., Schmitt, J., Schwope, A., Steinmetz, M., Strüder, L., Sunyaev, R., Tiedemann, L., Vongehr, M., Wilms, J., Erhard, M., Gutruf, S., Jugler, D., Kampf, D., Graue, R., Citterio, O., Valsecci, G., Vernani, D., Zimmerman, M., "UV, X-Ray, and Gamma-Ray Space Instrumentation for Astronomy XV". Ed. Siegmund, O.H. Proc. of the SPIE 6686, 668617 (2007)
Reiprich, T., Böhringer, H., 2002, ApJ 567, 716
Rosati P, Borgani S, Norman C, ARA&A 40, 539 (2002)
Vikhlinin A., Voevodkin A., Mullis C. R., VanSpeybroeck L., Quintana H., McNamara B. R., Gioia I., Hornstrup A., Henry J. P., Forman W. R., Jones C., ApJ 590, 15 (2003)

Mem. S.A.It. Suppl. Vol. 17, 165

Memorie della
Supplementi

The high-redshift Universe with the International X-ray Observatory

A. Comastri[1], P. Ranalli[2,1], R. Gilli[1], C. Vignali[2,1], M. Brusa[3], and F. Civano[4]

[1] INAF – Osservatorio Astronomico di Bologna, Via Ranzani 1, I-40127 Bologna, Italy
e-mail: andrea.comastri@oabo.inaf.it
[2] Dip. di Astronomia – Università di Bologna, Via Ranzani 1, I-40127 Bologna, Italy
[3] MPE, Giessenbachstrasse 1, D-85748 Garching, Germany
[4] Center for Astrophysics, 60 Garden Street, 02138 Cambridge MA, USA

Abstract. We discuss some of the main open issues related to the light–up and evolution of the first accreting sources powering high redshift luminous quasars. We discuss the perspectives of future deep X–ray surveys with the International X–ray Observatory and possible synergies with the Wide Field X-ray Telescope.

Key words. Galaxies: active – X-rays; Active Galactic Nuclei – galaxies: high-redshift

1. Introduction

The "dark ages" of the Universe ended when the UV radiation from the first objects reionized the intergalactic medium. This epoch began approximately at $6 < z < 14$ and so far has remained essentially unexplored. Investigating the end of the dark ages is extremely important to understand structure formation, since during this phase the first proto–galaxies and the first seed black holes, that would later grow into luminous quasars, formed. Observations of the most distant (z> 6) quasars (QSOs) thus probe the very early growth of supermassive black holes (SMBHs) in the centers of massive galaxies.

The high luminosities and broad line widths of the most distant QSOs require BH masses above $10^9 M_\odot$ (Fan et al. 2001; Willott et al. 2003). The formation of such systems within the first 700-800 Myr of cosmic time is a challenge for theoretical models (i.e. Volonteri & Rees 2005; Li et al. 2007; Begelman 2010). A number of possibilities have been proposed for the origin of the seed BHs (from Pop III stars to more massive objects resulting from the direct collapse of molecular clouds), the accretion rate (Eddington limited or super Eddington) and the merging rate of dark halos in the early Universe. Even though suitable combinations of the above parameters may explain the presence of massive BHs at $z \sim 6$, the processes responsible for their assembly and light–up are largely unknown. The search for and the study of the first QSOs is a key scientific goal of future X–ray missions and in particular of the Wide Field X–ray Telescope (WFXT; Rosati et al. 2010, this book) and the International X–ray Observatory (IXO; White et al. 2010).

Send offprint requests to: A. Comastri

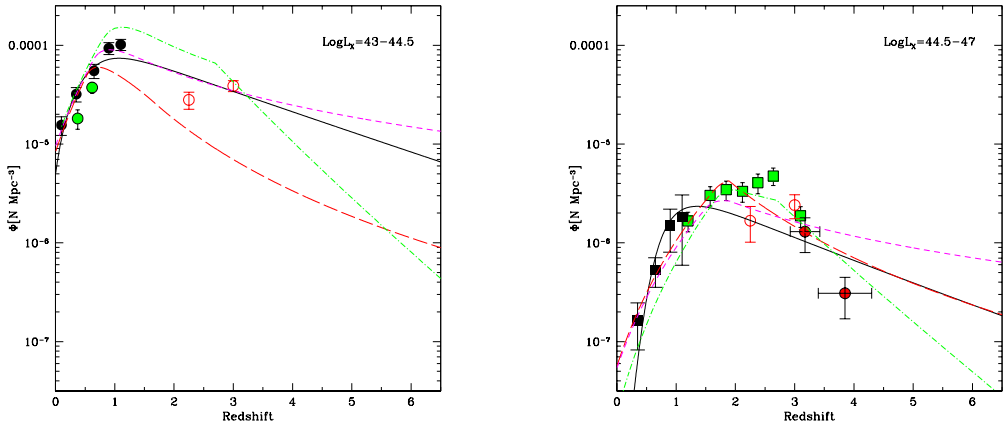

Fig. 1. The AGN number density, as determined by recent X-ray surveys, in two 2–10 keV luminosity ranges. *Left panel*: logL_X=43-44.5; *right panel*: logL_X=44.5-47. Green circles and squares at $z < 3$ are from the XMM-COSMOS survey (Brusa et al. 2010). Black circles and squares and open red circles at $2 < z < 3$ are from various surveys as described in Aird et al. (2010). Filled red circles at $z > 3$ in the right panel are from Brusa et al. (2009). The best fit results of the various determinations of the X–ray luminosity function from Aird et al (2010; black solid line), Ebrero et al. (2009; pink dashed curves), Silverman et al. (2008; red dashed curves) are reported in both panels. The green dot–dashed curves represent the expectations of the XRB synthesis model of Gilli et al. (2007).

2. Supermassive Black Holes in the early Universe

Most of the SMBH accretion luminosity is emitted in the optical/UV and X–ray bands. As a consequence, optical and X–ray surveys have played a major role in the discovery of high–redshift quasars.

2.1. Optical surveys

A major step forward in the study of the high redshift Universe was achieved thanks to the Sloan Digital Sky Survey (SDSS). In a series of papers, Fan and collaborators searched for $z > 5.7$ QSOs in different releases of the SDSS over an area of about 6600 deg^2 with a color selection (i–band drop out) technique (see Fan et al. 2001 for a detailed description). Their final sample includes 19 objects with $5.7 < z < 6.4$ and $M_{1450} < -26$. Using the same technique, the search for $z \simeq 6$ QSOs was recently extended towards lower luminosities ($M_{1450} \sim -24$) in the deep SDSS stripe by Jiang et al. (2008,2009), allowing the discovery of 12 additional objects. Thanks to the Canada France High Redshift Quasar Survey (CFHQS), which covers about 500 deg^2 down to fainter magnitudes, and applying a similar selection criterion, 19 additional QSOs at $z > 5.7$ have been found (Willott et al. 2007, 2009, 2010). The number of optically selected QSOs revealed up to $z \sim 6$ is large enough to determine their luminosity function. By combining the CFHQS data with the luminous SDSS QSOs, Willott et al. (2010) assembled a sample of 40 QSOs to estimate the $5.74 < z < 6.42$ luminosity function over the range $-24.7 < M_{1450} < -27.5$. Although the covariance between the slope and $M^{\star}_{1450}$ luminosity prevents strong constraints to be placed on either parameter, there is evidence for the detection of a break at $M^{\star}_{1450} \simeq -25.1$. As far as luminous QSOs are concerned, an exponential decline ($\propto 10^{-0.43z}$) in their space density from $z \sim 3$ to $z \sim 6$ has been clearly observed. Although SDSS has pushed the redshift record well above $z \sim 6$ with a statistics good enough to estimate the cosmological space density of high-z QSOs, it is crucial to point out that SDSS QSOs are among

the brightest and most extreme sources in the early Universe (in terms of luminosities and BH masses), and thus probably not representative of the QSO population at those redshifts.

2.2. X–ray surveys

The *Chandra* and XMM sensitivities to faint and hard X–ray sources has opened up a new era in the observations of the high redshift Universe. The systematic study of high–z ($>$ 4) optically selected QSOs was pioneered by Brandt and coworkers (i.e. Kaspi et al. 2000; Vignali et al. 2003; Shemmer et al. 2006); see Brandt et al. 2004 for a review) with pointed snapshot observations, and further expanded by cross correlating the SDSS catalogues with the XMM archive (Young et al. 2009) and the *Champ* project (Green et al. 2009). Multifrequency observations point towards the absence of evolution in the X–ray spectral index, absorption, metallicity, emission–line strengths and dust properties over a broad redshift range suggesting that the physical mechanisms powering luminous QSOs are insensitive to the significant changes on larger scales that occur at $z \simeq$ 0–6 (Maiolino 2006; Shemmer et al. 2006). Some departures from a self-similar evolution have emerged thanks to *Spitzer* near infrared observations of a small sample of $z \simeq$ 6 QSOs (Jiang et al. 2010). Two out of the 21 $z \simeq$6 QSOs observed by *Spitzer* do not show any detectable emission from hot dust. There is also evidence that hot dust free QSOs have the smallest BH masses in the sample (2–3 $\times$ $10^8 M_{\odot}$) and are accreting close to their Eddington limit, suggesting an early evolutionary stage.

A major improvement in the study of the cosmological evolution of the X–ray emission of moderate to high–z QSOs has been obtained in the last few years thanks to the large number of deep and medium–deep *Chandra* and XMM surveys. Large samples of X–ray selected objects were built, and by now the X–ray luminosity function is sampled up to $z \sim$ 3–4, down to X–ray luminosities of the order of a few $\times 10^{44}$ erg s^{-1} and to $z \sim$2–3 at lower luminosities (see Fig. 1; Brusa et al. 2009; Ebrero et al. 2009; Yencho et al. 2009; Aird et al. 2010; Fontanot et al. 2007).

At higher redshifts, present X–ray observations are highly incomplete, being strongly limited by the survey areas. The redshift records for X–ray selected QSOs are reached in the COSMOS survey (z = 5.41; Civano et al 2010 ApJ in prep.) and in the CLASXS survey (z = 5.40; Steffen et al. 2004), with only one spectroscopically identified object per survey. Deep and ultra–deep *Chandra* surveys in the CDFS and CDFN would be sensitive to lower X–ray luminosities, but the lack of area coverage is much more severe. Also in this case only one $z > 5$ spectroscopically confirmed AGN is found in the CDFN at z = 5.19, (Barger et al. 2005), and none in the CDFS (Luo et al. 2010). As a result, the space density of X–ray selected QSOs is still unconstrained at $z > 5$.

3. Beyond $z \sim 6$

The volume and surface density of the first QSOs can be estimated following two different approaches. A theoretical one, by building up semi analytical models (SAMs) which include a description as accurate as possible of the complex physical processes thought to be at work and key model parameters such as the seed BH mass, the accretion rate and the peak in the density field fluctuations above which they can start to form. Alternatively, an observational route may be followed. The best fit luminosity function and evolution, as measured by present X–ray surveys or by optical surveys can be extrapolated to high redshifts with some educated guesses on the optical to X–ray luminosity ratio.

Fig. 1 shows the most updated compilation of the X–ray luminosity function (XLF) parameterized with a Luminosity Dependent Density Evolution phenomenological model (LDDE; Silverman et al. 2008; Ebrero et al. 2009) or a Luminosity and Density Evolution model (LADE; Aird et al. 2010). The predictions based on the AGN synthesis model for the XRB of Gilli et al. (2007) are also shown, obtained by including an exponential cut–off in the XLF evolution at z=2.7, which is a good description of the observed space density of lu-

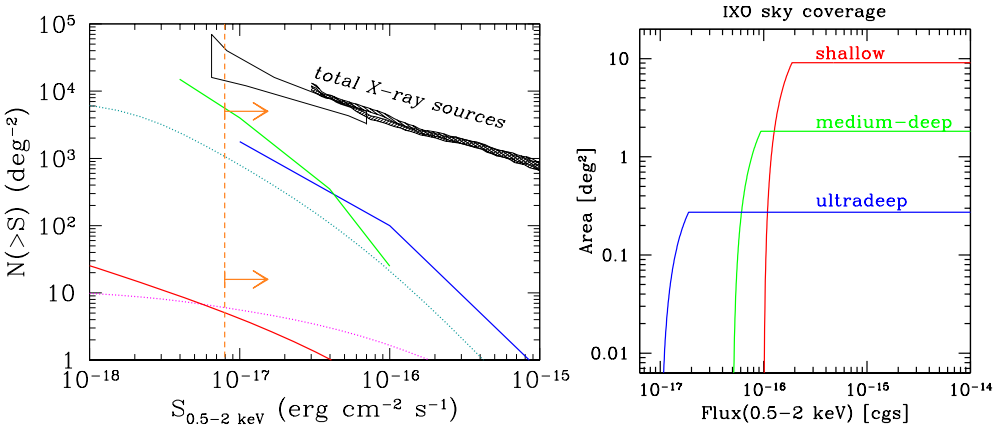

Fig. 2. *Left panel*: predicted AGN number counts at $z > 6$ for various semi-analytic models of BH/galaxy formation (solid lines): Salvaterra et al. (2007, green), Rhook & Haehnelt (2008, blue) and Marulli et al. (2009, red). Dotted curves show extrapolations of the luminosity functions adopted in the Gilli et al. (2007) model for the synthesis of the XRB (see text for details). The vertical orange line represents the IXO confusion limit (reached in about 2 Ms). *Right panel*: the sky coverage of a possible "survey" program (see text for details).

minous QSOs in the XMM–COSMOS survey (Brusa et al. 2009).

A detailed description of the best fit parameters of each XLF is beyond the purposes of this paper. Here we would like to stress that the extrapolations beyond the redshift range where the XLF was computed may differ by more than one order of magnitude. Moreover, the faint end of the XLF is poorly determined, even at relatively low redshifts (left panel of Fig. 1), making the predictions even more uncertain. The space density of $z > 6$ QSOs predicted by a few recent SAMs (Marulli et al. 2009; Salvaterra et al. 2007; Rhook & Haehnelt 2008) are compared with the extrapolation of the observed XLF in the left panel of Fig. 2.

The lower dotted curve corresponds to the "decline" model (cfr. Fig. 1) which is found to provide a good fit to the observed space density of $z \sim 3$–5 QSOs in the *Chandra*–COSMOS survey (Civano et al. 2010, in prep.). The upper dotted curve corresponds to an ad–hoc parameterization of the XLF high–redshift evolution named "maxXLF". The space density of low luminosity ($\log L_X < 44$) AGN is kept constant at $z > 4$. This model maximizes the predicted number of higher redshift QSOs, being at the same time in agreement with the observational results at lower z, hence the name "maxXLF" (see Fig. 1 in Gilli et al. 2010, this volume). Different choices for the evolution of the luminosity function (cfr. Fig. 1) would correspond to space densities in between the "decline" and the "maxXLF" predictions which should then be considered as a conservative and an optimistic estimate, respectively.

4. Breaking through the first typical AGN

The bulk of the population of high–z QSOs representative of the first accreting objects in the Universe is likely to be characterized, on average, by relatively low X–ray luminosities and BH masses. Large area optical and near–infrared surveys such as those foreseen with future ground-based facilities and space observatories like PANSTARRS, VISTA, LSST and JDEM/EUCLID will discover a large number of high-z QSOs. The above surveys will be biased against dust obscured QSOs and faint active nuclei for which the host galaxy starlight cannot be neglected.

X–ray observations can probe much lower luminosities and high absorption column densities. Moreover, the X–ray emission is the tell-

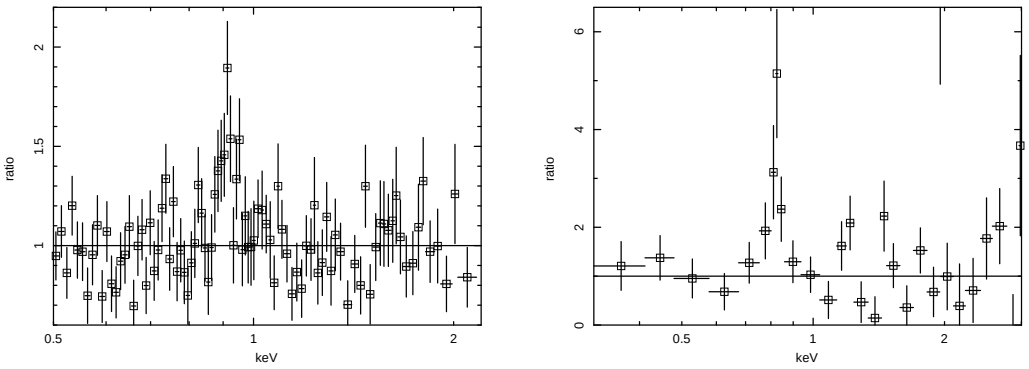

Fig. 3. Residuals wrt a single power law fit to IXO simulations. *Left panel*: a 100 ks simulation, including background, of a z = 6 QSO. The line EW of ∼ 40 eV observed frame (280 eV rest frame) is clearly seen at ∼ 0.9 keV. *Right panel*: a 1 Ms simulation, including background, of a Compton Thick AGN at z = 7. The characteristic strong iron line (EW ∼ 1.2 keV rest–frame) is easily recognizable.

tale of an accreting object. A blind search for X–ray selected $z \sim 5$–6 QSOs would require to survey several tens of square degrees to a depth comparable to that reached in the *Chandra* deep surveys (about 0.2 square degrees for a total observing time of 6 Ms) and is far beyond the capabilities of current X–ray facilities.

Thanks to its large effective area at 1 keV (~ 3 m^2) and good spatial resolution (5 arcsec HPD), IXO will perform deep surveys reaching limiting fluxes below 10^{-17} erg cm^{-2} s^{-1} in the 0.5–2 keV energy range (Fig. 2, left panel). The final sensitivity will depend on the actual number of faint sources which sets the confusion limit. In order to harvest a significant number of moderate luminosity, obscured AGN at $z > 6$ and to cope with the present large uncertainties on their predicted space density, a typical multi–cone observing strategy is mandatory.

A possible observational strategy for a multi–cone IXO survey with the Wide Field Imager (WFI) is shown in the right panel of Fig. 2. The total observing time invested in cosmological surveys would be of the order of 18 Ms broadly split in deep (3 pointings, 2 Ms each) medium (20 pointings, 300 ks each) and shallow (100 pointings, 60 ks each) corresponding to about 10 months of observing time assuming an efficiency of 70%, though it should be noted that shallower observations will be performed anyway for a wide range of scientific investigations.

The expected number of $z > 4$ QSOs will range from a few hundreds to more than a thousands, while at $z > 6$ the predicted number of sources could vary beween a dozen up to a few hundreds, reflecting the uncertainties reported in Fig. 1 and 2. Taking a median value, the total number of high–z QSOs will be sufficient to constrain the evolution of the faint end of the XLF down to $L_X \sim 5\times 10^{42}$ erg s^{-1} and up to $z \simeq 6$. IXO will also be able to detect the very first objects at $z \sim 10$, if they exist, and if their X–ray luminosity is larger than approximately 10^{43} erg s^{-1}. IXO deep surveys need to be performed over well studied sky areas at longer wavelengths to ease the process of source identification and redshift determination. The excellent IXO angular resolution and sensitivity coupled with the capabilities of JWST, ALMA, E-ELT and TMT will allow to study the assembly of early Black Holes and their host galaxies.

The large IXO collecting area is extremely well suited for detailed spectroscopic studies. According to the currently accepted models for the joint evolution of SMBH and their host galaxies (Hopkins et al. 2006; Lamastra et al. 2010), the fraction of obscured and heavily absorbed or Compton Thick ($N_H > 10^{24}$ cm^{-2}) AGN is predicted to increase with redshift (i.e. Menci et al. 2008). From an observational point of view, the issue of an increased

fraction of obscured AGN at high redshifts is still debated (see the discussion in Gilli et al. 2010). Irrespective of what the true fraction is, the study of heavily obscured AGN at high–z would bear important information on the formation and early growth of the first active galaxies. Primordial, gas and dust rich galaxies, should undergo a phase of high obscuration, gas accretion on the central BH and vigorous starformation, making deep hard X–ray observations an ideal tool for their discovery. The IXO spectroscopic capabilities are shown in the two panels of Fig. 3. The spectrum of a luminous ($L_X \simeq 3\times 10^{44}$ erg s^{-1}), mildly obscured ($N_H \sim 10^{23}$ cm^{-2}) QSO at z=6 is simulated with a 100 ks WFI exposure. The 6.4 keV iron line EW is assumed to be 280 eV rest–frame. The residuals, with respect to an absorbed power law fit show a line–like feature with an observed frame EW of $\sim$ 40 eV. In the right panel, the X–ray emission of a z =7, $L_X \sim 10^{43}$ erg s^{-1}, CT AGN is modeled with a pure reflection spectrum plus a strong (EW $\sim$ 1.2 keV rest–frame) iron Kα line. The residuals of the fit with the same model, without including line emission, show that the $K\alpha$ iron line can be used to directly measure source redshift with an accuracy of $\Delta z \simeq$0.2.

5. IXO and WFXT Synergies

The study of the first SMBH would greatly benefit from joint WFXT and IXO surveys. The synergies between the two proposed missions are obviously clear. The WFXT multitiered survey strategy is designed to maximize the yield in the discovery of high–z AGN. Detailed and quantitative estimates are extensively discussed in Gilli et al. (2010, this volume). IXO with its superior sensitivity to faint sources would be unique for spectroscopic follow–up of the large WFXT samples and to discover the faintest AGN at the highest redshifts. At the flux of 10^{-15} erg cm^{-2} s^{-1}, about 300 AGN at $z > 6$ are expected in the WFXT medium survey assuming a conservative "decline" model. Relatively inexpensive IXO pointings (100 ks each), would allow us to obtain spectra of the quality show in the left panel of Fig. 3, making possible to measure metal abundances and many other QSO physical parameters at very high–z.

References

Aird, J., et al. 2010, MNRAS, 401, 2531
Barger, A., et al. 2005, AJ, 129, 578
Begelman, M. 2010, MNRAS, 402, 673
Brandt, W.N., et al. 2004, arXiv:0411355
Brusa, M., et al. 2009, ApJ, 693, 8
Brusa, M., et al. 2010, ApJ, 716, 348
Ebrero, J., et al. 2009, A&A, 493, 55
Fan, X., et al. 2001, AJ, 122, 2833
Fontanot, F., et al. 2007, A&A, 461, 39
Gilli, R., Comastri, A., Hasinger, G. 2007, A&A, 463, 67
Gilli, R., et al. 2010, Proceedings of "X-ray Astronomy 2009" AIP Conf. Proc. (eds: A. Comastri, M. Cappi, L. Angelini) arXiv:1004.2412
Green, P., et al. 2009, ApJ, 690, 644
Hopkins, P.F., et al. 2006, ApJS, 163, 1
Jiang, L., et al. 2008, AJ, 135, 1057
Jiang, L., et al. 2009, AJ, 138, 305
Jiang, L., et al. 2010, Nature, 464, 380
Kaspi, S., et al. 2000, AJ, 119, 2031
Lamastra, A., et al. 2010, MNRAS, 405, 29
Li, Y., et al. 2007, ApJ, 665, 187
Luo, B. et al. 2010, ApJS, 187, 560
Maiolino, R., et al. 2006, arXiv:0306261
Marulli, F., et al. 2009, MNRAS, 396, 1404
Menci, N., et al. 2008, ApJ, 686, 219
Rhook, K. & Haehnelt, M. 2008, MNRAS, 389, 270
Salvaterra, R., et al. 2007, MNRAS, 374, 761
Shemmer, O., et al. 2006, ApJ, 644, 86
Steffen, A., et al. 2004, AJ, 128, 1483
Vignali, C., et al. 2003, AJ, 125, 2876
Volonteri, M. & Rees, M. 2005, ApJ, 633, 624
White, N.E., et al. 2010, Proceedings of "X-ray Astronomy 2009" AIP Conf. Proc. (eds: A. Comastri, M. Cappi, L. Angelini)
Willott, C., et al. 2003, ApJ, 587, L15
Willott, C., et al. 2007, AJ, 134, 2435
Willott, C., et al. 2009, AJ, 137, 3541
Willott, C., et al. 2010, AJ, 139, 906
Yencho, B., et al. 2009, ApJ, 698, 380
Young, M., et al. 2009, ApJS, 183, 17